THE
PHYSICAL REVIEW
A Journal of Experimental and Theoretical Physics Established by E. L. Nichols in 1893
VOL. 53, NO. 7 APRIL 1, 1938 SECOND SERIES

The Intensity of the Primary Cosmic Radiation and Its Energy Distribution*

THOMAS H. JOHNSON
Bartol Research Foundation of the Franklin Institute, Swarthmore, Pennsylvania
(Received February 15, 1938)

The number of primary cosmic rays incident upon one horizontal square centimeter at the top of the atmosphere is computed by dividing the total energy spent in ionization in an infinitely deep column of air by the average energy of a single primary ray. The energy is found by integrating under the ionization-depth curves of Bowen, Millikan, Neher and Haynes and the average energy per ray is computed from the minimum energy of the Lemaitre-Vallarta theory and a suitably chosen distribution function. Evidence for a low energy limit at 4.4×10^9 volts is found. The number of primary cosmic rays increases from 0.03 per cm² per sec. at the equator to 0.36 per cm² per sec. at latitudes above 45°. The total cosmic-ray current to the earth is 8×10^{17} rays per sec. or 0.13 amperes. If the distribution function is of the form AV^{-n}, where V is the energy of a ray and n and A are constants, it is shown that n is equal to or slightly less than 3.

THE cosmic-ray intensity when plotted against depth in the atmosphere rises from some low value at the top of the atmosphere, passes through a maximum, and then falls off at greater depths. The initial rise demonstrates the importance of secondary effects in the measured intensity and one is led to inquire what the primary intensity would be if the apparatus could be elevated above the atmosphere. Because of wall effects, which would become appreciable under those conditions, in the ionization measurements, and because of magnetic bending of secondaries[1] in the rarified atmosphere at great heights, the actual measurements at the greatest attainable heights must always exceed the primary intensity, but it is possible to arrive at the number of primary rays by means of a simple calculation.

The total energy expended in the production of ions within a column of air of unit cross section and infinite depth is equal to the energy incident upon its upper surface. This energy divided by the average energy of a primary cosmic ray is equal to the number of primary cosmic rays per unit area. The recent balloon flights of Bowen, Millikan, Neher and Haynes[2] have supplied the data required for the computation of the energy expended in the atmosphere at the latitudes 3°N, 39°N and 52°N geomagnetic latitude and the earlier results of Millikan and Cameron[3] can be used for the greater depths where latitude effects are negligibly small. The results of integrations under these curves, reduced to the total number of ions in an infinitely deep column of air one square centimeter in cross section, are given in

* This paper was written in response to a question which was raised in the laboratory as to what intensity one might expect to measure at the top of the atmosphere with a counter apparatus. Some of the results included in it have just appeared in a paper by Bowen, Millikan and Neher, Phys. Rev. **53**, 217 (1938).

[1] Kulenkampf, Naturwiss. **21**, 25 (1933).

[2] Bowen, Millikan and Neher, Phys. Rev. **52**, 80 (1937); Millikan, Neher and Haynes, Phys. Rev. **50**, 992 (1936).

[3] Millikan and Cameron, Phys. Rev. **37**, 235 (1931).

the first row of Table I. The major part of the ionization takes place in the atmosphere; out of the total of 1×10^8 ions at 52°N only 2.3×10^6 ions are produced below sea level and only 1×10^6 below 40 meters of water. The total energy, listed in the second row, is equal to the ionization multiplied by the energy required to produce one ion pair, assumed equal to 33 ev.

The minimum energies of the primary cosmic rays for each latitude are given by the theory of the cosmic-ray orbits in the earth's magnetic field, developed by Lemaitre and Vallarta.[4] Strictly speaking the minimum energy also depends upon the direction, but to a first approximation the value for the vertical direction may be taken as a mean value for the latitude in question. These minimum energy values are listed in the third row of the table. An upper limit to the number of rays may now be found by dividing the total energy by the minimum energy. The numbers found in this way are listed in the fourth row of the table. The average energy per ray can be computed from the minimum energy if the energy distribution function is known. This distribution would be uniquely determined by the data if the measurements had extended over a continuous range of latitudes,[5] but in order to interpolate between the experimental points and to extrapolate beyond them into the higher energies above the low energy limit for the equator, it is convenient to assume some form of the energy distribution with two disposable constants and to determine these from the data for the two lowest latitudes. The intensity at the highest latitude may be effected by the existence

TABLE I. *Intensity data for cosmic rays at various latitudes.*

GEOMAGNETIC LATITUDE	3°N	39°N	52°N
Ions per cm² per sec.	$3\cdot10^7$	$5.4\cdot10^7$	$10\cdot10^7$
Energy per cm² per sec. (electron volts)	$1\cdot10^9$	$1.7\cdot10^9$	$3.2\cdot10^9$
V_λ, low energy limit by the earth's field	$15\cdot10^9$	$8\cdot10^9$	$2\cdot10^9$
Upper limit to the number of cosmic rays per cm² per sec.	0.064	0.215	1.6
Average energy per ray $n=3$ law with limit at 4.4×10^9	3×10^{10}	1.6×10^{10}	0.88×10^{10}
Probable number of rays per cm² per sec.	0.032	0.11	0.36
Probable number per minute	1.9	6.5	21.8

[4] Lemaitre and Vallarta, Phys. Rev. **50**, 493 (1936).

[5] This was pointed out independently and nearly simultaneously by H. Zanstra, Naturwiss. **22**, 171 (1934) and the writer Phys. Rev. **45**, 574 (1934).

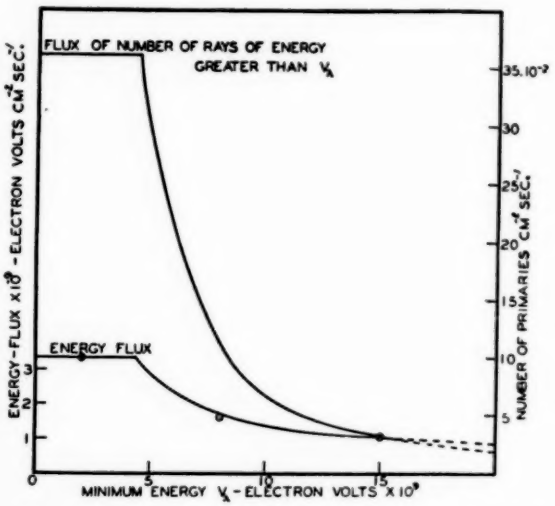

FIG. 1. The flux of the number of cosmic rays and the cosmic-ray energy for rays of energy greater than V_λ.

of a low energy limit to the primary cosmic radiation imposed by a solar magnetic field which introduces additional considerations. A reasonable distribution function will have a large value for low energies, will vanish asymptotically for high energies and will be positive and continuous over the range above the low energy limit. Below the low energy limit the function will be zero. An analytically convenient form of function is

$$j(V)=A\,V^{-n} \qquad V>V_0,$$
$$j(V)=0 \qquad V<V_0, \tag{1}$$

where $j(V)dV$ is the number of rays per horizontal square centimeter per second in the primary radiation in the energy range from V to $V+dV$. The total energy in latitude λ per cm² per sec. is

$$E_\lambda=\int_{V_\lambda}^{\infty} V\,j(V)\,dV=A\,V_\lambda^{-(n-2)}/(n-2)\,; \tag{2}$$

the total number of rays per cm² per sec. is

$$J_\lambda=A\,V_\lambda^{-(n-1)}/(n-1), \tag{3}$$

and the average energy per ray is

$$\bar{V}_\lambda=(n-1)\,V_\lambda/(n-2). \tag{4}$$

If n is determined from the experimental points for 3°N and 39°N, it is found that an exact fit is realized with $n=2.87$; the data are approximated within reasonable accuracy by $n=3$, $A=15\cdot10^{18}$. A plot of the total energy per cm² per sec. by rays

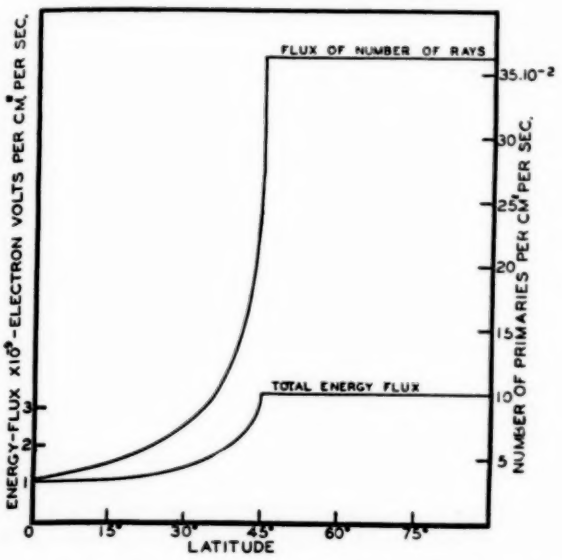

FIG. 2. The latitude effect of the primary cosmic radiation plotted in terms of numbers of rays per cm² per sec. and in terms of the total energy flux.

of energy greater than V, according to this distribution, is given in curve I of Fig. 1. The points realized from the integration of the experimental data are shown as circles. In order to include the point at 52°N it is necessary to assume that the lower energy limit occurs at 4.4×10^9 ev. (If an exponent less than $n=3$ were chosen this point would shift to slightly lower energies.) This corresponds to a knee in the latitude *vs* intensity curve at 45° which is in close agreement with the position of the observed knee. In the same figure the number of primary cosmic rays per cm² per sec. of energy greater than V is also plotted according to the corresponding distribution, Eq. (3) with $n=3$. Fig. 2 shows the same quantities plotted against latitude. In calculating the number of rays an average energy equal to twice the minimum energy, according to Eq. (4) with $n=3$, has been used.

The total number of cosmic rays incident upon the entire surface of the earth is given by the integral

$$N=4\pi R^2\int_0^{\pi/2} J(\lambda)\cos\lambda d\lambda$$

$$=8.0\times10^{17} \text{ rays per second.}$$

It is known that most of the primary cosmic rays are positive.[6] If they were all positive, the cosmic-ray current to the earth would be 0.13 amperes. In the absence of other currents this would charge the earth up at the rate of 180 volts per second. The total power of the cosmic-ray primaries is about one million kilowatts.

In the last row of Table I the number of primary cosmic rays per cm² per minute is given for each of the three latitudes. Since approximately one[7] cosmic ray per minute is incident upon a horizontal square centimeter at sea level these numbers represent approximately the ratios of the intensities at the top of the atmosphere to those at sea level.

[6] T. H. Johnson, Phys. Rev. **45**, 574 (1934).
[7] According to Street and Woodward this number is 1.25 rays per minute at sea level. Phys. Rev. **46**, 1029 (1934).

The Radioactivity of Potassium

ARTHUR BRAMLEY* AND A. KEITH BREWER
Bureau of Chemistry and Soils, U. S. Department of Agriculture, Washington, D. C.
(Received January 29, 1938)

The radioactivity of K was measured with a Geiger counter by placing a thick layer of the salt under a thin Al window. The results agree with those of Mühlhoff and give for the radioactive constants when corrected for the relative abundance of K^{40} the following values: $\lambda=(1.56\pm0.6)\times10^{-17}$ sec.$^{-1}$, and $T=(14.2\pm3.0)\times10^{+8}$ yr.

POTASSIUM has long been known to be radioactive. It emits two hard β-rays of velocity 0.83C and 0.93C in proportions 60 and 40 percent.[1] The disintegration constant has been determined by three different methods. Holmes and Lawson[2] using the data of Hoffmann give for the half-life, $T=1.5\times10^{12}$ years and for the disintegration constant $\lambda=1.40\times10^{-20}$ sec. Orban[3] by means of expansion chamber methods obtained $T=5\times10^{12}$ years and $\lambda=5\times10^{-21}$ sec. Mühlhoff,[4] from Geiger counter measurements, obtained $T=1.5\times10^{13}$ years and $\lambda=1.5\times10^{-21}$ sec. It will be observed that the various measurements differ by a factor of 10. The present experiment was undertaken, for the purpose of deciding which of these values was the more reliable.

Apparatus and Technique

The counter employed in these measurements was of the cylindrical form of metal construction. The counter chamber was made of heavy copper tube, with a perforated brass plate soldered to the lower end. An aluminum foil, 0.002 cm in thickness, was waxed over the plate. The area of the perforations was 1.4 square centimeters while the free inside dimensions of the chamber were 4.4×1.9 cm. The inner electrode was a polished nickel wire 0.15 cm in diameter supported by a hard rubber plug inserted in the upper end of the cylinder and extending for 2.5 cm down the barrel of the tube. The counter was operated at 1 cm of Hg pressure of dry air; the corresponding voltage lying in the range between 700 and 800. In normal operation the counter was run at 20 volts above the starting potential; under these conditions slight changes in pressure did not affect the counting rate.

The counts were amplified and recorded by means of a three-tube vacuum circuit and watch recorder described by Johnson and Street.[5] The technique employed was to measure the number of counts in the absence of any radioactive material. This was followed by measurements on a sample of finely powdered KCl supported in a glass dish placed directly below the aluminum foil window. These measurements were all made for an interval of either 6 or 15 minutes each depending on the set of experiments. They were repeated over a period of many hours.

Since commercial potassium salts are apt to be contaminated with radium, the KCl used in these experiments was prepared from K_2SO_4 and $BaCl_2$; any radium that might be present is removed along with the $BaSO_4$. Various samples of salt crystallized during the evaporation of the KCl containing filtrate showed no variations in radioactivity.

In the previous measurements performed by Mühlhoff with a Geiger counter, the salt was introduced into the counter itself whereas here the activity of the salt placed outside of the counter was measured. This procedure was followed because it was felt that the constants of the circuit such as number of spontaneous counts and sensitivity could be kept better under control. It had the disadvantage that the sensitivity was so low that thin films of KCl could not be used. However, for the thick films this was an advantage. In this case, the number of counts per minute for KCl was such that no correction need be applied to take care of the possibility that

* Washington, D. C.
[1] D. Bocciarilli, Atti accad. Lincei **17**, 830 (1933).
[2] A. Holmes and R. W. Lawson, Phil. Mag. **2**, 1218 (1926)
[3] Orban, Akad. Wiss. Wiess. Ber. **140**, 121 (1931).
[4] W. Mühlhoff, Ann. d. Physik **7**, 205 (1930).
[5] Johnson and Street, J. Frank. Inst. **215**, 293 (1933).

counts were missed on account of the low resolving time of the recording apparatus. Further, the number of counts arising from the β-ray emission was always greater than the spontaneous counts. In order to ascertain whether or not the performance of the counter was independent of the working conditions two independent sets of readings were taken. In the first set, the background was fairly high, of the order of 7 counts per minute, but this was compensated for to some extent by the higher efficiency of the counter. In the second set the background was exceptionally low. Although the count was as low as 2 per minute, the efficiency was less by only 10 percent on the average. It is gratifying to observe that these two independent runs lead to the same value for the disintegration constant to an accuracy far within the probable error. For the purpose of convenience in recording the data, these two runs will be described separately.

Counter Efficiency

The absolute efficiency of the counter was measured in the first series of runs by means of recording the counts from measured quantities of U_3O_8 and from $UO_2(NO_3)_2+6H_2O$. In the case of U_3O_8, 902 counts were obtained in 30 minutes from a sample containing 2.1×10^{-4} g per cm^2 total weight. The background count for a similar period was 240. This gives 15 2 counts per minute per cm^2. The number of counts to be expected is equal to one half-the number of disintegrations per gram of uranium times the amount present per cm^2. According to Rutherford, the number of disintegrations per gram of uranium per minute is 1.43×10^6. Since the sample contained 1.78×10^{-4} grams of uranium per cm^2, 135 counts per minute per cm^2 should have been recorded. The efficiency of the counter is in consequence $15.2/135=11.2$ percent. The efficiency obtained by using uranium nitrate instead of uranium oxide was 12.2 percent. The average efficiency is, therefore, 11.7 percent. The low efficiency observed is to be expected from the design of the counter. The geometry of the apparatus was such that only about one-half the β-particles leaving the surface can enter the chamber even if they were not absorbed by the thin Al window. Further the distribution of potential within the counter requires that a large part of the space adjacent to the window is insensitive. In addition the ionizing power of β-particles in air at N.T.P. for potassium and UX_2 varies from 28 to 23 ions per cm of path. At 1 cm pressure, therefore, the mean free path between ionizing collisions is about 3 cm. In consequence many β-rays will pass through the counter without ionizing, and hence will not be recorded.

Since the β-rays from UX_2 are slightly more penetrating than those from potassium it seems advisable to apply a correction factor of about 44 percent to the efficiency obtained for uranium. The effective efficiency for KCl is, therefore, close to 16.8 ± 4.0 percent. This estimate of the efficiency for KCl as compared to that for U_3O_8 was computed from the known differences in the hardness of the rays. The two beta-rays designated as UX_2 and UX_1 which are emitted in equal numbers from thin layers of uranium have an absorption coefficient in Al of 14.4 and 510, respectively. The percentage transmitted by the Al window on the counter—thickness 0.02 mm—is 97 and 36 percent, respectively. From the known values of 80×10^4 and 4.2×10^4 ev for the average energy of these same rays, the number of ions formed per cm of path in air under normal conditions is computed to be 25.2 and 60. With the aid of these numbers the probability of ionization in a chamber 3 cm long filled with air at 1 cm pressure can be found.[6] This probability turns out to be 0.63 and 0.79. Thus the value for the probability of ionization in the counter of a β-particle emitted by uranium is

$$(\tfrac{1}{2})(0.97\times0.63+0.36\times0.79)=0.46.$$

Potassium also emits two rays in the proportions of 40 to 60whose average energies are 350 and 133×10^3 ev, respectively. For these rays the average number of ions per cm of path in air at N.P.T. is 28 and 37. From a calculation similar to that for uranium, the final value of the probability of ionization in the counter for a beta-particle from potassium is 0.67. According to this reckoning the relative efficiency of potassium as compared to uranium in tripping off the counter should be $67/46=1.44$.

These limits of error were computed from estimates of the variability of the deposit of the

[6] Loeb, *Kinetic Theory of Gases* (McGraw-Hill), p. 45.

TABLE I. *Results obtained with a thick layer of pure* KCl. *Average number of counts/min./cm²* 6.3±0.3, *The error is the probable error of the total number of counts.*

SALT	MINUTES	COUNTS	COUNTS/MIN.	COUNTS/MIN.·CM²
Sample 1				
Blank	72	592	8.22	
KCl	72	1228	17.00	6.1±0.3
Sample 2				
Blank	120	251	2.09	
KCl	315	3117	11.19	6.5±0.3

uranium salts in thin films and of the path length of the β-particles in the counter. This last factor must be known before an adequate correction can be applied for the difference in ionizing power for the β-rays from uranium and potassium.

In the second set of experiments in which the sensitivity was tested with a sample of U_3O_8, the measured efficiency of 10.3 was somewhat lower. This gives for the effective efficiency for KCl, 14.8±0.4.

RESULTS

The results obtained with pure KCl are given in Table I. The difference between these two sets of data is not significant from a statistical viewpoint even when allowance is made for the difference in the effective efficiency of the counter for KCl, namely, 16.8 as compared to 14.8. For the purpose of future calculation, it is justifiable to treat the combined data as if it were a single sample.

Since the counts in any one interval are necessarily grouped statistically, the following examples given in Table II for typical six-minute intervals from which the above data were compiled will serve to illustrate the type of variations obtained. It will be observed that the net number of counts from KCl is materially in excess of the background and that the results for unit intervals do not scatter badly.

DISCUSSION

The computation of the disintegration constant from the results obtained with a thick layer of salt necessitates a knowledge of the absorption within the body of the salt. Orban[3] has treated this point in detail, hence only a brief outline of the method will suffice here. The number of disintegrations observed per second per square centimeter "n" is equal to the disintegration constant divided by two times the number of potassium atoms from which the β-rays can reach the surface. This latter quantity is equal to the number of potassium atoms per cubic centimeter in KCl times the average thickness from which the rays can penetrate. If the reciprocal of the absorption coefficient μ measured in KCl is taken for the average thickness, it follows that

$$n=\frac{\lambda}{2}\left(\frac{\rho}{\mu}\right)_{\mathrm{Al}}\frac{6.06\times10^{23}}{77}.$$

The most difficult point in the calculation of the disintegration constant from the observed number of counts is that of choosing an appropriate value for μ from the various estimates given in the literature. Campbell and Wood[7] give the absorption coefficient in cm^{-1} of aluminum for the two β-rays of potassium as 29 and 75 for the hard and soft rays, respectively. Since 40 percent of the rays are hard, the average absorption coefficient is computed to be 46 cm^{-1}. This value is in agreement with the determination of Orban of 46 cm^{-1} Al for a thickness of 0.05 cm Al. His calculation of the disintegration constant[3] of potassium is based on the validity of this measurement of the absorption coefficient. This value for the absorption coefficient is materially greater than that found by Kuban.[8] He gives for the absorption coefficient in Al 28 cm^{-1}. Since the values taken with an ionization chamber might well give an erroneous estimate of the number of beta-particles absorbed, it was decided to measure the absorption coefficient with this apparatus. The results of these measurements agree within the limit of error with the value determined by Kuban. For this reason the computation for $(\mu/\rho)_{\mathrm{Al}}$ was made with a value of 10.4.

TABLE II. *Statistical variation in the number of counts obtained during typical six-minute intervals.*

BLANK	34	46	46	46	48	44	48
KCl	90	104	108	110	82	92	88
Counts/cm²·min.	6.4	6.6	7.0	7.2	3.9	5.5	4.6

[7] Campbell and Wood, Proc. Camb. Phil. Soc. **14**, 15 (1906).
[8] Kuban, Wien Ber. **137**, 241 (1928).

The disintegration constant computed by the above method is

$$\lambda = (1.73 \pm 0.6) \times 10^{-21} \text{ sec.},$$

the average life is

$$\theta = 1.83 \times 10^{13} \text{ years}$$

and the half-life is

$$T = (12.8 \pm 3.0) \times 10^{12} \text{ years}.$$

The principal sources of error in the above values appear to enter through the method employed in determining the thickness of the layer from which rays reach the counter and through the estimation of the counter efficiency. In so far as can be told from the data at hand, these errors lie within the limits given. The present value of 13×10^{12} is to be compared with the previous values of 15×10^{12} obtained by Mühlhoff and 5×10^{12} years given by Orban.

It is now known that potassium is composed of three isotopes with mass numbers 39, 40 and 41.[9, 10] Smythe and Hemmendinger[11] have recently shown that of these only K^{40} is radioactive. Since the abundance[10] of K^{40} is given by the ratio $K/K^{40} = 9000$, the disintegration constant for K^{40} is obtained by multiplying the values given above by 9000. The radioactive constants for K^{40} then become:

$$\lambda = (1.56 \pm 0.6) \times 10^{-17} \text{ sec.}^{-1},$$
$$\theta = 20.3 \times 10^{8} \text{ yr.},$$
$$T = (14.2 \pm 3.0) \times 10^{8} \text{ yr.}$$

The writers wish to thank Dr. F. L. Curtiss, National Bureau of Standards, for many valuable suggestions in counter technique. One of us (A. B.) wishes to express his appreciation of the opportunity of cooperating with the members of the Fertilizer Research Division of the Bureau of Chemistry and Soils in the evaluation of these constants.

[9] A. O. Nier, Phys. Rev. **48**, 283 (1935).
[10] A. Keith Brewer, Phys. Rev. **48**, 640 (1935).
[11] Smythe and Hemmendinger, Phys. Rev. **51**, 178 (1937).

APRIL 1, 1938 PHYSICAL REVIEW VOLUME 53

The Nuclear Isomers of In^{116}

ALLAN C. G. MITCHELL AND LAWRENCE M. LANGER
Physics Department, New York University, University Heights, New York, N. Y.

(Received January 22, 1938)

The isomeric periods of In^{116} (13 seconds and 54 minutes), produced by the capture of slow neutrons by In^{115}, have been studied with the purpose of determining the energy level scheme for In^{116}. The γ-ray of energy 1.4 Mev previously measured by the authors has been shown to have a period of 54 minutes. No γ-ray of 13 second period could be found. The percentage transmission by boron of resonance neutrons which effect the two periods has been measured and found to be the same within the experimental error, for both periods. The value obtained for the percentage transmission of 0.0252 g/cm² B (uncorrected for obliquity) is 73.5 ± 3.0. The branching ratio $R(13 \text{ sec.})/R(54 \text{ min.})$ has been shown to be independent of the method of excitation and has the value 1.12 ± 0.06. From the known beta-ray end points and the energy of the gamma-ray an energy level diagram has been drawn up which accounts for all the experimental facts. The two excited levels of In^{116} from which disintegration takes place are separated by 0.3 Mev, the level corresponding to the 13 second period lying higher. Gamma-ray transitions between these two levels can be forbidden by choosing quantum numbers which differ by 5 units.

INTRODUCTION

THE element indium, when subjected to neutron bombardment, becomes radioactive and shows several periods. The most prominent periods are those of 13 seconds and 54 minutes discovered by Amaldi, d'Agostino and Segrè[1, 2] which were shown to result from the capture of slow neutrons by indium. Szillard and Chalmers[3] also found a period of 3.5 hours which they attributed to the action of fast neutrons on indium, since they obtained it when the neutrons were not slowed down by paraffin. They pointed out that, since indium has only two known isotopes, one of the isotopes must be responsible for two periods.

[1] E. Amaldi, O. d'Agostino, E. Segrè, Ricerca Scient. **5**, 2 (1934).
[2] E. Amaldi, O. d'Agostino, E. Fermi, B. Pontecorvo, F. Rasetti, and E. Segrè, Proc. Roy. Soc. **149**, 522 (1935).
[3] L. Szillard and T. A. Chalmers, Nature **135**, 98 (1935).

Recent investigations have added materially to our knowledge of the indium periods. From the work of Lawson and Cork,[4] who have made a thorough investigation of the indium periods which are obtained when this and neighboring elements are bombarded by various types of particles, it is clear that the 13 second and 54 minutes periods are to be attributed to In^{116}. In the present experiment indium was bombarded with slow neutrons, and under these conditions only two periods are observable;[5] namely 13 seconds, and 54 minutes due to In^{116}. In the present work we shall investigate the isomeric periods of In^{116} and shall show that a nuclear energy level scheme can be drawn up which will account satisfactorily for all of the experimental data.

The Beta-Ray Spectrum

The spectrum of the beta-rays associated with the two periods of indium has been studied in a cloud chamber by several investigators. Gaerttner, Turin and Crane[6] found, from the Konopinski-Uhlenbeck theory of beta-ray emission, an extrapolated end point of 3.2 Mev for the beta-ray associated with the 13 second period. The end point obtained by inspection appears to be about 3.1 Mev.

For the 54-minute period Gaerttner, Turin, and Crane obtained an extrapolated end point of 1.3 Mev while Brown and Mitchell,[7] using the same method found an extrapolated end point of 1.45 Mev. The end point obtained by inspection of the curves of the two sets of investigators is certainly not less than 1.3 Mev.

It is interesting to note that, although in some cases the K-U extrapolated end points are considerably higher than those obtained by inspection,[8] in the present case they appear to agree with the end points obtained by inspection to about 0.1 Mev. From all the data it seems that the best values for the end points are: for the 13 second period, 3.1 ± 0.1 Mev; for the 54 minute period 1.4 ± 0.1 Mev.

The Gamma-Rays

Mitchell and Langer[9] measured the gamma-rays associated with the 54-minute period of indium. The method they used was that of measuring the stopping power of aluminum for Compton electrons ejected from a light metal by the gamma-rays. The ejected electrons were allowed to pass through two thin walled counters arranged to count coincidences. The decrease in the number of coincidences per minute was measured as a function of the thickness of aluminum placed between the counters. The authors also showed, from straight absorption experiments, that the gamma-ray was monochromatic. From this fact and the results of the coincidence method they showed that the energy of the gamma-ray was 1.39 ± 0.10 Mev.

The Period of the Gamma-Ray Activity

We have performed a number of experiments in which we have measured the period of the gamma-rays. To do this we used two identical thin walled glass counters lined with a thin coating of silver. One counter was wrapped with lead foil to a thickness of 1.44 g/cm^2 (which stops beta-rays of energies up to 3.2 Mev) and was used to measure the gamma-rays. The other counter was used to measure the beta-rays. The counters were attached to a high speed amplifier and a thyratron scale of 4 or 8 recording mechanism. Indium foils were irradiated with neutrons from a radium beryllium source, containing 200 milligrams of radium salt. The neutron source was placed in a large paraffin cylinder, 4 cm below the top surface, and the indium samples were placed on top. In certain experiments an additional 5 cm of paraffin was placed behind the detector. The irradiation times varied from 1 to 15 minutes.

Since preliminary experiments showed that the period of the gamma-ray was about an hour, we irradiated samples of indium for periods of time ranging from 5 to 15 minutes, and started count-

[4] J. L. Lawson and J. M. Cork, Phys. Rev. **52**, 531 (1937).
[5] Mitchell (Phys. Rev. **53**, 269 (1938)) has shown that slow neutrons will produce an activity in indium with a 45-day period. This activity is due to In^{114} and does not appear in these experiments since the irradiation time is too short.
[6] E. R. Gaerttner, J. J. Turin and H. R. Crane, Phys. Rev. **49**, 793 (1936).
[7] M. V. Brown and A. C. G. Mitchell, Phys. Rev. **50**, 593 (1936).
[8] L. M. Langer and M. D. Whitaker, Phys. Rev. **51** 713 (1937).
[9] A. C. G. Mitchell and L. M. Langer, Phys. Rev. **52**, 137 (1937).

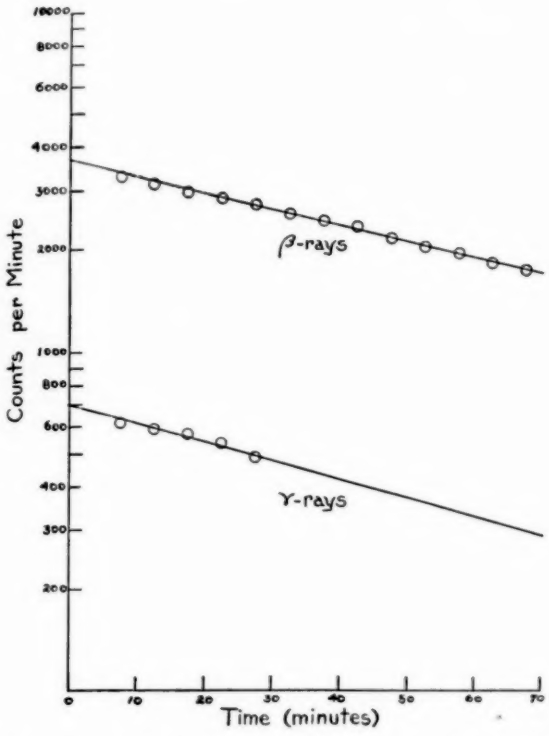

FIG. 1. Decay curves for the beta- and gamma-radiation of the 54-minute activity of indium (116).

ing 5 minutes after the end of the irradiation. With this procedure, any effect due to the 13 second period would be entirely negligible. Measurements on the beta-rays with the beta-ray counter, and on the gamma-rays with the gamma-ray counter, showed that the two periods were the same to within the experimental error, and had the value 55 ± 5 minutes. Fig. 1 shows decay curves for the beta- and gamma-rays taken with identical indium samples irradiated in the same manner. The samples were irradiated for 15 minutes. It will be seen that the initial intensity of the beta-ray count was 3700 per minute while that for the gamma-rays was 700 per minute. The ratio of the two is therefore

$$I(\gamma)/I(\beta)=700/3700=0.189.$$

This value, of course, has nothing to do with the number of gamma-ray quanta per disintegration since the gamma-ray counter was not calibrated in terms of quanta.

Experiments were now performed to see if there were any gamma-rays connected with the 13-second period. In these experiments the indium was irradiated for 1 minute on the paraffin cylinder and paraffin was placed behind the sample to increase the intensity. The sample was placed on the counter and readings were taken as soon after irradiation as possible, the first readings being taken in from 10–20 seconds after irradiation. Readings were taken every 10 seconds.

A typical set of data on the beta- and gamma-ray counters is shown in Table I. The first column shows the time after irradiation, the second the beta-ray count and the third the gamma-ray count. A scale-of-eight counter was used for recording the beta-ray count while a scale of four was used for the gamma-rays. Since the gamma-ray count was small and a scale of four counter was used the fluctuations are large. It will be seen at once from the table that the beta-ray activity decreases by a factor of ten, in the time interval under consideration, whereas the gamma-ray activity decreases but slightly. In the table the activity due to the 54-minute period has not been subtracted. Readings on the above experiments were carried on for 30 minutes after the end of the irradiation. The gamma-ray count showed a period of 54 minutes and the activity for the earlier times extrapolated from the complete decay curves, shows that the gamma-ray activity given in column 3 of the table is due to the gamma-rays of the longer period. Runs were taken with longer irradiation times to increase the accuracy, and a calculation shows that any gamma-ray activity obtained in the early part of the run can be attributed to the 54-minute activity.

EFFECT OF BORON ABSORPTION ON THE TWO ACTIVITIES

It is of interest to see whether the two isomeric periods of indium have the same resonance energy. In the case of the bromine isomers, of 18 minutes and 4 hour periods, Fleishmann[10] has shown that the resonance neutrons which excite the two isomeric periods show the same absorption coefficient in boron, from which it follows that the resonance state in which the neutron is captured by the bromine nucleus is the same for both isomeric periods. Moreover, he has

[10] R. Fleishmann, Zeits. f. Physik **107**, 205 (1937).

TABLE I. *Comparison of beta- and gamma-ray intensity for 13 second period of indium. (1 minute irradiation.)*

TIME AFTER IRRADIATION (SEC.)	BETA-RAYS (COUNTS/MIN.)	GAMMA-RAYS (COUNTS/MIN.)
0	—	—
10	—	—
20	—	—
30	5341	88
40	4381	40
50	3037	88
60	2221	88
70	1549	88
80	1021	88
90	781	40
100	637	88
110	397	40
120	493	40

shown that the ratio of the two activities is independent of whether the neutrons have been filtered through cadmium or not. In the case of indium there exists a set of measurements by Goldsmith and Rasetti[11] which appears to show that the two isomeric periods do not have the same resonance energy. In order to test this point we have measured the percentage of the resonance neutrons transmitted by boron for both periods.

To carry out these measurements the neutron source was situated in the paraffin cylinder, described above. Across the top of the paraffin was placed a cadmium sheet, 0.218 g/cm² thickness, and measurements were taken with and without a Pyrex sheet containing 0.0252 g/cm² of boron as absorber. In order to make as good measurements as possible on the 13-second period activity, arrangements were made to photograph the recording meter and the stop watch at frequent intervals during the early part of the run with a Sept camera. The procedure, therefore, was as follows: An indium detector was irradiated, with or without the Pyrex filter, for a period of either 5 or 10 minutes. It was placed on the beta-ray counter as soon after irradiation as possible and instantaneous pictures of the meter and stop watch were taken every two seconds until the count became to small in this time interval for accurate measurement. Counting was continued, by reading the meter visually, until the end of the fortieth minute. The initial activity of the 54-minute period was obtained by extrapolating back to zero time the observations taken at the later times, and the activity of the 13-second period was obtained in the same way from the data of the films, due account being taken of the activity arising from the 54-minute period during the earlier times.

The results are shown in Table II, in which the percentage of the activity due to neutrons transmitted through boron is shown in the last two columns. It will be seen that the transmission is the same, to within the limit of experimental error, for both periods.[12] It appears, therefore, that the neutron resonance energy is the same for both isomeric periods.

THE BRANCHING RATIO

We have measured the branching ratio for the process, *viz.*, the activity of the 13-second period to that of the 54-minute period, under various conditions of irradiation. This ratio is independent of the method of excitation of the sample, as is shown in Table III. Column 1 shows the method of irradiation. Thus, for example, the notation "paraffin only" indicates that the sample was placed directly on top of the paraffin cylinder containing the neutron source; Cd indicates that 0.218 g/cm² of cadmium was placed between the detector and the paraffin; and Cd+B, that 0.218 g/cm² of cadmium and 0.0252 g/cm² of boron (Pyrex plate) were interposed between source and paraffin. Column 2 shows the length of time of irradiation. In columns 3 and 4 are given the corrected initial rates of decay of the 13 second and 54 minute periods, respectively, in counts per second. These

TABLE II. *Boron absorption.*

CONDITIONS	IRRADIATION TIME (MIN.)	ACTIVITY (COUNTS PER MIN.)		PERCENT TRANSMISSION	
		13 SEC.	54 MIN.	13 SEC.	54 MIN.
0.218 g/cm² Cd	5	3850	225		
0.218 g/cm² Cd +0.0252 g/cm² B	5	2850	155	74.0	69.0
0.218 g/cm² Cd	10	4000	420		
0.218 g/cm² Cd +0.0252 g/cm² B	10	3000	312	75.0	74.5
				74.5 ±0.5	72.0 ±3.0

[11] H. H. Goldsmith and F. Rasetti, Phys. Rev. **50**, 328 (1936).

[12] Since the angular distribution of the neutrons is not particularly well known for the experimental arrangement we have used, we have not attempted to calculate the absorption coefficient or the absolute value of the resonance energy.

data were obtained in the manner usually employed in radioactive work, i.e., the initial activities were found by extrapolating the various decay curves to zero time after irradiation and then correcting these for irradiation time, so that all figures are given on the basis of infinite irradiation time for both periods. The ratio of these two results, called the branching ratio R (13 sec.)/R (54 min.), is shown in column 5 of Table III. It will be seen at once that the branching ratio is independent of the method of excitation and that it has the value 1.12 ± 0.06.

From the branching ratio one can calculate the number of radioactive atoms present in each isomeric state at zero time after infinite irradiation. Since the branching ratio has to do with the initial rate, the ratio of the number of atoms present in the two states will be given by

$$1.12=\frac{\lambda_{13}N_{13}}{\lambda_{54}N_{54}};$$

$$\frac{N_{13}}{N_{54}}=1.12\times\frac{2.14\times10^{-4}}{5.32\times10^{-2}}=0.446\times10^{-2}$$

using the values for λ_{13} and λ_{54} of 5.32×10^{-2} sec.$^{-1}$ and 2.14×10^{-4} sec.$^{-1}$, respectively.

The Energy Level Scheme

It has been suggested by Weizsäcker[13] that the nuclear isomers may be considered as metastable states in the excited parent nucleus. Transitions may occur from both excited states of the parent nucleus to various states in the product but, because of selection rules, transitions between the excited states of the parent either do not occur or the lives of these states are long compared to the lifetime for decay into the product. With this hypothesis as a basis we now have enough data to draw up a tentative energy level scheme for In^{116}.

Table III. *Determination of the branching ratio.*

Method of Excitation	Time of Irradiation (Min.)	Corrected Initial Rates R (counts/sec.)		R (13)/R (54)
		13 sec.	54 min.	
Paraffin only	5	133	135	0.99
Paraffin only	5	192	151	1.27
Paraffin only	5	166	148	1.12
Cd	5	64.1	58.3	1.10
Cd	10	66.6	58.3	1.14
Cd+B	5	47.5	40.1	1.18
Cd+B	5	50.0	48.0	1.04
Cd+B	10	50.0	43.3	1.15
			Average	1.12 ± 0.06

[13] C. F. v. Weizsäcker, Naturwiss. **24**, 813 (1936).

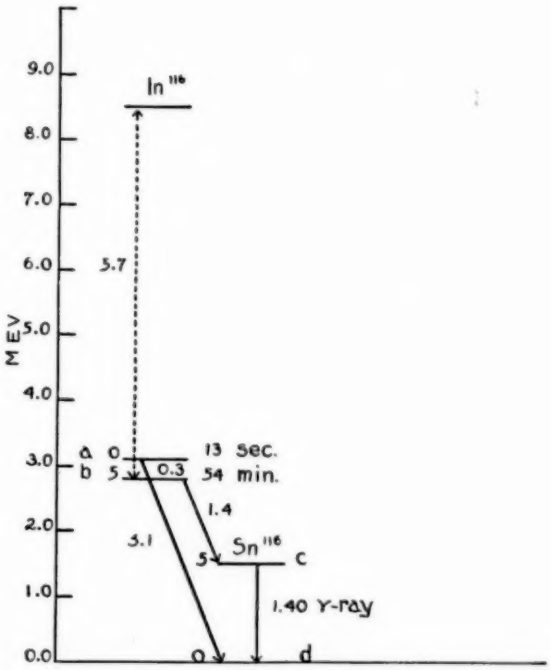

FIG. 2. Energy level system of indium (116).

Figure 2 shows the energy level scheme for the process. The states to the left of the diagram represent the parent nucleus In^{116} while those to the right represent the product Sn^{116}. Since the sum of the beta- and gamma-ray energies (2.8 Mev) connected with the 54-minute period is less than the beta-ray energy of the 13-second period, the energy level for the 54-minute period must lie lower than that of the 13-second period. Moreover, we have been unable to detect any gamma radiation of 13-second period. We have shown that the observed gamma-ray must be attributed to the 54-minute period. Furthermore, we have attributed the gamma-ray of 1.4 Mev energy to a transition in the product nucleus Sn^{116}. Although we have no proof at present that this is correct, it follows by analogy from the situation in the natural radioactive elements where it can be shown that the gamma-ray follows the disintegration and is attributed to a transition in the product.

One now has to explain why there is no observed gamma-ray transition between the levels a and b. The mean life for a gamma-ray depends on the angular momentum change for the transition and the energy of the gamma-ray according to the formula,[14] $\tau = 5\times10^{-21}(l!)^2(20/\hbar\omega)^{2l+1}$ seconds, where $\hbar\omega$ is the energy of the gamma-ray in millions of volts and l is the change in angular momentum during the process of emission. With the available energy taken as 0.3 Mev, one must choose an l which will make the mean life for the gamma-ray transition $a\rightarrow b$ long compared to the beta-ray transition $a\rightarrow d$. If one takes $l=5$ one obtains $\tau_\gamma = 139$ min. ($\lambda_\gamma = 0.83\times10^{-4}$ sec.$^{-1}$). Now, when one measures the period of the beta-rays from state a from the relation $e^{-\lambda t}$, the value of λ obtained is the sum of all the transition probabilities to all possible lower states. Hence

$$\lambda_{13} = \lambda_\gamma + \lambda_\beta = 5.32\times10^{-2} \text{ sec.}^{-1}$$

so that with the value of λ_γ given above for $l=5$, the ratio of the intensity of gamma-ray transition to the total is given by

$$\frac{I_\gamma}{I_{\text{total}}} = \frac{\lambda_\gamma}{\lambda_\gamma+\lambda_\beta} = \frac{0.0083\times10^{-2}}{5.32\times10^{-2}} = 0.0016 = 0.16 \text{ percent}$$

Thus, the gamma-ray emission would be undetectable in agreement with experiment. On the other hand, if one takes $l=4$ one obtains $\tau_\gamma = 7.57\times10^{-2}$ sec. ($\lambda_\gamma = 9.15$ sec.$^{-1}$). With this small value for τ_γ it will be seen that the total activity of the state a would decay in a time which is short compared to 13 seconds by gamma-ray emission so that no beta-ray emission with a period of 13 seconds would be observed. However, since a strong beta-ray emission of 13-second period is observed it follows that l cannot be less than 5.

The assignment of quantum numbers to the various levels cannot be made on a very sound basis. Some progress can be made, however, if one makes use of certain assumptions. In the first place the level d, ground state of Sn^{116}, probably has zero spin since the nucleus contains $4n$ particles. Furthermore, the beta-ray end points of both the 13 second and the 54 minute activities lie on the first Sargent curve for which $\Delta i = 0$. This suggests assigning the quantum number 0 to level a so that it will have the same quantum number as d. Similarly the levels b and c should have the same quantum numbers. Since the transition $a\rightarrow b$ is to be forbidden, it follows from the above calculation that the level b must be assigned the quantum number 5, and hence level c should also be given the quantum number 5. Finally, the assignment of the quantum number 5 to level c does not forbid the gamma-ray transition $c\rightarrow d$. A short calculation shows that, on account of the high energy of the gamma-ray (1.4 Mev), the mean life for the transition $c\rightarrow d$ is about 10^{-6} seconds.

Unfortunately, the energy of the gamma-radiation occuring in the process of the capture of slow neutrons by In^{115} to form In^{116} has not been measured. In this region of the periodic table the binding energy of the neutron is about 8.5 Mev, so that if the nucleus made a transition from the capture state to one of the states a or b with the emission of one quantum of radiation, one would expect a gamma-ray of 5.4 to 5.7 Mev energy. Now the branching ratio has been shown to be approximately unity, i.e. the rates at which nuclei are leaving states a and b are about the same. At equilibrium, therefore, the rates at which they are arriving in states a and b are also equal. If the states a and b are fed from the capture state by single transitions, one would expect large differences in the rates at which the states are populated on account of selection rules governing the gamma-ray transitions which depend on the quantum numbers of the state a and b as well as that of the capture state.[15] If cascade transitions occurred the effect of selection rules would be more or less obliterated so that the rates of arriving in states a and b would be approximately equal. It would be of interest, therefore, to make a measurement of the energy of the capture gamma-rays as it would elucidate the mechanism of the transitions between the capture state and the states a and b.

The authors wish to acknowledge their indebtedness to the American Philosophical Society for a grant from the Penrose Fund which made this work possible. They are also grateful to Dr. M. H. Johnson, Jr. for many helpful discussions.

[14] See H. A. Bethe, Rev. Mod. Phys. 9, 226 (1937).

[15] The quantum number of the capture state is probably 4 or 5, since In^{115} has a spin of 9/2 and the neutron is so slow that most of the capture occurs from the S wave.

A Critical Analysis of the Classical Experiments on the Relativistic Variation of Electron Mass

C. T. ZAHN AND A. H. SPEES
Department of Physics, University of Michigan, Ann Arbor, Michigan

(Received February 14, 1938)

In the course of a previous mathematical analysis of an improved method for the determination of the ratio e/m it was suggested that the generally accepted interpretations of the classical experiments of Bucherer and of Neumann might be subject to serious limitations. A similar analysis for the unmodified Bucherer-Neumann experiment is therefore carried out in the present paper. By this means it is discovered that Neumann's supposed velocity filter, even for the case of negligible scattering of electrons along the condenser plates, must have been completely broken down on the high velocity side, for values of $\beta>0.7$; and that, even for the lower velocities observed, the resolution width was approximately *as great as that equivalent to the whole relativistic mass effect*. Besides, it is found from this analysis that, with a certain choice of geometrical constants, a very poor resolving power may be concealed by spurious focusing effects—and that it was just this choice that Neumann, by trial, found it necessary to make in order to obtain sharp lines. It is also seen that, when the filter is open on the high velocity side, one may still obtain an apparent line, which may be considerably shifted from the position predicted by the simple theory, and which in extreme cases may form the edge of a heavily fogged region extending inward to the central zero line corresponding to $\beta=1$. This fogging can actually be seen very clearly in Neumann's photographs for $\beta=0.8$. Further, a consideration of the possible effect of scattering on such experiments shows that, when the resolving power is very near the critical limit at which the filter breaks down, the probability of leakage of high velocity scattered electrons through the filter becomes relatively large, especially when the spectrum of the source is distributed largely amongst velocities above that to be observed. Under these latter circumstances it is suggested that one might obtain seriously shifted lines, and even mistake for the expected line a spurious maximum due to the source distribution itself. Since the interpretations of Bucherer and of Neumann are based on such doubtful premises, a short discussion is given of other similar experiments designed to distinguish between the Abraham and the Lorentz electrons. So far as is known to the authors, it appears that, at least for the higher velocities, no very satisfactory experimental distinction between the two types of electron has as yet been made by direct electric and magnetic deflection methods. In view of the fundamental importance of such experiments it seems that much is left to be desired.

IN a recent article[1] the authors described a method for the determination of the ratio e/m for beta-particles. This method was developed for the purpose of determining the specific charge of *primary* beta-particles, as distinguished from the secondaries; and it consists essentially in a modification of the Bucherer-Neumann experiment in which the positions of the source and the detector are effectively interchanged and as detector a Geiger counter is used in a fixed position. Preliminary measurements showed a main central peak and two side peaks, the origin of which was not quite clear, since they could have been due either to the characteristics of the ideal instrument, or to scattering, or to a bona fide mass effect. On examining the literature it was found that only an incomplete discussion was given of the resolution limitations of the classical experiments of Bucherer and of Neumann. Bestelmeyer had at the time raised objections along these lines by questioning whether or not the finite resolving power of the apparatus might cause shifts in the density maximum of the observed photographic line. In partial answer to this objection Bucherer made only a very special resolution calculation for the case $\beta=0.3$; but, surprisingly, does not seem to have made similar tests for the cases of the higher velocities—although he found it impossible to obtain sharp lines for $\beta>0.8$. In fact, the general behavior of a condenser in crossed fields seems not to have been clearly understood at the time.

Since a more complete understanding of the behavior of the condenser in such experiments was necessary for a careful interpretation of the results obtained by the above-mentioned modified method, it was decided to make a mathematical analysis of the instrumental behavior. Although the system of rays involved in experiments of this type is rather complicated, it was found not too difficult to determine the resolution characteristics for a particular observation. In

[1] C. T. Zahn and A. H. Spees, Phys. Rev. **52**, 524 (1937). See also: C. T. Zahn and A. H. Spees, Phys. Rev. **53**, 357 (1938).

this way a clear idea of the resolution limitations of the experiment was obtained; and it appeared that the modified method had, in this regard, very decided advantages over the original method. Closely connected with the effective resolving properties of the condenser is the possible presence of radiation scattered from the condenser plates, since the resolving power for the scattered radiation decreases very rapidly as the point of scattering approaches the condenser exit. Another advantage consisted in the fact that the scattering was largely eliminated. (For a more complete discussion of this point see the above-mentioned article.[1])

In studying the system of rays involved in the modified method certain general relations were obtained for the behavior of electrons in the crossed fields between the plates of a shallow condenser. Since the latter problem was found not too difficult, it was decided to apply the same general method of analysis to the case of the Bucherer-Neumann experiment. This seemed to be particularly desirable, since from time to time questions have been raised in the literature as regards the interpretation of Neumann's results, especially at the higher velocities where the results should be more significant.

First, as has been mentioned, Bestelmeyer raised the question of the finite resolving power of the instrument. This question still does not seem to have been answered satisfactorily, although it is not so very difficult a matter to obtain a considerable amount of information in this connection. One would perhaps not expect very serious difficulties so long as one worked at velocities well below the limit at which resolution becomes impossible; but it should be remembered that the classical experiments were extended up to this limit. Besides, an examination of Neumann's original paper[2] shows that there were certain peculiar practical limitations on the ratio of the lengths of the electron path inside and outside of the condenser, which limitations were mentioned by Neumann, but left unexplained. Also the effect of scattering may be of great importance because of its effect on the resolving power. To take it into account quantitatively would be a very complicated problem in the case of the Bucherer experiment, but it should be of considerable value at least to determine the limitations of the apparatus for the idealized experiment where no scattering appears, and thereby to obtain a lower limit for the effect of the finite resolving power.

A further question which might be raised is the following. For a given experiment, with given values of β and a given relationship between mass and velocity, it is always possible to calculate the over-all spread in the momentum beam transmitted by the condenser. If this spread is of the order of magnitude of, or greater than the width of discrete peaks in the momentum distribution of the source, one must consider the possibility of false or shifted peaks due to the source itself. Except for the one particular case, $\beta=0.3$, no test along these lines seems to have been applied to the classical data.

It is not desired here to imply doubts as to the validity of the theory of relativity in this connection; but rather to point out that there are still certain rather serious difficulties, in the correct interpretation of Neumann's data, which make it impossible to state within what limits of error and over what region of velocities the theory of relativity has actually been verified experimentally by Neumann. Until a complete understanding of the resolution limitations is had and the effect of possible scattering is taken into account, such a statement will not be possible. In an experiment of such fundamental importance it seems especially desirable to have definite information as to the exact range of energies over which the theory of relativity has actually been verified. It is therefore the purpose of the present discussion to answer as many as possible of the above questions.

Theory of the Bucherer Experiment

In the development of the theory for the modified experiment[1] there were obtained certain general relations, which apply to the motion of the unscattered beam of electrons transmitted by a shallow condenser in crossed fields:

$$k_i=k(1-v_0/v), \tag{1}$$

where k_i is the curvature of the trajectory inside the condenser; k, that in the magnetic field alone; v, the velocity of the electron; v_0, the value of v

[2] G. Neumann, Ann. d. Physik **45**, 529 (1914).

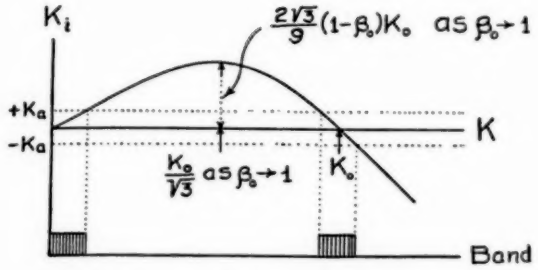

FIG. 1. Conditions for potential transmission of Lorentz electrons.

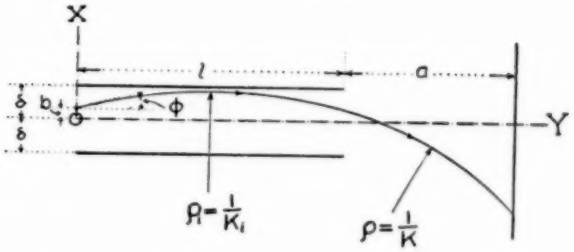

FIG. 2. Initial conditions imposed by the position of the source.

for which the electric and magnetic forces would be compensated and k_0 the curvature of an electron having a velocity v_0 in the magnetic field alone. When the relation between the mass and the velocity is given, it is possible to obtain an expression in terms of curvatures alone, which expression, for the case of Lorentz electrons, is:

$$k_i=k[1-((A^2+k^2)/(A^2+k_0^2))^{\frac{1}{2}}], \qquad (2)$$

where $A=eH/m_0c$. For the case of nonrelativity electrons this would have been:

$$k_i=k(1-k/k_0). \qquad (3)$$

It has been pointed out that for small spreads the resolution characteristics depend on $(\partial k_i/\partial k)_{k_0}$, and therefore on the particular relationship between k_i and k. One will therefore assume here that the theory of relativity is valid, and hence obtain the resolution limitations which would exist if the theory were true. The relativity relationship (2) is represented graphically in Fig. 1, where $k_a=16\delta/l^2$ is the maximum curvature of circles passing freely between the plates of the shallow condenser. The value k_a represents a geometrical limitation, and the band of velocities shown in the figure represents the only velocities which could be freely transmitted under any, circumstances. Transmission will, however, be further contingent on the proper initial conditions of the trajectories. As was pointed out in the previous article,[1] when either k_a becomes too large, or k_0 too small (i.e., v_0 too large) one reaches a condition where the two bands spread out to meet each other and cover the whole region of velocities greater than v_0, as well as a small range of velocities slightly less than v_0. This indicated very serious limitations on the Bucherer experiment for the higher velocities.

In Fig. 2 is shown a diagram representing the conditions of Neumann's experiment. The source may be imagined to be distributed over the plane $y=0$ at the left end of the condenser at values $x=b$ and with $|b|<\delta$. For each value of the source position b the condenser will behave slightly differently. The initial conditions for a "ray" are specified by the two geometrical variables b and ϕ, and the two variables k_i and k, which latter two give the curvatures of the trajectory inside and outside the condenser, respectively. In terms of these variables the equation of the trajectory may be written as follows, for small values of x. (For the purpose of resolution calculations it should suffice to make this approximation for the region outside as well as that inside the condenser.)

$$x=b+\phi y-y^2k_i/2 \qquad \text{for } 0\lesseqgtr y\lesseqgtr l, \qquad (4)$$

$$x=b+\phi(a+l)-l(l+2a)k_i/2-a^2k/2 \qquad \text{for } y=a>l. \qquad (5)$$

Cut-off conditions: In the previous article the general conditions for cut-off were expressed in terms of the three variables b, ϕ, and k_i. It was found that all rays *not* falling in the category defined by the following inequalities would be transmitted freely:

(I) $$+\delta\lesseqgtr b\lesseqgtr -\delta,$$

(II) $$+\delta\lesseqgtr b+\phi l-l^2k_i/2\lesseqgtr -\delta,$$

(III) Simultaneously:

$$0\lesseqgtr \phi/k_i\lesseqgtr l,$$
$$+\delta\lesseqgtr b+\phi^2/2k_i\lesseqgtr -\delta.$$

Condition (I), in the case of the Bucherer experiment, requires simply that the source lie between the condenser plates. One may then consider the effect of the conditions (II) and (III) for various

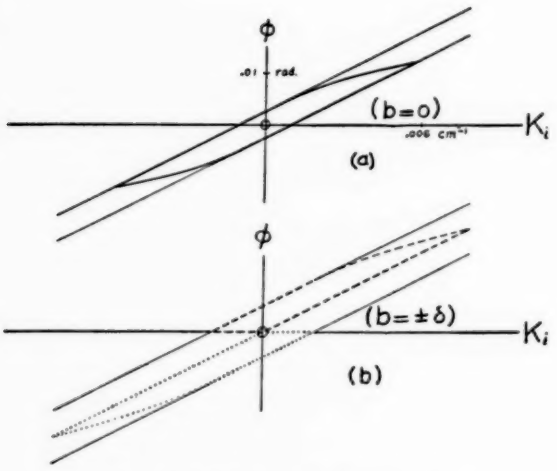

FIG. 3. Restricted areas in the ϕ, k_i plane.

values of b between $+\delta$ and $-\delta$. With a fixed value of b these conditions involve only the two variables ϕ and k_i; and restrict the transmitted rays to a certain area, in the ϕ, k_i plane, bounded by two parallel straight lines (end cut-off) and by two simple parabolae, each of which is tangent to one of the lines. In Fig 3a is shown the restricted area for the case of a source in the central plane $b=0$; and in Fig. 3b, the cases $b=+\delta$ (dotted lines) and $b=-\delta$ (broken lines). It may be noted in general that changing the sign of b corresponds to reflection of the restricted area through the origin.

For any given value of k_i the permissible spread in ϕ is given by the vertical section of the restricted area at a distance k_i from the origin; and, if the source is isotropic, this length represents the distribution function of the transmitted radiation in terms of k_i, to within a constant factor. (This, of course, will be true exactly, only if the spread is so narrow that the variations of the source distribution function are negligible.) It will also be obvious from the above-mentioned property of symmetry, that the integrated distribution function for the transmitted radiation from a source extending uniformly from $+\delta$ to $-\delta$ will be symmetrical around $k_i=0$. It may be noted further that as b changes from $b=0$ to $b=\pm\delta$ the maximum permissible values of $\pm\phi$ and $\pm k_i$ increase only by ratios $\pm 8/4.82$ and $\pm 16/11.65$, respectively. It is also rather easily seen that the effect of distributing the source over the distance 2δ is to give a beam in k_i somewhat sharper at the center, even if somewhat wider at the extreme ends. Hence the curve for $b=0$ may be regarded as giving a good qualitative picture of the resolution limitations.

The latter analysis determines the bundle of rays transmitted by the condenser, as a function of k_i. In order to obtain the spread in x, the measured deflection on the photographic plate, it is necessary to consider the equation of the trajectory *after the electron leaves the condenser*:

$$x=b+\phi(a+l)-l(l+2a)k_i/2-a^2k/2.$$

Now if the spread in k_i is small compared to k_0 one can set:

$$k_i=B(k-k_0), \quad \text{where} \quad B=(\partial k_i/\partial k)_{k_0}=-(1-\beta_0^2)$$

for Lorentz electrons. Then one can write:

$$x=-a^2k_0/2+b+\phi(a+l)-[l(l+2a)+a^2/B]k_i/2.$$

For the central compensated ray $b=\phi=k_i=0$, and $x=-a^2k_0/2\equiv x_0$; and setting $x-x_0\equiv\Delta x$, one may write:

$$\Delta x=b+\phi(a+l)-[l(l+2a)+a^2/B]k_i/2,$$

where Δx represents the departure from the ideal central line.

An examination of the latter equation shows that, if the constants of the apparatus be so chosen that for a given value of β_0 the coefficient of k_i vanish, then there will be energy focusing of the rays, and the line width will be due entirely to the spreads in ϕ and b. The condition for such energy focusing may be written:

$$l(l+2a)=a^2/(1-\beta_0^2)$$

or

$$l/a=((2-\beta_0^2)/(1-\beta_0^2))^{\frac{1}{2}}-1.$$

In Table I are shown the appropriate values of l/a for different values of β_0, under the condition for energy focusing.

Under the condition for energy focusing the maximum spreads in ϕ, corresponding to

TABLE I.

β_0	l/a
0.0	0.41
0.5	0.53
0.7	0.72
0.8	0.94
0.9	1.50
0.95	2.36

$b=\pm\delta$, are easily seen to be $\pm 8\delta/l$, and the corresponding limits in x are given by:

$$\Delta x=\pm(8a+7l)\delta/l. \tag{6}$$

Furthermore it is obvious from Fig. 3b that the distribution in Δx is symmetrical around $x=x_0$ and that this may be true even if the line is rather wide, unless so wide that $B=\partial k_i/\partial k$ is no longer practically constant over the whole width. Therefore, in order to insure that the line is symmetrical, it would be necessary to determine the limits in k_i involved, and to test for uniformity of B over the allowed interval.

The latter condition for the energy focus permits a rather wide spread in x; but if one notes that the integrated spread in ϕ, as a function of k_i, is symmetrical around the line $\phi=lk_i/2$ and for a given value of b. ϕ lies between the lines $\phi=lk_i/2\pm\delta/l-b/l$, one sees that one can overfocus the energies in such a way as largely to compensate for the variations in x due to the spread in ϕ, and thus obtain a best quasi-focus. This may be seen by writing the latter limiting values of ϕ into the equation for Δx. Then the limits of Δx are:

$$\Delta x=-(a/l)b\pm(a+l)\delta/l-a(l+a/B)k_i/2,$$

which shows that, if one chooses the ratio l/a in such a way that $(l+aB)=0$, or $l/a=1/(1-\beta_0^2)$, one obtains the best quasi-focus with: $\Delta x=-(a/l)b\pm(a+l)\delta/l$; or if one writes in the limiting cases $b=\pm\delta$, then:

$$\Delta x=\pm(1+2a/l)\delta. \tag{7}$$

One sees from the expressions (6) and (7) that for values of l of the same order as a, the spread Δx for the energy type of focusing is about five times as large as that associated with the best quasi-focus. In Table II are shown the values of the ratio l/a for the various values of β_0 under the conditions for the best quasi-focus.

It is noteworthy that for the energy focus one must have $l<a$ for values of $\beta_0\lesssim 0.8$, whereas for the quasi-focus one must have $l>a$, always. Before considering the actual numerical values involved in Neumann's experiments, it is of interest to recall certain statements made by Neumann as regards the particular practical conditions he found necessary in order to obtain sharp lines. He mentioned that the determination of deflections was extremely difficult; and that so long as he confined himself to small velocities ($\beta_0=0.4\rightarrow 0.6$), and small distances a (4 cm), he obtained very fine sharp lines; and that for $\beta_0=0.6$ the lines were already indistinct for $a=5$ cm, and for still greater velocities they were very broad even with $a=4$ cm. No attempt was made at an explanation of these rather peculiar facts, but they are easily seen to be in harmony with the predictions of the foregoing analysis, if one remembers that for Neumann's condenser $l=5$ cm. The condition for the quasi-focus requires that $a<l$, and this is just the condition, roughly expressed, that Neumann found necessary for sharp lines. Now Neumann's plate separation $2\delta=0.25$ mm and his deflections were $5\rightarrow 10$ mm. From (7) one calculates that the *total* width of the quasi-focus should be about 0.7 mm, approximately; but since the line may be sharpened at the center because of the vertical extension of the source, it may appear somewhat narrower than this value. If, on the other hand, the condition for energy focusing had held, the line width should have been about five times this latter value, or about 3.7 mm, which would have been very wide, indeed, in consideration of the fact that the total

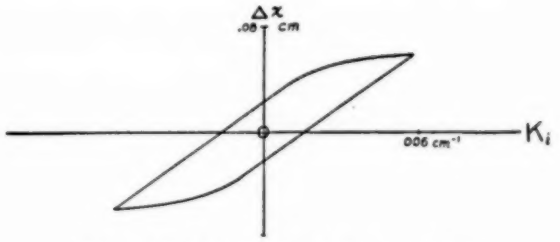

FIG. 4. Limiting values of the spread Δx.

TABLE II.

β_0	l/a
0.0	1.00
0.5	1.33
0.7	1.96
0.8	2.78
0.9	5.26

TABLE III. *Selected cases from Neumann's data.*

No.	H (GAUSS)	V (VOLTS)	β_0	DEFL. (CM)	a (CM)	ρ_0 (CM)
40	106.8	407.9	0.507	0.9714	4.1905	9.05
39	128.2	580.8	0.602	0.8961	4.1905	9.78
54	128.2	693.2	0.718	0.6427	4.2013	13.65
37	128.2	772.8	0.801	0.5004	4.1905	17.55

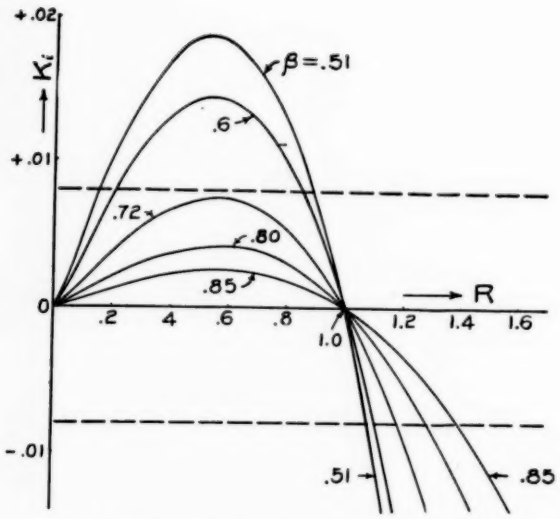

FIG. 5. Resolution conditions for Neumann's typical cases.

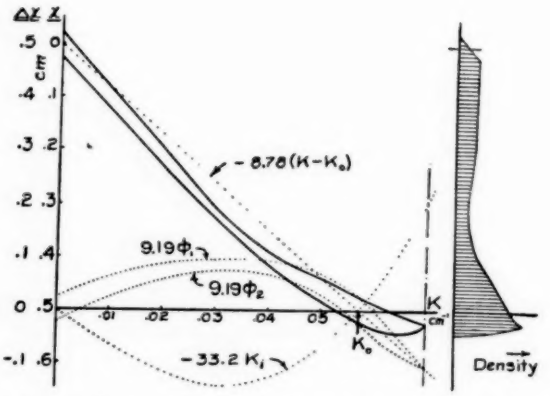

FIG. 6. Photographic density to be expected for Neumann's case $\beta=0.8$, if the source distribution function were uniform in terms of k, and if there were no scattering.

deflection was only 5→10 mm. It is therefore obvious that Neumann was by trial finding approximately the condition for the best quasi-focus, without knowing how poor the velocity resolution of his condenser really was.

NEUMANN'S DATA

In Table III are given some typical cases taken from Neumann's table. On the basis of these data and the foregoing analysis one can calculate the expected spreads in the various quantities involved. The general equation for the spread in x, not assuming any particular type of focus, is:

$$\Delta x = b + \phi(a+l) - [l(l+2a) - a^2/(1-\beta_0^2)]k_i/2 \quad (8)$$

and for Neumann's case No. 37, $\beta_0=0.801$ one can calculate the spreads for $b=0$, and also the restricted area, as shown in Fig. 3a. From these one can further calculate the limiting values of Δx corresponding to the contour of the restricted area and then plot against k_i, as shown in Fig. 4. In this way one finds a *total* expected line width of about 1.2 mm, which is about 25 percent of the total deflection 5 mm. This great line width need not of itself cause any serious difficulty, since it has been shown that the line should be symmetrical, provided that the derivative $\partial k_i/\partial k$ be practically constant over the allowed interval, and also that the k distribution function for the source be practically constant over the same interval. Therefore, it remains only to ascertain whether the actual spread in k is sufficiently small to justify the assumption of the latter conditions. It is of importance to recognize the fact that the focussing properties of the apparatus may conceal a condition where the spread in k could be very large, indeed.

In order to test for the width of the interval in k one can obtain a rough idea, at least, of the order of magnitude of the spread by assuming, as in the latter analysis, that the spread is actually small; that is, $\Delta k=\Delta k_i/B=\pm k_a/(1-\beta_0^2)$. In this way one obtains for the total spread in k a value which is actually as much as 78 percent of k_0 for Neumann's case $\beta_0=0.8$. It is therefore immediately obvious that the assumption of small spreads in this case cannot be valid, and that the observed line cannot be symmetrical. In fact, the spread in k is so large as to suggest that the velocity filter may have "broken down" completely on the side of the higher velocities. In any case, it will *not* be sufficient to calculate Δx from the equation (8). One must rather return to the original equation in which k_i and k both appear, and use the actual relation (2) between these two curvatures. This gives:

$$\Delta x = b + \phi(a+l) - l(l+2a)k_i/2 - a^2(k-k_0)/2. \quad (9)$$

In order to obtain an accurate idea of the way in which the ideal velocity filter should behave for Neumann's cases one can draw the actual graphs representing the relation (2) in k_i and k; or one can transform the relation to a more convenient form as follows. If, instead of k, one

introduces the dimensionless variable $k/k_0 \equiv R$, and if one notes that in general $k = A(1-\beta^2)^{\frac{1}{2}}/\beta$, or more specifically $k_0 = A(1-\beta_0^2)^{\frac{1}{2}}/\beta_0$, then one can write (2) as:

$$k_i = k_0 R[1 - \{1 + (R^2-1)(1-\beta_0^2)\}^{\frac{1}{2}}], \quad (10)$$

which enables one to determine k_i as a function of R for different particular experimental conditions specified by given values of $k_0 \equiv 1/\rho_0$ and β_0. With this method of representation the compensated condition is represented by $R=1$ for all values of k_0 and β_0, and the percentage spreads can be read directly from the graphs. In Fig. 5 are shown the graphs of (10) for Neumann's four typical cases (Table III) and also for the case later discussed by Schaeffer ($\beta_0 = 0.85$; $\rho_0 = 21.45$ cm; plate No. 50). The horizontal lines $k_i = \pm k_a = \pm 16\delta/l^2 = \pm 0.008$ correspond to the maximum and the minimum curvatures allowed by Neumann's condenser.

These curves show very definitely that the velocity filter behaves so poorly for $\beta_0 > 0.7$ that *some* radiation of all velocities $\beta > \beta_0$ may be transmitted. One may then ask why it was possible at all for Neumann to obtain apparent lines for the higher velocities β_0. By means of the relation (10), shown graphically in Fig. 5 for $\beta_0 = 0.8$, together with the cut-off conditions shown in Fig. 3a for the same case and for $b=0$, one can by using Eq. (9) calculate the allowed values of Δx for all values of k. The results of such a calculation, for the case of a line source in the central plane of the condenser, are shown in Fig. 6. From (9) it is easily seen that over a wide range in k the value of x is determined chiefly by the last term which represents the effect of the magnetic field after the electron has left the condenser space; since the first three terms are always restricted to small values, while k can vary from zero to a value somewhat greater than k_0. Hence one sees that the deflections $(-x)$, to be expected, will range all the way from a small negative value (due to the spread in ϕ) to a value somewhat greater than $(-x_0)$. In Fig. 6 are also shown, for the same case ($\beta_0 = 0.8$; $b=0$), the various individual contributions to Δx of the several terms of (9), all plotted against k, and drawn with dotted lines. For the term in ϕ there are two curves corresponding to the two limiting values ϕ_1 and ϕ_2 for a given value of k. Finally the limiting values of x, or of Δx are shown by the solid curve. The horizontal section of the area enclosed by the solid curve represents approximately the line density to be expected on the photographic plate for a source of uniform distribution in k. (For an actual source one must therefore multiply by the actual distribution function in terms of k.) These values are plotted on the right of the figure as a function of x. This density curve shows that even with the filter broken down there is a small tendency to transmit more radiation in the vicinity of $k = k_0$, and hence there may be an apparent line superimposed on the general fogging. One would expect the maximum density to occur at a value of x about 5 percent greater than x_0 when shifts or spurious peaks due to the variation in the k distribution, are neglected. The error introduced, *in this particular case*, by assuming that this point of maximum density corresponds to $x = x_0$ would be of such a nature as to make the mass appear less than the true value by about 5 percent. It is interesting to note that Neumann's value of e/m_0 for this case indicates a deviation from his other values by about 2.5 percent in the same direction. However, it should be remembered that the latter analysis was carried out for the case $b=0$, and that the variation of the source distribution density in k was neglected; and hence the results give only an approximate idea of the magnitude of the various spreads. In order to calculate the actual expected shift one would have to take into account the vertical extension of the source between the condenser plates. In principle this would be possible, even if somewhat laborious; but, as stated, the possibly important effect of the source distribution has also been neglected in the latter analysis. Since the velocity filter is "open" for $\beta_0 = 0.8$ over a wide range in k, as indicated by Fig. 6, one must then take the momentum distribution of the source into account. Actually, if the source has sharp maxima, one may expect the instrument under these conditions to behave rather as a momentum spectrograph; and consequently spurious, or seriously shifted maxima may appear on the photographic plate. Neumann stated that his source had a maximum at $\beta = 0.83$, which would definitely tend to produce a spurious maximum or a shifted maximum in the region of β_0. With this state of affairs it may easily be

understood how by chance considerable errors could compensate each other. For the case $\beta_0=0.85$, later discussed by Schaeffer, the maximum of the source at $\beta=0.83$ and that due to the velocity filter would by chance lie very close to each other, and one would again have a similar condition. It might then seem that Neumann was able to obtain lines at the higher velocities, at least partially because of the chance condition that in his experiments β_0 was near the value where his source distribution function had a maximum value.

As regards further qualitative predictions of the present analysis, the density curve of Fig. 6 indicates that the photographic plate should be considerably fogged between the zero line and the apparent line, and that the blackening should fall off rather suddenly at the outer edge of the line, with no fogging beyond it. On examining Neumann's photographs for $\beta_0=0.8$ one sees that this is actually the case, since the background inside the line is definitely darker than that outside. In the other photographs, for $\beta_0=0.7$, for example, this fogging is not pronounced. One might have expected fogging for this latter case also; but it should be remembered that the actual intensity must be obtained by a consideration of graphs of the type shown in Fig. 6 and of the source distribution function, and that the expected fogging for this case might be considerably less than that for the former case $\beta_0=0.8$. It may, however, be noted that Neumann, in his original paper, stated that small departures from the relativity theory were obtained for values $\beta_0>0.7$, which is just the value at which the present theory predicts complete breakdown of the velocity filter on the side of the higher velocities.

The above analysis was not intended to give an accurate correction for Neumann's data; but rather to indicate the general behavior of the condenser when it no longer selects a narrow band around k_0. While the actual density maximum of the apparent line is shifted by an amount of the order of only 5 percent, it is important to note that the various individual contributions to the spread Δx, as represented by the dotted curves of Fig. 6, are much greater, and because of the focusing tendency partially compensate each other to produce the resulting 5 percent. Without a detailed analysis for each individual case it would be impossible to state how large the errors might be, in general. These calculations then show how very important and necessary such an analysis really is, and how fallacious it may be to assume that the mere existence of fairly sharp photographic lines is a good criterion for the proper functioning of the velocity filter. This difficulty appears much more serious, when one remembers that the original object of the Bucherer-Neumann experiments was to distinguish between the two cases of the rigid Abraham electron and the contracting Lorentz electron, which two cases themselves differ by only a small amount.

One may now consider the spreads for the other cases of Neumann's data. As regards the spread Δk around k_0, if it is small, it should suffice to calculate it from the differential relation $(\partial k_i/\partial k)_{k_0}=-(1-\beta_0^2)$, taking the limiting values of k_i equal to $\pm k_a=\pm 16\delta/l^2=\pm 0.008$. In this way one obtains for the total fractional spread: $\Delta k/k_0=2k_a/(1-\beta_0^2)k_0=0.016/k_0(1-\beta_0^2)$ for Neumann's condenser. If the spread is large it must be obtained from the relation (2), or from the graphs of Fig. 6. The values of the *total* spread $\Delta k/k_0$ obtained in the above two ways are shown in Table IV. In the fourth column are given the approximate values of the percentage spread obtained from the derivative of relation (2) around k_0; and in the fifth column, the accurate values taken from the graphs of Eq. (10), including the individual spreads on the positive and negative sides of k_0. (The difference between the latter two individual values is an indication of the amount of dissymmetry, and 100 percent on the left hand side indicates complete breakdown on the high velocity side of k_0). One sees here that for the last three cases the filter has broken

TABLE IV. *Total spread $\Delta k/k_0$ from typical cases of Neumann's data.*

No.	β_0	$\rho_0=1/k_0$	Total Spread $\Delta k/k_0$		$(m-m_0)/m_0$
			Approx.	Equation (10)	
40	0.507	9.05	20%	11+ 9=20%	16%
39	0.602	9.78	24	15+11=26	25
54	0.718	13.65	45	100+18=118	44
37	0.801	17.55	78	100+29=129	67
50	0.85	21.45	124	100+39=139	90

down on the high velocity side; and that even for the smallest velocity, $\beta_0=0.5$, the spread is by no means small, in fact, as much as 20 percent. In consideration of the complexity of Neumann's source one might have expected, in this interval of 20 percent, to observe resolved peaks due to the source distribution, unless they were smoothed out either by the vertical extension of the source, by scattering, absorption, and deceleration at the condenser plates, or in the source itself, or by the spreads in the angle ϕ—in which case one would possibly expect just one wide peak. In the last column of Table IV is given the percentage excess of the relativistic mass over the rest mass m_0; that is, the whole percentage effect of the relativistic variation of mass. This reveals the astonishing and disturbing fact that the actual spreads in the beam transmitted by the condenser, even under the best conditions, were of approximately the same value as the momentum variation caused by the whole relativistic change of mass. It need not be emphasized, under these circumstances, that a special detailed analysis of the structure of the observed lines is necessary before attempting to interpret such data. An analysis of this sort is possible along the lines followed in the above discussion, for the case of negligible scattering; but it seems quite possible that scattering actually played a considerable, if not a predominant role in Neumann's experiments. Now, from the foregoing treatment it was seen, that, even apart from the consideration of scattering, the usual interpretations are subject to serious criticism. It may well be that the shifts mentioned above always compensate each other approximately, but it definitely requires proof; and such a proof seems difficult even for the case of the direct beam, not to mention the effect of scattering.

It may be recalled again that the experiments of Bucherer and of Neumann were designed to make a quantitative measurement of the relativistic variation of the electron mass with velocity and thereby to distinguish between the Abraham and the Lorentz electrons. If one examines Neumann's table (reference 2, p. 571) one finds that the values of e/m_0 calculated on the Lorentz theory are practically constant, as required by the theory, while those calculated on the Abraham theory vary by about 10 percent amongst themselves. Hence the validity of Neumann's interpretations rested on the accurate measurement of a 10 percent effect. Now if one considers the very large spreads actually present, the fact that they may be concealed by focusing effects, and the further serious consequence of possible scattering, it is not in any sense inconceivable, even if possibly improbable, that the corresponding uncertainties could have produced errors of as much as 10 percent and in such a way as to have masked a real variation of the Lorentz values and at the same time to have produced an apparent variation in possibly truly constant Abraham values.

On the basis of the foregoing discussion it seems fair to say that the Bucherer-Neumann experiments actually proved very little, if anything more than the Kauffmann experiments, which indicated a large qualitative increase of mass with velocity. One might say that their experiments gave a slight suggestion in favor of the relativity electron, but that the uncertainties of interpretation are so great as to give one very little feeling of certainty as regards a 10 percent effect. Indeed, it seems remarkable that they were able to obtain lines at all for the higher velocities in consideration of the exceedingly poor performance of their velocity filters. What seems very surprising is the fact that Bestelmeyer actually raised objections along the lines of the present treatment, but still it was not discovered how very poor the resolution of the velocity filter really was.

Although by tedious calculations it would in principle be possible to carry out a more thorough analysis of the system of rays for the direct radiation, the uncertainty of scattering makes it seem almost hopeless to arrive at any reliable conclusions on the basis of Neumann's data. Since Neumann's difficulties seemed to set in at just the velocity expected on the present theory *for the unscattered radiation*, it might seem that scattering was of no importance. On the other hand there are so many possibilities of spurious lines and shifts, and hence of compensating errors, that it would be dangerous to draw such a conclusion. In fact, it would seem to be extremely hazardous in general to draw conclusions from experiments on Bucherer's type of apparatus without a complete knowledge of the resolution

characteristics and of the scattering. For example, it seems possible that the scattering might be negligible for experiments at a value of β_0 in the upper part of the source spectrum; but for experiments at a value of β_0 in the lower part of the spectrum, the scattering might become the predominant factor, since as scattering occurs the electrons are progressively decelerated and there may be a very much greater chance of electrons finally reaching the allowed interval around β_0. It even seems possible that one could make experiments at a low velocity, with a spectrum largely composed of higher velocities—and, because of the relatively low distribution density for the low velocity, miss the expected line altogether—and at the same time, because of an open filter for the scattered radiation, obtain, instead, a rough momentum spectrogram somewhat like that of the source itself, and hence a spurious maximum. This seems all the more possible when one remembers that the density curve of Fig. 6, for example, must be multiplied by the distribution function in terms of k, and that the latter is obtained from the ordinary $H\rho$ distribution function by multiplying by ρ^2, which accentuates the higher energies and suppresses the lower energies by considerable factors.

If one should mistake this general maximum of the scattered spectrum for the theoretical line, one would come to the conclusion that the electrons were heavier than normal. On the authority of the long accepted results of Bucherer and Neumann, and without a knowledge of the critical conditions of the Bucherer experiment, it is easy to understand how one might unwittingly come to such a conclusion. In the previously mentioned investigation of continuous beta-rays a first attempt was made with the Bucherer method, and with a source of artificially radioactive phosphorus obtained by bombardment in the Michigan cyclotron. Fortunately, however, the intensity of the source was not sufficient to give visible blackening in a reasonably short time; and, as a result, an improved method was developed for the determination of the ratio e/m. Amongst other advantages of this method, the uncertainties of scattering were largely eliminated. This modified method also offers a means of measuring e/m more accurately than was possible by the original method; and it promises the possibility of extending the experimental study to velocities considerably greater than those previously reached in experiments of this general type.

Since the Bucherer-Neumann interpretations are based on such doubtful premises, a search was made in the literature for other experiments of the same general kind and for discussions of such experiments. In 1924 Doi[3] presented an analysis in which he claimed that the Bucherer experiments gave more support to a mass formula of his own than to that of Lorentz. Doi's basis of contention was that his own formula led to the correct curvatures for the Bucherer deflection traces, whereas the Lorentz formula did not. He also pointed out that the photographic traces were longer than expected from the theory. In a subsequent paper Schott[4] gave a criticism of Doi's analysis, directed chiefly at the latter's failure to consider the non-compensated rays, which falsify the traces near the ends.

Also Lewis[5] gave an analysis showing that the extension and fogging of the ends of the traces was due to the noncompensated rays. His calculations, in which scattering was neglected, gave the intensity distribution to be expected on the photographic plate, and he concluded that the Bucherer traces were in satisfactory agreement with his theory. It thus appears that none of the above-mentioned authors carried out calculations which revealed the resolution limitations of the method.

As regards experimental investigations, beside those of Bucherer and of Neumann, several others are to be found in the literature. Hupka,[6] working with high velocity cathode rays of velocities up to $\beta = 0.5$, obtained relative values of the electron mass at different velocities in order to decide between the formulae of Lorentz and of Abraham. His experimental method required a precise determination of accelerating potentials; and Heil[7] calculated that in Hupka's experiment a $\frac{1}{4}$ to $\frac{1}{2}$ percent error in the potential would have allowed a decision in favor of the Abraham theory, whereas Hupka claimed an accuracy of

[3] U. Doi, Phil. Mag. **49**, 434 (1925).
[4] G. A. Schott, Phil. Mag. **50**, 389 (1925).
[5] T. Lewis, Proc. Roy. Soc. **A107**, 544 (1925).
[6] E. Hupka, Ann. d. Physik **31**, 176 (1910).
[7] W. Heil, Ann. d. Physik **31**, 519 (1910) and **33**, 403 (1910).

only about ¼ percent. Hence these measurements do not provide the basis for a definite conclusion

Guye, Ratnowski and Lavanchy,[8] working with cathode rays of velocities $\beta=0.2$ to $\beta=0.5$, also used a comparison method; and they stated that their results spoke in favor of the Lorentz theory.

At higher velocities, Tricker[9] made observations on several *discrete* beta-ray lines from Ra B and Ra C, with velocities ranging from $\beta=0.363$ to $\beta=0.794$. Some of the above-mentioned uncertainties of the Bucherer type of experiment seem to have been recognized by Tricker, but he did not investigate them quantitatively as has been done in the present treatment. For his own experiments Tricker used a method which seems to be free from the latter type of uncertainty; but he stated that he could measure his photographic traces to within an accuracy of 2 percent, whereas the difference between the two types of electron amounts effectively to only 5 percent. Hence even Tricker's results do not provide a very satisfying basis for distinction between the Abraham and the Lorentz electrons.

In conclusion the authors wish gratefully to acknowledge support from the Horace H. Rackham School of Graduate Studies of the University of Michigan.

[8] See *Handbuch der Physik*, Vol. 22 (1926), p. 76.
[9] R. A. Tricker, Proc. Roy. Soc. **A109**, 384 (1925).

APRIL 1, 1938 PHYSICAL REVIEW VOLUME 53

A New Mass Spectrometer with Improved Focusing Properties

WALKER BLEAKNEY AND JOHN A. HIPPLE, JR.
Palmer Physical Laboratory, Princeton University, Princeton, New Jersey

(Received February 7, 1938)

The use of crossed electric and magnetic fields for a mass spectrometer is discussed. It is shown that this arrangement has perfect focusing properties; the focusing depends only on the m/e of the ion selected, and not on the velocity or direction of the charged particles entering the analyzer. The projection of the path in the plane perpendicular to the magnetic field is a trochoid. The theory necessary for the design of the apparatus is developed in some detail. A method of drawing the trochoids is described as well as a chart which is a great help in rapidly correlating the many variables. It is shown that there are two types of path to be considered, the curtate and the prolate. The former was employed in the first model constructed and gave encouraging results in spite of some structural difficulties encountered. The second apparatus was the prolate type and worked exceptionally well. Some typical mass spectra are shown. It was found that a distribution in energy amounting to 50 percent of the potential accelerating the ions had no effect on the resolution.

WHATEVER be the source of ions employed in mass-ray analysis one is always faced with a velocity distribution and an angular divergence of the charged particles. So-called "double-focus" mass spectrographs have recently been constructed by Bainbridge and Jordan,[1] Mattauch,[2] Dempster[3] and Aston.[4] References to other theoretical work bearing on these methods are to be found in these papers as well as in two recent publications by Cartan.[5] Considerable success has attended these efforts to construct a true e/m selector which is independent to some extent of the velocity and direction of the incident ions. However, in all the field combinations except the one which is the subject of this paper, the focusing that is obtained is not perfect and is limited to a small range of initial velocity and direction. Since there is an arrangement of fields which in theory possesses all the desirable qualities mentioned

[1] Bainbridge and Jordan, Phys. Rev. **50**, 282 (1936).
[2] Mattauch, Phys. Rev. **50**, 617 (1936).
[3] Dempster, Proc. Am. Phil. Soc. **75**, 755 (1935).
[4] Aston, Nature **137**, 357 (1936); Proc. Roy. Soc. **163A**, 205 (1937).
[5] Cartan, *Spectrographie de Masse*, (Hermann, 1937) (Actualités Scientifique 550); J. de phys. **8**, 453 (1937).

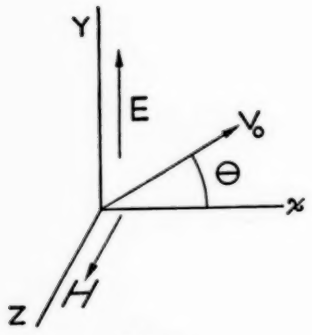

FIG. 1.

above for a mass spectrometer and is theoretically relatively simple, it seemed important to construct an apparatus which would take advantage of these unique properties. This is the type of instrument which is described below.

It is well known that the projection of the path of a charged particle in crossed electric and magnetic fields is a trochoid in the plane perpendicular to the magnetic field.[6] The arrangement of the fields is indicated in Fig. 1. The trochoid is a curve generated by a point on the plane of a circle which rolls on a plane as illustrated in Figs. 2, 3 and 4. In view of the fact that, in designing an instrument of this type, it is necessary to associate the various parameters of the trochoid with the fields and the geometry of the apparatus, the theory will be developed in some detail. In the figure, E and H represent the electric and magnetic fields, v_0 the component of the initial velocity in the $x-y$ plane, and θ the angle between v_0 and the x axis. The component of the initial velocity in the direction of the magnetic field can be neglected since it merely leads to an astigmatic broadening of the image in this direction, i.e. in the direction of the length of the defining slit. The equations of motion are

$$m\ddot{y}=Ee-(eH/c)\dot{x}, \tag{1}$$

$$m\ddot{x}=(eH/c)\dot{y}, \tag{2}$$

where E and e are in e.s.u. and H is in e.m.u. Choosing the origin of time so that when $t=0$, $x=y=0$, the solutions of these equations become

$$x=N\sin\varphi-N\sin(\gamma t+\varphi)+(Ec/H)t, \tag{3}$$

$$y=N\cos\varphi-N\cos(\gamma t+\varphi), \tag{4}$$

where N and φ are parameters depending on the initial velocity and γ is defined by the relation

$$\gamma=eH/mc. \tag{5}$$

The usual procedure of eliminating the time from the above two equations leads to complications. However, by comparison with the equations for the trochoid, the properties of the trochoid may be used to tell completely the motion of the charged particle through the crossed electric and magnetic fields provided the initial conditions are known. The following are the

[6] Page and Adams, *Principles of Electricity* (Van Nostrand, 1931).

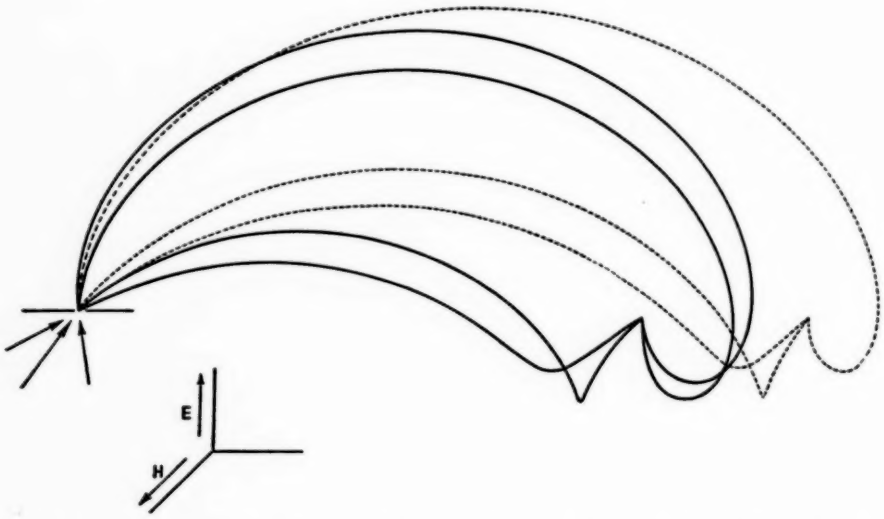

FIG. 2. Trochoidal paths corresponding to various initial conditions. The two foci represent two different values of m/e.

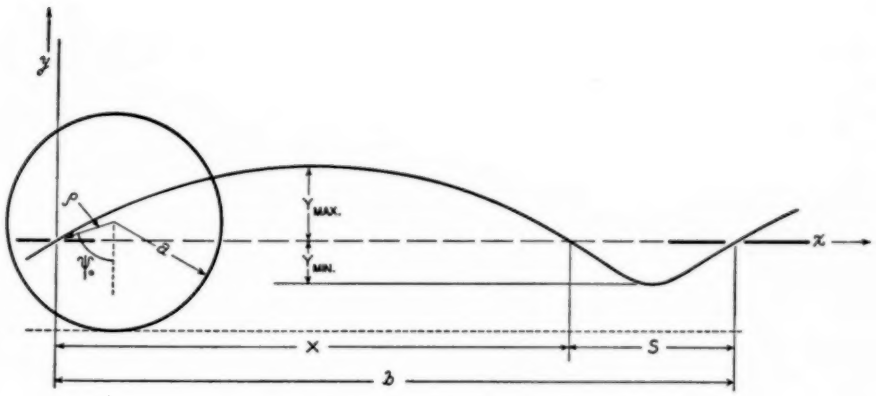

FIG. 3. The curtate cycloid.

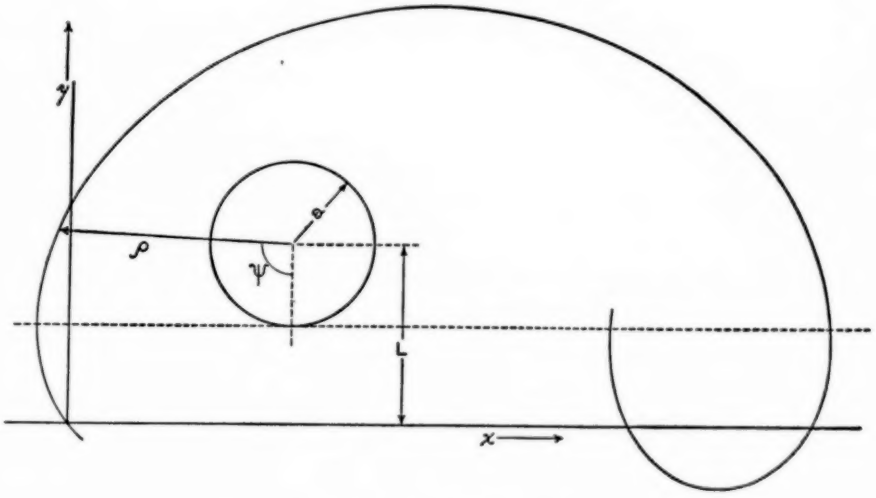

FIG. 4. The prolate cycloid.

equations for the trochoid (cf. Figs. 3 and 4):

$$x=a\psi-a\psi_0+\rho \sin \psi_0-\rho \sin \psi, \tag{6}$$

$$y=L-\rho \cos \psi=\rho \cos \psi_0-\rho \cos \psi. \tag{7}$$

The meaning of the symbols should be evident from the figures. In order to facilitate the discussion, the radius of the rolling circle will be called the primary radius, and the distance from the center of the rolling circle to the point whose locus describes the curve will be called the secondary radius. Thus the primary radius is a, and the secondary radius is ρ. By comparing Eqs. (6) and (7) with (3) and (4), it is evident that

$$a=Emc^2/eH^2 \tag{8}$$

and also that $N=\rho$, $(\gamma t+\varphi)=\psi$ and $\varphi=\psi_0$.

Equation (8) is the fundamental relation for this type of instrument. From the periodic property of the trochoid we get a very important result: the charged particles which have crossed a plane $y=$constant at a certain value of x, say x', will again cross this plane (going in the same direction) at a point $x=x'+b$ where b is given by

$$b=2a\pi=2\pi Emc^2/eH^2. \tag{9}$$

From the fact that none of the initial conditions appear in this equation it is evident that an initial distribution in velocity and direction is immaterial insofar as the focal line is concerned.

It is evident from (9) that m/e is proportional to b and hence the mass scale is accurately linear throughout the mass range. This is in striking

contrast to the usual Dempster type of mass spectrometer for which the analogous equation is

$$b^2=8Vmc^2/eH^2=(2r)^2, \tag{10}$$

where V is the potential accelerating the ions. In this case the masses vary as the square of the distance along the photographic plate. It seems pertinent to mention the Dempster type at this point since in general the same equipment may be used for the construction of this new type of instrument—an instrument which has been found to be a real improvement upon the former. In this connection a gain of a factor of two in the resolving power should be mentioned. From (10), the theoretical expression for the resolving power of the Dempster type instrument neglecting the imperfect focusing is

$$(m/\delta m)=(b/2\delta b). \tag{11}$$

From (8), the theoretical expression for the resolving power of the crossed-field type is

$$(m/\delta m)=(b/\delta b). \tag{12}$$

It must be remembered that Eq. (11) applies for the Dempster type only when the ion beam is perfectly homogeneous with regard to both direction and velocity. The perfect focusing should make it much more easy experimentally to approach the theoretical resolving power in the crossed-field instrument. The factor of two mentioned above is of tremendous importance since the only other method of increasing the resolving power consists in increasing b and decreasing the slit widths—a procedure having obvious limitations in practice. It might perhaps be supposed that the difficulty of getting a sufficiently uniform field would eclipse the gains mentioned above. Actually, as will be described below, it was found that the electric field did not have to be very uniform to provide a considerable improvement in resolution.

In order to design an instrument, it is necessary to know several other quantities connected with the trochoid in order that the path of the ions through the analyzer be known. Although, as explained above, the primary radius a does not depend on the initial conditions, the secondary radius ρ depends not only on the electric and magnetic fields, but also on the direction and magnitude of the initial velocity of the ions. By differentiation of (3) and (4) with respect to the time and substituting the conditions that when $t=0$, $\dot{x}=v_0\cos\theta$ and $\dot{y}=v_0\sin\theta$, the following relations are obtained

$$v_0\sin\theta=\rho\gamma\sin\psi_0, \tag{13}$$

$$v_0\cos\theta=(Ec/H)-\rho\gamma\cos\psi_0. \tag{14}$$

By elimination of ψ_0 from these two equations the following expression is obtained for the secondary radius

$$\rho=(1/\gamma)[v_0^2+(E^2c^2/H^2)-(2Ec/H)v_0\cos\theta]^{\frac{1}{2}}. \tag{15}$$

In order that the ions emerging from the exit slit will have traversed the same path regardless of the m/e selected, it is necessary that there should be a constant relationship between the accelerating voltage V_0 and the analyzing voltage V ($V=Ep$ where p is the distance apart of the condenser plates providing the field E). This important ratio will be denoted by β

$$\beta=(V_0/V). \tag{16}$$

A few more relations were found helpful in studying various orbits in order to select a group suitable for the particular apparatus being designed. Thus, in order that the ions will not strike the condenser plates providing the field in the analyzer, the maximum and minimum values of y must be known. From Fig. 3, it is seen that these are given by

$$y_{\max}=\rho\cos\psi_0+\rho, \tag{17}$$

$$y_{\min}=\rho\cos\psi_0-\rho. \tag{18}$$

Furthermore, to insure that the ions will not strike the structure of the apparatus around the exit slit, the points at which the ions cross the x axis must be known. It will be noted that there are two distinct types of paths: the first of these for which $\rho>a$ is shown in Fig. 4 and will be referred to as the prolate type; the second for which $\rho<a$ is shown in Fig. 3 and will be referred to as the curtate type path. This designation is consistent with the usual conventions in mathematical texts where the curves corresponding to $\rho>a$, $\rho=a$ and $\rho<a$ are called prolate cycloids, cycloids, and curtate cycloids, respectively. The trochoid is a general term which applies to the whole family. Since the cycloid has

cusps, this type of trajectory must be avoided; at the cusps there would be a building up of space charge and therefore a scattering of the ion beam. The distance s from the exit slit along the x axis to the preceding point at which the ions crossed this axis is given by

$$s=2[\rho \sin \psi_0-a\psi_0]. \tag{19}$$

As should be clear from Fig. 4, s is positive when $X>b$. Of course for the curtate path $X<b$ always so that in this case s is negative.

Using the constant β introduced above, Eq. (14) may now be put into the more convenient form

$$\rho=(b/2\pi)[(4\pi p/b)\beta+1 -4(\pi p/b)^{\frac{1}{2}}\beta^{\frac{1}{2}}\cos\theta]^{\frac{1}{2}}. \tag{20}$$

Another useful relation is

$$\rho\cos\psi_0=(b/2\pi)-(bp/\pi)^{\frac{1}{2}}\beta^{\frac{1}{2}}\cos\theta \tag{21}$$

since it appears in both (17) and (18). Since it is sometimes necessary in designing the apparatus to know the radius of curvature of the ions in the magnetic field alone, it is also of service to express this in terms of some of the quantities mentioned above.

$$r=(pb/\pi)^{\frac{1}{2}}\beta^{\frac{1}{2}}. \tag{22}$$

With so many variables to be considered, the design and operation of the crossed-field instrument is somewhat more complicated than the conventional type. For this reason several tools were developed that proved to be quite helpful. In the first place, it is evident that a method of easily drawing the trochoids would be desirable. The obvious method of rolling a disk along a straight edge is awkward and entirely unsatisfactory. Hence the following apparatus was devised: instead of rolling the disk containing the tracer, the disk is suspended from a fixed support and the paper, on which the drawing is to be made, is fastened to a board which is slid under the disk. A string looped around the disk and having its ends fastened to the ends of the board causes the disk to rotate as the board is moved. It is now very easy to draw either the curtate or the prolate cycloid. With this instrument available, it was found generally to be more convenient to reverse the usual procedure of calculating the orbit from the fields and the initial conditions; the orbit of the desired shape was now drawn and the various combinations of the variables that would give this orbit could then be calculated fairly easily by using some of the relations developed above. Fig. 2 shows some curves drawn with this instrument. The two different foci correspond to two different values of m/e. The trochoid drawer is useful also in any problem in which charged particles are being accelerated in the presence of a magnetic field; in any apparatus in which this occurs, it is necessary to know the paths of ions as they are accelerated to the entrance slit of the analyzer in order that the slits may be properly placed, and this is most easily determined graphically by means of the apparatus just described.

Another device that was found to be very helpful was a chart that aids in the rapid correlation of several of the variables. This chart is shown in Fig. 5 and is based upon the relation

$$(\partial b/\partial M)=(2\pi c^2M_P/e)(E/H^2) =(6.5\times10^4)[E(\text{volts/cm})/H^2], \tag{23}$$

where M is the mass in atomic weight units and M_P is the mass in grams of unit atomic weight. A diagonal represents a line of constant dispersion in centimeters per mass-unit. This chart will be of particular help in rapidly determining the fields required to focus a particular mass at a particular value of b as is necessary in the photographic method. Thus, suppose it is required to have mass 20 focused at $b=60$ cm. When this point is found on the chart, it is seen that the corresponding diagonal line (interpolated) is $(\partial b/\partial M)=3$, the value observed where this line cuts the mass one ordinate. Values of the electric and magnetic fields which correspond to any point on this diagonal line will be possible solutions of the problem. For example, $H=3100$ gauss and $E=450$ volts per cm could be chosen. However, the value of E will probably in general be kept as large as conveniently possible because of the desirability of keeping the ion velocity large.

It is of interest to notice that an initial velocity distribution should be useful in the crossed-field instrument since it should mean a more intense ion beam may be used. The velocity distribution causes the beam to spread out except at the foci

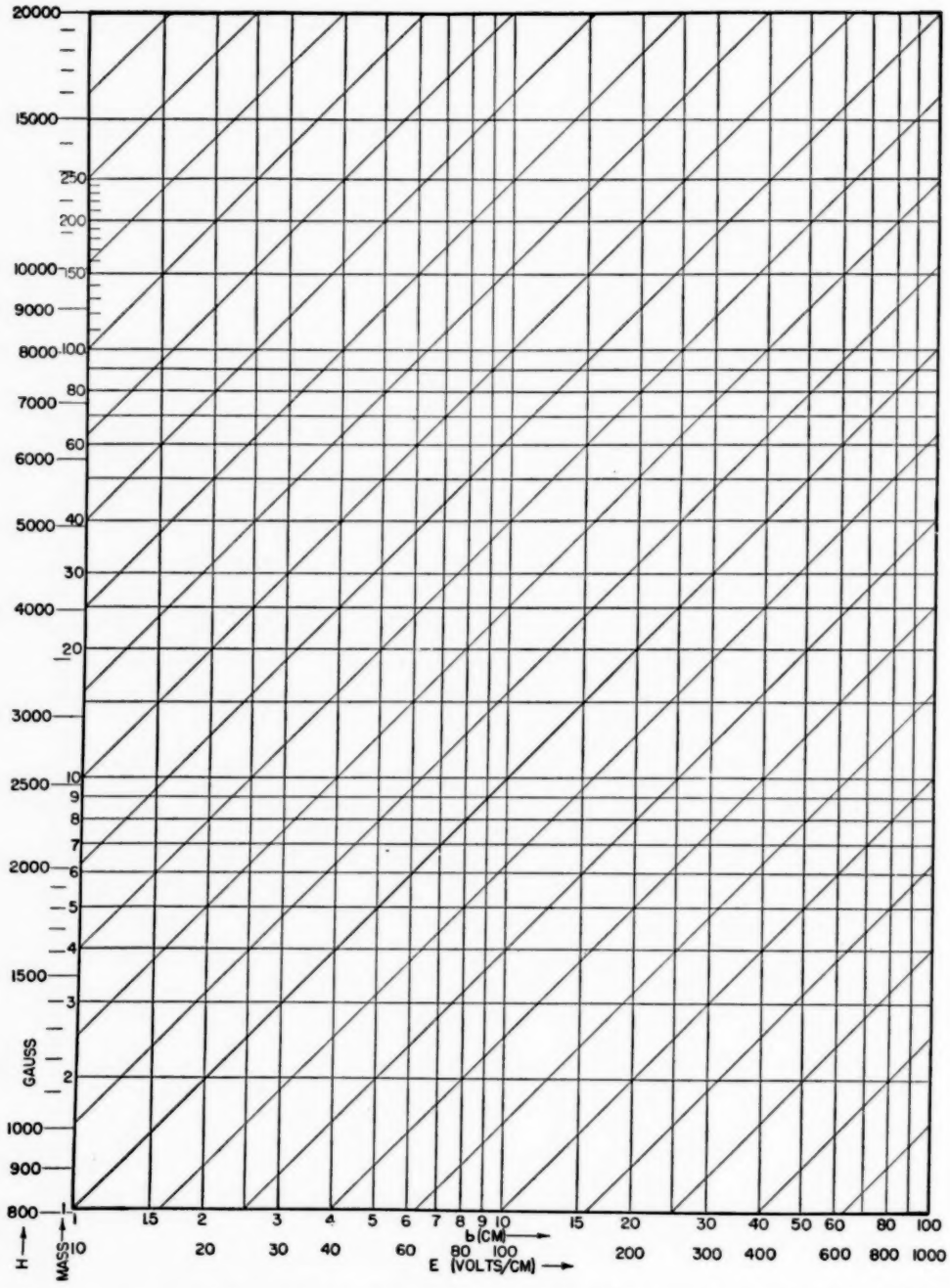

FIG. 5. A chart for rapidly correlating the variables appearing in the equation for b (E, H and M/e).

of the trochoid, thus decreasing the space charge effect.

THE CURTATE PATH: $\rho < a$

The ideal apparatus of the crossed-field type would be so designed that it would be easily adaptable for the use of either the curtate or the prolate path. However, in the small models here described it was not feasible to do this. The first apparatus was of the curtate type.

In this apparatus use was made of a small Pye electromagnet having a gap between the pole faces of $\frac{1}{2}$ inch. Under these circumstances the attainment of a uniform electric field

parallel to the pole faces represents a difficult problem. Fig. 6 indicates the manner in which the uniform electric field was obtained. The analyzing potential was applied between the plates I and II which are staggered as shown in order that the ions may enter and leave the crossed field region which constitutes the analyzer. These end plates, together with the center plate containing the entrance and exit slits, were supported by the two pairs of Bakelite cylinders III threaded with 100 threads per inch. Around each pair of cylinders was wound in a sort of double grating effect 3 mil Nichrome wire having a resistance of 68 ohms per foot. With this high resistance wire to provide a uniform potential gradient along the edges of the region between the plates, the electric field within the long narrow coil thus formed was quite uniform. The entrance and exit slits were 10 cm apart. The gap in the center plate to allow passage of the ion beam from the entrance slit to the exit slit was made with a length just slightly less than half the distance between the slits in order to prevent the collection of second or higher orders; if this gap were larger, there would be the possibility of collecting multiply charged ions of a certain mass at the same time as the singly charged ions of that mass; or, for ions having the same charge, there would be the possibility of collecting $M/2$ (and perhaps $M/3$, $M/4$, etc.) at the same time as M. By making the gap less than $b/2$ there is no possibility that any ions will be collected which have traversed several cycles of the trochoid.

In this particular apparatus, the proper value for b was calculated in the following manner. The condition to be fulfilled in order that no cycloids will be formed is that $\rho < a$. In terms of β it may readily be shown that this means that

$$\beta < [b/p\pi] \cos^2 \theta. \tag{24}$$

In this apparatus with $b=10$ cm., $p=4.5$ cm and $\theta=30°$

$$\beta < 0.53.$$

Taking $\beta=0.25$ it was found that the corresponding values of y_{max}, y_{min} and s calculated by means of Eqs. (17), (18), and (19) should lead to a possible trajectory for the ions through the instrument although perhaps not the best one. Actually, when the ions first reached the collector, the peaks observed were very ragged and ghosts were present. However, by adjusting β to the value 0.39, the peaks became very sharply defined. With the slits between 1 and 2 mm in width, the peaks for K^{39} and K^{41} were completely resolved. The nature of the peaks was found to be fairly sensitive to the adjustment of β. Of particular interest is the fact that a large percentage of the ions of a particular mass which passed through the first slit also passed through the second slit when the apparatus was properly adjusted.

It is to be emphasized that this model was constructed merely to show the possibilities of the method. The use of brass, Bakelite and other materials unsuitable in high vacuum technique prevented the application of this instrument to any extensive research. In spite of this, the results obtained with this model were quite satisfactory inasmuch as they showed clearly

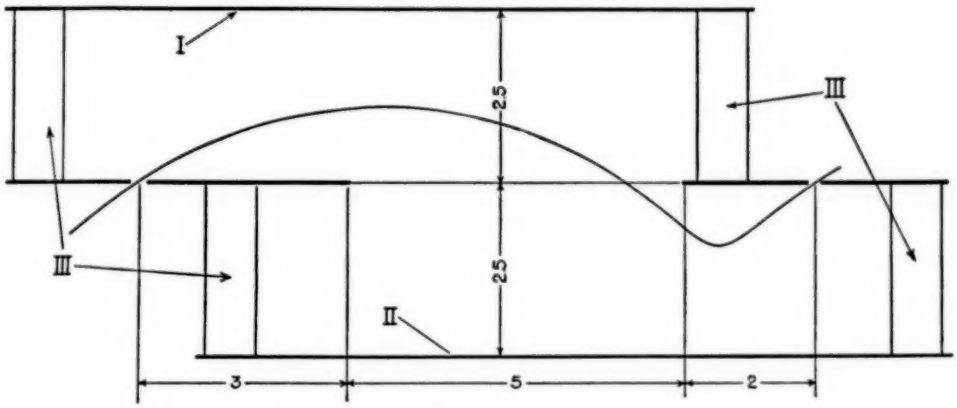

FIG. 6. Diagrammatic sketch of the curtate instrument.

the practicability of the use of crossed fields for a mass spectrometer and indicated the manner in which a better instrument should be designed. It is this instrument which is described below. A solenoid being available in the laboratory, the prolate path appeared to be the better choice in this case.

The Prolate Path: $\rho > a$

The fact that for this type of path $\theta = 90°$, approximately, furnishes considerable simplification both theoretically and experimentally. It is easier to get a good ion beam through the entrance slit to the analyzer when the ions pass this slit perpendicularly. It is true that, in contrast to the curtate path, the factor s (cf. Eq. (19)) becomes positive; this is a decided disadvantage since it means a loss in resolving power inasmuch as the slits cannot be placed at the extremities of the region of the uniform magnetic field. However, it was felt that, for the particular solenoid available, the advantages mentioned above would more than compensate for the loss in resolution. In addition, since the rather low magnetic field would limit the use of the instrument to the lower mass region, the resolving power should be more than sufficient at any rate. Actually this was found to be true.

There is no longer any difficulty about the occurrence of cycloids since the condition $\beta > 0$ is always satisfied. With the substitution $\theta = 90°$ the following simple relations are obtained:

$$\rho = (b/2\pi)[(4\pi p/b)\beta + 1]^{\frac{1}{2}},$$
$$y_{max} = a + \rho,$$
$$y_{min} = a - \rho,$$
$$s = 2[(\rho^2 - a^2)^{\frac{1}{2}} - a \cos^{-1}(a/\rho)].$$

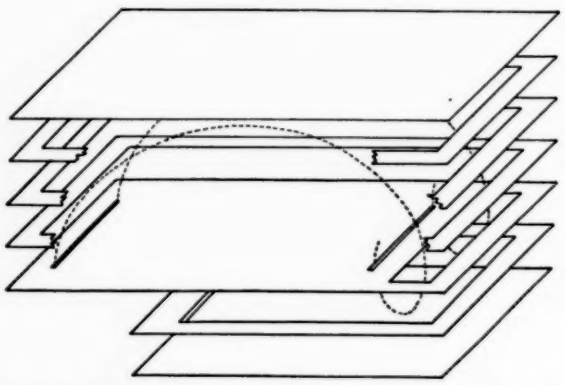

FIG. 7. Isometric view illustrating schematically the prolate instrument.

A suitable relation between b and s may now be determined. Naturally it is desirable to have b as great as possible and consequently s as small as possible to obtain the optimum theoretical resolving power; on the other hand, s must be of such magnitude that the ions of the highest mass with which the apparatus will be used, will have sufficient velocity throughout the orbit. Clearly the magnitude of the magnetic field available is a determining factor in the choice of the ratio between b and s. The kinetic energy is least at y_{min} and is given by the relation

$$V_{min} = V[\beta + (y_{min}/p)].$$

Unfortunately the maximum field attainable was 1000 gauss and $(b+s)$ had to be less than 9.5 cm. The most satisfactory solution seemed to be to take $a = 1$ cm and $\rho = 3$ cm making the ratio $(b/s) = 2$ approximately.

The new mass spectrometer was constructed entirely of glass, tantalum and tungsten. The electric field was obtained by stacking rectangular tantalum plates spaced 0.5 cm apart by means of glass spacers. This is illustrated schematically in the isometric drawing in Fig. 7. There were actually fifteen of these plates and a separate lead was brought out of the vacuum system for each one. Between the leads for successive plates 10,000 ohm resistors were inserted. The defining slits in the main plate were made 4 cm long and could be varied in width from the end of the solenoid by means of thin tungsten rods, each one being about three feet long. All of the electrical leads except for the filament were brought out the other end of the tube. The great number of these leads together with the long slit-adjusting rods on the other side of the apparatus caused the tube to become very long—about seven feet. The lead for the ion current was brought out through a separate reentrant tube with the tungsten seal close to the apparatus at the center of the solenoid. A long aluminum tube was inserted in the glass tube for shielding. The reentrant tube was waxed to the box housing the amplifier through a flexible connection and then evacuated with the amplifier. The ions were produced and accelerated into the analyzer in the same manner as described in an earlier apparatus.[7]

[7] Bleakney, Phys. Rev. **40**, 496 (1932).

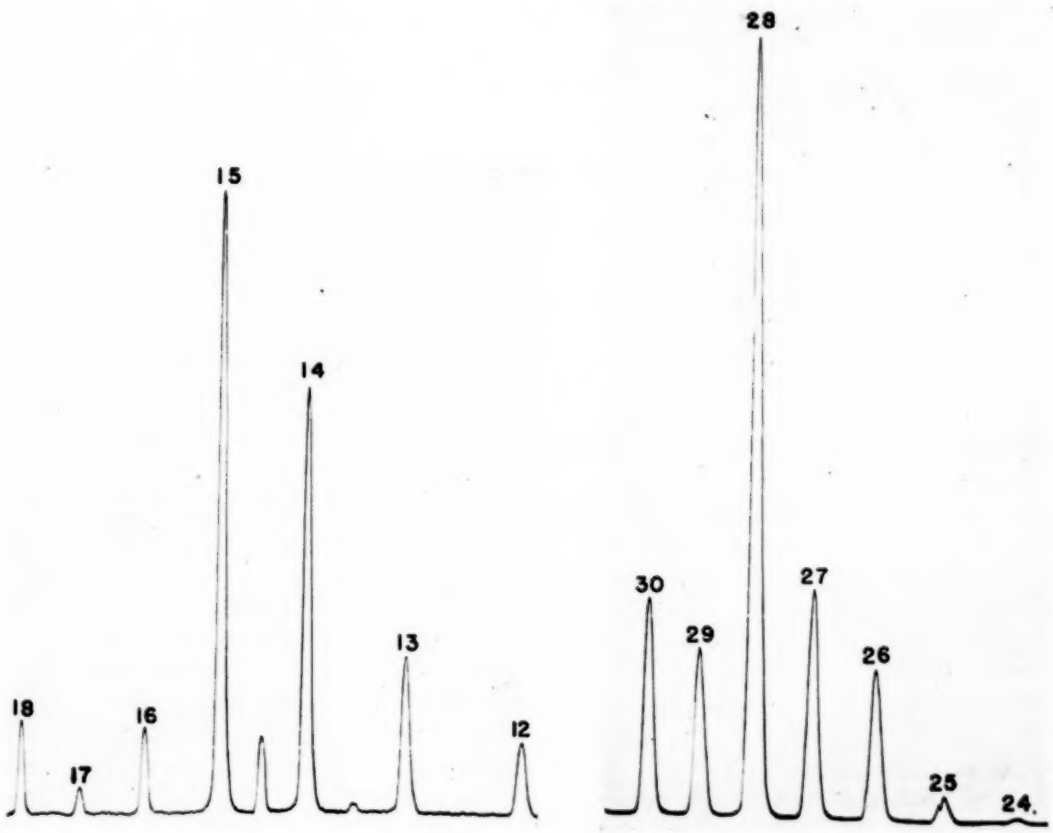

FIG. 8. Mass spectra obtained with ethane in the prolate instrument. The peaks at masses 14.5 and 13.5 are due to $C_2H_5^{++}$ and $C_2H_3^{++}$, respectively.

In Fig. 8 are shown some curves obtained with ethane in the apparatus just described. The analyzer slits were about 0.3 mm in width and, as mentioned previously, only 6 cm apart. The resolving power was greatly improved in comparison with the former tube with similar geometrical conditions. The curves were taken with the automatic recorder described previously.[8] It may at first appear that they are in contradiction to the earlier statement concerning the linear mass scale, but it must be remembered that the mass scale is linear in b as would be evident on a photographic plate. In this case the analyzing potential is being varied and the formula shows that M/e is proportional to the reciprocal of V.

In addition to the improved resolution, two striking facts were noted. In the first place, it was found that the effect of shorting the two central plates was very slight. In other words, the uniformity of the electric field does not constitute as great a problem as initially supposed. Secondly, in agreement with the theory, an initial velocity distribution was immaterial insofar as the focusing was concerned, but the magnitude of the distribution permissible was surprising. An a.c. component was superimposed on the d.c. accelerating potential of the ions and an energy fluctuation amounting to almost 50 percent of the average had practically no effect either on the intensity or resolution. However, it was impossible to show this effect unless condensers were placed across the analyzer to prevent the a.c. potential from disturbing the analyzing field.

It is hoped that a much larger apparatus will be completed in the near future.

[8] Smith, Bleakney, Smith and Lozier, Rev. Sci. Inst. **8**, 1 (1937).

The Dissociation of Ethane by Electron Impact

JOHN A. HIPPLE, JR.
Palmer Physical Laboratory, Princeton University, Princeton, New Jersey
(Received February 7, 1938)

The dissociation of C_2H_6 by electron impact has been investigated with a new mass spectrometer. One negative, two doubly-charged and fourteen positive ions have been observed corresponding to the various states of dissociation of the C_2H_6 molecule. An analysis is given of the processes taking place in the upper mass-range where unique interpretations of the results may be made. The difficulty of accurately determining the relative intensities of two ions having a large difference in mass is discussed as well as the meaning of the probable errors given for the measured appearance potentials.

IN several recent papers[1-3] it has been shown that interesting interpretations may be made of the electron dissociation processes in the more complicated molecules. These papers provide an introduction to this field as well as a review of the previous literature on the subject. The present paper represents an extension of this work to ethane.

The analysis of ethane was made with the new mass spectrometer described in the previous paper. The ions observed are listed in Table I. Mass spectra with this gas in the apparatus were given in the preceding paper along with the description of the apparatus. The fact that the ratio of the intensities of masses 30 and 15 is 100/9 serves to correlate the two mass ranges shown. The height of the mass 28 peak relative to mass 30 is interesting inasmuch as it shows that, for this molecule, it is more probable to strip off an electron and two hydrogen atoms than a single electron. A similar effect was found by Stewart and Olson[4] in propane and butane. A measurement of the appearance potential indicates that mass 16 is partly due to a methane impurity in the ethane. Of course the peaks at masses 18 and 17 come from water vapor.

In the discussion of the results the same notation will be used as in the previous papers on this subject which were mentioned above:

$A(X^+)$ ≡ Appearance potential of the ion X^+
$I(X)$ ≡ Ionization potential of X
$D(X)$ ≡ Energy of dissociation of X to atoms in the gaseous state.
$W(X^+)$ ≡ Excess energy (kinetic or excitational) appearing in the production of the ion X^+ from the parent molecule.

The first step in the analysis of the data is the calculation of the energies of the possible states of combination in which two carbon and six hydrogen atoms may exist. In methane there were nine states with which to deal and in ethylene twenty-three. In ethane there are forty-three possible combinations; and as a result, it was only possible to make a significant analysis of the data for the heavier masses. Only the combinations which are in the range in which interpretations were made are given in Table II. Most of the energies listed are obtained from Table VII of Kusch, Hustrulid and Tate using the value 25.0 volts for the state 2C+6H referred to C_2H_6 as zero.[5] The only state that cannot be obtained in this way is C_2H_5+H; this energy is taken as 2.9 volts, interpolated in the same manner as was done in ethylene.

$C_2H_6^+$. The ionization potential of C_2H_6 is 11.6±0.1 volts. Morris[6] measured the ionization potentials of C_2H_2, C_2H_4 and C_2H_6 as 12.3, 12.2 and 12.8 volts, respectively. Since the values for C_2H_2 and C_2H_4 were later determined spectroscopically to be 11.35 and 10.41 volts, Mulliken[7] suggested as a probable corrected experimental value 11.4 volts for C_2H_6 and felt that this was in reasonable agreement with the spectroscopic estimate. In a very early paper, Hughes and

[1] Smith, Phys. Rev. **51**, 263 (1937).
[2] Bleakney, Condon and Smith, J. Phys. Chem. **41**, 197 (1937).
[3] Kusch, Hustrulid and Tate, Phys. Rev. **52**, 843 (1937). This paper will henceforth be referred to as K, H and T.
[4] Stewart and Olson, J. Am. Chem. Soc. **53**, 1236 (1931).
[5] Bichowsky and Rossini, *Thermochemistry of Chemical Substances* (Reinhold, 1936).
[6] Morris, Phys. Rev. **32**, 942 (1928).
[7] Mulliken, J. Chem. Phys. **3**, 517 (1935).

TABLE II. *Energies of possible states of combination in which two carbon and six hydrogen atoms may exist.*

STATE	ENERGY (VOLTS)
$2C+6H$	25.0
CH_3+C+3H	14.4
CH_3+C+H_2+H	9.9
$CH_3+CH+2H$	10.9
CH_3+CH+H_2	6.4
CH_3+CH_2+H	7.4
CH_3+CH_3	3.8
C_2+6H	19.5
C_2+H_2+4H	15.0
C_2+2H_2+2H	10.6
C_2+3H_2	6.1
C_2H+5H	15.7
C_2H+H_2+3H	11.2
C_2H+2H_2+H	6.8
C_2H_2+4H	12.2
$C_2H_2+H_2+2H$	7.1
$C_2H_2+2H_2$	3.3
C_2H_3+3H	8.9
$C_2H_3+H_2+H$	4.4
C_2H_4+2H	5.8
$C_2H_4+H_2$	1.3
C_2H_5+H	2.9
C_2H_6	0.0

Dixon[8] measured the appearance potential of C_2H_6 as 10 volts.

$C_2H_5^+$. Since this ion appears at $A(C_2H_5^+)=12.7$ volts, the energy relation may be written

$$I(C_2H_5)+W(C_2H_5^+)+2.9=12.7 \text{ volts.}$$

This leads to an upper limit for the ionization potential

$$I(C_2H_5)\leq 9.8 \text{ volts.}$$

[8] Hughes and Dixon, Phys. Rev. **10**, 495 (1917).

$C_2H_4^+$. Using the value of $I(C_2H_4)=10.8$ volts obtained by K, H and T, it is evident that the process here must be

$$C_2H_6\rightarrow C_2H_4^+ + H_2$$

since the calculated energy required in this case is $10.8+1.3=12.1$ volts in agreement with the appearance potential observed. This means that $W(C_2H_4^+)=0$ within the limits of error. The process

$$C_2H_6\rightarrow C_2H_4^+ + 2H$$

requiring a minimum of 16.6 volts may possibly occur, but the ionization curve is rising too rapidly in this region as a function of the electron velocity to detect a second break.

$C_2H_3^+$. Of the two processes possible here, the one of lower energy appears to be the one that occurs. This is

$$C_2H_6\rightarrow C_2H_3^+ + H_2 + H$$

K, H and T showed that

$$I(C_2H_3)\leq 11.0 \text{ volts.}$$

If it is assumed that $I(C_2H_3)=11.0$ volts, then the minimum energy calculated for the above process is $11.0+4.4=15.4$ volts agreeing very well with the observed appearance potential $A(C_2H_3^+)=15.2\pm 0.3$ volts. This means that either the ion $C_2H_3^+$ is formed from both C_2H_6 and C_2H_4 with the same additional energy

TABLE I. *Ions observed in ethane.*

ION	ABUNDANCE	APPEARANCE POTENTIAL	PROBABLE PROCESS $C_2H_6\rightarrow$	CALCULATED MINIMUM ENERGY	EXCESS ENERGY OR DEDUCED $I(X)$ (VOLTS)
$C_2H_6^+$	100	11.6 ± 0.1	$C_2H_6^+$	$I(C_2H_6)$	$I(C_2H_6)=11.6$
$C_2H_5^+$	76	12.7 ± 0.2	$C_2H_5^+ + H$	$I(C_2H_5)+2.9$	$I(C_2H_5)\leq 9.8$
$C_2H_4^+$	360	12.1 ± 0.1	$C_2H_4^+ + H_2$	12.1	$W(C_2H_4^+)=0$
$C_2H_3^+$	105	15.2 ± 0.3	$C_2H_3^+ + H_2 + H$	$I(C_2H_3)+4.4$	$I(C_2H_3)\leq 10.8$
$C_2H_2^+$	62	15.0 ± 0.3	$C_2H_2^+ + 2H_2$	14.5	$W(C_2H_2^+)=0.5$
C_2H^+	12	27.0 ± 1.0	$C_2H^+ + H_2 + 3H$	$I(C_2H)+11.2$	$I(C_2H)\leq 15.8$
			$C_2H^+ + 5H$	$I(C_2H)+15.7$	$I(C_2H)\leq 11.3$
C_2^+	2.5	31.5 ± 1.0	$C_2^+ + H_2 + 4H$	31.5	$W(C_2^+)=0$
CH_3^+	9	14.2 ± 0.3	$CH_3^+ + CH_3$	$I(CH_3)+3.8$	$I(CH_3)\leq 10.4$
CH_2^+	6	16.2 ± 1.0			
CH^+	2.5	24.5 ± 1.0			
C^+	1	30.4 ± 1.5			
$C_2H_5^{++}$	1	32.0 ± 1.5			
$C_2H_3^{++}$	.1				
H_3^+	.5				
H_2^+	5.	28.0 ± 1.5			
		31.5 ± 1.5			
H^+	50.	20.8 ± 1.0			
H^-					

* Because of the great number of possibilities to be considered together with the larger uncertainty in the measured value of the appearance potential, an attempt at further interpretation does not seem to be worth while at present.

$W(C_2H_3^+)$ involved, or $I(C_2H_3)$ is actually about 11.0 volts. The second possibility appears more probable.

$C_2H_2^+$. From the work of Tate, Smith and Vaughn[9] on C_2H_2 it is known that $I(C_2H_2) = 11.2 \pm 0.1$ volts (a value in good agreement with Mulliken's spectroscopic value[7]). There are three possibilities here, but the only one that can occur at an energy low enough to agree with the observed $A(C_2H_2^+) = 15.0 \pm 0.3$ volts is

$$C_2H_6 \rightarrow C_2H_2^+ + 2H_2,$$

which can appear at $11.2 + 3.3 = 14.5$ volts. This means that $W(C_2H_2^+) = 0.5$ volts which is of the same order of magnitude as the probable error.

C_2H^+. This ion was observed at $A(C_2H^+) = 27.0 \pm 1.0$ volts. K, H and T found in their interpretation of C_2H_2 that $I(C_2H) \leq 14.3$ volts and in C_2H_4 that $I(C_2H) \leqq 13.8$ volts. This probably eliminates one of the three possibilities as demanding too great an amount of energy $W(C_2H^+)$ to be associated with the process. The process

$$C_2H_6 \rightarrow C_2H^+ + H_2 + 3H$$

leads to a value $I(C_2H) \leq 27.0 - 11.2 = 15.8$ volts. For agreement with K, H and T this means that $W(C_2H^+) \geq 2$ volts. The reaction

$$C_2H_6 \rightarrow C_2H^+ + 5H$$

means that $I(C_2H) \leq 11.3$ volts.

C_2^+. Although there are now four possibilities to be considered, the solution appears to be unique. K, H and T found that $I(C_2^+) \leq 16.5$ volts. In the reaction

$$C_2H_6 \rightarrow C_2^+ + H_2 + 4H$$

if $I(C_2^+)$ is taken as 16.5 volts, then the calculated minimum energy is 31.5 volts, agreeing with the observed appearance potential $A(C_2^+) = 31.5 \pm 1.0$ volts. Of the other three possibilities, one cannot occur at a potential this low and the other two would require that $W(C_2^+) \geq 4.4$ volts.

CH_3. In this case the explanation of the appearance potential $A(CH_3^+) = 14.2 \pm 0.3$ volts seems to be the lowest energy process

$$C_2H_6 \rightarrow CH_3^+ + CH_3.$$

From the relation

$$I(CH_3^+) + 3.8 + W(CH_3^+) = 14.2 \text{ volts}$$

the ionization potential is

$$I(CH_3) \leq 10.4 \text{ volts}.$$

This is to be compared with Smith's result from methane of $I(CH_3) \leq 9.9$ volts. Fraser and Jewett[10] obtained the value $I(CH_3) = 11.1 \pm 0.5$ volts by direct measurement on free CH_3 radicals and Mulliken[11] made a theoretical estimate of 8.5 volts for this ionization potential. Any of the other processes would lead to $I(CH_3) < 7.8$ volts and hence do not appear to be as consistent with these values as the reaction given above.

It does not seem significant to carry the detailed analysis beyond this point due to the number of possibilities which must be considered. The complexities of the analysis suggest that a careful study of the lower mass region would be unwarranted at present.

There is one very interesting fact to be noticed in regard to the analyses of C_2H_2, C_2H_4 and C_2H_6: in the first molecule only the atomic hydrogen ion was observed; in C_2H_4, both H^+ and H_2^+ were found; and finally in C_2H_6, it was discovered that H^+, H_2^+ and H_3^+ were all present. This is in agreement with the results that might be expected from the known structure of these molecules.

In the work of this nature there are two confusing points that need some further discussion. The first of these is concerned with the abundance of the hydrogen ions relative to the heavier masses. This quantity has been found to vary in different apparatuses in spite of the fact that the measurements in the upper mass region check rather well. For example, in the preliminary work done at Princeton on CH_4[12] the yield of hydrogen ions was found to be very small. Later Smith, using an apparatus of the same type but with increased sensitivity, found these ions to be rather abundant. Since, in this study of ethane, the hydrogen ions were found to be much more abundant than in any previous studies of hydrocarbons, a check was made on

[9] Tate, Smith and Vaughn, Phys. Rev. **48**, 523 (1935).

[10] Fraser and Jewett, Phys. Rev. **50**, 1091 (1936).

[11] Mulliken, J. Chem. Phys. **1**, 492 (1933).

[12] Hipple and Bleakney, Phys. Rev. **47**, 802(A) (1935).

the measurements by putting methane into this new apparatus; it was found that there was a relative increase of almost a factor of ten compared with Smith's measurements. This last increase can be partially explained by the fact that, because of the focusing properties of the new instrument, ions formed with kinetic energy will no longer cause a broadening of the main peak as in the case of magnetic focusing alone. When 75-volt electrons are used there must certainly be a great number of hydrogen ions formed with kinetic energy. However, the discrepancy existing when the two instruments are of the same type indicates that no great faith should be placed in the observed values in any event when there is so great a difference in mass. This is probably explained by a differential selection of the ions as they are accelerated from the ionization chamber into the analyzer. This last effect would of course vary with the geometrical conditions. It is due to a difference in the amount of kinetic energy associated with the formation of the ions as well as a difference in mass. Thus, if the accelerating slits in the ion gun are wide, the solid angle subtended with reference to the region in which the ions are formed will be correspondingly large; and this in turn means that a greater fraction of the ions formed with kinetic energy will enter the analyzer.

The second point that requires some discussion is the error given in the measured value of the appearance potential. Smith found that, if the conditions were varied over an extremely wide range, the uncertainty in the observed value of the appearance potential was somewhat increased; this is due to the difference in the shape of the initial portion of the molecular ionization curve as compared with that of the inert gas used for calibration. As a result, Smith was liberal in his estimate of the probable error. Certainly, under similar experimental conditions, the variation in successive measurements is much less than the errors he gives. Also the difference in the appearance potentials of the various ions is known to a greater accuracy than would be concluded from Smith's results. K, H and T evidently estimated their probable error from the internal consistency of the data taken under similar experimental conditions; since the results here given for ethane fit in so nicely with their results on ethylene, the same method of estimating the error in the measured appearance potential has been employed here.

The author is indebted to Mr. Morikawa formerly of the chemistry department for the preparation of the gas.[13] The author also wishes to express his grateful appreciation to Professor Walker Bleakney for the supervision of this work.

[13] Benedict, Morikawa, Barnes and Taylor, J. Chem. Phys. **5**, 1 (1937).

X-Ray and Optical Properties of Barium-Copper-Stearate Films

CLIFFORD HOLLEY
Ryerson Physical Laboratory, University of Chicago, Chicago, Illinois
(Received December 29, 1937)

Barium-copper-stearate films, built by the successive deposition of layers one molecule thick, were used as diffraction crystals to obtain x-ray spectra. The measurements show that for these films the x-ray spacing has a constant value of approximately 50.47A for films with the same composition, with thicknesses varying from 301 to 3000 layers, but varies with the percent of copper in the film; thin films produce as good spectra as do thick ones; the reflecting planes are regular and definite; the spacing is the same whether the molecules in adjacent layers are oriented in the same or in opposite directions; and the unit decrement of the index of refraction is 5.1×10^{-6}. From the total thickness of a film, as measured by a Michelson interferometer, the spacing of the molecular layers was found to be 24.23A. For the films in which the molecules in adjacent layers were oriented in opposite directions it was expected that the grating space would be twice the layer spacing, or 48.46A. The marked difference between this value and the x-ray spacing of 50.47A indicates that the x-ray spacing is not determined by the method of building the film.

A METHOD of building a multiple-layer film of the salt of a fatty acid on the surface of glass or metal by the successive deposition of layers one molecule thick has been reported by Blodgett.[1] By direct count during the building process the total number of layers in the film is known. The successful use of a film of 301 layers of barium stearate in diffracting x-rays in such manner as to produce fairly sharp lines[2] suggested the possibility of an independent and direct method of measuring the grating space of a crystal. Accordingly the grating space of such a film, used as a diffraction grating, was determined from the angle of reflection of a known x-ray line, and this spacing compared with that obtained by optical means with a film of a relatively large number of layers. The results of these experiments show, contrary to our expectations, that these surface films as they are now being made cannot be used thus to obtain reliable values of the absolute crystalline grating space.

For the work of this experiment Dr. Blodgett provided several films of barium-copper-stearate with thicknesses varying from 301 layers to 3000 layers. All the films except the one of 301 layers were built on optically flat surfaces of glass with an index of refraction nearly the same as that of the film. These films were built with the alternate layers of molecules oriented in opposite directions, i.e., the films were of the "*y*" type as described by Dr. Blodgett.[1] Earlier work with a 301-layer film of this type had indicated that the grating space was approximately 47.5A.[3] In order to obtain appreciable angles of diffraction and sufficient resolving power with so large a grating space it was necessary to use long wave-length x-rays, or a high diffraction order of the shorter wave-length x-rays, and a spectrometer with high dispersive power. For the longer wave-lengths of x-rays it was necessary to use a vacuum spectrograph in order to reduce absorption.

The x-ray apparatus is shown in Fig. 1. A Dershem type of metal x-ray tube *T* with tungsten target is placed approximately 60 cm from the crystal *X*, which in turn is the same distance from the photographic plate *P*. This provides Bragg focusing in a spectrometer with high dispersive power. The camera *C*, the copper tubes *A* and *B*, and the crystal chamber *D* form a gas tight compartment. *A* is connected to the x-ray tube, and *B* to the crystal chamber by sylphons. This permits limited freedom of motion. *D* is a removable steel cylinder with several open-

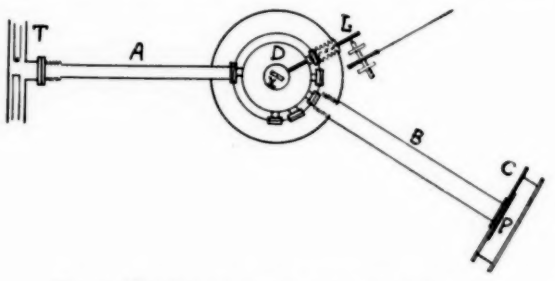

FIG. 1. Dershem vacuum x-ray spectrograph.

[1] Katharine B. Blodgett, J. Am. Chem. Soc. **57**, 1007 (1935).
[2] Clifford Holley and Seymour Bernstein, Phys. Rev. **49**, 403 (1936).
[3] Seymour Bernstein, unpublished master's thesis, University of Chicago, 1936.

ings in the side to provide for different positions of the camera. The crystal mounting, attached to a divided circle, can be moved by the lever L, which is attached through a sylphon. The cover of D can be removed to permit adjusting the crystal. All openings are closed by brass plugs seated with rubber gaskets. The bending of the sylphon permits the camera to be rotated through about 15°. When further motion is necessary, a different opening in D is used. With three cylinders in which the openings are at different positions, the entire angular position up to 90° can be covered. The lever L is oscillated by means of a pulley driven by an electric motor, and automatically reverses its direction at regular intervals. In practice the crystal oscillated through about 0.5°. The purpose of this oscillation was to eliminate the effect of crystal irregularities.

The constancy of the grating space among the different films was checked by matching x-ray reflections from the film against those from gypsum. With the film used as a crystal a photograph was taken of the fifth order tungsten $L\alpha_1$ line (1.47336A, crystal standard). The film was then replaced by a gypsum crystal and a photograph taken of the tungsten $L\gamma_1$ line (1.09630A, crystal standard). The photographic plate remained in the same position during the two exposures. Fig. 2 shows typical photographs obtained from films of 301, 1100, and 3000 layers, respectively, with an exposure time of 4.5 hours for the film, and 40 minutes for the gypsum. Tube current and voltage were approximately 25 ma and 25 kv, respectively. Photographs were taken from films with 301, 1100, 1100, 1130, 1900, 2990, 3000, and 3000 layers. The 2990-layer film and one of the 3000-layer films failed to give definite lines, but the remaining six films produced good lines. From

TABLE I. *Apparent grating spaces of films with different numbers of layers.*

NUMBER OF LAYERS IN FILM	DISTANCE BETWEEN THE TUNGSTEN $L\gamma_1$ AND FIFTH ORDER $L\alpha_1$ LINES	ANGLE OF REFLECTION OF THE FIFTH ORDER TUNGSTEN $L\alpha_1$ LINE	APPARENT GRATING SPACE OF FILM
301	1.21 mm	4° 12′ 17.7″	50.236A
1100	1.18	4 12 12.6	50.252
1100	1.13	4 12 4.0	50.280
1130	1.22	4 12 19.4	50.230
1900	1.12	4 12 2.3	50.285
3000	1.16	4 12 9.1	50.263

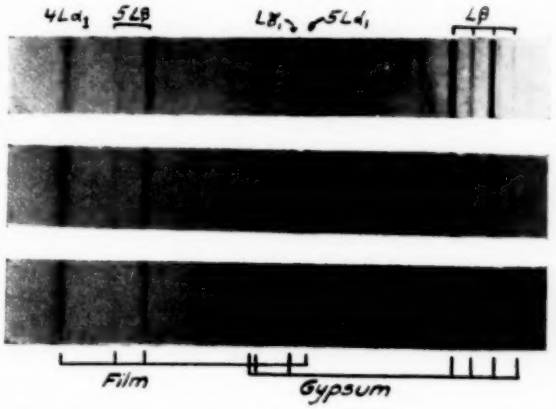

FIG. 2. Tungsten L series spectra from gypsum and films of 301 (upper), 1100 (middle), and 3000 (lower) layers.

the color of the films it was evident that those films failing to produce good spectra had a higher copper content than did the others. To check the effect of the copper, more films were used, some with no copper content and some with as much copper as they would take. A comparison of the spectra showed that the only apparent effect was a change in the spacing in the films.

The distance between the $L\alpha_1$ line from the molecular film and the $L\gamma_1$ line from the crystal on a given photographic plate was measured by a Dershem photoelectric photometer.[4] A graph of the intensity of blackening as a function of the distance along the plate located accurately the position of each line. Since the angle of reflection for the $L\gamma_1$ line was known, the angle of reflection of the $L\alpha_1$ line was thus determined without the use of spectrometer angle readings. The grating space of the film was then computed from Bragg's equation $n\lambda = 2d \sin\theta$ without correction for the index of refraction. Table I shows the distance between the two lines, the corresponding angle of reflection of the fifth order tungsten $L\alpha_1$, line and the apparent grating space of each film.

The results indicate that the spacing is the same for the different films, since there is a maximum difference of but 0.056 percent between the mean apparent value of d and its value for any one film. This difference may be due to the method of building, since, as indicated above, the spacing changes with the amount of copper present in the film.

Photometer curves of the fifth-order tungsten

[4] Elmer Dershem, Rev. Sci. Inst. **3**, 43 (1932).

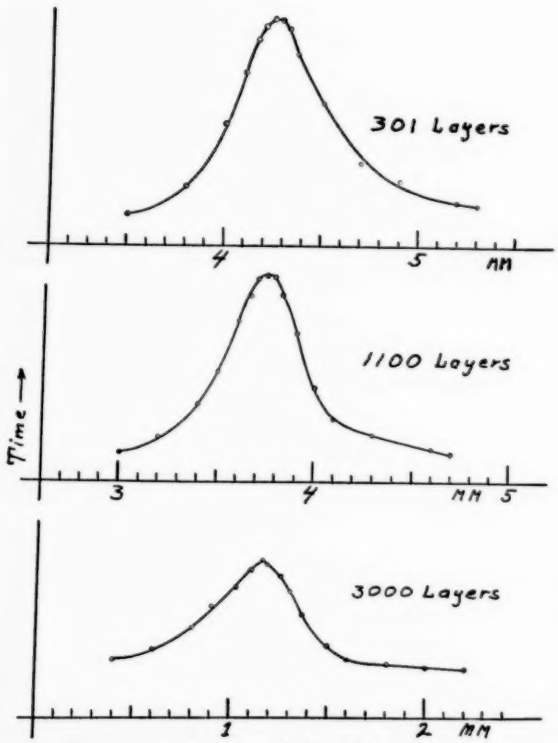

FIG. 3. Photometer curves of the fifth-order $L\alpha_1$ line of tungsten from barium-copper-stearate films.

$L\alpha_1$ line from the 301, 1100, and 3000-layer films are shown in Fig. 3 in which the distance along the photographic plate is plotted as abscissa and the time for a given electrometer deflection as ordinate. These curves show the line to be asymmetrical as diffracted by the films, but their sharpness indicates that the reflecting planes are quite regular and definite. However, curves from the second 1100-layer film and from the 1900-layer film showed small irregularities. With approximately the same exposure conditions the intensities of the lines from the different films were found to be roughly the same. This indicates that the upper layers only are effective in reflecting the x-rays.

The films were built on the optically flat surfaces of glass with a thick portion on the outer parts of each plate and 100 layers in the center. The distance from the surface of the thick part of the film to the surface of the 100-layer part was measured by means of a Michelson interferometer with the 5460.7A line of mercury as the source of light. This method of building the film was to prevent a difference in phase change in the light reflected from the two surfaces of the film. The fringes were very clear and quite straight across each part of the film except at the outer edges, where they were irregular. The thickness of each film was measured several hundred times. Thus it was possible to obtain the apparent thickness to the nearest hundredth of a fringe. With the 3000-layer film there were 25.73 fringes. The accuracy was then approximately 1/26 percent. Such measurements of the 1100-, 1900-, and 3000-layer films gave the spacing of the molecular layers as 24.26A, 24.27A, and 24.23A, respectively. From earlier work[2] it was expected that the heads of the molecules in alternate planes would act as the reflecting planes. Therefore the grating spaces would be twice the above values. In the case of the 3000-layer film, on which the measurements were most reliable because its thickness was greatest, the value of the grating space would be 48.46A. This value is 1.8A, or 3.6 percent less than the spacing found from x-ray measurements given in Table I.

To check some possible sources of error, which might cause the wide discrepancy between the spacing measurements as determined by optical and x-ray methods, the following experiments were tried: (1) X-ray photographs were taken with the film in air and in a vacuum. The spacing was the same for the two conditions. (2) Onto one of the films Mr. Bernstein evaporated a layer of aluminum to eliminate any possible phase-change difference in the reflection of the light from the thick and thin portions of the film in the interferometer measurements. The aluminum film caused no change in the relative positions of the fringes across the boundary lines. (3) The possibility of a phase change error was also eliminated

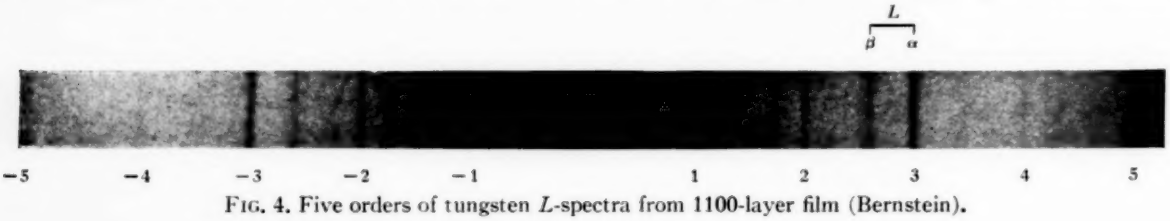

FIG. 4. Five orders of tungsten L-spectra from 1100-layer film (Bernstein).

by computing the spacing for 1900 layers from the difference in the number of fringes for the 1100-layer and the 3000-layer films. This measurement yielded the grating space as 48.36A, a value in fairly good agreement with the direct measurement of the 3000-layer film. (4) Photographs were taken with two films in which all the molecules were oriented in the same direction, i.e., the films were of the "*x*" type as described by Dr. Blodgett.[1] If the molecular layers were deposited one on another in discrete sheets, an x-ray grating space of about 24A, corresponding to the length of a single molecule, would be expected. Actually a grating space of about twice this magnitude was found, just as for the other type of film.

Thus it becomes evident that the optical measurement of the spacing of the molecular layers of these films does not yield the x-ray grating space. In a preliminary report of these measurements[5] an error in identification of a spectral line led to the opposite conclusion, that the optical and x-ray spacings were consistent. The fact that the x-ray spacing has a fixed value, which differs from the increment in thickness of each added double layer would seem to imply that this spacing is due to a crystalline arrangement of the molecules within the film.

In the x-ray determination of the grating space given above it was assumed that the index of refraction of the film was unity. Fig. 4 shows a photograph by Mr. Bernstein of five orders of the *L* spectrum of tungsten from a 1100-layer film, on each side of the primary beam. From this photograph he has determined the apparent values of the grating space and the index of refraction. The apparent values of *d* for the first, second, third, fourth, and fifth orders are 49.11A, 50.07A, 50.19A, 50.23A, and 50.30A, respectively. The unit decrement of the index of refraction is 5.1×10^{-6}. The agreement between this more directly measured value of 50.30A for the fifth order and the more precise mean value of 50.26A obtained above by comparison with the position of the $L\gamma_1$ line from gypsum confirms the validity of the method we have used. When the correction of 0.05A for the index of refraction is made, the x-ray measurements yield 50.35A for the true grating space as based on the crystal wave-length standard, or 50.47A as based on the ruled grating standard.[6] The latter value was computed by using Bearden's weighted average of 1.00248 as the ratio between the ruled grating and crystal wave-length values.[7]

It may be noted that the theoretical calculation of the unit decrement from dispersion theory[8] yields but 3.4×10^{-6} for the tungsten *L* spectrum, a value some 33 percent less than the experimental value. The correction for refraction in the film is in any case a minor one and does not alter the conclusions drawn above.

A final point of interest in the study of the films is that the spacing increases with age. The optical measurements show that in five months the spacing in the 1100-layer film increased by 0.22 percent, and that in the 3000-layer film increased by 0.45 percent. This suggests that the molecules probably reorient and adjust themselves in a more nearly crystalline arrangement. The use of such a film as a crystal for x-ray work thus necessitates completing the experiment within a relatively short time, or aging the film for a time sufficient to permit final orientation of the molecules.

The results of this investigation indicate that (1) most films prepared by this method show definite crystalline arrangement of the molecules with the spacing of the layers the same for all films of the same composition, but some films fail to show any such definite arrangement of the molecules; (2) thin films are as effective as thick ones in diffracting x-rays; (3) the thickness of the film increases with age; (4) the reflecting planes are not provided by the method of building, but are probably due to crystalline arrangement of the molecules in the film.

The writer wishes to express his thanks to the following people for their help in completing this experiment: To Professor A. H. Compton for suggesting the problem and guiding the work; to Dr. Katharine B. Blodgett for much time and labor spent in building the films; to Dr. Elmer Dershem and Professor G. S. Monk for valuable help in the mechanical aspects of the problem; and to Mr. Seymour Bernstein for his helpful collaboration.

[5] Clifford Holley, Phys. Rev. **51**, 1000 (1937).

[6] In a preliminary report (Clifford Holley and Seymour Bernstein, Phys. Rev. **52**, 525 (1937)) these values were given as 50.31A and 50.43A, respectively.

[7] J. A. Bearden, Phys. Rev. **48**, 385 (1935).

[8] A. H. Compton and S. K. Allison, *X-Rays in Theory and Experiment*, p. 496.

Focusing of an X-Ray Beam by a Rocksalt Crystal

R. M. Bozorth and F. E. Haworth
Bell Telephone Laboratories, Inc., New York, N.Y.

(Received February 14, 1938)

A single crystal of rocksalt (halite) has been bent plastically and cut so that x-rays of a narrow range of wave-lengths coming from the focal point of the x-ray tube, are focused at another point. In this way the divergent beam from the x-ray tube (about 6° divergence) is monochromatized and concentrated so that the intensities of the Fe $K\alpha$ lines are about 30 times as great as when monochromatized by reflection from a plane crystal. The point of focus was placed on the reflection circle of a Seeman-Bohlin focusing camera and powder photographs were taken, the advantage over the usual arrangement being that the background (due to undesired wave-lengths) is much diminished without any serious loss of intensity in the lines.

Introduction

In recent years a number of curved crystal x-ray spectrographs have been constructed and used for determining wave-lengths and widths of x-ray spectrum lines. So far, however, little attention has been paid to the application of curved crystals to the study of the structure of materials by x-ray diffraction, although Cauchois[1] has pointed out the advantages of monochromatization and of reduced exposure time which may result from the use of curved mica sheets.

DuMond and Kirkpatrick[2] suggested as early as 1930 that improved focusing may be obtained by both bending and cutting a crystal. Later, independently, Johansson[3] made the same suggestion and built a spectrograph employing a quartz crystal bent and cut in appropriate manner.

We have now adapted this principle to powder photograph technique and have produced an intense beam of x-rays which contain a narrow range of wave-lengths and converge to a sharp line focus. This has been accomplished by using a curved crystal of rocksalt. A thin piece is cleaved and is bent plastically under water to the required radius. Then on the concave side is ground a surface of half the radius, the ground surface is etched away and the crystal is ready for use.

This method has several advantages over those previously used. The crystal can easily be obtained and prepared; no difficult cutting and grinding are required as with quartz. Any reasonable thickness of crystal can be bent with as small a radius of curvature as desired. It can be mounted without being held in a form, since it has "set" after plastic deformation. The reflecting power is large because all of the atoms reflect in phase and because the crystal is "imperfect" in the Darwin sense, and the absorption is relatively small because the atoms are relatively light and the rays are reflected from the surface rather than transmitted through the whole crystal.

Preparation of the Crystal

The crystal was cleaved from a single crystal cube of unknown origin, weighing about 200 grams. A section $3.3\times1.7\times0.24$ cm^3 was selected and bent as follows. A metal form was prepared as shown in Fig. 1, with one convex and one concave cylindrical surface each having a radius of curvature of 20 cm. The form and crystal section were immersed in a concentrated solution of sodium chloride and the crystal surfaces rubbed several times with the fingers. The crystal was then placed in the form as shown, a piece of paper placed between the crystal and the concave surface of the form, and the screws tightened with considerable pressure while still in the solution. The screws were then loosened and the crystal wiped dry. The concave surface of the crystal was ground to a radius of 10 cm by rubbing it on emery paper stretched over a metal form of that radius. After this the surface was etched with water until the crystal became transparent, and it was then mounted by sticking the convex side to a rod with beeswax.

[1] Y. Cauchois, Comptes rendus **195**, 228 (1932).
[2] J. W. DuMond and H. A. Kirkpatrick, Rev. Sci. Inst. **1**, 88 (1930).
[3] T. Johansson, Zeits f. Physik **82**, 507 (1933).

Measurement of Intensities and Crystal Perfections

Figure 2 shows the relative positions of the x-ray tube, crystal and focus, for perfect focusing after reflection in the second order from (100) planes ($\theta = 20.1°$). A Philips structure research tube with an iron target was used, and the crystal was adjusted to reflect the $K\alpha$ radiation from the line source, as follows. A fluorescent screen was placed at A and the crystal rotated until the $K\alpha$ radiation was most intense. The reflection so obtained was spread over a band of a few millimeters width and usually was not uniform over this band. The crystal was then moved nearer or farther from the x-ray tube and the crystal again rotated into the reflection position, and this continued until the band attained a maximum of uniformity and intensity showing that the source of x-rays and the surface of the crystal lay on the same circle.

The intensity at the focus obtained with the arrangement of Fig. 2, was compared with that obtained when a plane cleaved crystal, from the same specimen as the bent crystal, was substituted for the bent crystal. In order to be able to compare this intensity ratio with what would be expected theoretically, measurements were made of the widths of the source of x-rays and the beam at the point of focus after reflection from the crystal, of the crystal perfection of the bent and the straight crystals, and of the integrated intensities from the plane crystal and a small portion of the bent crystal.

Size of source of x-rays

A pinhole photograph of the target was taken with a pinhole about 0.05 mm in diameter and showed an image 1.5 cm long and about 0.3 mm wide. A better value of the width was obtained

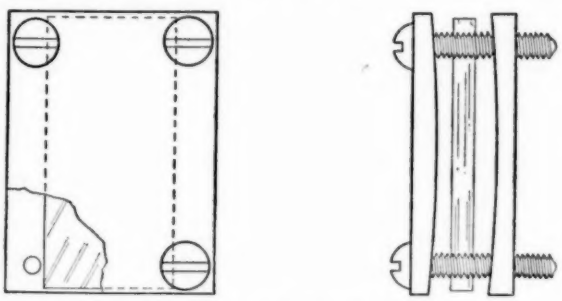

Fig. 1. Form for bending rocksalt crystal.

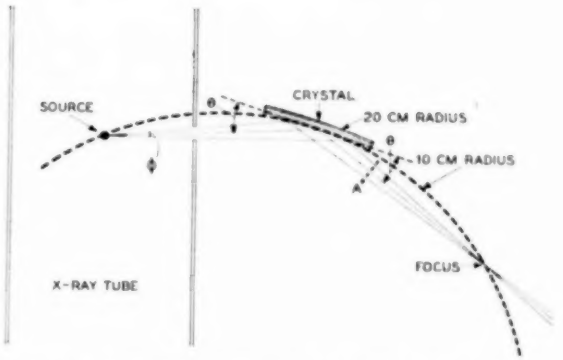

Fig. 2. Focusing arrangement for bent cut crystal.

with a slit 0.02 mm wide placed parallel to the line source of x-rays. The size of the slit was determined by exposing a fine grained plate placed just beyond the slit and measuring the image with a microscope. The width of the image on a plate placed 10 cm behind the slit (20 cm from the target) was measured with a microphotometer because its edges were not sufficiently sharp for good microscopic determination. When a scanning slit of 0.02 mm was used the width of the microphotometer curve at half-maximum intensity was 0.27 mm, and this is equal to the width of the source of x-rays as viewed from a point in the middle of the diverging x-ray beam. The divergence of the beam was found to be 5.7° or 0.10 radian.

Width of focus of x-ray beam

The width of the focus of the $K\alpha$ lines was also determined by microphotometering a photographic plate. The narrowest part of the reflected beam was determined by trial; a series of photographs was taken by displacing the plate between exposures, 0.2 mm in the direction of the beam and about 1 cm at right angles thereto. The width so determined was 0.25 mm at half-maximum intensity, equal within the experimental error to the width of the x-ray source, although the distribution of intensity over the cross section is more uniform at the source than at the focus.

Perfection of straight and bent crystals

The cleavage surface of the original crystal was apparently more perfect than average. A carefully cleaved specimen was placed in a beam limited by a single 0.1 mm slit and a photographic plate placed in the reflected beam 100 cm from

the crystal with the crystal set so as to give maximum intensity of reflection. This showed apparent resolution of the $K\alpha$ doublet but not nearly as good resolution as that obtained with etched quartz under the same conditions. A microphotometer curve showed a minimum between the α_1 and α_2 lines 67 percent of the height of the α_2 maximum. From this and the known shape of the lines[4] it was estimated that the angular range of the mosaic elements was about 30″ (between half-maximum points). This is considerably less than the usual width[5] of about 400″ but greater than the 14″ observed by Renninger.[6] The integrated intensity was determined in arbitrary units by microphotometering and was 63 percent of that of a similar surface that had been ground with fine emery paper.

The perfection of the cut bent crystal could not be estimated in the same way as the straight crystal because of its focusing properties. It was therefore set so as to reflect general radiation having wave-lengths lying between those of the α- and β-radiation, and the width of the reflected band measured at the point of focus. The angle this length (0.63 mm) subtends at the center of the crystal is twice the angular range of the mosaic (at half-maximum). The mosaic range was thus found to be 17′ (0.0050 radian).

The percent reflection of the relatively perfect crystal was measured roughly by successive reflection from two similar crystals. The first crystal was set for maximum reflection with a fluorescent screen. The second crystal was placed in the once-reflected beam parallel to the first crystal and the reflection from it could also be observed with a fluorescent screen after resting the eyes. From exposures taken with the plate between the two crystals and beyond the second it was estimated that the intensity for the latter position was 15 percent of that for the former.

For use in calculations to be discussed later it was desired to know the integrated reflection of the $K\alpha$ doublet from the bent crystal when it was in a nonfocusing position. It was assumed that this integrated reflection was the same as that which would be given by a plane crystal having the same mosaic structure with respect to its surface as the curved crystal had with respect to its atomic planes. To measure this the crystal was turned as shown in Fig. 3 and set for maximum intensity of reflection around the vertical axis. The single slit near the crystal was 0.3 mm high. The image on the plate P was microphotometered across the densest part of the line and the area under the density *vs.* distance curve compared with that measured when the crystal having the good cleavage surface was substituted for the bent crystal and the reflected x-rays allowed to fall for the same length of time onto another portion of the same plate. According to the results, the integrated intensity of the curved crystal was 2.2 times that of the relatively perfect crystal which was the same specimen as that referred to above.

The perfection of bending

If the crystal of rocksalt were bent uniformly at all points, a fluorescent screen placed at A in Fig. 2 would show a uniform illumination across the band. Actually some nonuniformity was observed, and to measure this a plate was placed in the reflected beam 20 cm beyond the focus. The band is thus spread out to a width of about 2 cm, and the intensity of each element of the width is proportional to the reflecting power of the corresponding portion of the crystal. The photograph is reproduced in Fig. 4(a), and the density curve across the image, obtained by microphotometering, is shown in Fig. 4(b). Although the nonuniformities are easily detected by eye, the density curve shows that the total intensity is 64 percent of that which would have been attained if each point of the crystal had reflected with maximum intensity. Presumably then the curved crystal reflects more than half as intensely as it would if perfectly bent. This will be discussed more in the next section.

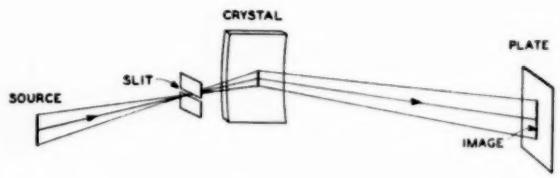

FIG. 3. Measurement of mosaic spread in curved crystal.

[4] L. G. Parratt, Phys. Rev. **44**, 695 (1933); and reference 8, second citation.
[5] R. M. Bozorth and F. E. Haworth, Phys. Rev. **45**, 821 (1934) and other literature there cited.
[6] M. Renninger, Zeits. f. Krist. **89**, 344 (1934).

"Berg" photographs

To show the perfection of the cleaved crystals as compared with more imperfect crystals of rocksalt and with more perfect crystals of quartz, photographs were taken similarly to those of K. Berg,[7] as shown in Fig. 5. The nonuniformity in the orientations of the mosaic elements in the more imperfect rocksalt crystal is well marked. The difference between the more perfect rocksalt crystal and the quartz crystal is not brought out by this method.

Intensities from straight and bent crystals

The integrated intensity at the focus of the beam reflected from the bent crystal, was compared with the beam reflected from the most perfect of the cleaved specimens. The bent crystal was placed as shown in Fig. 2, the straight crystal was placed later in the same position, and the plate was placed at the position of the focus of the bent crystal. After several trials, the perfect crystal was exposed 30 times as long as the bent crystal, and microphotometric measurements of the integrated intensities across the middle of the lines showed them to be equal, within one percent, for equal x-ray tube space-currents and voltages. Thus the intensity of the beam from the bent crystal was 30 times that from the relatively perfect plane crystal.

FIG. 4a.

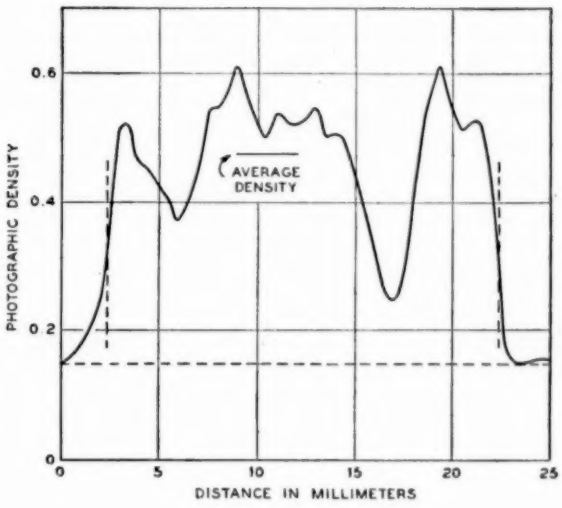

FIG. 4b.

FIG. 4. Photograph (and microphotometer record) of beam in off-focus position (see Fig. 2).

POWDER PHOTOGRAPHS WITH BENT CRYSTAL

To test the value of the bent crystal for structure investigations, the arrangement of Fig. 6(a) was used. The point of focus of the rays coming from the bent crystal was placed on the circumference of the "reflection circle" of radius 8 cm, on which lie also the specimen and the film. Well defined reflections from the (311) and (220) planes were visible after an exposure of one minute of a specimen of annealed permalloy, which was rotated during exposure.

To compare the intensities of the lines and the diffuse background with those secured with the usual arrangement, photographs were taken[8] as shown in Fig. 6(b) with a 0.2 mm slit placed as close as possible to the tube. Microphotometry showed that for equal exposure times of 17 minutes the integrated intensity of the (311) lines (α doublet) was 0.67 as great with the method of Fig. 6(a) as with that of Fig. 6(b). The maximum photographic densities were respectively 0.31 and 0.43 above background.

The great advantage of the method of Fig. 6(a) is the low intensity of the diffuse background. In the photograph taken with the curved crystal, the back ground is only one-eighth as intense as that in the photograph taken by the more usual method. The actual densities observed were 0.154 and 0.020 above those of the unexposed portions of the films.

It should be pointed out that a larger portion of the permalloy specimen was illuminated by the

[7] K. Berg, Naturwiss. **19**, 391 (1931).
[8] F. E. Haworth, Bell Lab. Record **16**, 66 (1937) and Phys. Rev. **52**, 613 (1937).

x-ray beam in the arrangement of Fig. 6(a). This is because the whole divergence of the beam from the x-ray tube could here be used, whereas in the arrangement of Fig. 6(b) the divergence is limited by the width of the slit and of the focal spot of the target. This difference is a consequence of the geometry of the tube. The width of the specimen covered by the beam was 1.6 cm in the one case and 0.2 cm in the other.

Limit of Intensity Attainable

DuMond and Kirkpatrick[2] have given the conditions for perfect focusing for both reflecting and transmitting types of bent and cut crystals. For the former type the radius of curvature, R, of the reflecting planes must be twice the radius of curvature r, of the surface of the crystal. Johansson[3] has taken into account the change in lattice spacing throughout an *elastically* bent crystal of thickness, t, and shown that the condition for perfect focusing is

$$R=2r+t/2,$$

the circle of radius r passing through the source and focus and bisecting the crystal. For a *plastically* bent crystal, however, the elastic stresses are negligibly small and the condition is simply $R=2r$, and the reflecting surface is placed on the reflection circle.

The intensity of reflection from the bent crystal is obviously dependent upon the length of crystal illuminated, the reflecting power of each element of crystal, the size of the x-ray source in relation to the mosaic structure of the crystal, and the perfection of the bending and cutting. As shown in Fig. 7(a), let W be the width of the source of x-rays and consider the reflection from some point near the center of the crystal. At this point reflection will take place from all points of the source provided the angle, τ, subtended by the source is smaller than the angular range, ϵ_b, of the mosaic structure. Experimentally, as described above, ϵ_b was found to be 0.0050 radian and

$$\tau=W/(2r\sin\theta)$$

was 0.0039 radian. Thus if the bending has been done uniformly and the cutting accurately, each point of the source should reflect from each point of the crystal surface. That the cutting has been done accurately is indicated by the fact that the focus is the same size as the source. That the bending has been done rather imperfectly is shown by the photograph reproduced in Fig. 4; this indicates that the loss in reflecting power due to this cause was about 36 percent.

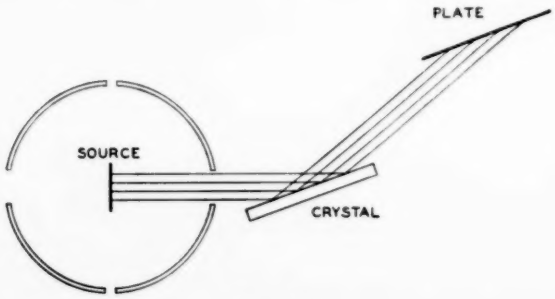

Fig. 5a.

Comparison with plane crystal

The integrated reflection from a stationary plane crystal is proportional to the width of the source, which determines the length of crystal that reflects, and may depend also on the mosaic structure of the crystal. As indicated in Fig. 7(b)

Fig. 5b.

Fig. 5. Method of investigating gross structure of surface layers of crystal, according to Berg, and photographs so taken of "perfect" quartz crystal, of relatively perfect rocksalt crystal, and very imperfect rocksalt crystal, respectively.

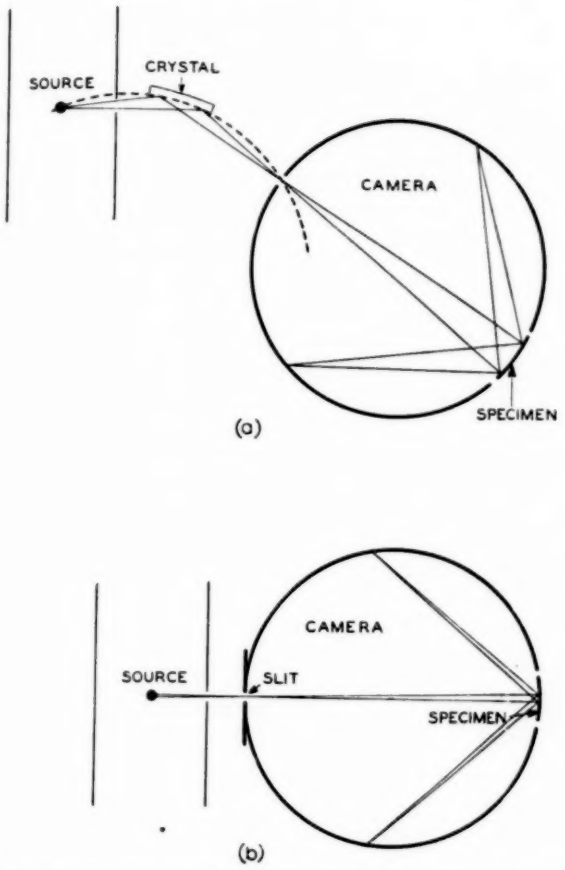

FIG. 6. Arrangements for taking powder photographs with and without curved crystal, for comparison.

the length, l_p, of crystal reflecting is

$$l_p = W/\sin\theta$$

equal in our case to $0.027/0.343 = 0.079$ cm. Since the mosaic range in the relatively perfect crystal used for the comparison of intensities was $\epsilon_p = 0.00015$ radian (30″) and the angle the source subtended at the center of the crystal is over twenty-five times this (0.0039 radian), the length of crystal reflecting is not appreciably affected by the mosaic structure.

We should expect the ratio of intensities reflected from the bent and plane crystals to depend on several factors. The most important of these is the ratio l_b/l_p. Another is the ratio R_b/R_p, of the integrated reflections from equal areas of surface of the bent and plane crystals; this is given by the ratio 2.2 determined as described in an earlier section. The remaining factor, f_b, takes account of imperfect bending and is the ratio of

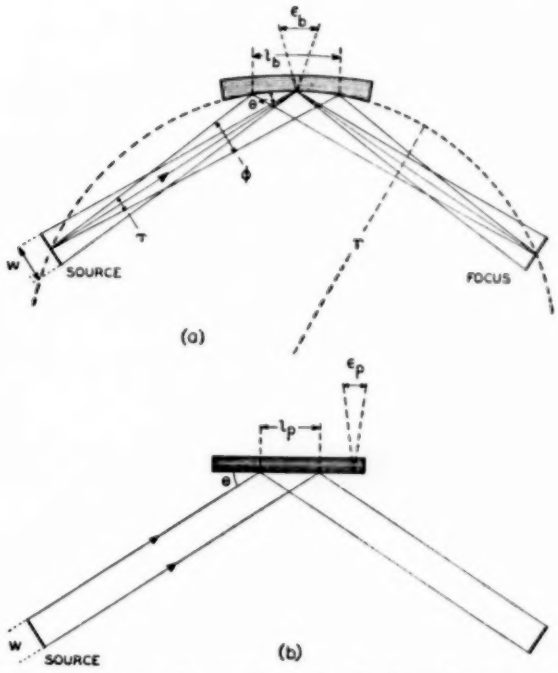

FIG. 7. Diagrams for analysis of reflections from curved and straight crystals.

the average to maximum intensity reflecting from different parts of the crystal, as derived from the photograph of Fig. 4. The value of f_b was 0.64. Thus the ratio of intensities, I_b/I_p, of reflection from the bent and plane crystals should be

$$I_b/I_p = (l_b/l_p)(R_b/R_p)f_b.$$

Using the appropriate values $l_b/l_p = 2\Phi r(\sin\theta)/W = 2\times 0.100\times 10\times 0.343/0.027 = 25$, $R_b/R_p = 2.2$, $f_b = 0.64$, we find that

$$I_b/I_p = 35.$$

This is in fairly close agreement with the ratio 30 determined by direct comparison of intensities as described above, and indicates that the factors affecting the ratio have been correctly chosen. The discrepancy may be due to the variation of R_b/R_p from point to point over the crystal surface.

This result indicates also that one cannot expect to increase the intensity of reflection from the bent crystal by a very large factor except by increasing the divergence of the beam and consequently the area of crystal covered. The factor f_b can be increased only 1.6 times, and the value of R_b can probably be increased in about the same ratio as judged from the work of Renninger.[6]

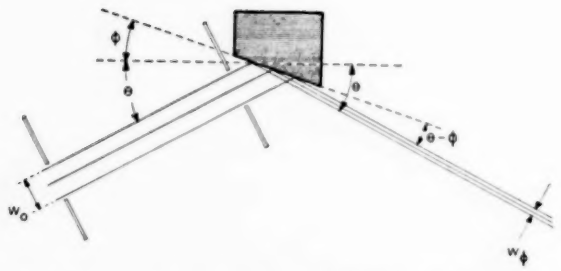

FIG. 8. Diagram for analysis of Fankuchen's method.

Fankuchen's method of concentration of an x-ray beam

Fankuchen[9] has suggested a method for monochromatizing and intensifying a beam of x-rays, which is depicted in Fig. 8. The surface of a crystal is cut at an angle to the reflecting planes such that the reflected beam makes a smaller angle with the surface than the incident beam does. Let θ be the Bragg angle, and Φ the angle the reflecting planes make with the surface upon which falls a parallel beam of width W_0. We are to compare the intensity and width of the reflected beam for any value of Φ with the intensity and width for $\Phi=0$. If the whole beam is reflected from the surface without absorption, the width of the reflected beam, W_Φ, may be made as small as desired by choosing a small enough value of $\theta-\Phi$. Then the ratio

$$W_0/W_\Phi=\sin\alpha/\sin\beta,$$

in which $\alpha=\theta+\Phi$ and $\beta=\theta-\Phi$ are the angles that the incident and reflected beams make with the surface, represents the advantage gained because it is equal to the power per unit width of reflected beam, as compared with that for $\Phi=0$.

But the absorption which actually occurs nullifies most of this advantage. Because of absorption the energy of the reflected beam is proportional[10] to

$$A_\Phi=\sin\beta/(\sin\alpha+\sin\beta).$$

The advantage of the method can be measured by the energy per unit width of reflected beam, compared with that for $\Phi=0$. With absorption this is

$$(W_0/W_\Phi)\cdot(A_\Phi/A_0)=2\sin\alpha/(\sin\alpha+\sin\beta).$$

The maximum value of this expression is 2, and occurs when $\beta=0$, or $\Phi=\theta$. Thus at best the intensity obtainable by this method of cutting is only twice that obtained by simply reflecting from a surface parallel to the reflecting planes, and is considerably less than that attained by the method we have described, using the rocksalt crystal.

Other materials

It is interesting to consider what other materials might be superior to rocksalt. It is desirable to have a plastic material that is made of compact atoms of relatively low average atomic number, and has widely spaced reflecting planes for which the crystal structure factor is large. Among such materials may be mentioned graphite, organic compounds, aluminum, magnesium, and possibly lithium fluoride. One of us (F.E.H.) has already used a bent cut crystal of quartz in which the reflecting planes are (101) instead of (100) as used (in the third order) by Johansson. Although the (101) planes reflect about three times as strongly as the (100) planes in the first order, and are by far the most strongly reflecting planes in quartz, the intensity of the beam focused by such a quartz crystal was much less than that focused by the rocksalt. This is probably due to the relatively great perfection and small structure factor of the quartz.

[9] I. Fankuchen, Nature **139**, 193 (1937).

[10] P. Debye and H. Menke, Ergeb. d. techn. Röntgenkunde, Leipsig **2**, 15 (1931).

Emission of Radiation in the Positive Column of a Mercury Arc

BENTLEY T. BARNES AND ELLIOT Q. ADAMS
Incandescent Lamp Department, General Electric Company, Nela Park, Cleveland, Ohio

(Received February 26, 1937)

Intensities, corrected for absorption, of the principal spectral lines of wave-lengths 2259 to 11,289A are given for 4-ampere mercury arcs operated at vapor pressures of 0.03, 20, 450, and 500 mm (Hg). The variation across the arc of the intensity per unit area is given for twenty of these spectral lines. Plots of spectral intensity data were made on two alternative hypotheses: (1) That the concentrations of atoms in excited states are in a Boltzmann equilibrium with one another and that transition probabilities are proportional to $w_{AB}/[\lambda^2(n_A^*+n_B^*)(n_A^*-n_B^*)^2]$, where w_{AB} is the Kronig *a priori* probability, λ is the wave-length of the emitted radiation, and n_A^* and n_B^* are the effective quantum numbers of the upper and lower levels; (2) that all downward transitions are radiative and that the rate of excitation to a given level is proportional to the product of the *a priori* probability of the level and the concentration of electrons with energies which do not differ from the minimum for excitation by more than a constant amount. A Maxwellian distribution of velocities was assumed. The method of plotting is such that, if either hypothesis were correct and if the corrections for absorption were of the proper magnitude, the points on the corresponding plot would all fall on a straight line. Characteristic deviations of the points from a linear relationship are found on each type of plot. Both types of plot indicate that the electron temperature varies little with distance from the axis. This is in disagreement with Elenbaas' theory of the mechanism of a high pressure mercury arc.

ELENBAAS has made an extensive study[1] of the characteristics of mercury arcs operating at pressures ranging from about 10 mm to 760 mm (Hg). He has concluded that many of the characteristics of the discharge can be explained by assuming a Boltzmann-Saha equilibrium between electrons, normal atoms, excited atoms and ions. He assumes that the electrons have a Maxwellian distribution of velocities with an electron temperature approximately the same as the gas temperature. The variation of the gradient with tube diameter, pressure and current computed from this theory agrees well with experimental results. The measured intensities of spectral lines are also in fair agreement with the theory. However, the comparisons with calculated values are limited to three lines, of which only one was actually measured, and no corrections for absorption were made. A more extensive study of the emission of radiation in mercury arcs seemed desirable. Accordingly, a series of measurements on mercury arcs operated at vapor pressures of 0.03, 20, 450, and 500 mm (Hg) was made in this laboratory.

SET-UP AND METHODS

One experimental set-up used in this investigation is shown in Fig. 1. The quartz lens L is set at its principal focal distance from the entrance slit of the monochromator. If the slit height is small compared to the focal length of the lens, this optical system transmits only rays which are approximately parallel to the optical axis when they strike the lens. By manipulating the shutters S, radiation from only tube B, or from both tubes, may be allowed to enter the monochromator. The diaphragm D determines the cross-sectional area of the beam of radiation received from the tubes A and B: to obtain radiation from the entire width of the arc, a diaphragm 2 cm wide and 1.3 cm high was used; to obtain a narrow beam of radiation from some portion of the arc, a diaphragm 2.3 mm wide was used.

The dispersing instrument for the radiation measurements was the quartz double monochromator previously described.[2] This made it possible to measure the weaker lines in the spectrum without appreciable error from stray radiation. The receiver for the intensity measurements was a calibrated photoelectric tube: a "bubble-window" sodium tube for ultraviolet or a caesium tube for visible and infra-red radiation.

The discharge tubes were of Corning No. 972 glass ("high transmission" Corex) and the bubble windows (W) were only 3 to 7 mils thick at the center. The average transmission per window determined on one tube was 0.81 for λ11289,

[1] W. Elenbaas, Physica **1**, 211, 673 (1934); **2**, 155, 169 (1935).

[2] W. E. Forsythe and B. T. Barnes, Rev. Sci. Inst. **4**, 289 (1933).

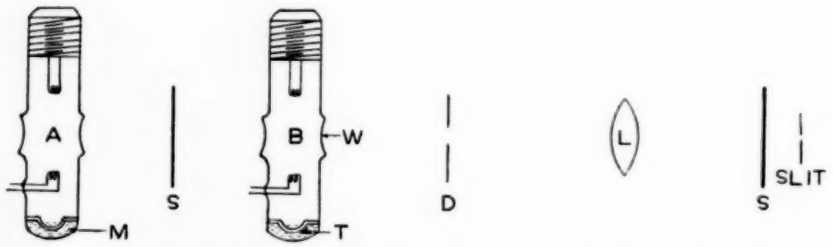

FIG. 1. Diagram of set-up. *A* and *B*, mercury vapor discharge tubes; *W*, thin "bubble" window; *M*, mercury pool; *T*, thermocouple tube; *D*, diaphragm; *L*, lens; *S*, shutter.

0.55 for λ5461, 0.22 for λ2967, and 0.06 for λ2259. The losses at the windows are rather large. They probably are due chiefly to scattering caused by striations and to absorption and scattering by material evaporated or sputtered onto the windows from the electrodes. Another tube had a transmission for λ2259 of 0.54 per window when new and 0.22 after several long runs.

Both electrodes in each tube were oxide-coated tungsten spirals which could be heated by means

TABLE I. *Spectral radiant intensities for positive column of 4-ampere* Hg *arc in tube 36* mm *in diameter. Also spectral transmittance of vapor along radius of tube for radiation from a similar tube.*

Nominal Wave-length	Lines and Transitions			Argon Press. 5 mm at 25°C			None		
				Hg Press (mm) 450	20	0.030	20	500	500
				Arc Voltage 51	23	10.6	17	49	49
				Milliwatts per Steradian per cm Arc					Transmittance
11289A	11289 $7^3P_2-7^3S_1$			9.5	0.35	0.3		9.6	0.93
10140	10140 $7^1S_0-6^1P_1$			32.	2.31	1.26	1.96	39.	.90
7087	7092 $8^3P_0-7^3S_1$	7082 $8^3P_1-7^3S_1$		0.22	.020			.29	.90
6907	6907.5 $8^3P_2-7^3S_1$			.086	0.05		.03	1.03	.90
6716	6716 $8^1P_1-7^1S_0$			0.11	.017			.14	.93
6234	6234 $9^1P_1-7^1S_0$			0.12				.10	.95
5780	5770 $6^3D_2-6^1P_1$	5790 $6^3D_1-6^1P_1$	5791 $6^1D_2-6^1P_1$	89.	5.0	0.87	2.38	89.	.81
5461	5461 $7^3S_1-6^3P_2$			133.	22.1	4.3	12.2	133.	.58
4916	4916 $8^1S_0-6^1P_1$			0.56	0.10			1.17	.86
4358	4358 $7^3S_1-6^3P_1$			112.	21.	3.05	10.1	111.	.54
4078	4078 $7^1S_0-6^3P_1$			7.0	0.51		.79	8.8	.70
4047	4047 $7^3S_1-6^3P_0$			67.	12.8	1.78	5.4	73.	.56
3906	3906 $8^1D_2-6^1P_1$	3902 $8^3D_2-6^1P_1$	3904 $8^3D_1-6^1P_1$	0.95	0.06			1.35	.82
3654	3650 $6^3D_3-6^3P_2$	3655 $6^3D_2-6^3P_2$ 3663.3 $6^1D_2-6^3P_2$	3662.9 $6^3D_1-6^3P_2$	123.	9.5	1.44	3.40	145.	.70
3341	3341 $8^3S_1-6^3P_2$			10.5	0.90	0.07	.29	11.8	.70
3129	3125.7 $6^3D_2-6^3P_1$	3131.6 $6^3D_1-6^3P_1$	3131.8 $6^1D_2-6^3P_1$	88.	9.5	1.53	3.79	110.	.61
3022	3021.5 $7^3D_3-6^3P_2$	3023.5 $7^3D_2-6^3P_2$ 3027.5 $7^1D_2-6^3P_2$	3025.6 $7^3D_1-6^3P_2$	33.	1.94	0.14	.69	41.5	.71

of step-down transformers with two insulated secondary coils. All of the data for this article were taken on d.c. with only the cathode heated. In some cases external heating of the cathode was used only in starting the arc.

The temperature of the mercury pool in each tube was determined by means of a thermocouple threaded through the tube, T (Fig. 1), which dips into the mercury pool, M, at the bottom of the lamp. A furnace surrounding the lower part of each lamp made it possible to raise the vapor pressure at will. The upper part of each lamp was wrapped with asbestos tape to make it hotter than the mercury pool when the arc was in operation. This kept the windows free of condensed mercury and made the temperature of the mercury pool a reliable measure of the vapor pressure.

Ordinarily both tubes were operated at the same pressure and current. Tube A (Fig. 1) was kept in a fixed position with its axis intersecting the axis of the optical system. Tube B was mounted on a slow-motion screw so that it could be moved sidewise (perpendicular to plane of Fig. 1). Tube A was used as a source for determining the absorption of tube B. These absorption data were used to correct the spectral intensity data taken on tube B for the effect of absorption by the vapor and the thin window. This was done by dividing the measured inten-

TABLE I.—*Continued.*

Nominal Wave-Length	Lines and Transitions			Argon Press. 5 mm at 25°C			None		
				Hg Press (mm) 450	20	0.030	20	500	500
				Arc Voltage 51	23	10.6	17	49	49
				Milliwatts per Steradian per cm Arc					Transmittance
2967A	2967 $6^3D_1-6^3P_0$			19.5	2.7	0.42	1.07	22.6	0.68
2925	2925 $9^3S_1-6^3P_2$			1.75	.077	.010		1.91	.85
2894	2893.6 $8^3S_1-6^3P_1$			7.5	.52	.07	.225	9.2	.66
2804	2803.5 $8^3D_3-6^3P_2$	2804.5 $8^3D_2-6^3P_2$	2805.3 $8^3D_1-6^3P_2$	11.	.58	.03	.22	15.0	.81
		2806.7 $8^1D_2-6^3P_2$							
2753	2753 $8^3S_1-6^3P_0$			3.6	.20			4.7	.71
2699	2698.8 $9^3D_3-6^3P_2$	2699.4 $9^3D_2-6^3P_2$	2699.8 $9^3D_1-6^3P_2$	3.8	.18		.11	5.8	.82
		2700.8 $9^1D_2-6^3P_2$							
2652	2652 $7^3D_2-6^3P_1$	2654 $7^3D_1-6^3P_1$	2655 $7^1D_2-6^3P_1$	24.	1.21	.14	.69	35.	.64
2576	2576 $9^3S_1-6^3P_1$			1.25	.10			2.3	.78
2537	2535 $7^3D_1-6^3P_0$	2536.5 $6^3P_1-6^1S_0$		48.	10.4	15.	7.0	56.	.55
2483	2482.0 $8^3D_2-6^3P_1$	2482.7 $8^3D_1-6^3P_1$	2483.8 $8^1D_2-6^3P_1$	7.4	.44		.29	13.8	.70
2464	2464 $9^3S_1-6^3P_0$			.62	.03			1.14	.72
2447	2447 $10^3S_1-6^3P_1$			.57	.03			.82	.75
2399	2399.4 $9^3D_2-6^3P_1$	2399.7 $9^3D_1-6^3P_1$	2400.6 $9^1D_2-6^3P_1$	2.8	.19			5.6	.72
2378	2378 $8^3D_1-6^3P_0$			2.6	.17			5.5	.68
2353	2352.4 $10^3D_2-6^3P_1$	2352.65 $10^3D_1-6^3P_1$	2353.2 $10^1D_2-6^3P_1$	1.33	.11			2.9	.72
2323	2323.0 $11^3D_2-6^3P_1$	2323.2 $11^3D_1-6^3P_1$	2323.6 $11^1D_2-6^3P_1$	.60	.05			1.42	.76
2302	2302 $9^3D_1-6^3P_0$			1.33	.03			3.1	.72
2259	2259 $10^3D_1-6^3P_0$			.53	.04			1.65	.68

TABLE II. *Spectral intensities per unit of projected area (microwatts per steradian per* mm² *) for positive column of 4-ampere* Hg *arc in tube 36* mm *in diameter.*

Partial Pressure of Hg	450 mm			20 mm			0.030 mm	
Nominal Wave-Length	On Arc Axis	5 mm From Arc Axis	8 mm From Arc Axis	On Arc Axis	5 mm From Arc Axis	8 mm From Arc Axis	On Arc Axis	10 mm From Arc Axis
11289	96	15.4	4.6				1.1	0.5
10140	388	71.	17.2	14.2	8.0	3.5	5.9	3.0
5780	780	150.	39.	17.5	11.	5.0	5.3	3.0
5461	1140	336.	97.	91.	50.	29.	23.6	14.2
4358	1090	297.	78.	91.	50.	29.	10.8	7.0
4078	56	11.6	3.8				.8	.47
4047	740	199.	48.	72.	41.	19.	8.3	5.3
3654	1720	315.	81.	74.	45.	20.	4.2	2.9
3341	156	33.7	12.3	5.7	4.0	2.2	.21	.12
3129	1140	231.	64.	69.	46.	22.	4.4	2.95
3022	530	84.	25.3	11.6	7.7	3.7	.39	.34
2967	268	52.	17.3	13.5	9.6	6.1	1.28	.82
2925	20	6.7	3.1				.017	.012
2894	98	21.3	7.2	4.4	2.6	1.3	.196	.115
2804	135	28.4	9.2	4.3	2.6	1.2	.078	.047
2652	372	75.	21.	13.8	7.9	3.9	.32	.18
2537	570	192.	86.				62.	50.
2483	119	24.3	7.2	4.6	2.6	1.0		
2399	62	13.	3.2					
2378	58	11.	2.9					

sities by the square root of the transmission of the entire tube for the beam from tube *A*. If the thin windows are identical and the absorption in the vapor is small (<10 percent), such a procedure is quite satisfactory.[3] If the absorption in the vapor is fairly high (>20 percent), changes in line contours cause the absorption per unit length to decrease as radiation passes through the vapor. This tends to make the above correction for absorption too small. On the other hand, for a strictly monochromatic portion of a spectral line, the average transmission of the vapor for radiation from an arc centered about the axis of the tube will be greater than the square root of the transmission of the entire width of the tube. Thus these two errors tend to counterbalance each other. Re-radiation of part of the absorbed energy at the same wave-length would tend to make the correction for absorption too large.

Spectral Intensity Data

Table I gives the intensities, corrected for absorption,[4] of the line radiation from the positive column of 4-ampere mercury arcs. The measured radiation came from a region midway between the electrodes. Each tube had an arc gap of 7 cm and an internal diameter of about 36 mm. The last three columns of this table give data on a tube containing only mercury vapor; the preceding three columns give data on tubes with 5 mm argon pressure (measured at 25°C with arc not running). The partial pressure of mercury vapor and the arc voltage are given at the top of each column. The arc voltage includes an electrode drop which is estimated to be between 6 and 20 volts. The data for 450 mm pressure are averages of intensities for two tubes; the values for 20 mm mercury pressure in a tube containing argon were obtained on only one of these tubes and those for 0.030 mm on the other one. For the weaker lines, approximate correc-

[3] Provided that relatively few of the downward transitions are radiative. If all downward transitions were radiative, there would be little or no correction for absorption in the vapor.

[4] Of both thin window and vapor, except for data for weak lines. In these cases, correction made only for absorption of thin window (measured with tube at room temperature). The absorption in the vapor for the weak lines is relatively small. This is shown by the last column of Table I which gives a rough approximation to the transmission, for radiation from a similar arc, of the vapor along a radius of the tube. These are data obtained on the tube without argon when it was operated at 4 amperes and 500 mm pressure. The values for the shorter wave-lengths are too low because the over-all transmission was divided by the transmission of the window at room temperature, instead of its transmission at operating temperature. The transmissions for all the lines of wave-lengths less than 2482A, except perhaps for λ2378, probably should be between 0.90 and 1.00.

tions for continuous radiation included in the measurements were made by subtracting from the deflection at the line setting the average of the deflections given by the continuous radiation and weak lines on the two sides of the line setting. These corrections were 70 to 85 percent of the original deflection for λ's 2576, 6234, 6716 and 7087, about 55 percent for λ2259 and less than 50 percent for all other lines.

In many cases several lines were included in a single measurement. Table I lists these lines, together with the corresponding transitions. The designations for the levels are those used by Bacher and Goudsmit.[5] The order of listing the terms corresponds to designation of term values as positive with respect to the ground state, as recommended by Condon and Shortley.[6]

The values in Table I represent radiation from the full width of the arc. Table II gives the intensity per unit area, treating the arc as if it were a flat emitting surface, for points at different distances from the axial plane of the arc which is parallel to the axis of the optical system. These data were obtained on the tubes containing argon and were corrected for absorption of the tube wall and of the vapor in the same manner as the data of Table I. They represent the summation of the radiation emitted along a diameter or some other chord of the tube.

Discussion

Table II shows the variation in intensity across a projected image of the positive column. However, this variation is roughly the same[7] as the variation along a radius of the amount of radiation emitted per unit of volume. To this degree of approximation, the data of Table II will represent the relative intensity of emission per unit volume at the axis of the arc and at different distances from the axis. If the laws governing the excitation of mercury atoms and the subsequent emission of radiation were known, the spectral distribution of the emitted radiation would indicate the distribution of electron velocities at these same points. If these velocity distributions are Maxwellian, they may be described completely by assigning an electron temperature to each of them.

If there is "natural excitation," i.e., if the concentrations of atoms in all the states[8] of a given level are equal, the emitted radiation is isotropic. If, in addition, the population of the lower level for a given line is so low that self-absorption may be neglected, the intensity (per steradian) of the line due to all transitions from level A to level B is given by

$$J_{AB}=(16\pi^3 c/3\lambda^4)N_A S_{AB} \qquad (1)$$

in which N_A = concentration of atoms in each state of the upper level, c = velocity of light, λ = wave-length of emitted radiation, S = strength of line, as defined by Condon and Shortley (reference 6, p. 98).

The intensity (per steradian) of a spectral line, expressed in terms of the oscillator strength f used in dispersion theory, is[9]

$$J_{AB}=(2\pi he^2/\mu\lambda^3)(2j_A+1)N_A f_{AB} \qquad (2)$$

where h = Planck's constant, e = electronic charge, μ = mass of electron, j = inner quantum number.

We shall introduce the quantity

$$\varphi_{AB}\equiv(2j_A+1)f_{AB}.$$

Then
$$J_{AB}=(2\pi he^2/\mu\lambda^3)N_A\varphi_{AB}. \qquad (3)$$

It is customary to assume that, within a multiplet, the "line strengths" S are proportional to the *a priori* probabilities of Kronig[10] for the corresponding transitions. In the article immediately following this one, reasons are given for assuming that φ_{AB} is proportional to the Kronig factors divided by some function of

Table III. *Relative a priori probabilities of transition in a two-electron atom.*

	$^1S_0$	$^1D_2$		
$^1P_1$	12	120		
	$^3S_1$	$^3D_1$	$^3D_2$	$^3D_3$
$^3P_0$	4	40		
$^3P_1$	12	30	90	
$^3P_2$	20	2	30	168

[5] *Atomic Energy States* (McGraw-Hill Co., New York, 1932).

[6] E. U. Condon and G. H. Shortley, *Theory of Atomic Spectra* (Cambridge University Press, 1935), p. 5.

[7] See article immediately following this one. Also, W. Elenbaas, Physica **1**, 680 (1934).

[8] The nomenclature is that used by Condon and Shortley; see reference 6, page 97–8.

[9] See reference 6, page 108.

[10] Kronig, Zeits. f. Physik **33**, 261 (1925). See Table III of the present article for the Kronig probabilities for Hg.

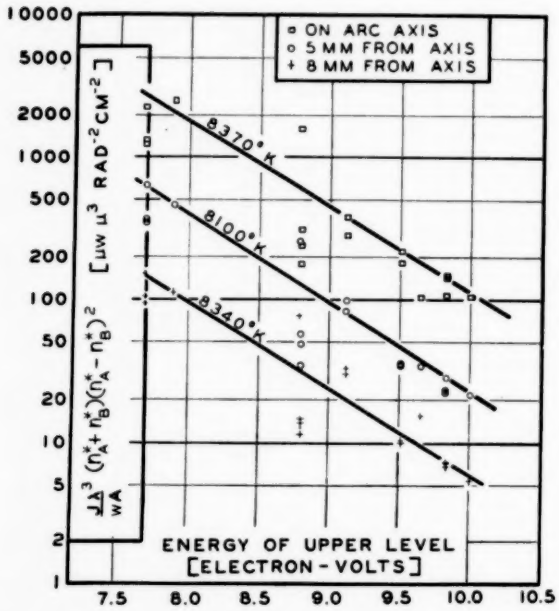

FIG. 2. Boltzmann plots of radiant intensity per unit of projected area at three different distances from arc axis for tubes containing argon. Each point represents a spectral line. (See Table IV.) Arc current 4.0 amperes; vapor pressure 450 mm. Ordinate is microwatts per steradian per cm² multiplied by cube of wave-length in microns and by indicated function of effective quantum numbers, and divided by *a priori* probability of transition as given by Kronig. Abscissa is energy, with respect to 6^1S_0, of upper level for corresponding transition. The computed electron temperature is written above each straight line.

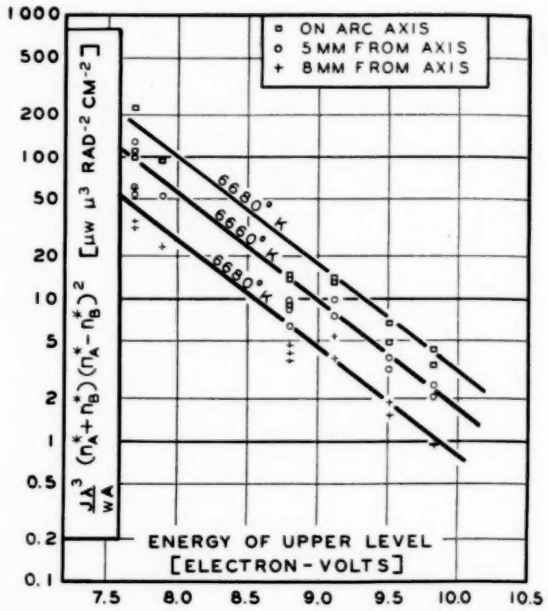

FIG. 3. Boltzmann plots of radiant intensity per unit of projected area at three different distances from arc axis for tubes containing argon. Arc current 4.0 amperes; vapor pressure 20 mm. Coordinates as in Fig. 2.

the effective quantum numbers of the upper and lower levels.

In case there is a Boltzmann equilibrium between electronic and atomic energies in an element of volume, then the concentration of atoms excited to state A would be

$$N_A = N_0 e^{-\epsilon V_A/kT} \qquad (4)$$

in which N_0 = concentration of atoms in ground state, ϵV_A = energy of excited state A with respect to ground level, k = Boltzmann constant, T = electron temperature. Since each level of the atom is composed of $2j+1$ states, the total population in the level is $(2j+1)N$.

Equations (3) and (4) give, for the case of a Boltzmann equilibrium and negligible self-absorption, $J\lambda^3 \propto \varphi e^{-\epsilon V/kT}$ or

$$\ln (J\lambda^3/\varphi) = \text{const.} - \epsilon V/kT. \qquad (5)$$

in this case, if $\log (J\lambda^3/\varphi)$ be plotted against ϵV, the points lie on a straight line, whose slopes is a measure of the electron temperature.

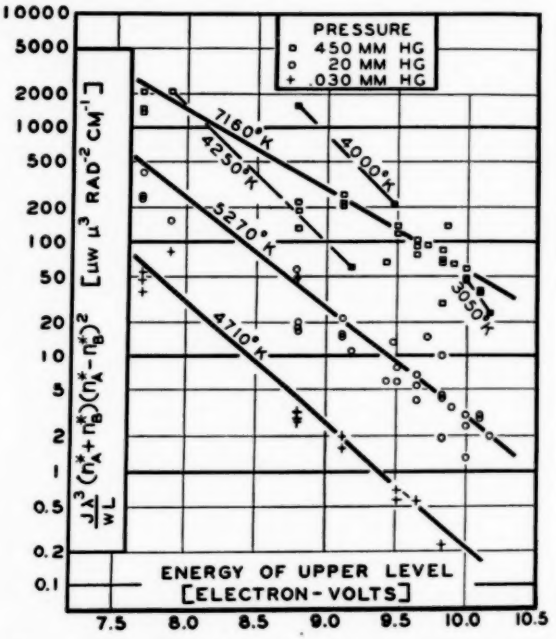

FIG. 4. Boltzmann plots of radiant intensity per unit length of arc for three different vapor pressures for tubes containing argon. Arc current 4.0 amperes. Ordinate is microwatts per steradian per cm of arc multiplied by cube of wave-length in microns and by indicated function of effective quantum numbers, and divided by *a priori* probability of transition as given by Kronig.

It is obviously impossible to isolate the radiation from an element of volume over which N_0

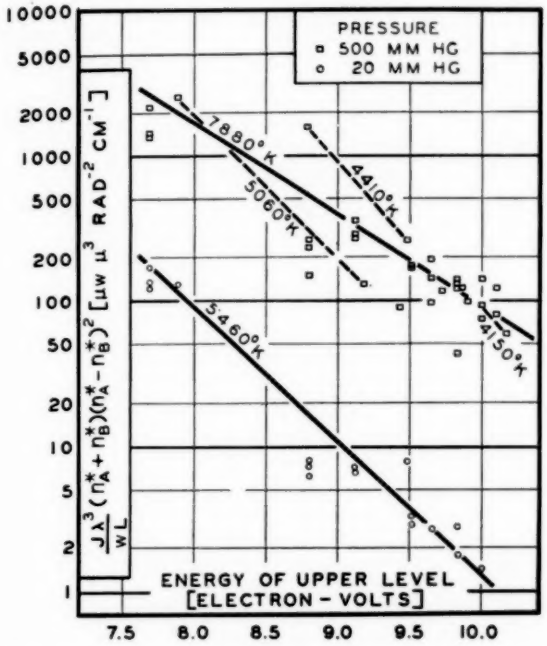

FIG. 5. Boltzmann plots of radiant intensity per unit length of arc at two different vapor pressures for tube without argon. Arc current 4.0 amperes. Ordinates as in Fig. 4.

and T are certainly constant. However, if there were a Boltzmann equilibrium at each point in the arc and if the values of φ were known for all the lines, the data of Table II would serve to give values of T which would not be much less than the maxima for the portions of the discharge concerned. This is true because the intensity of the radiation of a given wave-length would vary with T as

$$e^{-eV/kT}/N_0.$$

(N_0 probably would not vary much faster than the reciprocal of T. Hence the effect of the exponential would predominate and most of the radiation would come from portions of the discharge for which T is near its maximum value.)

Since the "transition strength" φ is not known for any mercury line except λ2537 and λ1849, Eq. (5) cannot be used to test for the existence of a Boltzmann equilibrium in a mercury arc. However, one may take plausible values for φ and see whether a semi-logarithmic plot corresponding to (5) gives a linear arrangement of points and a reasonable value of electron temperature. We shall asume that

$$\varphi_{AB} \propto w_{AB}/[(n_A^*+n_B^*)(n_A^*-n_B^*)^2],$$

where w_{AB} is the Kronig *a priori* probability of transition from level A to level B, as given in Table III; n_A^* and n_B^* are the effective quantum numbers of A and B, respectively. Figs. 2 and 3 give the plots, on this basis, of the data of Table II for 450 and 20 mm mercury vapor pressure, respectively. A straight line has been drawn among each set of points on Figs. 2 and 3. The electron temperature corresponding to the slope is given above each of these lines.

Figs. 2 and 3 show that the spectral distributions of the radiation from different portions of the arc are approximately the same. Since this is the case, there is theoretical justification for making a similar plot for the radiation from the entire width of the arc. Fig. 4 is a plot of the data of Table I for the tubes containing argon. This table is more accurate and includes more lines than Table II. The data for a mercury vapor pressure of 0.030 mm are included in Fig. 4 although a Boltzmann equilibrium is not ex-

TABLE IV. *Lines due to downward transitions from a given level of the mercury atom. Lines in parentheses not measured. Lines in brackets not included in Boltzmann plots.*

Upper Level	7^3S_1	7^1S_0	7^3P_2	6^3D	8^3S_1	8^1S_0	8^3P_{01}	8^3P_2	7^3D^*
Energy (Electron-Volts)	7.69	7.89	8.78	8.80	9.12	9.18	9.43	9.48	9.51
Lines	4047	10140	11289	3650–63	2753	4916	7082–92	6907	3021–28
Lines	5461	[4078]		3125–32	3341				2652–55
Lines	4358			2967	2894				(2535)
Lines				[5770–91]					
Upper Level	9^3S_1	8^1P_1	$8D$	9^1P_1	10^3S_1	9^3D^*	10^3D^*	11^3D^*	
Energy (Electron-Volts)	9.65	9.72	9.83	9.86	9.90	10.0	10.1	10.17	
Lines	2464	6716	2378	6234	2447	2302	2259	2323–24	
Lines	2576		2482–84			2399–2401	2352–53		
Lines	2925		2803–07			2699–2701	(2640)		
Lines			3906						

* Intercombination line from corresponding $^1D_2$ level included.

pected at this pressure. However, the average deviation of the points from a straight line is hardly as great as that of the corresponding points for either 450 mm or 20 mm pressure.

The electron temperatures indicated by the solid lines drawn among the points in the upper two plots on Fig. 4 should be approximately equal to the weighted mean of the electron temperatures indicated by the straight lines on Figs. 2 and 3, respectively. This is not the case. The discrepancies are too large to ascribe to differences between discharge conditions on successive runs. A detailed examination indicated that unintentional differences in the procedures used for correcting for absorption, for taking a weighted mean of the data for the two tubes used for the high pressure runs, and for drawing representative straight lines among the widely divergent points might account for much of the discrepancy.

The solid lines were drawn among the points on Fig. 4 in the same manner as on Figs. 2 and 3. The dashed lines connect points corresponding to transitions having the same lower level and having upper levels differing only in total quantum number. The significance of the electron temperatures indicated by these dashed lines is discussed in the article immediately following this one.

Figure 5 is a plot, on the same basis as Fig. 4, of the data in Table I for the tube without argon. The solid and dashed lines were drawn as on Fig. 4. The points on this plot for a pressure of 500 mm may be identified by means of Table IV. The lines in each multiplet are listed in the order in which they appear on the graph, the uppermost point on the graph corresponding to the line listed first in the table. Table IV does not serve to identify points on the other plots, except for the cases where only one line is listed for each upper level.

In each plot on Figs. 2 to 5, the points for the lines in a multiplet have a much greater spread than is to be expected from errors in intensity measurements. (The deviation caused by 5 percent error would be barely perceptible.) Consequently, either the assumptions concerning transition strengths are incorrect or the proper correction for absorption was not made. Since the highest point for a multiplet is generally that

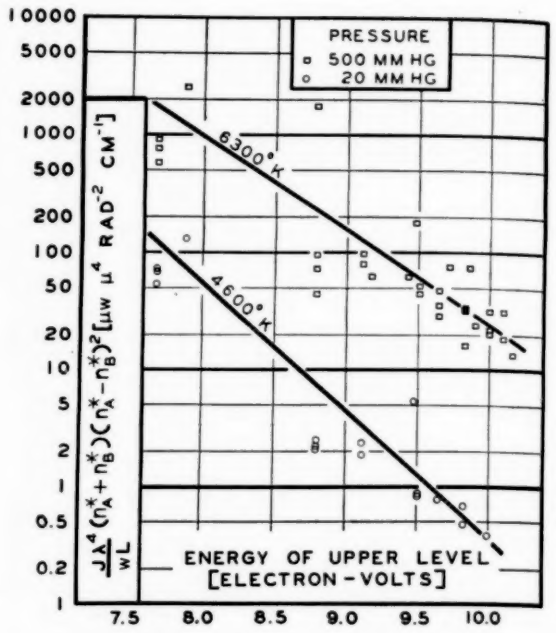

FIG. 6. Plots as in Fig. 5 except that intensities are multiplied by λ^4 instead of λ^3.

for the component with the least self-absorption, the correction for absorption may have been too small. To allow for this possibility, the straight lines on Figs. 2 to 5 were drawn somewhat above the points for strongly absorbed triplets.

The large deviation of points for certain transitions from the corresponding straight lines in Figs. 2 to 5 suggests that either a Boltzmann equilibrium does not exist or the transition strengths are not proportional to $w/[(n_A^*+n_B^*)\cdot(n_A^*-n_B^*)^2]$. Two other formulas for transition strength were tested out. For the data plotted in the upper part of Fig. 5, the expression $\varphi=w/(n_A^*-n_B^*)^3$ gave a plot with about the same spread of points as Fig. 5. The point for λ11289 came much nearer to the straight line drawn among the other points, but the points for λ's 7087, 4916, and 3906 were further from the straight line than in Fig. 5. The straight line drawn on this plot indicated an electron temperature of 14,500°K. Since an electron temperature of the order of 6000°K is sufficient to account for measured line breadths[11] and for the electrical characteristics of the arc, a temperature of nearly 15,000°K appears improbable.

[11] See article immediately following this one.

For the data plotted in Fig. 4, the formula $\varphi=w$ gave plots with a greater spread of points than those in Fig. 4. The electron temperature indicated by a representative straight line drawn among the points on the plot for 450 mm pressure would be less than 3800°K. This is too low to account for measured line breadths or for the electrical characteristics of the arc.

Although we believe that it is incorrect to identify the "line strength" S with the *a priori* probability of transition, we have made some Boltzmann plots on this basis. From Eq. (1)

$$\log (J\lambda^4/S)=\text{const.}-\epsilon V/kT. \qquad (6)$$

Fig. 6 is a plot of the data in Table I for 500 mm Hg pressure, in which Eq. (6) is used and it is assumed that $S=w/[(n_A{}^*+n_B{}^*)(n_A{}^*-n_B{}^*)^2]$. The only difference between Figs. 6 and 5 is that intensities are multiplied by λ^4 in the one case and λ^3 in the other. Since the points of wavelengths less than 2967A are all on the right hand side of the plot, multiplication of intensities by λ^4 instead of λ^3 reduces the electron temperature indicated by a straight line drawn among the points. It also makes the points for λ10140 and λ11289 come considerably above the general level of the other points. Otherwise, the spread of the points is much the same on the two plots.

Plots based on Eq. (6), using for the line strength S the formulas $w/[n_A{}^*n_B{}^*(n_A{}^*-n_B{}^*)^2]$, $w/(n_A{}^*n_B{}^*)^3$, $w/n_A{}^{*3}$ and w alone, all showed greater spreads of points than Fig. 6. The same was true of plots using $w/n_A{}^3$ and $w/(n_An_B)^3$, where n_A and n_B are the total quantum numbers of the upper and lower states, respectively. The electron temperatures given by straight lines drawn on these plots among the points for 500 mm pressure ranged from about 6500°K for the plot using $S=w/[n_A{}^*n_B{}^*(n_A{}^*-n_B{}^*)^2]$ to approximately 3000°K for the plot using $S=w$. Since the criteria used in drawing these straight lines (assumption that λ10140 and λ11289 points are too high and points for strongly absorbed lines are too low) are questionable, the electron temperatures obtained from their slopes are of no value except for rough comparisons.

Since certain points on each Boltzmann plot deviated from the straight lines by amounts equal to many times the errors in intensity measurements, we conclude that either (1) a Boltzmann equilibrium does not exist, or (2) none of the formulas used for transition probability are even approximately correct, or (3) the absorption losses for the strongest lines range from 90 to 95 percent instead of the experimental values of 30 to 50 percent. Although alternative (2) or (3) may be true, it seems proper to inquire whether a Boltzmann equilibrium should exist in a four-ampere mercury arc, even with a pressure as high as 500 mm. A Boltzmann equilibrium cannot be set up between the excited levels of an atom unless the total rate of downward transitions from each level is many times the total rate of radiation of quanta in the spectral lines corresponding to these transitions. Consequently, the probability of excitation to the level must far exceed the probability of radiative transition from it. This can be true only if there is a high concentration of electrons of sufficient velocity for exciting to the level or if there is no "permitted" radiative transition from the level. The latter case need not be considered here because the populations in levels above 6^3P_2 are our chief concern. The question as to the sufficiency of the supply of electrons cannot be answered without a knowledge of the electron temperature and the transition probabilities for all the processes under consideration. However, a study of other discharges in which a Boltzmann equilibrium seems to exist may indicate whether such an equilibrium in a mercury discharge is equally probable.

Populations in excited states corresponding approximately to a Boltzmann equilibrium have been reported[12] for a neon discharge. Here the energy required to excite an atom from the ground level directly to the highest level under consideration was only 14 percent greater than that for the lowest excited level. In the mercury atom, the energy required for direct excitation to the 7^3S_1 level is 65 percent greater than that for excitation to the 6^3P_0 level; the energy for direct excitation to the $8D$ levels is 2.11 times that for the 6^3P_0 level. This relatively greater spacing of the excited levels in Hg may make establishment of a Boltzmann equilibrium relatively more difficult than in a similar Ne discharge. Furthermore, the electron temperature

[12] H. Kopfermann and R. Ladenburg, Naturwiss. **19**, 513 (1931).

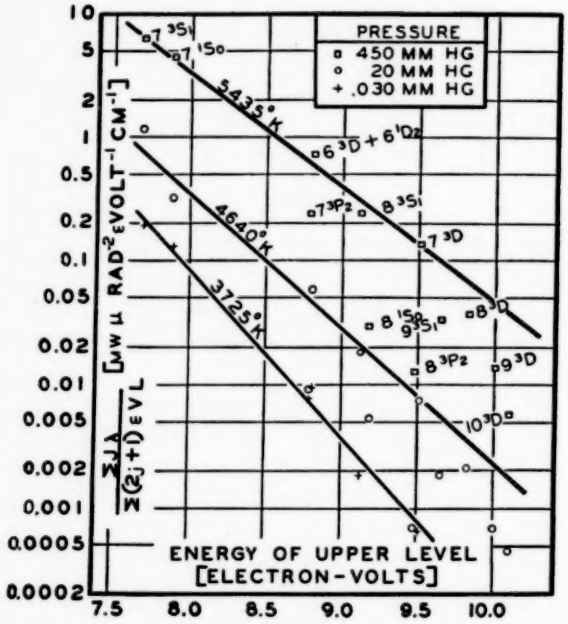

FIG. 7. "Excitation" plots of radiant intensity per unit length of arc for three different vapor pressures for tubes containing argon. Arc current 4.0 amperes. Ordinate is sum, for all downward transitions from a level or group of levels, of the milliwatts per steradian per cm of arc times wavelength in microns, divided by energy in electron-volts and by *a priori* probability of level or group. Designation of level or group of levels is given for upper set of points.

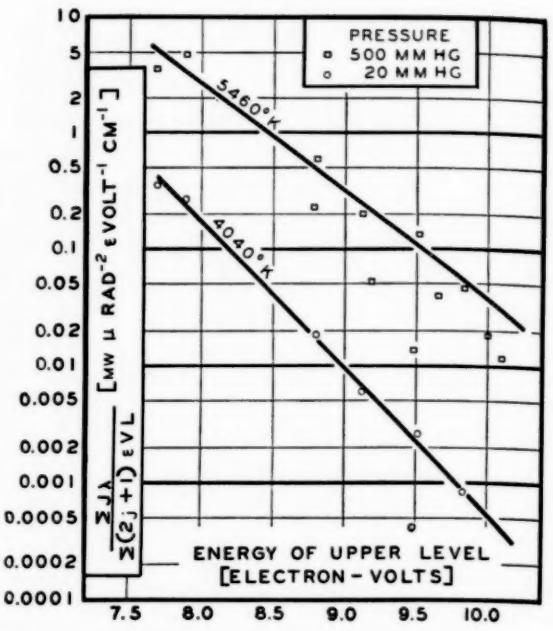

FIG. 8. "Excitation" plot of radiant intensity per unit length of arc at two different vapor pressures for tube without argon. Arc current 4.0 amperes. Ordinates as in Fig. 7.

values (18,000–20,000°K) obtained by Kopfermann and Ladenburg[12] for a neon discharge at 0.7 amp. and 1 mm pressure are much higher than that indicated by Fig. 5 for a 4 amp. Hg arc at 500 mm pressure. This partially offsets the higher excitation energies required for neon atoms. On the other hand, the higher pressure and current density favor the establishment of a Boltzmann equilibrium in the mercury arc mentioned above.

In the case of a carbon arc burning in air the spectral distribution within the CN band at 3883A indicates a Boltzmann equilibrium among the corresponding upper levels. It is possible that this equilibrium exists only between these closely spaced levels, not between all the levels of the CN molecule. This would probably be true if the mechanism for establishing equilibrium is most effective when the amounts of energy to be transferred are small.

Since spectral intensity data for a mercury discharge do not fit well on any of the Boltzmann plots that we have made, it seems proper to inquire whether some other type of plot would be more suitable. If radiation is the major factor in dissipating the energy of excited states, line intensities may be quite different from those obtaining in a Boltzmann equilibrium. For example, if all downward transitions were radiative, transition probabilities would determine only the relative intensities of different lines from the same upper level; line intensities would be determined primarily by the rate of excitation to the upper level concerned. If this rate is proportional[13] to $(2j+1)$ times the number of collisions between unexcited atoms and electrons with energies which do not differ by more than a certain amount from the energy required for excitation, and if the distribution of electron velocities is Maxwellian,[14] then the total rate of transitions from a given upper level will be

[13] This is a reasonable assumption provided that the supply of electrons of the proper velocities is not unduly diminished by the excitation which takes place. Subsequent collisions of the second kind which transfer the excitation to another level with approximately the same energy (within 0.01 electron-volt) need not concern us because, in the following discussion, the rates of transition from such levels are all added together before any plot of the data is made.

[14] A Maxwellian distribution of electron velocities usually exists in the positive column of an arc. See I. Langmuir and K. T. Compton, Rev. Mod. Phys. 2, 222 (1930).

proportional to $(2j+1)\epsilon V e^{-\epsilon V/kT}$. The factor $(2j+1)$ takes account of the $2j+1$ states in each level.

Then $$\log_{10} \sum J\lambda/[(2j+1)\epsilon V] = C - (5040/T)\,\epsilon V,$$

where λ is the wave-length and J the intensity of a given line. The summation is made for all the transitions from a given upper level. C is a constant for a given set of discharge conditions and ϵV is the energy of the upper level with respect to the ground level (or any other level, if C is changed to correspond). Thus, a semi-logarithmic plot of $\Sigma J\lambda/[(2j+1)\epsilon V]$ against ϵV would give a straight line whose slope would be a measure of the electron temperature, T. For brevity, such plots will be called "excitation" plots.

If all downward transitions are radiative and if radiative transitions from an excited level are much more probable than excitation to a still higher level, absorption of radiation in the vapor will have little net effect on the number of emitted quanta due to transitions from a given level. Consequently no correction should be made for absorption in the vapor. Elimination of the correction for the absorption of the vapor from all the data of Tables I and II was not possible. However, data on the transmission of the thin window when cold were available in most cases. These were used to correct the measured intensities, although the correction was doubtless too small in the far ultraviolet because hot glass has a greater absorption than cold. A plot of the energy per centimeter of arc, received from the entire width of the arc, is given in Fig. 7 for the tubes containing argon, and in Fig. 8 for the tube without argon.

The points on the graphs and the lines used for obtaining the plotted values may be identified by referring to Table IV. The designation of the upper level for each group of radiative transitions is indicated on Fig. 7 opposite the points for the highest pressure. In cases where lines due to transitions from several neighboring levels are included in one intensity measurement, the sum of the $J\lambda$'s for all the lines due to transitions from the group of levels is divided by $\Sigma(2j+1)$. When one of the lines of a triplet was not measured or not separated from a much stronger line (for example, λ2535), the summation was completed by assuming the relative intensities within the triplet to be proportional to $w/[\lambda^3(n_A^*+n_B^*)\cdot(n_A^*-n_B^*)^2]$, where w is the *a priori* probability of a transition as given by Table III.

The points for some of the weaker lines are further from the straight lines in Figs. 7 and 8 than in Figs. 4 and 5. On the other hand, the points for λ11289 lie nearer to the corresponding straight lines in Figs. 7 and 8 than in Figs. 4 and 5. Except for the data for λ11289, the points for the principal transitions from levels less than 9.8 electron volts above the ground level lie fairly near to the straight lines in Figs. 7 and 8. The deviations of the points representing transitions from the 8^1S_0, 8^3P_2, 9^3S_1 and the 8^3D to 10^3D levels are discussed in the article immediately following this one.

Conclusions

1. The electron temperature in a mercury arc varies little with distance from the arc axis. This is in disagreement with Elenbaas' theory of the mechanism of a high pressure mercury arc.

2. A decrease of electron temperature with decreasing mercury vapor pressure appears to be well established, regardless of the theoretical basis for plotting the intensity data.

3. The existence of a Boltzmann equilibrium in a high pressure mercury arc cannot be proved or disproved at present because the probability of a radiative transition from one level to another is not known as yet.

4. Various arbitrary but more or less plausible formulas for transition probability were tried out. None of them made the points on a Boltzmann plot lie on a straight line.

5. On Boltzmann plots, the points for strongly absorbed lines generally fall below a straight line drawn among the points for weakly absorbed lines. While this may be due to incorrect formulas for transition probabilities, it may indicate that the correction for absorption was too low. This is to be expected whenever a line is reversed in the arc used as a source for absorption measurements.

6. "Excitation" plots, based on the assumption that nearly all downward transitions are radiative, showed deviations of the points from

representative straight lines. These deviations were of the same order of magnitude as those on the best Boltzmann plots. The latter plots are based on the assumption that relatively few downward transitions are radiative and that the probabilities of radiative transition are proportional to $w_{AB}/[\lambda^2(n_A^*+n_B^*)(n_A^*-n_B^*)^2]$ where w_{AB} is the Kronig *a priori* probability, n_A^* and n_B^* are the effective quantum numbers of the upper and lower levels, and λ is the wave-length of the emitted radiation.

7. Representative straight lines drawn among the points on the Boltzmann plots described above gave electron temperatures of 7160 and 7880°K for mercury vapor pressures of 450 and 500 mm, respectively. Similar lines on the corresponding "excitation" plots gave electron temperatures of 5435 and 5460°K, respectively. Line breadth measurements and theoretical calculations set forth in the paper immediately following this one indicate that the electron temperature is at least 6000°K at these two pressures. The electron temperatures indicated by the "excitation" plots agree with this computed minimum value within the limits of uncertainty set by the scatter of the points on these plots. The electron temperatures indicated by the Boltzmann plots are not impossible, but are much higher than is required by the measured line breadths and the electrical characteristics of the arc. This conclusion is contingent on the formula chosen for transition probabilities.

8. Since neither excitation probabilities nor the probabilities of downward transitions are known, no quantitative basis is available for choosing between the hypothesis of a Boltzmann equilibrium and the hypothesis of an excitation-radiation balance.

APRIL 1, 1938 PHYSICAL REVIEW VOLUME 53

The Mechanism of the Positive Column in Mercury Vapor at Intermediate Pressures

ELLIOT Q. ADAMS and BENTLEY T. BARNES
Incandescent Lamp Department, General Electric Company, Nela Park, Cleveland, Ohio
(Received February 26, 1937)

Calculations based on the radiant intensity for the principal spectral lines of 4-ampere mercury arcs at 450 mm and 500 mm (Hg) pressure, indicate for low quantum states a dynamic equilibrium with electrons at approximately 6000°K, the temperature indicated by the absolute spectral intensity for three reversed lines. For high quantum states differing only in total quantum number, there appears to be a tendency toward Boltzmann equilibrium due to collision with normal atoms at approximately the temperature (2500°K) calculated from the heat balance by Langmuir's theory of conduction and convection in gases. This agrees with predictions from the principle of *spectroscopic stability*.

THE electric discharge[1] in the inert gases or in mercury vapor offers the advantage of a relatively simple system: a single molecular species[2] with no rotational energy, and incapable of any other dissociation than that into electrons and positive ions. Yet even this simple system is effectively a system of three components, atoms, ions, and electrons, present in different concentrations, and obeying different laws of motion.

The fact that some of the atoms are excited will have no material influence on the mechanical behavior of the gas, since the mass of the atom is not altered appreciably, and since collision of the second kind, whether between atoms or between an atom and a positive ion, will rarely have any other effect than an exchange of roles.[3] Collisions

[1] The discharge in mercury at atmospheric pressure is customarily referred to as a mercury arc. By Ornstein and Brinkman's definition (Physica **1**, 797 (1934)) it is a high pressure glow discharge, if, as we now believe, the electron temperature is significantly higher than the gas temperature.

[2] Mercury molecules and molecule ions are present in the discharge and may play an essential role, but in concentrations which will not affect significantly the mechanical and thermal properties of the vapor. Energy of electron excitation or spin is not ordinarily called "rotational energy."

[3] See, however, section on "Collision with Normal Atoms."

of the second kind between positive ions are improbable both because of the low ion concentration and because of electrostatic repulsion.

"Elastic" collisions of ions and electrons with atoms will not be numerous or violent enough to disturb the Maxwellian distribution of atomic velocities, but will transfer energy and momentum, raising the gas temperature and causing electrophoretic effects. Since most of the current is carried by electrons, these will furnish most of the energy; since the volume charge in the tube is predominantly positive, the electrophoretic effects at higher pressures will be produced chiefly by the positive ions—while at low pressures the greater transfer of axial momentum to the walls by the ions will more than compensate for the effect of the excess positive charge.[4]

Energy Balance

The dissipation of energy in the positive column involves three main processes: radiation, recombination of ions and electrons, and conduction and convection of heat. The laws of the conduction and convection of heat from a heated cylinder to a cooler surrounding gas have been worked out by Langmuir.[5] On the basis that almost all the temperature fall is concentrated in a quasi-stationary film of gas between the solid cylinder (of diameter a) and a concentric cylinder of diameter b, and by the use of the integrated form of the differential equation for the flow of heat between isothermal surfaces one obtains

$$\mathbf{W}=\mathbf{s}(\varphi_1-\varphi_0)=\mathbf{s}\int_{T_0}^{T_1}\mathbf{k}dT. \qquad (1)$$

In this $\mathbf{W}$ is the power lost by thermal conduction per cm of length, $\mathbf{s}$ is the "shape factor,"[6] likewise per cm of length, (for concentric cylinders $\mathbf{s}=2\pi/(\ln(b/a))$, and φ_1, as indicated, is the integral of the thermal conductivity $\mathbf{k}$ from some reference temperature, e.g., 0°C, to the temperature T_1. φ_0 is the same integral for the lower temperature, T_0.

For a convex cylinder, the diameter of the virtual limit of thermal conduction, b, is related to the diameter of the solid cylinder, a, by the equation of Adams[5]

$$b\ln b/a=2B, \qquad (2)$$

where B is the film thickness for an infinite plane surface. The assumptions used in deriving this formula do not hold for the present case of a concave cylinder cooler than the enclosed gas, but the qualitative statement may be made that the film thickness in a discharge tube at atmospheric pressure will be somewhat greater than for an infinite plane surface, i.e., $>B$.

For mercury vapor at atmospheric pressure, Langmuir found $B=0.0784$ cm, from which a round figure of 0.08 cm may be taken as the film thickness in Elenbaas' tube of 2.0 cm internal diameter with mercury vapor at atmospheric pressure.[7] As the precision of the data does not justify interpolation in Langmuir's table of integrated heat conductivity of gases ($\varphi=\int\mathbf{k}dT$), 2500°K, 900°K, and 300°K will be taken as the respective temperatures of the mercury vapor, tube, and surroundings; the thickness of the tube walls will be assumed to be 0.1 cm, and the film thickness of air outside the tube 0.4 cm.

The rate of flow of heat from the mercury vapor to the tube is

$$\mathbf{W}=\mathbf{s}\varphi=\pi(1.96/0.08)(0.481-0.062)$$
$$=32.2\text{ watt cm}^{-1}. \qquad (3)$$

The rate of flow of heat from the tube to the surrounding is

$$\mathbf{W}=\mathbf{s}\varphi+A\sigma(T^4-T_0^4)$$
$$=\pi(2.6/0.4)(0.297-0.039)+\pi\times2.2\times3.70$$
$$=5.3+25.6=30.9\text{ watt cm}^{-1}. \qquad (4)$$

Elenbaas estimated the heat flux lost by conduction and convection as 70 percent of 43.8 w cm^{-1}, the input per cm of positive column.

$$\mathbf{W}=0.70\times43.8=30.7\text{ watt cm}^{-1}. \qquad (5)$$

Whereas Elenbaas[7] found discrepancies as great as a factor of four by assuming that convection could be neglected, the calculation above,

[4] I. Langmuir, J. Frank. Inst. **196**, 751–62 (1923).

[5] I. Langmuir, Phys. Rev. **34**, 401–22 (1912). Langmuir's value of φ, the temperature integral of thermal conductivity of mercury vapor, was calculated from an assumed value of the Sutherland viscosity constant and may be considerably in error. Since we are using the value of B (film thickness for a plane surface) computed from this value of φ and Langmuir's data taken at atmospheric pressure, to calculate convection *at atmospheric pressure*, only a second-order error will be introduced by any uncertainty in φ.

[6] I. Langmuir, E. Q. Adams, and G. S. Meikle, Trans. Am. Electrochem. Soc. **24**, 53–84 (1913).

[7] W. Elenbaas, Physica **1**, 211–24 (1934) esp. p. 222.

based on measured[5] convection losses agrees well within the precision of the data used in the calculation.

Distribution Over the Cross Section

It follows that (at atmospheric pressure) up to within a millimeter of the wall of the tube the mercury vapor temperature is substantially constant and approximately 2500°K. The electron temperature (as judged from the relative intensity of the various lines of mercury) cannot be less than 3500°K, and therefore the vapor and the electrons are *not* in thermal equilibrium with one another. Since the electrons in all parts of the tube cross section are moving in an equal electromotive gradient through vapor of constant temperature and pressure, the electron temperature, mean free path (as concerns collision with mercury atoms) and drift velocity must likewise be uniform, and the relative spectral distribution should be uniform over the cross section, as has been found to be the case.[8]

If the radiant flux resulting from the collisions of a single electron is the same in all parts of the cross section of the tube, any variation in steradiancy,[9] beyond the cosine effect of the cylindrical cross section, must be attributed to a change in electron concentration. This in turn is due to the radial electromotive gradient due to the excess of positive ions over electrons. The experimentally determined variation in steradiancy ($\mathfrak{B}$) indicates a nearly Gaussian distribution of electron concentration. (For this special case it may be shown that the radial and pinacoidal[10] variations of electron concentration follow the same law.)

$$dJ/dV=(dJ/dV)_0e^{-r^2/a^2}\equiv(dJ/dV)_0e^{-x^2/a^2}e^{-y^2/a^2}, \quad (6)$$

where J is radiant intensity, V is volume, and x and y are the components, across and along the line of sight, of the distance r from the axis. a is a parameter defining the radial distribution and subscript 0 indicates the axial value of the derivative dJ/dV.

$$\mathfrak{B}=\int(dJ/dV)\,dy=a(dJ/dV)_0e^{-x^2/a^2}\int e^{-y^2/a^2}d(y/a), \quad (7)$$

where $\mathfrak{B}$ is steradiancy (surface density of radiant intensity).

If the value of dJ/dV at the wall is negligibly small with respect to $(dJ/dV)_0$, the integral becomes the complete integral

$$\int_{-\infty}^{+\infty}e^{-t^2}dt=\pi^{\frac{1}{2}}, \quad (8)$$

$$\mathfrak{B}=a\pi^{\frac{1}{2}}(dJ/dV)_0e^{-x^2/a^2}. \quad (9)$$

While this equation accounts almost quantitatively for the distribution of steradiancy near the axial plane of the discharge, it cannot be expected to apply to the entire cross section of the tube, for a Gaussian distribution of electron concentration implies a parabolic distribution of electric potential, which in turn requires a uniform volume concentration of (net) positive charge. Near the axis of the tube the radial electric potential gradient is small and the convective stirring of the mercury vapor will be sufficient to keep the concentration of positive ions practically uniform. Where the potential gradient is greater and the stirring less vigorous, a radial concentration gradient of positive ions can be maintained and it is improbable that the net positive charge will remain unchanged.

The electron distribution at a distance from the axis cannot be determined precisely from the distribution of steradiancy, for the strongest lines in the discharge are all due to transitions whose lower level is 6^3P_0, 6^3P_1, or 6^3P_2. Absorption and re-emission should increase the peripheral intensity of these lines relative to those due to transitions to higher levels, as is found to be the case.[8]

Formation and Neutralization of Mercury Molecule Ions

Calculations indicate that the net positive volume charge is a small fraction ($\leqq 10^{-3}$) of the concentration of positive ions, hence the rapid decrease in the concentrations of positive ions and electrons with increasing radius cannot be

[8] See preceding article.

[9] Cf. W. E. Forsythe, *et al, The Measurement of Radiant Energy* (McGraw-Hill Book Co., Ltd., New York and London, 1937), especially p. 3. See also Rev. Sci. Inst. **7**, 322 (1936).

[10] From the Greek, pinax = slab.

accounted for by recombination at the walls. The direct recombination of atomic positive ions and electrons is a rather improbable process; hence the possible intervention of mercury molecules and molecule ions must be considered.

Mercurous salts have been shown[11] to be derived from the doubly-charged molecule ion, Hg_2^{++}. The stability of such a grouping in aqueous solution and in solid compounds,[12] proves the possibility of a strong bonding between mercury atoms. The absorption spectrum of unexcited mercury shows a strong band, which is to be attributed to molecules of two atoms of mercury,[13] on the long wave side of λ2537A. Foote[14] and Houtermans[14] found ionization produced by irradiation with λ2537 in mixtures of mercury vapor and argon, which they assigned to a reaction of mercury atoms in the 6^3P_0 and 6^3P_1 states:

$$Hg\ (6^3P_0)+Hg\ (6^3P_1)=Hg_2^+ +\epsilon^- +K.E. \quad (10)$$

and Foote, Ruark and Chenault[15] observed under similar conditions a blue-green band emission which they attributed to the interaction of two 6^3P_0 mercury atoms

$$2\ Hg\ (6^3P_0)=Hg_2+\text{radiant energy} \quad (11)$$

or

$$2\ Hg\ (6^3P_0)=2\ Hg+K.E.+\text{radiant energy}. \quad (12)$$

The existence of the molecule ion makes possible the reaction

$$Hg+Hg^+=Hg_2^+ +\text{radiant energy}. \quad (13)$$

Since the concentration of atomic mercury is high and constant, this reaction would be apparently unimolecular in (Hg^+). The neutralization reaction:

$$Hg_2^+ +\epsilon^- =Hg_2+\text{radiant energy} \quad (14)$$

or

$$Hg_2^+ +\epsilon^- =2\ Hg+K.E.+\text{radiant energy} \quad (15)$$

would be much more probable than the direct neutralization of the atomic ion, since many more degrees of freedom are available to store energy and prevent the reionization of the molecule. Let it be assumed that it is enough more rapid than (13) to make (13) the rate-determining step, and the disappearance of positive ions effectively unimolecular.

Such a reaction sequence in a region of the tube in which ions are not being produced would give a concentration of positive ions (and hence of electrons)

$$C=ar^{-\frac{1}{2}}e^{-br}, \quad (16)$$

where (b) and (a) are constants dependent, respectively, on the rate of destruction of ions in the outer parts of the tube and on the rate of production of ions near the axis of the tube.

A production of ions proportional to the first power of the current density will be equivalent to a reduction in the rate of neutralization of ions, since both processes are proportional to the ion concentration. The maintenance of the discharge then requires some process of ionization proportional to a higher power of the current density. Cumulative ionization by electrons is most likely to occur where the concentrations of electrons and of excited atoms are the greatest, namely near the axis of the tube. The electron temperature of approximately 6000°K estimated from the kinetics of radiation, is high enough to account for a reasonable amount of ionization of mercury atoms in this region of the tube.

A Priori Probabilities

In the estimation of electronic (or atomic) temperatures from relative line intensities, allowance needs to be made for the *a priori* probabilities of the states and processes involved.

It should be noted that the "strength"[16] of

[11] Cf. G. A. Linhart, J. Am. Chem. Soc. **38**, 2356–61 (1916). G. A. Linhart and E. Q. Adams, J. Am. Chem. Soc. **39**, 948–50 (1917).

[12] Ch. Mauguin, Comptes rendus **178**, 1913–6 (1924). E. Hylleraas, Physik Zeits. **26**, 811–4 (1925). R. J. Havighurst, Am. J. Sci. **10**, 15–28 (1925); J. Am. Chem. Soc. **48** 2113–25 (1926). H. Mark and J. Steinbach, Zeits. f. Krist. **64**, 79–112 (1926).

[13] J. Franck and W. Grotrian, Zeits. f. tech. Physik **3**, 194–7 (1922). The fact that the intensity of this band, at constant *concentration* of mercury, decreases with rising temperature, indicates that the band is due to an actual Hg_2 molecule, and not to a "virtual" molecule existing only during collisions.

[14] P. D. Foote, Phys. Rev. **29**, 609 (1927). F. G. Houtermans, Zeits. f. Physik **41**, 140–54 (1927). Cf. A. L. Hughes, Wash. Univ. Studies, N.S., Sci. Tech. **2**, 25–30 (1929). It should be emphasized that the energy of two excited 6^3P_1 atoms is insufficient to ionize an *atom* of mercury.

[15] P. D. Foote, A. E. Ruark and R. L. Chenault, Phys. Rev. **37**, 1685 (1931).

[16] E. U. Condon and Shortley, *Theory of Atomic Spectra* (Cambridge University Press, 1935), p. 98: $S\ (A, B)$ = *line strength* = sum of the squared matrix components for the transition $A \rightarrow B$.

Condon and Shortley, S, is not the same as the "strength"[17] of Ladenburg, f.

Following Dirac,[18] Condon and Shortley identify the matrix components with the components of the electric amplitude, $\epsilon\mathbf{r}$ (ϵ = electron charge, $\mathbf{r}$ = displacement from point of rest of the equivalent oscillator.) The "oscillator strengths" of Ladenburg, being abstract numbers, and shown by Thomas[19] and by Kuhn[20] to obey a sum rule first suggested by Van Vleck[21] seem to the authors more likely, *a priori*, to be given by formulas involving only quantum numbers. For the special case of an $S \rightleftarrows P$ resonance transition, e.g., sodium, where $f_{BA} \cong \frac{1}{3}$, Ladenburg and Minkowski[22] have shown that the resonance life is approximately equal to that of the classical oscillator of equal $h\nu$.

The question is one of normalization. Since the most satisfactory tests of intensity formulas have been with close multiplets and the Zeeman and Stark effects, the question as to the power to which the frequency enters has not greatly concerned the experimental workers. Thus Frerichs[23] wrote, "Es spielt da die wichtige, experimentell noch unentschiedene frage hinein, ob die Summenregeln für die Intensitäten J oder die 'Sprungzahlen' J/ν gelten (vgl. u.)"[!] while earlier in the same year Schrödinger had given[24] two formulas for the dipole moment, in the second of which the frequency as a factor was eliminated in the process of normalization, without any proof that the method of normalization used is correct, other than a reference to Heisenberg. Now Heisenberg[25] has stated the quantum condition in the form:

$$2\pi m\{b^2(n, n-1; m, m-1)\omega(n, n-1) - b^2(n, n-1; m-1, m)\omega(n, n-1)\} = (m+\text{const.})\,h$$

for the special case of the Zeeman effect of a quantized rotator, where the first m is electronic mass. Elsewhere n is a rotational and m a magnetic quantum number. The b's are the amplitudes of the perturbed circular orbits, ω is angular velocity, and h the Planck constant. For a multiply-periodic system there would be a summation in which the ω's would not all be equal. Taking account of the known relation of Einstein's coefficient B to the squared amplitude, a^2,

$$B = (8\pi^3\epsilon^2/3h^2)a^2$$

(and $\omega = 2\pi\nu$) it can be seen that the total-summation rule of Van Vleck, Thomas, Reiche and Kuhn, is just such a summation.

This summation, it should be emphasized, is an algebraic one. If it is to be applied to individual electrons, account must be taken of transitions which cannot occur because both the upper and lower levels are filled. As stated by Kronig and Kramers[26] "Solange die Koppelung der Elektronen gegen die sonstigen vorhandenen Kräfte sehr Klein ist, bewirkt das Pauliverbot einfach ein Wegfallen der Oszillatoren der einzelnen Elektronen, die Übergängen nach schon besetzen Zuständen entsprechen, und zwar in Paaren von positiven und negativen Oszillatoren gleicher Frequenz und Stärke, während die übrigen Oszillatoren unbeeinflusst bleiben." It is thus possible, e.g., for the first term of a principal series to have an aggregate f value of unity, in spite of the existence of other permitted upward transitions.

For comparison with the *a priori* multiplet-transition probabilities of Kronig,[27] w_{AB}, it is

---

[17] R. Ladenburg, Rev. Mod. Phys. **5**, 243 (1933):

f_{kj} = *oscillator strength* (Condon and Shortley, reference 16, p. 108)
= number of dispersion electrons, per atom in the state j, associated with the transition $j \rightarrow k$.

[18] P. A. M. Dirac, Proc. Roy. Soc. **A111**, 281–305, 405–23 (1926). On p. 302 Dirac states, "We cannot actually determine the amplitudes at present because we do not know the action and angle variables corresponding to the r's and P_r's. If, however, we assume that the Fourier expansion of r does not involve p, j, ϕ, or ψ, then when $x/r, y/r, z/r$ are expanded as Fourier series in $e^{i\phi}$, $e^{i\psi}$, the ratios of the coefficients will give the ratios of the corresponding amplitudes. We can thus determine the relative intensities of the lines of a multiplet and of the components into which these lines are split in a weak magnetic field.

[19] W. Thomas, Naturwiss. **13**, 627 (1925); F. Reiche and W. Thomas, Zeits. f. Physik **34**, 510–25 (1925).

[20] W. Kuhn, Zeits. f. Physik **33**, 408–12 (1925).

[21] J. H. Van Vleck, Phys. Rev. **24**, 359–60 (1924); Bull. Nat. Res. Council **10**, (54) 152 (1926).

[22] R. Ladenburg and R. Minkowski, Zeits f. Physik **6**, 163 (1921). At that time the *a priori* probabilities of the $3S$ and $3P$ levels of sodium were not known, but an expression was given explicitly relating the radiational decay time to the *a priori* probabilities "$g_{1.5s}$, g_{2p_1}, g_{2p_2}" and the classical decay time, τ.

[23] R. Frerichs, Ann. d. Physik **81**, 840 (1926).

[24] E. Schrödinger, Ann. d. Physik **79**, 755; **80**, 464 (1926).

[25] W. Heisenberg, Zeits. f. Physik **33**, 892 (1925).

[26] R. de L. Kronig and H. A. Kramers, Zeits. f. Physik **48**, 178 (1928).

[27] R. de L. Kronig, Zeits. f. Physik **33**, 261–72 (1925). A common factor of 16 has been omitted in Table III of the preceding article.

more convenient to deal with the symmetrical function $(2j_A+1)f_{AB}=-(2j_B+1)\,f_{BA}\equiv\varphi_{AB}$, where[28] j_A is the inner quantum number of state A, and f_{AB} is the "oscillator strength" for the transition $A\rightarrow B$.

The "transition strength" φ_{AB} depends on the total quantum numbers as well as on the Kronig probability, w_{AB}. For purposes of computation, this last has been divided by $(n_A^*+n_B^*)\cdot(n_A^*-n_B^*)^2$ as a function which satisfies the correspondence principle both for series, and for transitions between nearly circular orbits. (n_A^* and n_B^* are the effective quantum numbers for states A and B.) This is to be regarded, however, as a makeshift, pending the evaluation of the appropriate radial quantum integrals.[29]

Similarly, in default of an exact knowledge of the collision area for various processes as a function of electron velocity, it has been assumed that the rate of excitation by electron collision is proportional to the *a priori* probability $(2j_A+1)$ of the upper state and to the rate of collisions with electrons whose energy exceeds the energy of transition by not more than a constant energy. This assumption gives $\Sigma J\lambda/[(2j_A+1)\epsilon V]$ as the function which should vary exponentially with the energy, ϵV, of the upper level, A, in the event that the excitation by electron collision is the rate-determining step, and that practically all downward transitions are radiative.

[28] The transition strength φ_{AB} should not be confused with the heat-conductivity integral $\varphi=\int\mathbf{k}dT$ of Langmuir.

[29] This function does not reproduce well the intensities of the first five lines of the principal series of sodium $nP_{\frac{1}{2},\frac{3}{2}}-3S_{\frac{1}{2}}$, but gives good agreement for larger values of n:

n	λ	$f_{AB}(n_A^*+n_B^*)(n_A^*-n_B^*)^2$
3	5893A	87.3
4	3303	5.3
5	2853	7.44
6	2680	5.26
7	2594	4.10
8	2544	3.57
9	2512	3.36
10	2491	3.26
11	2476	3.27
12	2464	3.28
13	2456	3.30
14	2449	3.38
15	2444	3.46
16	2440	3.55
17	2437	3.44
18	2434	3.41

For the principal series of lithium and of cesium on which less work has been done, the agreement of the formula with the experimental values of intensity is not as good as with sodium.

Temperature Estimate from Line Intensity

The principle that the spectral steradiancy of the arc cannot exceed that of a black body at a temperature equal to the electron temperature permits the setting of a lower limit to the electron temperature. The ratio of the steradiancy for a given emission line to the spectral steradiancy of a black body at that wave-length sets a lower limit for the effective line width, for any assumed black-body temperature.

Line widths were measured on films taken on a 21-foot concave grating with 30,000 lines per inch, for a mercury arc at approximately 450 mm (Hg) pressure. We are indebted to our colleague, Mr. A. Poritsky, of the Cleveland Wire Works of the General Electric Company, for these spectrograms.

Table I compares the result of calculations for λλ4047, 4358 and 5461A, and assumed temperatures of 3000°, 4000°, 5000°, and 6000°K (using $c_1=1.177\times10^{-2}$ cm² w rad^{-2} and $c_2=1.432$ cm °K in the Planck radiation formula) with the net widths of these three reversed[30] lines. It may be concluded that the electron temperature is at least 6000°K.

Collision with Normal Atoms

It remains to take into account the possible influence of collisions with normal atoms upon

Table I. *Width of reversed lines calculated for different temperatures and observed values.*

Wave-length	Observed w rad^{-2} cm^{-2}	Line-width				
		Calculated				Observed
		3000°K	4000°K	5000°K	6000°K	
4047A	0.074	91A	4.7A	0.81A	0.25A	0.21A
4358	0.109	83	5.4	1.04	0.35	0.25
5461	0.114	29	3.3	0.89	0.37	0.33

[30] With an unreversed line there will be no assurance that the absorption is great enough to give black-body steradiancy even at the central wave-length. It may be pointed out that this degree of absorption does not necessarily invalidate the assumption on which the excitation plot is based: that all downward transitions are radiative. Since that plot uses measurements of the radiation from the entire width of the arc, absorption followed by reemission of the same triplet will not affect the estimate of the rate of excitation to the common upper level, 7^3S_1. The short wave-length wing, region of reversal, and long wave-length wing, respectively, of the three lines measured were: λ4047: 0.095, 0.07, 0.115; λ4358: 0.115, 0.12, 0.14; λ5461: 0.15, 0.10, 0.175A. These figures are the averages of readings by four observers. We are indebted to P. D. Cargill, Miss M. A. Easley, and W. J. Karash for these comparator readings.

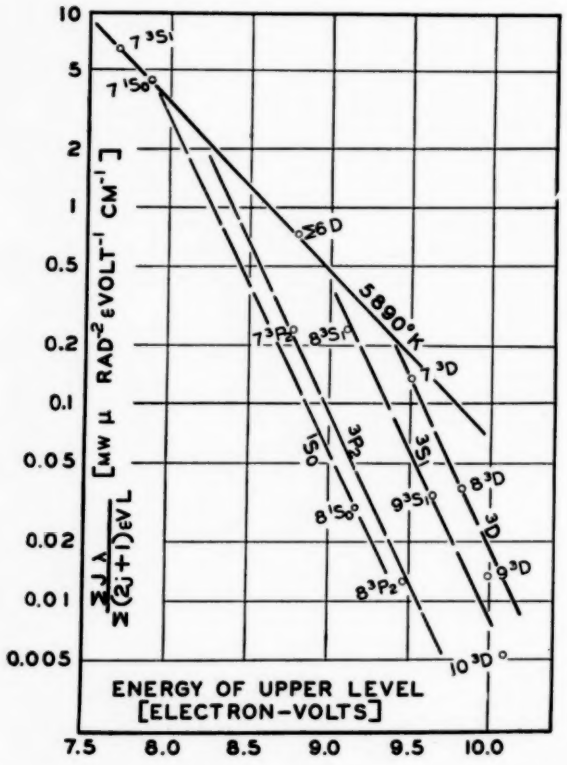

FIG. 1. Plots of $\Sigma J\lambda/[\Sigma(2j+1)\epsilon VL]$ for various types of upper state.

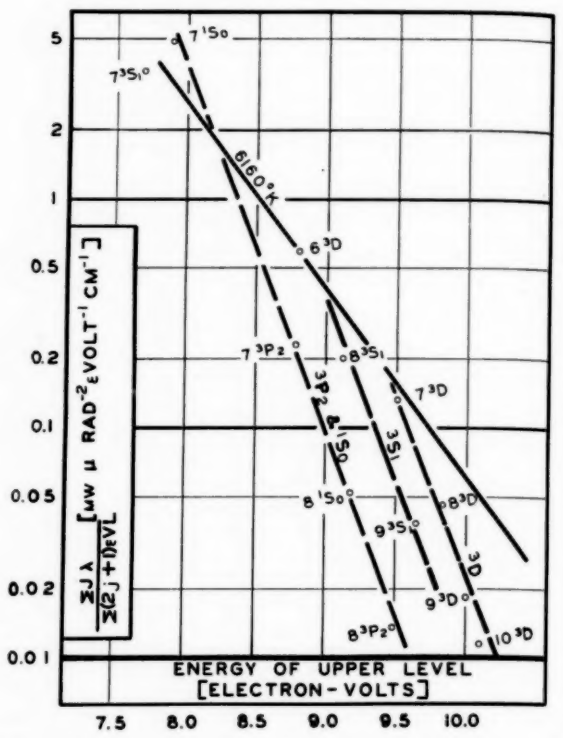

FIG. 2. Plots of $\Sigma J\lambda/[\Sigma(2j+1)\epsilon VL]$ for various types of upper state.

the relative concentrations of the higher excited states. It is well established that such collisions will not be inelastic for mercury in the ground state; but when the orbital radius becomes comparable[31] with the mean distance between mercury atoms, and the energy differences between states become less than the thermal kinetic energy of the atoms, neither geometric nor energetic considerations forbid inelastic collisions. Since the colliding normal atom will suffer no change except in velocity, the principle of *spectroscopic stability*[32] demands that the most probable transitions be those in which neither j nor S changes, i.e., to states differing only in total quantum number from the initial state.

In the case of the discharge at 450 mm (Hg) pressure, sufficient data are available to permit a search for such an effect of atomic collisions. Figs. 1 and 2, plots of $\Sigma\lambda J/(\Sigma(2j+1)\epsilon VL)$ show that for each type of upper state, $^1S_0$, $^3P_2$, $^3S_1$ and ΣD, for low total quantum number the rates of excitation as measured by the totality of radiative transitions from any state lie on a line whose slope indicates an electron temperature of 5890°K for 450 mm Hg pressure, and 6160°K for 500 mm Hg pressure, while for high total quantum number, they lie on a series of nearly parallel lines.

[31] Since the radius of the first Bohr orbit of hydrogen is 0.528A, the classical radius of a circular orbit with $n=10$ should be 53A; the "maximum elongation" for an electron in the corresponding s-orbit, on account of quantum defect, will be less than this (about 30A). Since the number of molecules in a cubic centimeter of gas at 273°K and 1 atmosphere is 2.706×10^{19}, at 2500°K and 450 mm (Hg) pressure, the distance between molecules in cubic array would be 83A.

[32] A collision between a normal and an excited mercury atom may be regarded from two alternative points of view: the temporary exposure of the excited atom to the perturbing field of the colliding normal atom, or the formation and subsequent dissociation of an Hg_2 molecule. For an inelastic collision, the collision must be close enough to relax to some extent the quantization of the excited atom (from the former point of view) or to destroy the one-to-one correlation between atomic and molecular states with the result that an atom may leave in a configuration different from that in which it enters the molecuie (from the second). Since one of the atoms is in a $^1S_0$ state, and S, L and j for the other are small, a change in S, L or j is unlikely, and the most probable change is in the largest quantum number, n, of the excited electron. This change may be either a promotion or a demotion, and since the energy difference is added to or taken from the atomic kinetic energy, the ratio of the rates of the two processes will depend on the atomic temperature.

As an indication of the atomic temperature, these pairs of points have been connected on the Boltzmann diagrams, Figs. 4 and 5 of the preceding paper, by dotted lines.

The slopes of these lines indicate temperatures of 4250°K, 4000°K, 3050°K, 5060°K, 4410°K, 4150°K, intermediate between the temperatures of the electrons and of the atoms.[33] Whether the higher members of the same series would give a closer approach to the atomic temperature is a question which cannot be answered experimentally as the line intensities become too weak to measure. It seems certain, however, that collisions of the second kind with unexcited atoms are a significant factor in determining the concentrations of higher states.

Persistence of Radiation

The continuance of radiation after the current has been interrupted cannot be accounted for quantitatively by the kinetic energy of the electrons. The only apparently significant stores of energy are in the kinetic energy of the atoms and the excitation energy of the $6P$ states. Since the atomic-Boltzmann equilibrium has been shown to remove energy from the higher excited states, during the steady state, and since the radiation pattern does not change discontinuously when the current is interrupted[34] the atoms must be a sink rather than a source of energy, at least until the electron temperature has fallen nearly to that of the atoms. Rough calculations based on a Boltzmann equilibrium between the electron velocity and the excitation[35] to the 6^3P states, indicate that the stored energy is of the right order of magnitude. In making these calculations it must be remembered that only about 10 percent of the power input is radiated, and that nonradiative dissipative processes and binary collisions of excited atoms to yield molecules or molecule ions may be expected to fall off more rapidly than the atomic radiative processes.

[33] It may be of interest to note that the calculated electron temperature is approximately that of the surface of the sun, and the atomic temperature that of the filament of a tungsten lamp. According to the theory of Elenbaas, reference 7, the electron temperature and the gas temperature are equal, and vary with the distance from the axis; according to the present theory, they are uniform, and unequal. The wall temperature, the maximum electron temperature and the mean gas temperature are substantially the same in both.

[34] H. Witte, Zeits. f. Physik **88**, 415–35 (1934).
[35] V. Fabrikant and V. Pulwer, Comptes rendus U.S.S.R. **3**, 439 (1934).

APRIL 1, 1938 PHYSICAL REVIEW VOLUME 53

The Signs of the Nuclear Magnetic Moments of Li^6 and K^{41}*

John E. Gorham
Columbia University, New York, N. Y.

(Received February 14, 1938)

Nonadiabatic transitions between magnetic quantum states of atoms in an atomic beam were used to determine the signs of the nuclear magnetic moments of Li^6 and K^{41}. The nuclei of these isotopes were found to have positive magnetic moments.

Schuler's[1] determination of the sign of the nuclear magnetic moment of Li^6 was based upon intensity measurements of h.f.s. separations which were incompletely resolved. In view of the uncertainties which arose in connection with the spectroscopic determination of the sign of the nuclear moment of K^{39} because of incomplete resolution of the h.f.s.,[2, 3] it was considered desirable to determine the sign of the nuclear moment of Li^6 by the method of atomic beams. In the case of K^{41} it was of interest to see if the addition of two neutrons changes the sign of the

* Publication assisted by the Ernest Kempton Adams Fund for Physical Research of Columbia University.
[1] Schuler, Zeits. f. Physik **99**, 285 (1935).
[2] D. A. Jackson and H. Kuhn, Nature **137**, 107 (1936).
[3] D. A. Jackson and H. Kuhn, Nature **140**, 276 (1937).

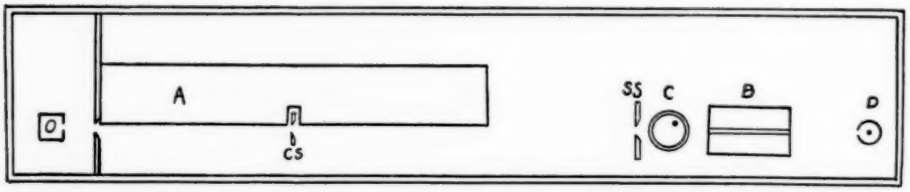

FIG. 1. Diagram of the apparatus viewed from above. *O*, oven; *A*, weak *A* field; *CS*, collimating slit; *SS*, selecting slit; *C*, transition field; *B*, strong *B* field; *D*, detector.

nuclear magnetic moment relative to the sign of the moment of K^{39}.

The method of nonadiabatic transitions between magnetic quantum states of atoms in an atomic beam, suggested by Rabi,[4, 5] has been applied to obtain the signs of the nuclear magnetic moments of the hydrogens by Kellogg, Rabi and Zacharias,[6] and of the more abundant alkali metals by Torrey,[7] and Millman and Zacharias.[8]

Manley,[9] and Manley and Millman[10] have determined the nuclear spins and hyperfine separations of the K^{41} and Li^6 nuclei. The nuclear spins and hyperfine separations of K^{39} and Li^7 in the normal state are known from the work of Millman,[11] and Fox and Rabi.[12]

METHOD

The method employed in this experiment was somewhat different from the procedure of previous workers because of the fact that the K^{41} and Li^6 isotopes have abundances of less than 10 percent, and their h.f.s. separations are very small. It was therefore necessary in the first place to use a very long beam to attain sufficient resolution, and to use a procedure which would conserve the intensities of these isotopes relative to the background of the more abundant isotopes.

To this end the weak *A* field, shown in Fig. 1, was set at a value necessary to produce the zero moment of the isotope to be studied. A selector slit was placed in the path of the beam to cut out all atoms not in the zero moment state, aside from the background of the fast, undeflected atoms in other states possessing moments different from zero.

The subsequent analysis of the beam was effected by means of the transition field *C*, and the strong analyzing field *B*. In the *B* field the atoms in the two zero moment levels were separated spatially into a Stern-Gerlach pattern of two broad peaks. If one set the detector on either of these two peaks one could study the variation of its intensity with the current in the wires producing the *C* field. A direct comparison between this variation and the corresponding variation of the more abundant isotope of known sign then permitted one to infer the sign of the moment immediately. If the change of intensity of the less abundant isotope is the same as that of the more abundant isotope the signs of the moments of the two isotopes must be the same. Conversely, if the changes of intensity are of opposite sign, the signs of the moments must be unlike.

APPARATUS

The apparatus, as shown in Fig. 1, consisted of a long brass tube which contained an oven, slit system of the usual type, and a nonhomogeneous deflecting field 153 cm long produced by the usual system of a pair of wires carrying current in opposite directions. This part of the apparatus was identical with that used by Manley[9] and Manley and Millman.[10] To this tube was added another section, 30 cm long and 5 in. in diameter, which contained the transition field, strong field and the detecting filament.

The *C* field, shown in Fig. 1, consisted of a copper wire mounted inside and parallel to the axis of a brass cylinder, 3 cm in diameter and 5 cm long. The cylinder was mounted on a double brass-to-brass ground joint so that it could be moved laterally with respect to the

[4] Rabi, Phys. Rev. **49**, 324 (1936).
[5] Rabi, Phys. Rev. **51**, 652 (1937).
[6] Kellogg, Rabi and Zacharias, Phys. Rev. **50**, 472 (1936).
[7] Torrey, Phys. Rev. **51**, 501 (1937).
[8] Millman and Zacharias, Phys. Rev. **51**, 380A (1937).
[9] Manley, Phys. Rev. **49**, 921 (1936).
[10] Manley and Millman, Phys. Rev. **51**, 19 (1937).
[11] Millman, Phys. Rev. **47**, 739 (1935).
[12] Fox and Rabi, Phys. Rev. **48**, 746 (1935).

beam, and also rotated about its own axis, which was vertical. It was found that when a current of about nine amperes was sent down the wire and up through the wall of the cylinder the magnetic field due to this current combined with the field normally present in the laboratory to form a transition field having characteristics which were quite satisfactory for the performance of this experiment.*

In order to produce a strong, nonhomogeneous B field with a small expenditure of power the following type of iron magnet was used. A slot was made in the walls of, and parallel to the axis of an Armco iron cylinder. The slot was 10 cm long and 1.33 mm wide at its widest place. The outside diameter of the cylinder was 3.75 cm, and the walls were about 0.6 cm thick. Fig. 2 shows a cross section of the cylinder. The vertical dash represents the beam in the slot. The faces of the slot were arcs of circles which were approximately tangent at a point diametrically opposite the slot. This configuration gave a ratio of field to gradient of field of about 2 cm. A current of 12 amperes through eight turns of water-cooled copper tubing wound on the walls of the cylinder produced a magnetic field of about two thousand gauss in the slot. In this field the alkali atoms had over-all magnetic moments of approximately plus or minus one Bohr magneton, irrespective of their magnetic quantum state. The nuclear and electronic magnetic moments were completely uncoupled in the strong field.

The over-all length of the beam was about 230 cm. It was found that sufficient beam intensity could be obtained at the detector when the vapor pressure of the alkali vapor in the oven was about 1 mm, and the pressure in the rest of the apparatus was better than 10^{-6} mm of mercury.

Procedure for K^{41}

The positions of the oven, collimating slit, and receiving slit were varied until the beam was running parallel to the A field at a predetermined distance from the field wires where the field characteristics were sufficiently uniform. This was done as described by Manley.[9]

The C and B field currents were set equal to zero and the current of the A field was varied until K^{41} atoms having zero magnetic moment were most abundant at the receiving slit set to receive undeflected atoms. The resolving power of the A field because of its high ratio of gradient to field, and great length, was such as to permit complete separation of the zero moment atoms from the other K^{41} atoms which did not have zero moment, and from the K^{39} atoms

The B field current was then set equal to twelve amperes to produce a field of about two thousand gauss in the slot through which the atoms passed. A conventional Stern-Gerlach pattern of the atoms deflected in this B field was obtained by moving the filament across the beam, and noting the positive ion current as a function of the filament position. This field strength just completely separated the two peaks of maximum intensity on either side of the center of the Stern-Gerlach pattern. One peak was composed of atoms of lower F value belonging to one zero moment level. The other peak was composed of atoms having the higher F value. Identification of the F values of the peaks was sufficient to enable one to determine the sign of the nuclear magnetic moment.

Atoms of lower F value will not undergo any change of intensity in the strong field pattern after passing through the transition field.[4] Atoms of higher F value will undergo transitions to

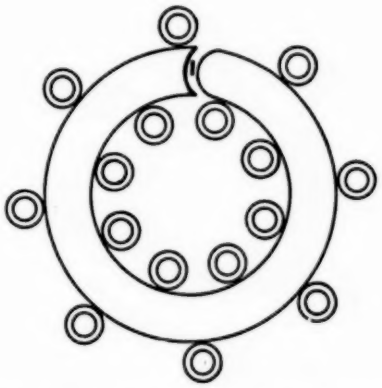

FIG. 2. Cross section of the strong field electromagnet. The dash in the slot shows the position of the beam.

* Previous workers in this laboratory have used iron cylinders instead of brass ones, but it was found that the rapid changes in field at the boundaries of the iron effected transitions when the current through the wires was zero. Then by varying the current it was possible to observe increases as well as decreases of intensity of levels which should show only one or the other of the effects. When the brass cylinder was used such spurious transitions were not observed.

magnetic states having moments of opposite sign in the strong field, if the transition field current is suitably chosen. Thus the higher F peak will show a decrease in intensity. Since the C field was located before the B field, the atoms actually making the transition will appear at the same peak as do the atoms of the lower F value. Thus the peak primarily due to atoms of lower F value will show an increase of intensity just equal to the decrease of the other peak intensity.

The filament was set at the Stern-Gerlach peak composed of atoms having positive moment in the B field. The magnitude of the C field current was varied continuously from zero to 9.6 amperes, and the intensity of the peak simultaneously measured. A similar procedure was followed for the atoms having negative moment.

The A field current was changed first to just less than, and then to just larger than the K^{41} zero moment value, and the procedure described in the preceding paragraph was repeated.

Results for K^{41}

When the intensity of the zero moment components was being observed the B field negative moment peak showed a decrease of 30.8 ± 2.3 percent for the optimum value of the C field current. Within the limits of the precision of the experiment the intensity of the positive moment peak was increased by a number of centimeters of galvanometer deflection equal to that lost by the negative peak. No increase in intensity of the negative peak nor decrease in intensity of the positive peak was observed for any value of the C field current.

When the value of the weak field current was either just larger or just smaller than that required to produce K^{41} atoms of zero magnetic moment the changes in intensity of the strong field positive and the negative moment peaks were qualitatively the same as those observed for K^{41} atoms having zero magnetic moment. The number of centimeters of galvanometer deflection corresponding to a change in peak intensity was smaller than that observed for the K^{41} zero moment atoms. Therefore the effect observed for the zero moment could not have been due to atoms forming the background.

The K^{39} zero moment atoms behaved in a similar manner, and Torrey[7] has shown that the sign of the nuclear magnetic moment of K^{39} is positive. The author has verified this result with the present apparatus. Therefore, it is concluded that the sign of the nuclear magnetic moment of K^{41} is positive.

Procedure for Li^6

The resolving power of the A field was not great enough to separate the Li^6 zero moment peak from the background of Li^7 atoms and molecules. That is, when the current through the A field wires produced a field in which the two Li^6 magnetic quantum levels had zero magnetic moments, and were consequently undeflected by the field, the faster atoms of the Li^7 state $m=0$ were not deflected enough to miss the receiving slit. Therefore, in order to determine the sign of the moment of Li^6, it was necessary to follow a procedure which was somewhat different from that used in the case of K^{41}.

As the A field current was varied from fifteen to twenty-seven amperes the percentage of the atoms, passed through the receiving slit and belonging to the zero moment levels of Li^6, varied from about five percent to about twenty-nine percent. The maximum percent abundance was obtained when the A field was set at the Li^6 zero moment peak value. On either side of this A field the percent abundance of Li^6 atoms decreased. The method of calculating the abundances of the various states at the receiving slit has been described by Manley and Millman.[10] The intensity of the Li^6 zero moment atoms arriving at the detector was easily calculated, since the Li^7 zero moment intensity at the filament, the isotopic abundance ratio, and the population factor for the Li^6 and Li^7 levels were known.

The A field current was varied from 15 to 27 amperes in steps of two amperes. At each value of the A field current the C field was used as described in connection with the determination of the sign of the moment of K^{41}. A similar procedure was repeated for A field currents of 35, 40 and 45 amperes.

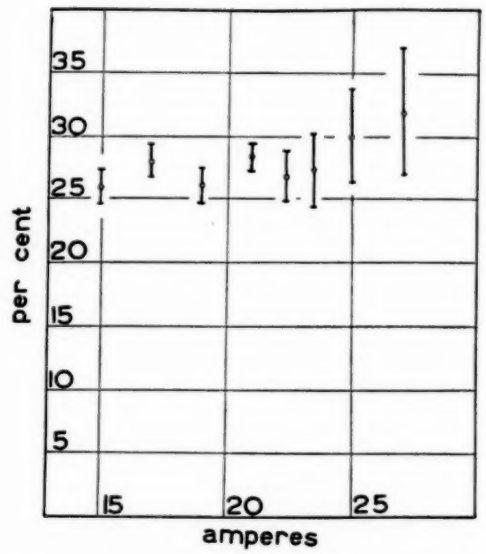

FIG. 3. Percent change in intensity of Li^6 negative strong field peak as a function of the weak field current.

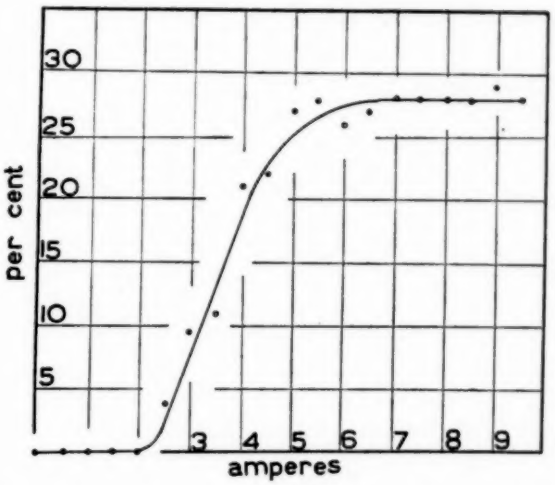

FIG. 4. Percent change in intensity of negative strong field peak as a function of transition field current.

RESULTS FOR Li^6

For values of the A field current between 15 and 45 amperes a decrease in intensity of the negative B field peak was observed as the C field current was varied from 0 to 9.6 amperes. A corresponding increase in intensity of the positive peak was observed.

Figure 3 shows the effect of the C field plotted, not in absolute value, but as the percent change of the intensity of this peak, for the various values of the current in the A field wires. It is to be noticed that within the limits of error indicated in the diagram this change is independent of the value of the A field current. However, when the A field current is 15 amperes about five percent of the intensity is due to Li^6, at 22.5 amperes, 29 percent, and at 27 amperes, 15 percent. Hence it seems quite apparent that the Li^6 atoms were behaving like the Li^7 atoms and the sign of the Li^6 moment is therefore positive. This is in agreement with the predictions of Bethe and Bacher,[13] Inglis,[14] and Rose and Bethe.[15]

This conclusion is further supported by the results shown in Fig. 4; here the percent change of intensity of the negative peak is plotted as a function of the current in the C field wires for the fixed value of 22.5 amperes in the A field wires. Similar curves were made for all the other values of the A field current and they are all essentially the same. Hence it seems implausible to assume that the background Li^7 atoms were making transitions to an abnormal degree in the region of the greatest abundance of Li^6; thus masking null or negative effects of Li^6. Such an abnormality is certainly not to be expected from the theory of this experiment.

The author would like to thank Professor I. I. Rabi for suggesting the problem, and for his valuable suggestions during the course of the experiment. He would also like to thank the other members of the atomic beams laboratory for helpful discussions.

[13] Bethe and Bacher, Rev. Mod. Phys. **8**, 182 (1936).
[14] D. L. Inglis, Phys. Rev. **51**, 531 (1937).
[15] Rose and Bethe, Phys. Rev. **51**, 205 (1937).

Term Values in Carbon*

C. W. UFFORD
Allegheny College, Meadville, Pennsylvania
(Received January 24, 1938)

The energies of the terms of the normal state of C I, $1s^2\ 2s^2\ 2p^2$, and of the excited state, $1s^2\ 2s\ 2p^3$, are calculated with one-electron functions for a self-consistent field. The effect of the interaction of $1s^2\ 2s^2\ 2p^2$ and $1s^2\ 2p^4$ is also included. Tables are given of the radial integrals, of the absolute energies of the terms, and of the separations of the terms. $1s^2\ 2s\ 2p^3\ {}^5S$ is found 3.16 volts above the ground state $2p^2\ {}^3P$.

THE energies of the terms of the normal state of C I, $1s^2\ 2s^2\ 2p^2$, and of the excited state, $1s^2\ 2s\ 2p^3$, are here calculated from Torrance's[1] values of the one-electron functions for a self-consistent field. The method is that used by Hartree and Black.[2] The values of the radial integrals F, G, and I are given in Table I. The I and F^0 integrals were checked by the method of H and B. The G integrals and F^2 were checked by calculating the difference between pairs of integrals, e.g., excited state minus normal state. Thus let Δ represent the difference of a function obtained by subtracting the function for the normal state from that for the excited state. Then in the notation of H and B,

$$\Delta\rho(\alpha\beta|r)=P_0(\alpha|r)\Delta P_0(\beta|r)+P_0(\beta|r)\Delta P_0(\alpha|r)+\Delta P_0(\alpha|r)\Delta P_0(\beta|r) \quad (1)$$

and

$$\Delta I_k(\alpha\beta:\gamma\delta)=\int_0^\infty r^{-1}\{\Delta\rho(\alpha\beta|r)\,Y_k(\gamma\delta|r)+[\rho(\alpha\beta|r)+\Delta\rho(\alpha\beta|r)]\Delta Y_k(\gamma\delta|r)\}dr, \quad (2)$$

where $P_0(\alpha|r)$, $P_0(\beta|r)$, $\rho(\alpha\beta|r)$ and $Y_k(\gamma\delta|r)$ are the functions belonging to the normal state; and $\Delta Y_k(\alpha\beta|r)$ is calculated by replacing $\rho(\alpha\beta|r)$ by $\Delta\rho(\alpha\beta|r)$ in (13) and (14) of H and B. The errors in the integrals computed in this way are given in Table I.

Fried working with Shortley[3] has found $F^2(2p,\ 2p)=0.2137$ independently for the normal state by numerical integration of the differential equations given in H and B. This agrees well with the value given in Table I considering the different method used.

The term values were found from the radial integrals by Slater's[4] method. The coefficients of the integrals for $1s^2\ 2s^2\ 2p^2$ are given in Table IV of H and B. The energies of $1s^2\ 2s\ 2p^3$ are[5]

$$2I(1s)+I(2s)+3I(2p)+F^0(1s,\ 1s)+2F^0(1s,\ 2s)+6F^0(1s,\ 2p)+3F^0(2s,\ 2p)+3F^0(2p,\ 2p)-G^0(1s,\ 2s)$$

$$-G^1(1s,\ 2p)+\begin{cases} {}^1P & 0 & {}^3P & -\frac{2}{3}G^1(2s,\ 2p) \\ {}^1D & -\frac{6}{25}F^2(2p,\ 2p) & {}^3D & -\frac{6}{25}F^2(2p,\ 2p)\ -\frac{2}{3}G^1(2s,\ 2p) \\ {}^3S & -1\frac{5}{25}F^2(2p,\ 2p)+\frac{1}{3}G^1(2s,\ 2p) & {}^5S & -1\frac{5}{25}F^2(2p,\ 2p)-G^1(2s,\ 2p) \end{cases}$$

Table II gives the energy values of the terms. The term values are also given when allowance is made for the approximate value of the interaction of $1s^2\ 2s^2\ 2p^2$ with $1s^2\ 2p^4$ as calculated by the method of Hartree and Swirles.[6] Here the integrals used in finding the terms of $1s^2\ 2p^4$ are

* Presented at the Washington meeting of the American Physical Society, April 1937: Phys. Rev. **51**, 1020A (1937). Small errors in the values given there are corrected here.

[1] C. C. Torrance, Phys. Rev. **46**, 388 (1934). I am grateful to Dr. Torrance for letting me have these functions before publication.

[2] D. R. Hartree and M. M. Black, Proc. Roy. Soc. **A139** 311 (1933). This paper will be referred to as H and B. In Table V, p. 331, for O II $2s^2\ 2p^3\ {}^4S$ observed, 1.301 should be 1.290 which improves the agreement with the calculations and gives differences varying in the same way as those of O III and O.

[3] I am grateful to Dr. G. H. Shortley for sending me this unpublished result.

[4] J. C. Slater, Phys. Rev. **34**, 1293 (1929).

[5] Cf. Condon and Shortley: *Theory of Atomic Spectra* (Cambridge 1935) p. 199. The sign of G_1 in ${}^3S$ should be reversed. Also M. H. Johnson, Jr., Phys. Rev. **39**, 209 (1932).

[6] D. R. Hartree and Bertha Swirles, Proc. Camb. Phil. Soc. **33**, 240 (1937).

TABLE I. *Values of the radial integral I, F and G for* C I.

	Normal State $1s^2\ 2s^2\ 2p^2$	Error	Excited State $1s^2\ 2s\ 2p^3$	Error
$I(1s)$	−17.9324	8×10^{-5}	−17.9359	14×10^{-5}
$I(2s)$	− 3.7239	2	− 3.7381	5
$I(2p)$	− 3.2430	28	− 3.2839	44
$F^0(1s, 1s)$	3.5050		3.5110	
$F^0(1s, 2s)$	0.7666	2	0.7708	1
$F^0(1s, 2p)$	0.7131	3	0.7250	1
$F^0(2s, 2s)$	0.5477		0.5516	
$F^0(2s, 2p)$	0.5134	4	0.5212	4
$F^0(2p, 2p)$	0.4844		0.4954	
$F^2(2p, 2p)$	0.2134	6	0.2197	6
$G^0(1s, 2s)$	0.0412	0	0.0416	0
$G^1(1s, 2p)$	0.0532	21	0.0547	21
$G^1(2s, 2p)$	0.3154	0	0.3217	0

TABLE II. *Absolute term values in* C I. *Atomic units.*

	Normal State $1s^2\ 2s^2\ 2p^2$	With interaction $1s^2\ 2s^2\ 2p^2 - 1s^2\ 2p^4$	Excited State $1s^2\ 2s\ 2p^3$	
^3P	−37.6599	−37.6756	^5S −37.5590	^3S −37.1301
^1D	−37.6087	−37.6244	^3D −37.3727	^1D −37.1582
^1S	−37.5319	−37.5945	^3P −37.3200	^1P −37.1055

taken from $1s^2\ 2s\ 2p^3$ instead of from $1s^2\ 2s^2\ 2p^2$. The separations of the terms together with the observed values of Edlén[7] and the values calculated by Bacher and Goudsmit[8] are given in Table III. The lowest term ^5S of $1s^2\ 2s\ 2p^3$, which has not been observed. is calculated to be 3.16 volts above the ground state $2p^2\ ^3P$.

It is also interesting to compare these calculations with those of Van Vleck[9] done empirically by the use of Johnson's formulas,[5] and with those of Beardsley[10] who used approximate wave functions. The radial integrals of Table I are not greatly different from those found by Van Vleck and Beardsley. The terms of $2s\ 2p^3$ are similar to those obtained by them, except that ^5S falls somewhat higher than the rather low value found by Beardsley.

TABLE III. *Term values of* C I. *Wave numbers measured from* $1s^2\ 2s^2\ 2p\ ^2P_{\frac{1}{2}}$.

		Calculated*	With interaction* $1s^2\ 2s^2\ 2p^2 - 1s^2\ 2p^4$	Observed	Bacher and Goudsmit
$1s^2\ 2s^2\ 2p^2$	^3P	91965	91284	90786	88155
	^1D	80727	80047	80622	77910
	^1S	63872	73485	69167	71431
$1s^2\ 2s\ 2p^3$	^5S	69820	65694	58000†	55894
	^3D	28931	24805	26727	26053
	^3P	17365	13239	15560	17827
	^1D	−18146	−22272	− 7000†	−14027
	^3S	−24313	−28439	−14984	−24412
	^1P	−29712	−33838	−29000†	−22326

* The absolute positions of the calculated values have been adjusted by least squares to agree with the observed values below the ionization potential. The differences only of the terms are theoretically significant. To determine their absolute position relative to $1s^2\ 2s^2\ 2p\ ^2P_{\frac{1}{2}}$, the energy of the latter would have to be calculated.

† The observed value of ^5S is estimated by Edlén, reference 7, from the irregular doublet law. The values of ^1D and ^1P are estimated from the irregular doublet law and comparison with O III and N II. No combinations are observed for these levels.

The interaction of $1s^2\ 2s^2\ 2p^2$ with $1s^2\ 2p^4$ is seen to be in the right direction for all the terms below the ionization potential. The correction introduced is, however, too large except in the case of $2p^2\ ^3P$ and $2s\ 2p^3\ ^5S$. It is also too large for the interval ratio in $1s^2\ 2s^2\ 2p^2$ as was the case in O III[6].

C I: $(^1D - {}^1S)/(^3P - {}^1D)$, Slater 1.50, interaction 0.59, observed 1.13, and Bacher and Goudsmit 0.63.

Interaction also improves slightly the value of the ionization potential of the normal state of C I. Ionization potential: calculated 1019.66 volts, with interaction $1s^2\ 2s^2\ 2p^2 - 1s^2\ 2p^4$ 1020.09 volts, and observed 1024.84 volts.[7] Were it possible to include the interaction of all configurations, good agreement between theory and experiment might be expected.

I am grateful indeed to Dr. C. C. Torrance who suggested this problem and took an interest in its progress. I am also indebted to the many FERA and NYA students who have helped with the numerical integration.

[7] B. Edlén, Nova Acta Regiae Societatis Scientiarum Upsaliensis, [IV] **9**, No. 6 (1933); condensed in Zeits. f. Physik **84**, 746 (1933).

[8] R. F. Bacher and S. Goudsmit, Phys. Rev. **46**, 948 (1934).

[9] J. H. Van Vleck, J. Chem. Phys. **2**, 297 (1934).

[10] N. F. Beardsley, Phys. Rev. **39**, 913 (1932).

Photoelectric and Thermionic Investigations of Thoriated Tungsten Surfaces

ALLEN KING*
Department of Physics, University of Rochester, Rochester, New York
(Received January 31, 1938)

Photoelectric and thermionic data were obtained over a wide range of temperatures for several activations of a thoriated tungsten filament. The temperature dependence of the thermionic and photoelectric work functions are quite different. It is shown that this is to be expected for a nonuniform surface. The measured current density in either case is $i=(1/A)\int_s i_s\,ds$, in which i_s is given by either the Richardson-Dushman or the Fowler-DuBridge equation and A is the total emitting area. On the basis of a simple patch theory the integrations are carried out and show that (1) the saturation electron emission is independent of the size of the patches; (2) the observed or characteristic thermionic and photoelectric work functions for composite surfaces are different at low temperatures and approach each other at high temperatures; (3) the maximum and minimum values of the work function for a given surface do not vary linearly with temperature.

INTRODUCTION

THE well-known experimental fact that the coefficient A in Richardson's equation for thermionic emission is not a universal constant has presented a problem of both experimental and theoretical interest. Actually several lines of evidence indicate that the discrepancy between A and the theoretical constant

$$U=4\pi^2mk^2e/h^3=120 \text{ amp./cm}^2\text{/deg.}^2 \quad (1)$$

may be ascribed to a temperature coefficient of the work function.[1] That is, in the equation

$$i=UT^2e^{-w/T} \quad (2)$$

the work function w may be a function of both temperature and applied field. Because Richardson lines usually are straight, it is assumed that higher derivatives of w than the first with respect to temperature are vanishingly small, so that

$$w=w_0+\alpha t, \quad (3)$$

in which w_0 and α are constants characteristic of the emitting surface, and may also be functions of the applied field.[2] Experimental values of A are related to the corresponding values of α through the equation

$$\alpha=2.303(\log U-\log A). \quad (3')$$

It is of course desirable to check this relation through independent measurements of α by other methods.

D. B. Langmuir[3] measured the contact potential difference between a tungsten filament and a tantalum anode as a function of temperature. He attempted to fit his results with a straight line, the slope of which he made equal to the negative of the temperature coefficient of the work function found by Nottingham from thermionic data.[4] His results are questioned in a recent paper by Reimann.[4a]

A more direct method of obtaining the temperature coefficient of the work function is to determine w for several different temperatures by the application of Fowler's theory to photoelectric data. In this way Brattain and Becker[5] deduced a value for the coefficient of palladium from the data of DuBridge and Roehr.[6] It was recognized, however, that more accurate data were needed.

Linford,[7] Smith,[8] and Glover[9] have shown that Fowler's theory may be applied to the composite surface of thorium on tungsten. Since a rather large temperature variation of the work function was to be expected for such a surface, it seemed worth while to make a more detailed study of the photoelectric and thermionic properties of thoriated tungsten.

APPARATUS AND PROCEDURE

The experimental tube was constructed in accordance with the conventional design in which

* Now at Rensselaer Polytechnic Institute, Troy, New York.
[1] Becker and Brattain, Phys. Rev. **45**, 694 (1934).
[2] Rose, Phys. Rev. **49**, 838 (1936).
[3] D. B. Langmuir, Phys. Rev. **49**, 428 (1936).
[4] Nottingham, Phys. Rev. **49**, 78 (1936); *a*, Reimann, Proc. Roy. Soc. **163**, 499 (1937).
[5] Reference 1, page 702.
[6] DuBridge and Roehr, Phys. Rev. **39**, 99 (1932).
[7] Linford, Rev. Mod. Phys. **5**, 34 (1933).
[8] Smith and DuBridge, Phys. Rev. **46**, 339 (1934).
[9] Glover, Ph.D. dissertation, University of Rochester, Spring, 1935.

three nickel cylinders are placed end to end and coaxial with the filament. The two end ones were connected together and used as guard rings; the middle one was fastened to a separate insulated support and was connected to a tungsten side lead. A molybdenum spring held the filament taut.[10] Potential leads were welded to either end of the filament. Through a slit in the central cylinder, opposite a quartz window, the filament could be illuminated for the photoelectric measurements. An ionization gauge and getter filaments of Th-W wire were included in the assembly.

Bake-outs of the whole assembly up to 500°C were alternated with bombardment and furnacing of the cylinders over a period of two weeks. During this procedure all the filaments were properly aged and thoroughly outgassed. The tube was finally sealed off the vacuum system and further cleaned up with the getter filaments until a pressure much less than 10^{-7} mm Hg was obtained.[11]

In order to control accurately the temperature of the filament, a circuit was constructed, which allowed values of the current to be read and maintained to better than one part in a thousand.

For the accelerating potential several B batteries were kept in a well-shielded dry box. A type P wall galvanometer in series with approximately 100 megohms was used as a high resistance voltmeter to measure it. All the measurements reported here were made for 100 volts collecting potential ($\sim$2640 volts/cm). An error of one-half volt was not significant since the work function approaches a constant value for about 100 volts applied potential as indicated on the work function—voltage diagrams determined by Glover[9] and by Brattain and Becker.[12]

A DuBridge-Brown amplifier[13] and a Leeds and Northrup type R galvanometer were used for photoelectric and weak thermionic measurements. This system allowed emission currents from 10^{-15} to 10^{-6} amperes to be measured. A multimeter, also in the circuit, could be employed for even greater emissions.

In order to obtain the temperature of the central part of the filament, a temperature *versus* current curve was made. The filament was "long" down to a temperature of 760°K and, therefore, in the thermionic range no lead loss corrections were necessary.[14] For this region and, in fact, down to a temperature of 600°K the Langmuir-Jones,[15] Forsythe-Watson,[16] and Forsythe-Worthing[17] tables were used, and a satisfactory scale was established. Points on it were checked with a pyrometer and also with an auxiliary tube. For that part of the curve from room temperature to 600°K the tables and formulas of Langmuir and Taylor were used.[18] In this region the temperature depends to a large extent upon the bulb temperature which, in these experiments, was taken to be equal to room temperature. For this reason two curves were determined for room temperatures of 292° and 302°K, respectively; and for intermediate values of room temperature, the filament temperatures were obtained by interpolation between them. Actually, these calculations were extended to 700°K. Temperatures between 600° and 800°K were determined so that the high and low ends of the two curves joined smoothly and yielded reasonable values in this region.

For the photoelectric measurements, spectral lines from a Cooper-Hewitt Uviarc were resolved by a single Bausch and Lomb monochromator with quartz lenses to focus the individual lines on the filament. Slit widths of 0.05 mm were used. A special table was built upon which to mount the monochromator and arc, so that they could be properly adjusted. Effects of stray light were investigated and found to be negligible. The relative intensities of the arc lines were measured with a vacuum thermopile connected to a high sensitivity low resistance galvanometer.

After activating the filament, thermionic emission measurements were made for both increasing and decreasing temperatures over a range where the surface was not altered by further activation or dispersion. Then at a series of temperatures below the thermionic range photoelectric data

[10] Blodgett and Langmuir, Rev. Sci. Inst. **5**, 321 (1934).
[11] Pressures less than 5×10^{-8} mm Hg were unmeasurable with the apparatus used.
[12] Brattain and Becker, Phys. Rev. **43**, 428 (1933).
[13] DuBridge and Brown, Rev. Sci. Inst. **4**, 532 (1932).
[14] Langmuir, MacLane and Blodgett, Phys. Rev. **35**, 478 (1930).
[15] Langmuir and Jones, G. E. Rev. **30**, 310, 354, 408 (1927).
[16] Forsythe and Watson, J. O. S. A. **24**, 114 (1934).
[17] Forsythe and Worthing, Astrophys. J. **61**, 126 (1925).
[18] Taylor and Langmuir, Phys. Rev. **50**, 68 (1936); J. O. S. A. **25**, 321 (1935).

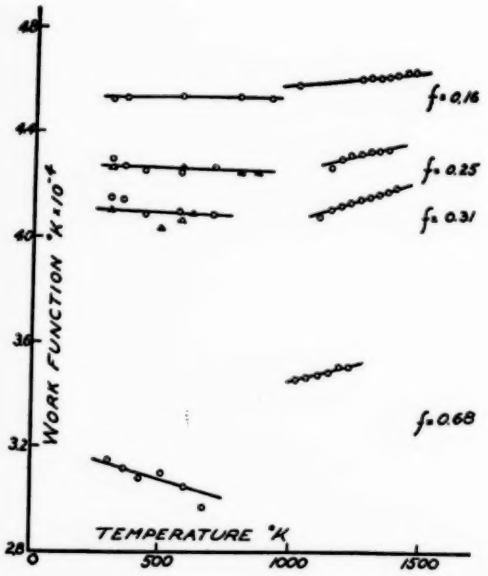

FIG. 1. Work function *versus* temperature curves for several activations of a thoriated tungsten surface, low temperature portions from photoelectric and high temperature portions from thermionic data. Small triangles represent data obtained on the following day of a regular run (represented by circles).

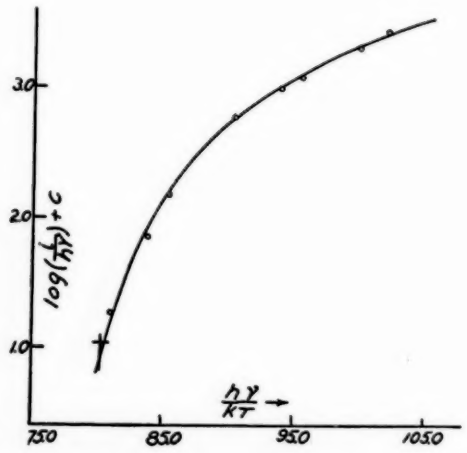

FIG. 2. Fowler plot of photoelectric data from a thoriated tungsten surface for which $f=0.16$ and $T=564.6°$K. The work function was found to be 45370°K.

were taken. Sufficient time was allowed between changes of temperature so that equilibrium conditions became established. At the end of a complete run the amplifier was calibrated. In this manner sufficient photoelectric data were secured so that Fowler plots could be made and work functions determined for a series of temperatures on surfaces of different activations.

ANALYSIS AND INTERPRETATION OF DATA

The thermionic emission currents were first reduced to those for unit apparent surface. Then these values were introduced into the equation

$$w=2.303T\{\log U-\log i/T^2\}, \qquad (4)$$

in which $\log U$ was taken equal to 2.074. In this manner the *characteristic thermionic work functions* for a series of filament temperatures at various activations of the surface were determined. For any given activation these work functions are found to vary linearly with temperature with a *positive* increasing slope as seen in the right-hand group of line segments in Fig. 1.

The photoelectric emission currents, on the other hand, were plotted as $\log (i/h\nu)$ against $h\nu/kT$ for each temperature and activation. A representative set of points fitted to a Fowler theoretical curve is shown in Fig. 2. The currents have been reduced to amperes per unit intensity of light. By an appropriate horizontal and vertical shift, the experimental points are brought into coincidence with the theoretical curve. Then the vertical shift corresponds to the absorption probability per quantum of light denoted by B; and the horizontal shift is just $h\nu_0/kT=w_p'/T$ in which w_p' is called the *characteristic photoelectric work function* in degrees Kelvin. If the values of w_p' are plotted against the corresponding temperatures T, a curve is obtained which has a generally *negative* slope. The data are shown in the left-hand group of lines in Fig. 1.

Only a slight temperature dependence of the measured values of B was noted, so that the effect of temperature on the absorption probability factor may be neglected.

The state of activation of the surfaces are described by "f numbers," which were determined from the observed thermionic work functions at 1274°K and the data of Brattain and Becker.[12] If these work functions are plotted against the corresponding f numbers the familiar parabola-like curve is obtained as seen in Fig. 3 (broken line). On the other hand, if the photoelectric work functions for 300° and 670°K are plotted against the same f numbers, straight lines with negative slopes result. (Solid lines of Fig. 3.)

According to the simple theory,[1] it would be

expected that the photoelectric and thermionic work functions at a given temperature, as determined in the above manner, would be identical. This would mean that the low temperature (photoelectric) and high temperature (thermionic) portions of the work function plots of Fig. 1 would join together into a smooth line. For the cleanest surfaces ($f=0.16$) this condition is approximately fulfilled, within experimental error. The discrepancy between the photoelectric and thermionic data becomes progressively worse as thorium is added to the surface. In fact, for thoriated surfaces the temperature coefficients of the photoelectric and thermionic work functions are of opposite sign. Some reasons for this discrepancy must be found.

In the first place it seems evident that the discrepancy cannot be attributed to experimental error. Errors as large as 10 percent in reading the photoelectric and thermionic emission currents would have a negligible effect on the work function determinations; and the precision of current and light intensity measurements was considerably better than this for the most part. It is impossible to attribute any appreciable portion of the discrepancy to errors in the temperature scale. On the other hand, if one assumes the true emitting area of the filament to be greater than the apparent area by a factor of 1.3 (which appears to be a reasonable estimate[19–21]), the discrepancy between photoelectric and thermionic measurements become worse.

Another possible source of error is that due to the accumulation of impurities on the surface during the course of a day's run. Readings of the thermionic emission for a given activation were repeated, however, on the following days, and in every case the emission for a given temperature remained practically unchanged. The vacuum conditions were good enough, and the filament had been well aged and outgassed so that this result was not unexpected. Values of the photoelectric work functions, on the other hand, varied somewhat from one day to the next. This variation appears to be outside the total experimental error as seen in Fig. 1, but is still of the order of only one percent.

[19] Tonks, Phys. Rev. **38**, 1030 (1931).
[20] Langmuir, J. Am. Chem. Soc. **54**, 2798 (1932).
[21] de Boer, *Electron Emission and Absorption Phenomena* (Cambridge, 1936), p. 72.

On the basis of the above observations, there is some evidence that a rearrangement of patches or a redistribution of thorium adatoms occurs with temperature and time. The differences between thermionic and photoelectric work functions, however, are not accounted for properly.

Since experimental errors are insufficient to explain the difference, the simple theory used for the reduction of the data must be examined. One could, of course, bring the data into agreement by inserting into Eq. (4) a suitably chosen value for the surface transmission coefficient. For example, the data for $f=0.68$ would reduce to a single smooth line of negative slope by assuming a *transmission* coefficient of approximately 5.0×10^{-3}. In view of other evidence relating to the values of electron reflection coefficients at metal surfaces this value appears unreasonably small. It appears necessary, therefore, to seek elsewhere to account for the major portion of the discrepancy.

Both the thermionic and photoelectric equations are deduced for clean, uniform surfaces. If however, W_a and W_i vary from point to point on the surface the equations will not be applicable to the emission from the whole surface. Work

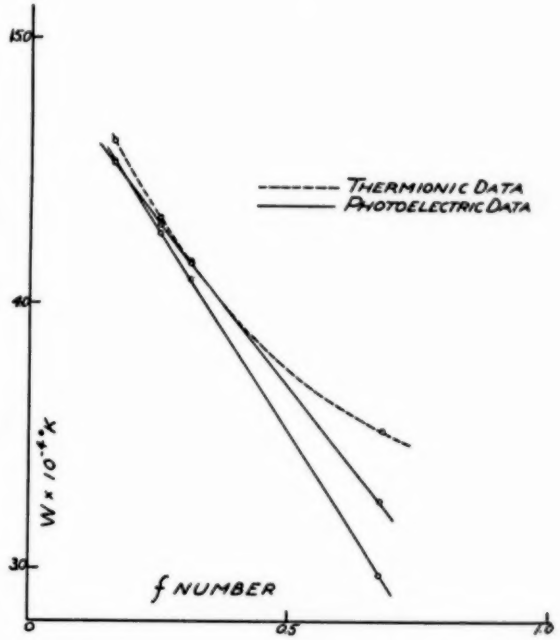

FIG. 3. Work function *versus* f numbers. The thermionic curve is plotted for a temperature of 1270°K; the upper photoelectric curve for 300°K; and the lower one for 670°K.

functions determined by means of these equations, therefore, will be average values for the whole surface and may be called "characteristic work functions." However, the thermionic and photoelectric emission equations are different in form, so that there is no reason to expect these average or characteristic work functions to be the same for the two processes or to show the same temperature dependence.

Theory

In both the thermionic and photoelectric theoretical equations the work function w in degrees Kelvin is equal to $(W_a - W_i)/k$; in which W_a is the height of the surface barrier in energy units, W_i is an integration constant, and k is Boltzmann's constant. To a high degree of approximation W_i is given by the relation

$$W_i = (h^2/2m)\{3nf/4\pi G\}^{\frac{2}{3}},$$

where n is the number of atoms per cubic centimeter; f is the number of free electrons per atom, which is usually assumed to be equal to the number of valence electrons; and G is the statistical weight, which is equal to 2 for electrons. Since W_i depends upon n, which in turn may change with temperature, it follows that W_i is a function of temperature.

On the other hand, W_a should decrease in value as the distance between surface atoms is increased; hence, due to thermal expansion, the work function should decrease with rising temperature. Detailed calculations have been made by Bridgman,[22] Herzfeld,[23] and Wigner.[24] Experimental results have not been sufficiently precise, however, to indicate the correctness of these theories.

In any case, the above theories are developed for uniform surfaces. Composite surfaces, on the other hand, give rise to more complex phenomena. To explain the anomolous Schottky effect, for instance, Langmuir suggested that adatoms were grouped in patches which have a profound influence upon the thermionic emission at low accelerating fields.[25] This suggestion was developed by Linford[26] and Becker and Rojansky;[27] and later it was modified by Becker[28] and by Nottingham.[4] In the following discussion in which a phenomenological theory is described, patches are assumed to exist; but their exact nature is not investigated.

For any electron emission whatever, the current density is given by the relation

$$i = (1/A)\int i_s ds, \tag{5}$$

in which ds is an element of the total emitting area A and i_s is the current density of that element. The assumption will now be made that the element ds is clean and pure, so that the Richardson-Dushman or the Fowler equation may be applied to it, depending upon whether the emission is thermal or photoelectric. The further assumption is made that the field is such that all the electrons are collected by the anode.

For the thermionic case i_s is given by the relation

$$i_s = UT^2 e^{-w_s/T}, \tag{6}$$

in which U is the universal constant (1), and w_s is the surface work function, which is assumed to vary from point to point, i.e.,

$$w_s = T\left\{a + b\cos\frac{\pi x}{t}\cos\frac{\pi y}{r}\right\}. \tag{7}$$

Here a and b are functions of temperature and applied field, and t and r are the lengths of the sides of a single rectangular patch. All values of w_s are found over the area $\frac{1}{2}tr$, so that upon insertion of the above relations in Eq. (5) the integration may be extended from $x=y=0$ to $x=t/2$ and $y=r$. That is

$$i = \frac{2}{tr}UT^2 e^{-a}\int_0^{t/2}\int_0^{r}\exp\left[-b\cos\frac{\pi x}{t}\cos\frac{\pi y}{r}\right]dx\,dy, \tag{8}$$

in which A has been replaced by $\frac{1}{2}tr$.

The exponential under the integral sign now is expanded in a Taylor's series and integrated term by term. There results

$$i = UT^2 e^{-a}S(b), \tag{9}$$

in which
$$S(b) = 1 + \sum_{n=1}^{\infty}\frac{(2n)!}{2^{4n}(n!)^4}b^{2n}. \tag{10}$$

[22] Bridgman, Phys. Rev. **31**, 90, 862 (1925).
[23] Herzfeld, Phys. Rev. **35**, 248 (1930).
[24] Wigner, Phys. Rev. **49**, 696 (1936).
[25] Langmuir, Gen. Elec. Rev. **23**, 503, 589 (1920).
[26] Linford, Phys. Rev. **37**, 1018 (1931) and reference 7.
[27] Becker and Rojansky, see footnote of reference 7, p. 50.
[28] Becker, Rev. Mod. Phys. **7**, 95 (1935).

This series is convergent for all finite values of b. Values of $S(b)$ and $\log S(b)$ are given in Table I.[29]

The observed total emission i may be assumed to obey an equation similar to (6). That is

$$i = UT^2 e^{-w/T}. \tag{11}$$

in which w has already been called the characteristic thermionic work function of the surface. Substitute this value of i in Eq. (9) and take logarithms. Then

$$w = aT - 2.303T \log S(b). \tag{12}$$

From Eq. (7) it is evident that

$$a = (w_{\max} + w_{\min})/2T \tag{13}$$

and

$$b = (w_{\max} - w_{\min})/2T. \tag{13'}$$

In this manner the measured work function has been related to the temperature and the maximum and minimum values of w. Already one important conclusion may be drawn; namely the characteristic thermionic work function is independent of the size of the patches. By means of a different method of analysis Becker came to the same conclusion.[28]

If now the derivative of w with respect to temperature is taken, there results

$$\frac{dw}{dT} = \frac{1}{2}\left\{1 - \frac{b}{2}\frac{R(b)}{S(b)}\right\}\frac{dw_{\max}}{dT} + \frac{1}{2}\left\{1 + \frac{b}{2}\frac{R(b)}{S(b)}\right\}\frac{dw_{\min}}{dT} - 2.303 \log S(b) + \frac{b^2}{2}\frac{R(b)}{S(b)}, \tag{14}$$

TABLE I. *Values of functions $S(b)$ and $R(b)$.*

b	$S(b)$	LOG $S(b)$	$R(b)$
0	1.000	0	0.5000
1	1.131	0.0535	0.5485
2	1.603	0.2049	0.7155
4	5.197	0.7157	1.813
6	23.57	1.3724	6.250
8	127.7	2.1064	1.4405
10	742	2.8704	132.5
12	4521	3.6552	
15	7.188×10^{4}	4.8566	8914
20	7.928×10^{6}	6.8992	

[29] Values of $S(b)$ were calculated from the series:

$$S(b) = 1 + 0.125b^2 + 5.859\times10^{-3}b^4 + 1.356\times10^{-4}b^6 + 1.854\times10^{-6}b^8 + 1.669\times10^{-8}b^{10} + 1.062\times10^{-10}b^{12} + 5.033\times10^{-13}b^{14} + 1.843\times10^{-15}b^{16} + 5.373\times10^{-18}b^{18} + 1.276\times10^{-20}b^{20} + 2.517\times10^{-23}b^{22} + 4.187\times10^{-26}b^{24} + 5.956\times10^{-29}b^{26} + 7.325\times10^{-32}b^{28} + 7.868\times10^{-35}b^{30} + 7.428\times10^{-38}b^{32} + 6.240\times10^{-41}b^{34} + 4.674\times10^{-44}b^{36} + 3.159\times10^{-47}b^{38} + 1.925\times10^{-50}b^{40}.$$

Coefficients of the terms in which $n>15$ were calculated by means of the relation: $2.303 \log C_n = 2n(0.3068 - 2.303 \log n) - 3.4539 \log n - 2.4103 - 7/24n$. The series $R(b)$ is related to $S(b)$ by Eq. (15).

in which

$$R(b) = -\frac{2}{b}\frac{dS(b)}{db} = -\frac{1}{2}\left\{1 + \sum_{n=1}^{\infty}\frac{(2n)!(2n+1)}{2^{4n}(n!)^4(n+1)^2}b^{2n}\right\}. \tag{15}$$

Values of $R(b)$ are given in Table I.

A similar operation is now carried out for the photoelectric aspect of the problem. In this case

$$i_s = \beta_s UT^2 \varphi(x_s), \tag{16}$$

in which β_s is the absorption probability and

$$\varphi(x_s) = \frac{x_s^2}{2} + \frac{\pi^2}{6} + \sum_{n=1}^{\infty}\frac{(-1)^n}{n^2}e^{-nx_s} \tag{17}$$

for $x_s \geqslant 0$; and

$$\varphi(x_s) = -\sum_{n=1}^{\infty}\frac{(-1)^n}{n^2}e^{nx_s} \tag{17'}$$

for $x_s \leqslant 0$ where

$$x_s = h\nu/kT - w_s/T.$$

If now β_s is assumed to be independent of the surface condition, frequency, and temperature in the neighborhood of the threshold;

$$\varphi(x) = \frac{1}{A}\int_s \varphi(x_s)\cdot ds. \tag{18}$$

In Fig. 4 is plotted the diagram of a single patch over which the work function is given by Eq. (7). Maximum values of w occur at $x=0$, $y=0$ and $x=t$, $y=r$. Minimum values occur at $x=0$, $y=r$ and $x=t$, $y=0$. Contours of equal values of w are shown in Fig. 4 at M, N, etc. Evidently the pair of bisecting lines AB and CD are loci of points at which

$$w = (w_{\max} + w_{\min})/2 = aT.$$

It is clear that if $h\nu/k > w_{\max}$ then Eq. (17) must be used; and if $h\nu/k < w_{\min}$ Eq. (17') must be used. On the other hand, if $w_{\min} < h\nu/k < w_{\max}$, then Eq. (17) is used for that portion of the patch for which $x_s > 0$ and (17') for that portion for which $x_s < 0$. Since the general solution of the problem is rather difficult and involves an extra parameter, only three special cases will be discussed.

(1) For $h\nu/k = w_{\max} = T(a+b)$,

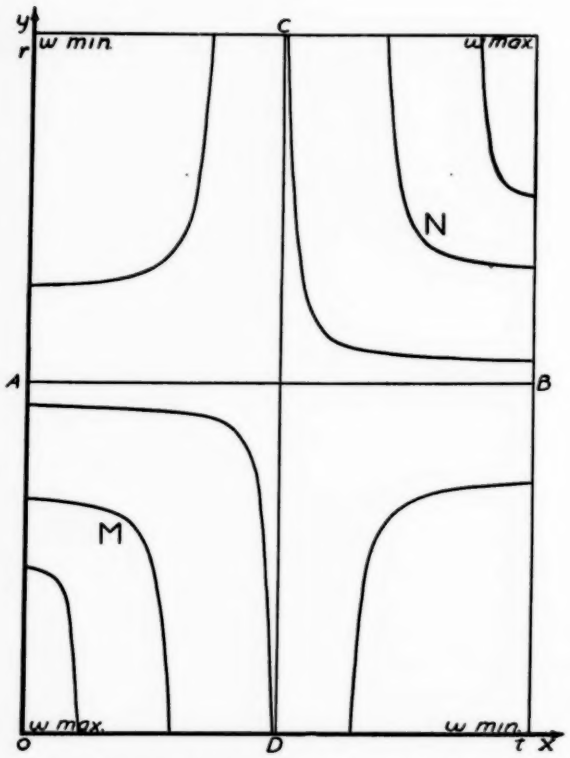

FIG. 4. Diagram of a single patch over which all values of the work functions from $w_{\min}$ to $w_{\max}$ exist. Curves such as MN represent loci of points on the surface where a given work function is found.

$$\varphi(x)=\frac{2}{tr}\int_0^{t/2}\int_0^{r}\left\{\frac{b^2}{2}\left(1-2\cos\frac{\pi x}{t}\cos\frac{\pi y}{r}+\cos^2\frac{\pi x}{t}\cos^2\frac{\pi y}{r}\right)+\frac{\pi^2}{6}+\sum_{n=1}^{\infty}\frac{(-1)^n}{n^2}e^{-nb}\cdot\exp\left[nb\cos\frac{\pi x}{t}\cos\frac{\pi y}{r}\right]\right\}dxdy$$

$$=\frac{5b^2}{8}+\frac{\pi^2}{6}+\sum_{n=1}^{\infty}\frac{(-1)^n}{n^2}e^{-nb}S(nb), \tag{19}$$

in which $S(nb)$ is the same series that occurred in the thermionic equations.

(2) For $h\nu/k=w_{\min}=T(a-b)$

$$\varphi(x)=-\frac{2}{tr}\sum_{n=1}^{\infty}\frac{(-1)^n}{n^2}e^{-nb}\int_0^{t/2}\int_0^{r}\cdot\exp\left[-nb\cos\frac{\pi x}{t}\cos\frac{\pi y}{r}\right]dxdy$$

$$=-\sum_{n=1}^{\infty}\frac{(-1)^n}{n^2}e^{-nb}S(nb). \tag{20}$$

(3) For $h\nu/k=(w_{\max}+w_{\min})/2=aT$

$$\varphi(x)=\frac{2}{tr}\int_0^{t/2}\int_{r/2}^{r}\left\{\frac{b^2}{2}\cos^2\frac{\pi x}{t}\cos^2\frac{\pi y}{r}+\frac{\pi^2}{6}+\sum_{n=1}^{\infty}\frac{(-1)^n}{n^2}\exp\left[nb\cos\frac{\pi x}{t}\cos\frac{\pi y}{r}\right]\right\}dxdy$$

$$-\frac{2}{tr}\int_0^{t/2}\int_0^{r/2}\sum_{n=1}^{\infty}\frac{(-1)^n}{n^2}\cdot\exp\left[-nb\cos\frac{\pi x}{t}\cos\frac{\pi y}{r}\right]dxdy$$

$$=\frac{b^2}{16}+\frac{\pi^2}{12}. \tag{21}$$

Since (21) is always positive it is apparent that $h\nu/k=(w_{\max}+w_{\min})/2$ must always be above the threshold for composite surfaces. Usually this value of the frequency lies near the threshold; so that for a given b it is possible to solve for x and thereby obtain a value of w from

$$w=T(a-x), \tag{22}$$

where w has already been termed the characteristic photoelectric work function.

Equations (12) and (22) can be identical for a given temperature only if

$$x=2.303\log S(b) \tag{23}$$

for which Eq. (21) is satisfied. This condition obtains for $b=0$. Thus *the thermionic and photoelectric work functions are equal only in the case of a uniform surface or for a composite surface at extremely high temperatures.*

By differentiating Eq. (22) with respect to temperature there results

$$\frac{dw}{dT}=\frac{1}{2}\left(1-\frac{b}{8}\frac{dx}{d\varphi}\right)\frac{dw_{\max}}{dT}+\frac{1}{2}\left(1+\frac{b}{8}\frac{dx}{d\varphi}\right)\frac{dw_{\min}}{dT}-x+\frac{b^2}{8}\frac{dx}{d\varphi}, \tag{24}$$

in which

$$d\varphi/dx=2.303\log(1+e^x), \tag{25}$$

where x is related to b by Eq. (21). Eqs. (14) and (24) are identical for a given temperature when the coefficients of $dw_{\max}/dT$ and $dw_{\min}/dT$ are

the same in the two equations. Only $b=0$ will satisfy these conditions. Thus *the temperature coefficients of the thermionic and photoelectric work functions are identical only for uniform surfaces or for composite surfaces at extremely high temperatures.*

From these results it follows that the thermionic and photoelectric work function versus temperature curve for composite surfaces must differ from one another at low temperatures and approach each other asymptotically at high temperatures.

Without a knowledge of either w_{max} or w_{min} it is difficult to carry out any calculations of a quantitative nature. Becker states that $2\mu=0.88$ electron volts for $f=0.33$ and $T=1270°K$; that is, $w_{max}-w_{min}=10{,}270°K$ and, therefore $b=4.045$. If it is assumed that dw_{max}/dT and dw_{min}/dT are constants and an attempt is made to evaluate them by trial and error in terms of the above reported data for $f=0.31$, no values will satisfy the theoretical equations. This result indicates that dw_{max}/dT and dw_{min}/dT may be functions of temperature.

Conclusion

The above analysis has been given in some detail since it leads to the important conclusion that for nonuniform surfaces in general simultaneous measurements of the photoelectric and thermionic work functions will not be expected to yield values which are equal or which show the same temperature coefficient. The experimental measurements reported herein constitute an excellent example. A similar argument could be extended to contact potential measurements since these involve a still different type of averaging over the surface. We thus find that values of α deduced from thermionic measurements and Eq. (4) cannot be checked by other measurements except for surfaces over which the work function is uniform. Reimann[4a] has recently found this expected lack of agreement between values of α deduced from Eq. (4) and from contact potential measurements, but he attributes the difference to a reflection coefficient. Our analysis would indicate that this is not justified.

Furthermore, as is seen from Eq. (14), thermionic measurements will yield an apparent temperature coefficient of w even for patched surfaces for which the work function at each and every point is actually independent of temperature. This is because the relative contribution of individual areas to the total emission will change with temperature. Consideration of the numerical values in Table I shows that in this case α will be positive and hence $A<U$, as is nearly always observed.

The author wishes to express his appreciation to the faculty of the University of Rochester for the Research Fellowship in Physics which allowed him to complete the experimental program. Special acknowledgment is made to Professor L. A. DuBridge for his invaluable advice during the progress of the research, to Dr. Alan Glover for the use of his preliminary results as a guide for the experimental procedure, to Dr. Fred Seitz for helpful discussions, and to the Bausch and Lomb Optical Company for the loan of a monochromator.

The Force on the Cathode of a Copper Arc

RANDAL M. ROBERTSON*
George Eastman Research Laboratories, Massachusetts Institute of Technology, Cambridge, Massachusetts
(Received February 7, 1938)

The force on the cathode in the electric arc, previously examined either in air at atmospheric pressure or in vacuum, is studied as a function of pressure. For the copper arc in nitrogen the force is found to remain of the order of magnitude of the values observed in air down to a pressure of about 5 mm, and then to increase sharply but smoothly to the much larger forces observed in vacuum. Various aspects of the arc are examined in this transition region. Curves showing force as a function of current at various pressures of hydrogen and nitrogen are given. A brief study of the stability of the vacuum arc is included, as well as a summary of the various theories put forward to explain the phenomenon.

INTRODUCTION

THE mechanical force exerted on the electrodes in the electric arc has been studied under two distinct sets of experimental conditions. On the one hand, various observers,[1–3] chiefly Duffield, Burnham, and Davis,[1, 2] have measured the force on both cathode and anode in arcs of different electrode materials running in air at atmospheric pressure. The forces found in these measurements, in which currents up to 10 amperes were used, are of the order of a dyne per ampere. Studies have also been made,[4, 5] in which hollow carbon electrodes and delicate manometers were used to determine the actual gas pressure at the electrodes. On the other hand, Tanberg[6] has measured the force on the cathode of the copper arc in vacuum, finding the force to be about 17 dynes per ampere in the range 10–30 amperes. Creedy, Lucas and Easton,[7] using currents as high as 150 amperes, found correspondingly high values for the force in the vacuum arc with several electrode materials. The force on the cathode in the mercury arc has also been the object of study.[8–10]

The lack of adequate experimental data has made the interpretation of these results very difficult. In particular, no studies have been made of the region intermediate between the two cases. It was therefore decided to study the force on the cathode of the copper arc at different pressures. Nitrogen was used instead of air in order to effect some simplification of the already complicated experimental conditions. The present paper is an attempt to summarize the results obtained in such a form as to be of most use to those desiring to pursue the subject further. No final conclusions can be drawn as to the nature of the force, but it is shown that there is a continuous transition, occurring in the region below 5 mm, from the small forces found at higher pressures to the large forces found at lower. Curves are shown for force as a function of current for pressures up to 500 mm, but it is the writer's opinion that measurements at the higher pressures, while qualitatively instructive, are of little value from the quantitative point of view because of disturbing effects notably convection and chemical action.

The statement has been made[6] that "an electric arc can be drawn even in very high vacuum by separating two metal contacts carrying current of the order of a few amperes." Some tests were carried out under reasonably clean surface

TABLE I. *Conditions under which a copper arc would not operate.*

p (MM)	V_0 (VOLTS)	i_a (AMP)
	115	0–30
10^{-3}–10^{-5}	230	0–30
	600	0–10

* Now at the Research Laboratories of the Norton Company, Worcester, Massachusetts.
[1] Duffield, Burnham and Davis, Phil. Trans. Roy. Soc. **A220**, 109 (1920).
[2] Duffield, Burnham and Davis, Proc. Roy. Soc. **A97**, 326 (1920).
[3] Sellerio, Phil. Mag. **44**, 765 (1922).
[4] Dewar, Proc. Roy. Soc. **33**, 262 (1882).
[5] Beer and Tyndall, Phil. Mag. **42**, 956 (1921).
[6] Tanberg, Phys. Rev. **35**, 1080 (1930).
[7] Creedy, Lucas and Easton, Trans. A.I.E.E. **53**, 1454 (1934).
[8] Stark and Reich, Physik. Zeits. **4**, 323 (1902).
[9] Stark and Cassuto, Physik. Zeits. **5**, 269 (1904).
[10] Kobel, Phys. Rev. **36**, 1636 (1930).

and vacuum conditions to define the region of stable arcing. The arc was considered stable if on separating the electrodes a discharge persisted for as long as 15 seconds. In the first place it was established that no copper arc would run in the residual gases of the system under the conditions given in Table I. p is the pressure in mm as read on the McLeod gauge, V_0 the open circuit voltage and i_s the short circuit current. The ranges given indicate the range tried and do not necessarily mean that the arc is stable for points outside. In the second place, tests were carried out for the copper arc in nitrogen at $i_s=20$ amperes and $V_0=230$ volts. The region of stable arcing was found to extend down to about 0.1 mm, below which pressure no arc of any length whatsoever could be maintained. No appreciable increase in range of stability was effected by the introduction of inductances of various sizes into the circuit. It would appear that further study of the stability of the so-called vacuum arc is desirable.

A pendulum deflection method of measuring the force was decided upon as being easiest to manipulate in a closed chamber. In such an experiment the measured total force is made up of a number of components. Most of the forces encountered tend to increase the arc length and such forces will be referred to as "positive." Those such as convection tending to decrease the arc length are called "negative." There are electromagnetic forces caused by interaction of the current, I, in the pendulum with both the earth's field and the field due to the rest of the circuit. These are proportional to I and I^2, respectively. Electrostatic forces, depending on the potential distribution between the electrodes are negligibly small. A disturbing factor, which cannot readily be evaluated is convection, which we will take to include all effects due to large scale movements of the surrounding gas. Radiometer forces are small but must be considered in a full account. Evolution of occluded gases, suggested as a possible cause of the high vacuum forces,[11] would produce a transient effect.

Any forces measured which cannot be attributed to a combination of the above forces must be explained by effects intimately connected with the arc mechanism. To account for the

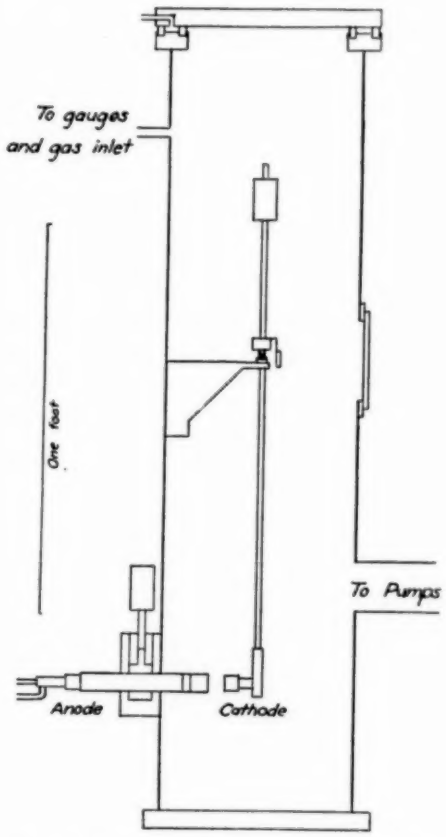

FIG. 1. Schematic diagram of the apparatus used in this work.

observed facts several theories have been put forward. Electrons emitted from the cathode spot will produce a reaction force of the right order of magnitude to explain that observed at the higher pressures. This was suggested by Duffield.[1, 2] A vapor stream emerging from a high temperature region at the cathode would give such a force. Tanberg and his co-workers[6, 12–14] put forward this theory to explain the force in the vacuum arc. The hypothesis was supported by the fact that a force was observed on a vane suspended in front of the cathode. Ions falling through the cathode fall of the arc and remaining on the electrode after neutralization produce no net force. However if the atoms come off after neutralization with a fraction $(1-\alpha)$ of their incident kinetic energy, where α is the accommodation coefficient for ions, a reaction force is pro-

[11] Wellman, Phys. Rev. **38**, 1077 (1931).

[12] Berkey and Tanberg, Phys. Rev. **38**, 296 (1931).
[13] Berkey and Mason, Phys. Rev. **38**, 943 (1931).
[14] Mason, Elec. Eng. **52**, 702 (1933).

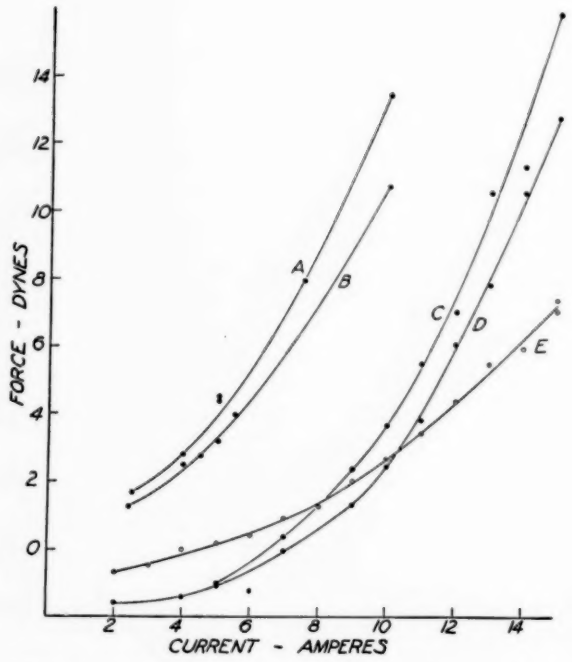

FIG. 2. Force on the cathode of a copper arc, arc length 5 mm, running in *A*, hydrogen at 50 mm pressure; *B*, hydrogen at 100 mm pressure; *C*, nitrogen at 20 mm pressure; *D*, nitrogen at 100 mm pressure; *E*, nitrogen at 500 mm pressure.

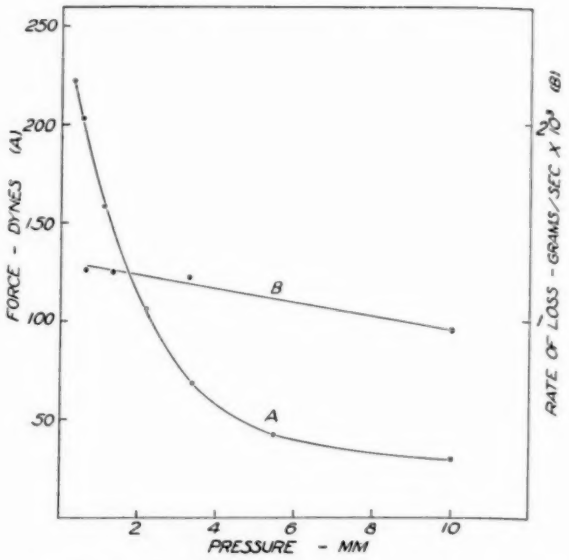

FIG. 3. *A*. Force on the cathode of a copper arc, current 15 amperes, arc length 1 cm, in nitrogen. *B*. Rate of loss of material from the cathode of a copper arc under the above conditions.

duced. Compton[15, 16] has shown that for reasonable assumed values of α this force is of the right order of magnitude to explain the force in vacuum. Tonks[17] calculated the force due to plasma electrons which were reflected from the cathode sheath and found that large forces could thus be accounted for. Risch and Ludi[18, 19] have suggested that there may be a large number of atoms near the cathode ionized as many as five or six times. If there is a sort of accommodation coefficient whereby some of the energy of ionization is turned into kinetic energy of rebound when the ion strikes the cathode, a large force could be accounted for. It should be noted that none of these theories points to a satisfactory explanation of the observed variation of force with pressure.

EXPERIMENTAL METHOD

In Fig. 1 are shown the main features of the experimental setup. The pendulum was mounted in a brass tank with removable top, which could be evacuated by means of a large Apiezon oil pump, the resulting pressure being measured on a McLeod gauge. Liquid air was used to keep mercury vapor from the gauge and oil vapor from the pumps out of the system. The best vacuum obtainable was about 10^{-6} mm. Gases were introduced into the system through purifying devices to remove water and oxygen, pressures above 10 mm being measured on a closed end manometer.

The pendulum consisted of a Duralumin rod supported on steel points resting in steel cups. The copper cathode rod was mounted in an aluminum block at the lower end of the pendulum. At the top was an adjustable counterweight which controlled the sensitivity. It was necessary to surround the cathode with a quartz sleeve to keep the cathode spot from wandering. The copper was turned down a little near the end to leave a small gap between it and the quartz. The current was brought into the pendulum by means of fine wires led down from a bar above to side arms at the axis of the pendulum. About one or two number 40 copper wires per ampere were sufficient. The effect of these wires on the sensitivity was tested and found to be negligible.

The external circuit was arranged to reduce electromagnetic effects to a minimum, but it was

[15] K. T. Compton, Phys. Rev. **36**, 706 (1930).
[16] K. T. Compton, Proc. Nat. Acad. Sci. **18**, 705 (1932).
[17] Tonks, Phys. Rev. **46**, 278 (1934).
[18] Risch, Helv. Phys. Acta, **4**, 122 (1931).
[19] Ludi and Risch, Zeits. f. Physik. **75**, 813 (1932).

necessary to mount the pendulum with its axis of rotation in a north and south direction, so that a "negative" force is present owing to interaction of the current in the pendulum with the earth's field. The current travels vertically in the pendulum for 25.4 cm below the axis and horizontally in the cathode rod for 2.5 cm. The anode rod, which was fixed and parallel to the cathode, was 22.9 cm in length.

The arc was started by contact between the cathode and the water cooled copper anode, which could be moved backward and forward through an Apiezon grease and graphite packed joint. Since the damping in the pendulum was very small, the anode and cathode had to be separated with great care to prevent violent oscillation being set up. With high currents and large forces the pendulum was often kicked away violently when the arc struck. Therefore a device was introduced consisting of an arm controlled through a packed joint which held the cathode steady while contact was being made. The arc length was measured by means of an enlarged image of the arc thrown on a screen.

The pendulum deflection was measured with a mirror mounted at the axis of the pendulum and a scale 2.2 meters away. The sensitivities used varied from 0.3 dynes per mm to 10 dynes per mm. Readings were taken in the following manner. The arc having been started and the current adjusted, the pendulum was in general in motion with small amplitude. For long periods, a cross hair was focused on the vertical scale and readings were taken of successive maxima and minima with the arc running and then with the arc extinguished. The difference between the mean positions was calculated and by the use of the previously determined sensitivity the force was found. For short periods, when readings could not be taken directly, a photographic method was used. The image of a horizontal line filament was focused on a strip of bromide paper. With the arc running the light source was turned on and the image allowed to move up and down a few times. The source was then put out and the arc extinguished. The paper was then displaced slightly and the light turned on to record the zero. It is not necessary to move the paper continuously since the successive maxima are marked by quite sharp lines on the developed paper.

Experimental Results

In Fig. 2 is shown the result of measurements made of force as a function of current for different pressures of nitrogen and hydrogen down to 10 mm. The points plotted are actual experimental points to which no corrections have been applied. No quantitative correction being possible for some extraneous effects, convection in particular, it was considered useless to apply any others. In general, points were taken both ascending and descending the curves to check the reproducibility of the effect. In this experiment the diameter of the cathode was $\frac{1}{4}$ inch and the arc length 0.5 cm. The forces found are of the same order of magnitude as those observed by Duffield, Burnham, and Davis. At low current the force is negative for nitrogen. In hydrogen the force is greater than in nitrogen and there is no tendency to negative forces. In both cases the force increases slowly with decreasing pressure. These facts may be explained in terms of convection effects which would be smaller for hydrogen and for lower pressures of either gas. The difference in shape between the curve for nitrogen at 500 mm and the other two nitrogen curves was

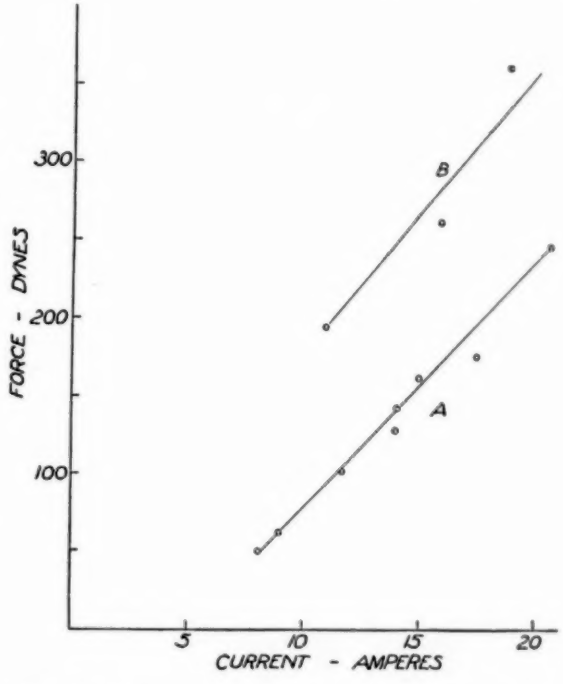

FIG. 4. *A*. Force on the cathode of a copper arc, arc length 1 cm, in nitrogen at 1 mm pressure. *B*. Force observed by Tanberg in the vacuum arc.

accompanied by a change in the form of the arc from type II (Hagenbach's notation[20]) where the red anode end of the arc is concentrated at a point to type I where the anode end is a diffuse red glow.

Thus for pressures as low as 10 mm there is no sign of the large forces observed by Tanberg in the vacuum arc. Fig. 3, however, shows the result of a series of measurements of force as a function of pressure for the 15 ampere copper arc in nitrogen. The cathode diameter was 0.3 inches and the arc length 1 cm. The force is seen to rise from a value at 10 mm comparable to that observed by Duffield, Burnham, and Davis to a force at 0.3 mm of the order of magnitude of that found by Tanberg in the vacuum arc. In this transition region several aspects of the arc were examined for possible correlation:

(1) Appearance. There was no marked change in the appearance of the arc apart from a gradual broadening with decreasing pressure.

(2) Voltage. The arc voltage remained constant at about 20 volts throughout the range.

(3) Material lost by the cathode. Some measurements were taken of the loss of material per second as a function of pressure. The cathode rod was weighed before and after a 30 second period of arcing at 15 amperes. The result is shown in Fig. 3, curve *B*. There is no apparent correlation. The values found are much larger than those observed by Tanberg who observed a rate of loss at 15 amperes of about 0.23 milligrams per second.

[20] Hagenbach and Veillon, Physik Zeits. **11**, 833 (1910).

It is clear from these results that the transition to the high forces is gradual, and that the high force is not characteristic of a special type of discharge setting in discontinuously at low pressures.

In Fig. 4 are given results of measurements taken in nitrogen at 1 mm pressure of force as a function of current. Some of Tanberg's vacuum arc figures are given for comparison. The chief difficulty in these measurements is the tendency of the arc to strike in the crack between quartz and copper. The force is then greatly reduced. This might lead to the supposition of two types of vacuum arc if the arc were not visible to the observer.

In conclusion I should like to thank those who have cooperated with me in this research, particularly Professor E. S. Lamar whose constant contact with the work has been a source of inspiration and genuine assistance and Dr. K. T. Compton who has offered much helpful advice.

APRIL 1, 1938 PHYSICAL REVIEW VOLUME 53

Internal Friction in Solids

IV. Relation Between Cold Work and Internal Friction

CLARENCE ZENER
College of the City of New York
(Received February 7, 1938)

Previous investigators have found that cold working of metals has a marked effect upon internal friction, increasing it, in certain cases, by a factor of more than ten. In the present paper it is assumed that the effect of cold work upon internal friction is due to the residual internal stresses which it produces. During vibration these residual stresses give rise to fluctuations in temperature, and thus to local heat currents, which are inevitably associated with a rise in entropy, i.e., with internal friction. A formula is obtained for this internal friction in terms of the energy associated with the residual stresses, and the temperature variation of the modulus of rigidity. It gives the observed order of magnitude. According to the theory developed in this paper, the measurement of the internal friction of a cold worked specimen over a wide frequency range and for various types of vibration will give not only the mean square of the residual stresses, but also their preferred axes, if any, and the mean linear dimensions of their inhomogeneities.

§1. INTRODUCTION

THE writer has recently investigated, both theoretically and experimentally, that part of the internal friction of solids which is associated with stress inhomogeneities.[1–4] These stress

[1] C. Zener, Phys. Rev. **52**, 230 (1937).
[2] C. Zener, Nature **140**, 895 (1937).
[3] C. Zener, Phys. Rev. **53**, 90 (1938).
[4] C. Zener, W. Otis, R. Nuckolls, Phys. Rev. **53**, 100 (1938).

inhomogeneities give rise to fluctuations in temperature, and hence to local heat currents, which are inevitably associated with a rise of entropy, i.e., with internal friction. Various types of stress inhomogeneities were studied: those inherent in the type of vibration, as in transverse vibrations of reeds and wires; those due to cavities; those due to the elastic anisotropy and random orientation of the individual crystallites. In this paper we study the internal friction due to the stresses, necessarily inhomogeneous, resulting from cold work.

That cold work has a marked effect upon internal friction has already been demonstrated by Wegel and Walther[5] for copper, by Förster and Köster[6] for steel and brass. Cold worked specimens were annealed at various temperatures, and their internal friction was then measured at room temperature. Their results are shown in Fig. 1. The frequencies used were approximately 1000, 1400, 9000 cycles/sec. for steel, brass, and copper, respectively. They attributed the initial drop of internal friction with an increase of annealing temperature as due to the relaxation of the internal stresses by annealing. They attributed the final rise of internal friction with annealing above the recrystallization temperature as due to an increase in grain size. The theoretical relation between internal friction and grain size has already been developed.[3]

According to the theory here developed, the internal friction due to cold working is a special example of thermoelastic internal friction. Hence it has a maximum at a frequency of the order of magnitude of D/L^2, where D is the thermal diffusion constant, and L is the mean linear dimension of the inhomogeneities in stress. The precise variation of the internal friction with frequency depends upon the detailed distribution of the residual stresses. However, its integral with respect to the logarithm of the frequency depends only upon the mean squares of the residual stresses. It reduces to a particularly simple expression when all residual stresses except shearing stresses are negligible, as is probably the case in

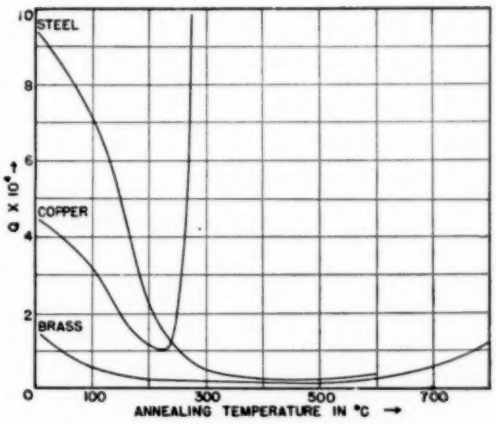

FIG. 1. Effect of annealing temperature upon cold worked specimens. Curve for copper by Wegel and Walther, curves for brass and steel by Förster and Köster.

cold worked specimens. This is

$$\int_{-\infty}^{\infty} Q^{-1} d \log_{10} \nu = 1.36 r(\theta/T)(d \log G/d \log T)^2.$$

Here G is the modulus of rigidity, T the absolute temperature, θ is the measure of cold work introduced by Quinney and Taylor.[7] θ times the specific heat per unit volume is the volume density of the energy associated with the residual stresses. They have obtained values of $\theta = 5°$ for copper, brass, aluminum, nickel, and mild steel. The factor r is a measure of the correlation between the residual stresses and the additional stress due to vibration. Values are given in Table I for special cases. Taking the values of $(d \log G/d \log T)^2$ from Table II, we see that the calculated internal friction due to cold work is of the same order of magnitude as the observed values in Fig. 1.

The theory developed in this paper shows that the measurement of the internal friction of cold worked samples over a wide frequency range, and for various types of vibration, will give not only the energy associated with the residual stresses, but also their preferred directions and their mean linear dimensions.

§2. General Theory

The general theory of thermoelastic internal friction has been developed only for the case of metals with microscopic cubic symmetry and

[5] R. L. Wegel and H. Walther, Physics **6**, 141 (1935).
[6] F. Förster and W. Köster, Zeits. f. Metallkunde **29**, 116 (1937).
[7] H. Quinney and G. I. Taylor, Proc. Roy. Soc. **163**, 157 (1937).

TABLE I. *Correlation factor.*

RESIDUAL STRESS	VIBRATION STRESS	r
Produced by torsion across xy plane	Torsion across xy plane	1
Produced by torsion across xy plane	Z_z	0
No preferred axis	Torsion	1/5
No preferred axis	Only one principal stress	$2(1+\sigma)/15$

TABLE II. *Variation of shear modulus with temperature at* 20°C.

METAL	$G^{-1}(dG/dT)\times 10^{4}$*	$(d \log G/d \log T)^2$
Lead	79	5.7
Zinc	48	2.1
Aluminum	25	0.56
Silver	8.2	0.060
Copper	4.5	0.020
Nickel	3.3	0.010
Iron	3.0	0.0081
Platinum	1.8	0.0029

* *Handbuch der Experimentalphysik*, Vol. 5, p. 251.

with no residual stresses. Hence in order to study the effect of cold work we must first develop the general theory making no assumptions concerning the microscopic symmetry or the magnitude of the residual stresses. This is done in the present section.

The internal friction Q^{-1} (natural logarithmic decrement/π) is given by[3]

$$Q^{-1}=(1/2\pi)\Delta E/E, \tag{1}$$

where ΔE is the energy loss per cycle, and E is the vibrational energy. We proceed to evaluate ΔE as in reference 3, without making the special assumptions there made.

The vibrational energy $\Delta w\, dv$ lost per cycle in an element of volume dv is given by

$$\Delta w=\nu^{-1}\text{ time average of } (X_x\, de_{xx}/dt+\cdots X_y\, de_{xy}/dt). \tag{2}$$

Each stress consists of three parts. The first is the residual stress at the mean temperature T_0, e.g., X_x'. The second part is a linear function of the strains e_{xx}, $\cdots$ referred to the nonvibrating sample at temperature T_0. The third part is proportional to the deviation ΔT of the temperature from its mean. Thus

$$X_x=X_x'+\{(\partial X_x/\partial e_{xx})_{T_0}e_{xx}+\cdots\}+(\partial X_x/\partial T)_e\Delta T. \tag{3}$$

The subscript e denotes that all strains are held constant in the differentiation. Although no assumption is made concerning the size of the residual strains and stresses, we assume the fluctuations in strains, e_{xx}, etc., as well as the fluctuation in temperature ΔT to be first-order small quantities. This temperature fluctuation is in turn related to the strains by the equation

$$d\,\Delta T/dt=(\partial T/\partial t)_e+(\partial T/\partial t)_S. \tag{4}$$

Here $(\partial T/\partial t)_e$ denotes the ordinary diffusion term, while $(\partial T/\partial t)_S$ denotes that contribution to $d\,\Delta T/dt$ which comes from adiabatic changes in the strains.

The temperature variation ΔT is contained in the relation between stress and strain, while the equation determining ΔT contains the strains. Hence the evaluation of Δw involves the simultaneous solution of the elastic equations of motion and of the diffusion equation (4). Since the temperature fluctuation affects the strains only very slightly, we shall obtain the solution by a perturbation method.

In the first approximation for the stresses we assume $\Delta T=0$. The first approximation to the strains is then obtained by solving the usual isothermal elastic equations of motion. These are then substituted into Eq. (4) to obtain the first approximation to ΔT. Substituting this first approximation for ΔT and for the strains into Eq. (3), we obtain a second approximation for the stresses. Finally, substitution of these approximations into Eq. (2) gives

$$\Delta w=\nu^{-1}\text{ time average of } \{(\partial X_x/\partial T)_e de_{xx}/dt+\cdots(\partial X_y/\partial T)_e de_{xy}/dt\}.$$

We now simplify this equation by making use of the following thermodynamical formulae

$$(\partial X_x/\partial T)_e=(C/T)(\partial T/\partial e_{xx})_S,\quad \text{etc.},$$

which are obtained from the condition that $TdS+(X_x de_{xx}+\cdots X_y de_{xy})$ be a perfect differential. Here C refers to the specific heat at constant strains, per unit volume. In the derivative $(\partial T/\partial e_{xx})_S$ all strains except e_{xx} are kept constant. We obtain, after integrating over the solid,

$$\Delta E=(C/T\nu)\times\text{time average of } \int(\partial T/\partial t)_S\Delta T\, dv. \tag{5}$$

The problem of formally solving Eq. (4) for ΔT, and then performing the time average and integration in Eq. (5), has been solved in the appendix of reference 3. Making use of this solution we obtain

$$Q^{-1}=(C/2ET)\Sigma\tau_k^2\nu_k\nu/(\nu_k^2+\nu^2). \qquad (6)$$

The constants τ_k and ν_k are interpreted as follows. We imagine the vibration to proceed adiabatically. The fluctuation ΔT of the temperature from its mean T_0 then has a maximum when the strains are a maximum. We denote by τ this maximum value of ΔT. We next expand τ in terms of the normalized eigenfunctions of a differential equation similar to Eq. (a-5) of that reference, the appropriate boundary condition being obtained by requiring that no heat flow across the boundary of the solid. The coefficients in this expansion are denoted by τ_k. The eigenwert of the differential equation are given by $2\pi\nu_k$.

A simplification is introduced by integrating with respect to the log of ν.

$$\int_{-\infty}^{\infty}Q^{-1}d(\log_e\nu)=(\pi C/4\mathcal{E}T)\langle\tau^2\rangle_{Av}. \qquad (7)$$

Here $\mathcal{E}$ refers to the average energy of vibration per unit volume. Av refers to a space average. In obtaining Eq. (7) we have assumed $\langle\tau\rangle_{Av}$ to vanish. If this assumption is not valid, then $\langle\tau^2\rangle_{Av}$ must be replaced by $\langle\tau^2\rangle_{Av}-\langle\tau\rangle_{Av}^2$.

§3. Effect of Residual Stresses

In applying the general Eq. (7) to a cold worked specimen, we must first obtain an explicit expression for the amplitude $\tau(x, y, z)$ of the temperature fluctuation for an idealized adiabatic vibration. If we denote the maximum values of the stresses accompanying the vibration by $\Delta X_x, \cdots$, then

$$\tau=(\partial T/\partial X_x)_{S,\,\pi}\Delta X_x+\cdots.$$

The suffix π denotes that all stresses are held constant except that with respect to which the differentiation is taken. We now apply to this expression the thermodynamical transformations

$$(\partial T/\partial X_x)_{S,\,\pi}=-(T/C)(\partial e_{xx}/\partial T)_{\text{stresses}}, \quad \text{etc.},$$

which are obtained from the requirement that $d(\text{energy density})-d(X_xe_{xx}+\cdots)$ be a perfect differential. We obtain

$$\tau=-(T/C)\{(\partial e_{xx}/\partial T)_{\text{stresses}}\Delta X_x+\cdots\}. \qquad (8)$$

We must now examine in detail the temperature dependence of the strains. An elementary region will be said to have zero strain when all stresses are zero, and when the temperature has its average value T_0. Then

$$e_{xx}=\alpha_{xx}(T-T_0)+\mathbf{E}^{-1}\{X_x-\sigma(Y_y+Z_z)\}, \quad \text{etc.},$$
$$e_{xy}=G^{-1}X_y, \quad \text{etc.}$$

Here α_{xx} refers to the thermal expansion coefficient for zero stresses. In obtaining the temperature variation of the strains, we shall assume the vibration stresses $\Delta X_x, \cdots$ to be negligible compared with the residual stresses $X_x', \cdots$. Then

$$(\partial e_{xy}/\partial T)_{\text{stresses}}=(dG^{-1}/dT)X_y', \quad \text{etc.}$$

Now $(\partial e_{xx}/\partial T)_{\text{stresses}}$ contains the temperature variation of the two elastic constants $\mathbf{E}$ and σ. The observation that the internal strains are mostly shears enables us to simplify the expression for $(\partial e_{xx}/\partial T)_{\text{stresses}}$ by assuming the dilation, and hence $X_x'+Y_y'+Z_z'$, to be exactly zero. Using the relation $\mathbf{E}/2(1+\sigma)=G$, we obtain

$$(\partial e_{xx}/\partial T)_{\text{stresses}}=\alpha_{xx}+\tfrac{1}{2}(dG^{-1}/dT)X_x', \quad \text{etc.}$$

Substitution of these results into Eq. (8) gives

$$\begin{aligned}\tau=&-(T/C)\{\alpha_{xx}\Delta X_x+\cdots\}\\&+C^{-1}G^{-1}(d\log G/d\log T)\\&\times\{\tfrac{1}{2}(X_x'\Delta X_x+Y_y'\Delta Y_y+Z_z'\Delta Z_z)\\&+(Y_z'\Delta Y_z+Z_x'\Delta Z_x+X_y'\Delta X_y)\}.\end{aligned}$$

In the general theory developed for the special case of no internal stresses, it was found that internal friction was caused by the inhomogeneities in the dilations accompanying vibration. In this paper we are studying the other extreme case, where internal friction is due primarily to the residual stresses. The first term of τ will thus be omitted. The effects of internal stresses and of inhomogeneities in dilation may actually be separated only if their contributions to internal friction are appreciable in different frequency ranges. This will be the case where the linear dimensions of the inhomogeneities of dilation and of residual stresses are of different orders of magnitude.

Our final expression for $\langle\tau^2\rangle_{Av}$ is obtained by taking the square of the above equation, and averaging over the solid. Let $\mathcal{E}$, as before, denote the average volume density of the strain energy associated with ΔX_x, $\cdots$, and $\mathcal{E}'$, as well as θC, the average volume density of the energy associated with the residual stresses X_x', $\cdots$. Introducing the dimensionless quantity

$$r = \text{space average of } \{\tfrac{1}{2}(X_x'\Delta X_x + Y_y'\Delta Y_y + Z_z'\Delta Z_z) + (Y_z'\Delta Y_z + Z_x'\Delta Z_x + X_y'\Delta X_y)\}^2/(4G^2\mathcal{E}\mathcal{E}') \quad (9)$$

we obtain, after substituting $\langle\tau^2\rangle_{Av}$ into Eq. (7),

$$\int_{-\infty}^{\infty} Q^{-1} d(\log_e \nu) = \pi r(\theta/T)(d\log G/d\log T)^2.$$

§4. Correlation Factor

In this section we shall calculate for a variety of cases the correlation factor r, defined by Eq. (9). Use will be made of the standard formulae for the volume density of energy, u, associated with the stresses X_x, $\cdots$,[8]

$$u = \tfrac{1}{2}[(X_x + Y_y + Z_z)^2/\mathbf{E} + (Y_z^2 + Z_z^2 + X_y^2 - Y_yX_x - Z_zX_x - X_xY_y)/G] \quad (10)$$

and for the stress transformation[9]

$$\Xi_\Xi = l^2X_x + m^2Y_y + n^2Z_z + 2(mnY_z + nlZ_x + lmX_y), \quad (11)$$

where l, m, n are the direction cosines of the Ξ axis. We shall assume (1) that the residual stresses have no macroscopic variation, (2) that the dilation associated with the residual stress is zero, i.e.,

$$X_x' + Y_y' + Z_z' = 0. \quad (12)$$

[8] R. V. Southwell, *Theory of Elasticity* (Oxford, 1936), p. 314.
[9] Reference 8, p. 269.

We first consider the case in which for each volume element the only nonvanishing residual stress is Z_μ', where the μ axis lies in the xy plane and passes through the volume element. Such residual stresses are produced by the torsion of a circular rod. Then $\mathcal{E}' = Z_\mu'^2/2G$. If also ΔZ_μ is the only nonvanishing vibration stress, then $\mathcal{E} = \Delta Z_\mu^2/2G$, and so $r = 1$. If, on the other hand, ΔZ_z is the only nonvanishing vibration stress, the space average of each term in Eq. (9) vanishes, giving $r = 0$.

We next consider the case where the residual shearing stresses have no preferred axis. If the only nonvanishing vibration stress is ΔZ_μ, we have

$$r = \langle Z_\mu'^2\rangle_{Av}/(2G\mathcal{E}'),$$

while if the only nonvanishing vibration stress is ΔZ_z, we have

$$r = \mathbf{E}Z_z'^2/(8G^2\mathcal{E}').$$

An explicit expression for $\mathcal{E}'$ is obtained by substituting into Eq. (10) the two relations

$$\langle X_x'Y_y'\rangle_{Av} = -\tfrac{1}{2}\langle X_x'^2\rangle_{Av} \quad \text{etc.},$$

and

$$4\langle X_y'^2\rangle_{Av} = 3\langle X_x'^2\rangle_{Av} \quad \text{etc.}$$

The first relation is obtained by squaring Eq. (12) and averaging over the solid, using of course the condition of no preferred axis. The second relation is obtained by squaring Eq. (11), averaging over the solid and over all directions Ξ, and upon using the first relation. We obtain

$$\mathcal{E}' = (5/2G)\langle Z_\mu'^2\rangle_{Av} = (15/8G)\langle Z_z'^2\rangle_{Av}$$

and hence, for the two examples,

$$r = \tfrac{1}{5}$$

and

$$r = (\mathbf{E}/15G) = 2(1+\sigma)/15,$$

where σ is Poisson's ratio.

The Effect of Hydrostatic Pressure on the Susceptibility of Rochelle Salt

DENNISON BANCROFT
Research Laboratory of Physics, Harvard University, Cambridge, Massachusetts
(Received February 4, 1938)

The electric susceptibility of Rochelle salt has been studied as a function of both temperature and hydrostatic pressure. Both the upper and lower critical temperatures are altered by the pressure, but the pressure coefficients for the alterations are different in the two cases. An attempt is made to correlate the experiment with statistical mechanical theory, but it is found that the theory is not sufficiently explicit to provide a quantitative explanation of the results.

THE anomalous variation of the electric susceptibility of Rochelle salt in the temperature range from $-40°$C to $+40°$C is so well known as to require little comment. Suffice it to say that as the temperature is increased from $-40°$, the dielectric constant rises to an effectively infinite value at $-18°$, remains infinite to $+24°$, then falls rapidly to normal values. This phenomenon has been exhaustively investigated by Mueller[1] and others. The behavior is thus characterized by two critical temperatures, $-18°$ and $+23.7°$, the explanation of which has been semi-quantitatively discussed by Fowler.[2] According to his theory, the effects are due to polar molecules within the crystal lattice: the lower critical temperature marks the onset of free dipole rotation, while the upper marks the point at which thermal agitation prevents universal alignment of the dipoles.

In the present paper, we measure the susceptibility as a function of temperature and hydrostatic pressure to 10,000 atmospheres over the temperature range $-20°$ to $+60°$. The pressure is found to produce a marked alteration of the critical temperatures; this effect is studied to an accuracy of $\pm 0.1°$C and ± 10 kg/cm^2. The apparatus is simple and conventional. Pressure is developed within a steel cylinder whose inside dimensions are roughly $\frac{5}{8}''\times 8''$. The equipment for producing the pressure has been exhaustively described by Bridgman.[3] The steel cylinder containing the specimen was surrounded by an oil bath whose temperature could be varied at will. The liquid used for developing the pressure was petroleum ether.

Tinfoil electrodes were cemented to the proper faces of the Rochelle salt crystals, and one lead was brought out of the pressure chamber through an insulated plug; the other lead was grounded. The crystal was freely suspended by its leads, which were as tenuous as possible, in order to eliminate mechanical constraints. The capacity from the insulated lead to ground was measured by means of a General Radio Company type 216 capacity bridge, used in a substitution method. The voltage on the crystal was controlled at 2.0 r.m.s. volts, 1000 cycles. No bias potential was used. Stray capacity effects were eliminated by a blank run made on a piece of glass similar in size and shape to the crystals used. No change in capacity with pressure was detected in this case; accordingly the correction amounted to a constant capacity to ground, which was subtracted from the capacity as measured in order to compute the true capacity of the crystal.

The crystals were furnished through the kindness of the Brush Development Company. Three crystals were used, whose dimensions were:

I. $0.424\times 0.970\times 3.65$ centimeters,
II. $0.356\times 0.869\times 2.27$ centimeters,
III. $0.313\times 0.904\times 2.54$ centimeters.

In all cases the shortest dimension lay along the "*a*" axis, and the electrodes were, of course, attached to the large faces. No attempt was made to study the effect of pressure on the normal values of the susceptibility which one obtains at right angles to this axis. The crystals are extremely fragile, and unfortunately the data from all three specimens had to be combined in order to get a complete picture of the behavior. It was

[1] Hans Mueller, Phys. Rev. **47**, 175 (1935).
[2] R. H. Fowler, *Statistical Mechanics*, second edition (Cambridge University Press, 1936) p. 816 *et seq.*
[3] P. W. Bridgman, *The Physics of High Pressure* (Bell and Sons, 1931).

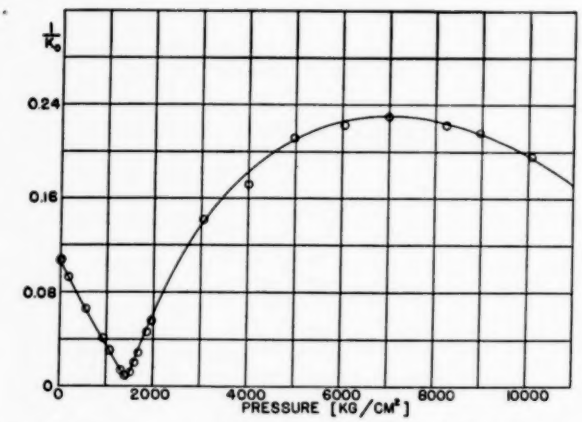

FIG. 1. The reciprocal susceptibility of Rochelle salt as a function of pressure at 40°C.

found that a relatively small but sudden change in pressure would almost invariably crack the crystal.

The absolute accuracy of the values obtained for the susceptibility is not high, partly because of the small specimens, partly because of the relatively large corrections for stray capacity, necessitated by the proximity of the specimen to the steel cylinder. Where it is possible to compare the results obtained with those of Mueller, our susceptibilities agree with his to better than 5 percent. The points observed, however, fell upon curves sufficiently smooth to enable one to estimate the position of the critical points to the accuracy of the temperature and pressure measurements. The runs were made at constant temperature, and the pressure was varied in steps of 1000 atmospheres, except where additional points seemed desirable. Considerable time was required to establish satisfactory thermal equilibrium after a change in pressure, particularly in the regions where the dielectric constant was extremely sensitive to small thermal changes.

Figure 1 shows the data obtained in the run at 40.0°. Following Mueller, the reciprocal susceptibility, $1/k_0$, is plotted. Of course the susceptibility in the critical region (above 1500 atmos. in this particular case) is a somewhat arbitrary quantity, since here the dielectric constant is effectively infinite, the material showing hysteresis and the other properties characteristic of the "ferromagnetic" state. On the other hand, outside the critical region, the properties are quite well defined, the observed dielectric constant being independent of both frequency and field strength. Fig. 2 shows the family of curves of which Fig. 1 shows only a single example. It will be noted that

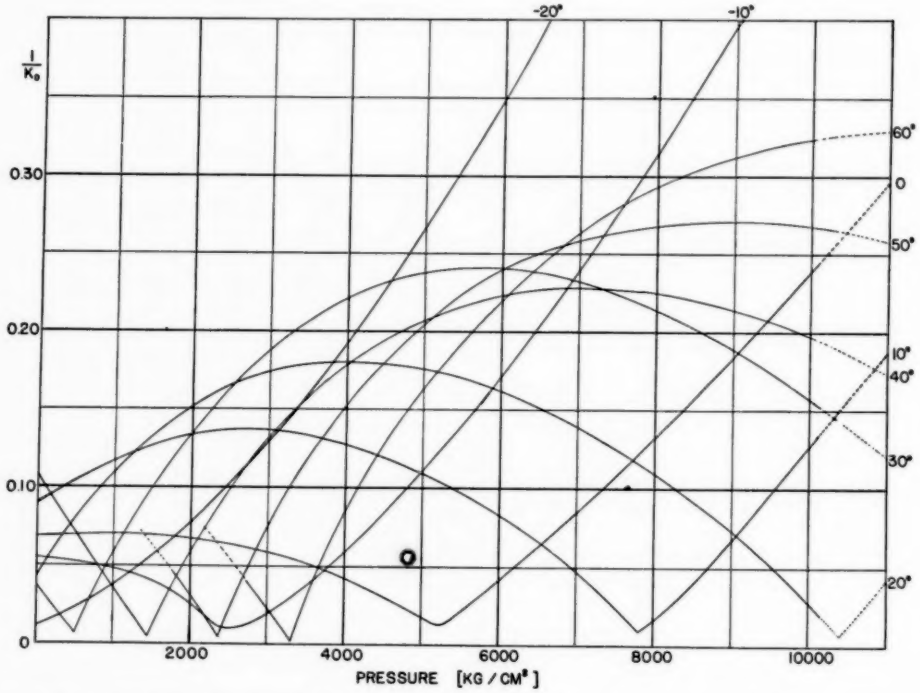

FIG. 2. The reciprocal susceptibility of Rochelle salt as a function of pressure for temperatures from −20°C to +60°C.

above 20°, the lower critical temperature occurs at too high a pressure to be observed. While it would have been possible to carry the measurements to a somewhat higher pressure, the general behavior of the critical points is so well illustrated in the low pressure range that it seemed hardly worth while. It is of some interest to note that as the temperature is increased, the height of the maximum to which the observed dielectric constant rises becomes larger and larger, i.e. $1/k_0$ approaches zero more and more closely. A value of k_0 of 80 was actually observed at 60°, and only the limitation of the bridge prevented the observation of an even larger apparent susceptibility.

No attempt has been made to "fair" the curves of Fig. 2 by plotting the data in the $1/k_0-T$ plane. Close examination of Fig. 2 will reveal that irregularities would appear in such a plot; these are due to the fact that the several specimens used did not give perfectly concordant results. Nevertheless the curves are sufficiently accurate to allow one to determine the position of the critical points with some confidence.

Figure 3 shows the loci of the critical points in the $T-P$ plane. The loci are approximately straight lines, and are adequately represented by the equations

$$\begin{aligned} T_u &= 1.073\times10^{-2}\,p+24.5, \\ T_l &= 3.769\times10^{-3}\,p-19.4. \end{aligned} \tag{1}$$

The critical temperatures at one atmosphere do not agree with Mueller's as well as one would desire, but the discrepancy is doubtless to be traced to the definition of the critical temperature. For the purposes of the present paper it is assumed to lie at the break in the curves shown in Fig. 2.

Figure 2 shows clearly that a discontinuity exists in the temperature and pressure derivatives of the reciprocal susceptibility. It is a matter of pure geometry to deduce an analog of the Clausius-Clapeyron equation, *viz.*

$$\frac{dp}{dT}=-\frac{[(\partial/\partial T)(1/k_0)]_1-[(\partial/\partial T)(1/k_0)]_2}{[(\partial/\partial p)(1/k_0)]_1-[(\partial/\partial p)(1/k_0)]_2}, \tag{2}$$

where the subscripts denote values of the derivatives taken on either side of the discontinuity, and dp/dT gives the slope of the locus of the discontinuity in the $T-P$ plane. For our purposes it is of more interest to extend the straight parts

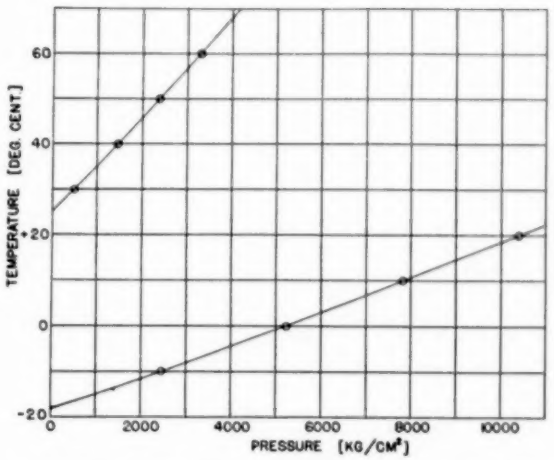

FIG. 3. The critical temperatures of Rochelle salt as a function of pressure.

of the curves of Fig. 2 until they intersect the p-axis. We then note that

$$\frac{dT}{dp}=-\frac{(\partial/\partial p)(1/k_0)}{(\partial/\partial T)(1/k_0)}, \tag{3}$$

where now the partial derivatives indicate the slope of the lines where they intersect the axis, and where dT/dp gives the slope of the locus of these intersections, which is nearly the same as what we have plotted in Fig. 3. The latter formula permits a correlation between the present results and those of Mueller. For the upper critical temperature our data yield (extrapolating to 1 atmos.) $(\partial/\partial p)(1/k_0)=-6.1\times10^{-5}$, while Mueller's results for the same temperature and pressure give $(\partial/\partial T)(1/k_0)=5.6\times10^{-3}$. Thus $(dT/dp)_u=1.09\times10^{-2}$. By a similar calculation for the lower temperature, one finds $(dT/dp)_l=2.5\times10^{-3}$. The agreement with Eq. (1) is most satisfactory for the upper critical temperature. In the other case one must remember that the discontinuity is not well marked, and that the extrapolation of both our data and Mueller's to a zero value of $1/k_0$ is far from a precise mathematical process.

The alteration observed in the critical temperatures is to be attributed in some way to the distortion of the lattice under pressure. Most methods of straining the crystal introduce mechanical constraints which, as Mueller has pointed out, completely remove the dielectric anomaly. In applying hydrostatic pressure, how-

ever, the only constraint introduced is the viscous reaction of the pressure medium, which at most would be expected to produce a gradual diminution of the anomalous behavior as the liquid becomes more viscous with pressure. Hence the effect of constraints can hardly be cited to account for the phenomenon observed.

Turning to Fowler's theory, we find a formula for the dielectric constant

$$\eta=1+\frac{4\pi}{\gamma}\frac{1-\beta T/2T_1}{(T_1/2\beta T_u)-1+(\beta T/2T_1)}, \quad (4)$$

where the critical temperatures are

$$T_1=\beta W_0/k \quad \text{and} \quad T_u=\gamma n\mu^2/3k.$$

Here W_0 is the energy of the molecular field in the absence of dipole rotation, β is a parameter, roughly equal to $\frac{1}{2}$, which serves to distinguish between rotating and nonrotating dipoles, n is the number of dipoles in unit volume, μ is the dipole strength, γ is the so-called "Lorentz factor" appearing in the formula $F'=F+\gamma P$ which gives the effective field in terms of the applied field and the polarization, and k is Boltzmann's constant. The lower critical temperature is determined by the onset of free dipole rotation; the upper by strict analogy with the Weiss-Langevin theory of ferromagnetism.

As the lattice is strained by pressure, we expect that, to a rough approximation, the expressions determining the critical temperatures will depend in some way upon the volume. If we assume that these expressions are proportional to some power of the volume, we arrive at the conclusion

$$TV^{\delta}=\text{constant}, \quad (5)$$

where T is either critical temperature, and δ may be expected to have different values in the two cases. The data obtained permit the calculation of the exponent δ for both cases on the assumption that the curves of Fig. 3 are those described by Eq. (5). For since the compressibility and thermal expansion are known at atmospheric pressure, we may easily compute the slopes of the curves defined by Eq. (5) where they intersect the T axis. The slopes are

$$dT/dP=T\delta\kappa/(1+T\delta\alpha),$$

α and κ being the volume coefficient of thermal expansion and the compressibility, respectively. Bridgman[4] gives the compressibility as 60×10^{-7} kg/cm^2, and the thermal expansion as given in the *International Critical Tables* is 143×10^{-6}. Taking $T_1=254°$ and $T_u=297°$ we, find

$$\delta_1=2.7 \quad \text{and} \quad \delta_u=8.4.$$

Thus at the lower critical temperature we conclude that

$$\beta W_0\sim V^{-2.7}.$$

Such variation of βW_0 is at least within striking distance of what one would expect, for β is a loosely defined quantity, and might change somewhat as the lattice is distorted, while W_0 would fall off as the third power of the distance for a linear array of dipoles.

At the upper critical temperature, on the other hand,

$$\gamma n\mu^2\sim V^{-8.4}.$$

In this case, $n\sim V^{-1}$, but even so the conclusion seems inevitable that $\gamma\mu^2\sim V^{-7.4}$. It is to be noted that both the compressibility and the thermal expansion of Rochelle salt are strongly aeolotropic, but even so, it is difficult to see how $\gamma\mu^2$ can vary so remarkably with changes in volume.

The somewhat crude application of Fowler's theory as outlined above indicates that no really satisfactory quantitative explanation of the effects observed can be given until more exact data are available on the crystal structure and the arrangement of the dipoles within the lattice. In particular a theory which will permit accurate calculation of the factor, γ, seems highly desirable. While nothing in the experiment contradicts any part of the theory, it must be admitted that the theory does very little in the way of reproducing the experimental facts.

In conclusion it is a pleasure to acknowledge the counsel of Professor Bridgman in carrying out the experimental part of the work, and of Dr. John Bardeen in the discussion of the theoretical aspects of the problem.

[4] P. W. Bridgman, Proc. Am. Acad. **64**, 51 (1929).

On Eddington's Treatment of Dirac's Equation

BORIS PODOLSKY
Graduate School, University of Cincinnati, Cincinnati, Ohio
(Received January 20, 1938)

Eddington, in his book *Relativity Theory of Protons and Electrons*, makes statements to the effect that the invariance of Dirac's equation is an elementary consequence of the tensor form which it acquires in the new wave tensor calculus, in which it is merely an identity derivable on epistemological principles and not on physical hypothesis. It is shown in this article that the invariance of Dirac's equation referred to by Eddington is a purely formal one, while the invariance which is of particular interest in quantum mechanics depends upon the physical interpretation of the wave function. The generalization of physical interpretation suggested by Eddington's work, however, has the desirable quality of leaving Dirac's equation invariant in the physical sense. It is further shown that in the derivation of Dirac's equation Eddington makes use of the usual physical assumptions, but in somewhat disguised form.

I. INTRODUCTION

IN his remarkable book,[1] *Relativity Theory of Protons and Electrons*, Eddington justly lauds the new form of tensor calculus, which he developed in response to the "*challenge to those who specialized in relativity theory*" contained in the invariance of Dirac's equation. The new tensor calculus, called by him the *wave tensor calculus*, is the basis of the entire book, which amply demonstrates the usefulness of this new mathematical tool. Among the many remarkable statements of the book one finds some that are evidently directed against the "challenge" of Dirac's equation; they are to the effect that the invariance of Dirac's equation is a trivial consequence of the tensor form that it acquires in the new calculus and that in this calculus it is merely an identity.

The object of this article is to show that neither of these claims is justified and, incidentally, to bring to light a certain positive, although considerably less spectacular, achievement of Eddington's method of physical interpretation of Dirac's wave functions.

Eddington's claims are astonishing and would, if they were true, profoundly modify our attitude toward Dirac's equations and to physics in general. In fact, it is hard to see what could produce a more fundamental alteration of a physicist's point of view than to find out that a theory, which to him was a brilliant induction from thousands of experiments involving efforts of several generations, can be shown by Eddington to be a mere identity, by considerations that are[2] "purely deductive, being based on epistemological principles and not on physical hypothesis." I must therefore quote Eddington, in order to show that he really makes such claims:

"Thus the invariance of Dirac's equation for relativity transformations, which was a novel kind of invariance from the point of view of ordinary tensor calculus, is an elementary consequence of wave tensor calculus."[3]

". . . the basal vector ψ has the transformation properties of Dirac's ψ, and in fact satisfies identically an equation identifiable with Dirac's wave equation."[4]

"We have made this comparison with Dirac's equation in order to ascertain the current nomenclature. . . . It would be foreign to our plan to intermingle the current semi-empirical theory with the purely deductive theory that we are developing. . . ."[5]

II. INVARIANCE OF DIRAC'S EQUATION

Dirac's equation is first introduced in the two equivalent forms:

$$H\psi=0 \quad \text{and} \quad \chi^*H=0; \tag{1}$$

where ψ and χ^* are four-component quantities, "wave-vectors," which transform according to equations

$$\psi'=q\psi \quad \text{and} \quad \chi^{*\prime}=\chi^*q', \tag{2}$$

[1] Cambridge University Press, 1936.

[2] Reference 1, page 5.
[3] Reference 1, page 63.
[4] Reference 1, page 77.
[5] Reference 1, page 119.

q and q' being 4×4 matrices satisfying the equations

$$qq'=q'q=1; \tag{3}$$

H, which Eddington calls the hamiltonian, is here

$$H=E_1p_1+E_2p_2+E_3p_3+E_4p_4-m, \tag{4}$$

where it is required to be a mixed wave tensor of second rank, thus transforming according to the equation

$$H'=qHq'; \tag{5}$$

E's are four of the five anti-commuting 4×4 matrices E_1, E_2, E_3, E_4, E_5, which are analogous to Dirac's α's, except that their squares are each equal to -1, instead of $+1$. By taking products of these, a set of 16 linearly independent 4×4 matrices (E^- symbols) may be formed, which can then be numbered in some convenient way from E_1 to E_{16}. Then an arbitrary 4×4 matrix can be represented as a linear combination of these. Thus, if T is such a matrix,

$$T=\sum_1^{16} t_\beta E_\beta. \tag{6}$$

Eddington observes that a transformation of the type (5) does not alter the structure of the set of the 16 E^- symbols (that is, after the transformation has been applied to each E^- symbol, the transformed matrices satisfy the same commutation and algebraic relations), and he therefore choses to regard them as mixed wave tensors of second rank.

The connection between wave tensors and space tensors (the ordinary tensors) is established in the following way: Let T of Eq. (6) be subjected to transformation (5) and the resulting matrix be again expressed in terms of the 16 E^- symbols; that is, let

$$T'=qTq'=\sum_1^{16} t_\beta' E_\beta; \tag{7}$$

then Eqs. (6) and (7) define t_β' in terms of t_β. These t_β are now regarded as components of ordinary tensors, and t_β' as their values after the transformation. In fact, Eddington shows that, if we restrict ourselves to such choice of matrices q that (t_1, t_2, t_3, t_4) transform like the coordinates of four-space in a four-dimensional rotation, the 16 t's break up into four groups, as follows:[6]

1. (t_1, t_2, t_3, t_4) transform as the components of a four-vector,
2. $(t_{15}, t_{25}, t_{35}, t_{45})$ transform as another four-vector,
3. $(t_{12}, t_{23}, t_{31}, t_{14}, t_{24}, t_{34})$ transform as a six-vector, and
4. t_5 and t_{16} are invariant.

It is evident then that if all the components of T belonging to one or more of these groups vanish, they remain zeros after a transformation of this restricted type.

Since in the hamiltonian (4) the coefficients (p_1, p_2, p_3, p_4) and m correspond respectively to group 1 and to t_{16} ($t_{16}=im$), and transform as a four-vector and an invariant, respectively, H will behave as a mixed wave tensor of second rank under ordinary relativity transformations, when expressed in the form (5). Thus, Eqs. (1) may be regarded as wave tensor equations; their transformations being, for example,

$$H'\psi'=qHq'q\psi=qH\psi=q0=0. \tag{8}$$

It is this invariance of the form of Eqs. (1) that leads Eddington to conclude[3] that "invariance of Dirac's equation . . . is an elementary consequence of wave tensor calculus." The invariance of which Eddington speaks is thus a purely formal one; it is a question of so transforming all physical quantities, that an equation which is set up in one coordinate system preserves its form in other coordinate systems.

However, the problem of invariance of Dirac's equations, as it appears in quantum mechanics, is somewhat different. Having chosen a coordinate system and a set of E^- symbols, we write down the hamiltonian (4) and the corresponding Dirac's equations (1). From the solutions of these we derive certain physical conclusions. The question then is this: had we chosen a different set of E's but the *same* coordinate system, would we have obtained the *same* physical conclusions? Or, conversely, had we chosen a *different* coordinate system, but the same set of E's, would our conclusions in the new coordinate system be *properly related* to those obtained in the old? Evidently these questions cannot be answered on the basis of formal invariance of Dirac's equa-

[6] The notation for the 16 E^- symbols implied here is based on the following scheme: $E_iE_j=E_{ij}=-E_jE_i$, $(i,j=0,1,..5)$; $E_{oi}=E_i$; $E_{16}=(-1)^{\frac{1}{2}}$.

tions alone, because the answer must depend upon the way in which physical consequences are to be derived from the wave functions. It turns out that both of the above questions can be answered in the affirmative in Eddington's theory, if a proper choice is made of the physically significant quantities.

Eddington supposes that physically significant is

$$J=\psi\chi^*=\psi_\alpha\chi_\beta, \quad (\alpha,\beta=1,2,3,4). \tag{9}$$

Since J is a 4×4 matrix, it can be represented as a linear combination of E^- symbols, thus:

$$J=\sum_1^{16} j_\mu E_\mu; \tag{10}$$

where j_μ are a set of suitable coefficients, which can be computed by the formula[7]

$$j_\mu=-\tfrac{1}{4}\chi^*E_\mu\psi. \tag{11}$$

The coefficients j_μ are thus analogous to the current-density vector of the usual Dirac's theory; the first four components of j_μ being in fact proportional to it, when χ^* is chosen equal to $\bar{\psi}^*$.

Now, because of the way in which E^- symbols transform, Eq. (7) can be written in the form

$$T'=\sum_1^{16} t_\mu E_\mu'=\sum_1^{16} t_\mu' E_\mu, \tag{12}$$

which shows that a *change in E's without a change of coordinate system*, as well as a *Lorentz transformation of coordinate system without a change in E's* (since t_1, t_2, t_3, t_4 transform as coordinates), can each be represented by the wave tensor transformation of the form $T'=qTq'$. The tensor character of Dirac's equations then insures that the wave-vectors transform in accordance with Eq. (2). Thus, J transforms as a mixed wave tensor of second rank:

$$J'=\psi'\chi^{*\prime}=q\psi\chi^*q'=qJq'. \tag{13}$$

If now this transformation is used to represent a change in E^- symbols from a set E_μ to a set $E_\mu'=qE_\mu q'$, we have

$$J'=qJq'=\sum_1^{16} j_\mu qE_\mu q'=\sum_1^{16} j_\mu E_\mu'. \tag{14}$$

Thus, the set of coefficients j_μ *remain unchanged*. This could also be seen directly; for, by the use of Eq. (11), we have

$$j_\mu'=-\tfrac{1}{4}\chi^{*\prime}E_\mu'\psi'=-\tfrac{1}{4}\chi^*q'qE_\mu q'q\psi$$
$$=-\tfrac{1}{4}\chi^*E_\mu\psi=j_\mu.$$

If, on the other hand, the E^- symbols remain unchanged, then comparison of Eq. (14) with Eq. (12) shows that j_μ must transform as the corresponding t_μ; in particular, the first four components will transform as the components of a four-vector.

These considerations show that Dirac's equations are invariant in this physical sense, even when the whole set of 16 quantities j_μ (but *not* J itself) are regarded as physically significant.

III. Dirac's Equation as an Identity

Eddington shows[8] that the equations

$$(E_1j_1+E_2j_2+E_3j_3+E_4j_4-E_{16}j_{16})\psi=0 \tag{15}$$

and

$$j_5=0 \tag{16}$$

are consequences of Dirac's equations, and asserts that Eq. (15) is *equivalent* to Dirac's equation. He then shows[9] that equation

$$(E_1j_1+E_2j_2+E_3j_3+E_4j_4$$
$$+E_5j_5-E_{16}j_{16})\psi=0 \tag{17}$$

is a consequence of the definitions (9) and (10) and of the properties of E^- symbols. Eq. (17) is thus an identity. These equations are the basis for the above quoted statement, to the effect that ψ satisfies identically an equation identifiable with Dirac's equation. The implication is that Dirac's equation is thus derived "purely deductively" from "epistemological principles." This implication is, however, unjustified.

First, it seems to me that too little is made of the fact that to derive Eq. (15) from Eq. (17) it is

[7] Reference 1, page 37, formula (3.37).

[8] Reference 1, page 65.

[9] Reference 1, page 67.

necessary to make the additional assumption $j_5=0$. Eddington dismisses this assumption by saying that "By omitting j_5 he (Dirac) restricts the equation to stream vectors which have zero component normal to space time; otherwise his equation is a perfectly general one. . . ." It seems to me that the limitation $j_5=0$ cannot be derived from epistemological principles, but must be based on physical experience.

Second, and more important, Eq. (15) is *not* equivalent to Dirac's equation, although it is a consequence of it. To show the equivalence of the two, it would be necessary to show also that, conversely, Dirac's equation can be derived from Eq. (15). But this is obviously impossible, since Dirac's equation contains quantities (p_1, p_2, p_3, p_4) not contained in Eq. (15). In deriving Eqs. (15) and (16) from Dirac's equation Eddington ingeniously eliminates them, but they cannot be again introduced without the use of either Dirac's equation or, equivalently, of physical experience. One can of course define them by means of the equations

$$j_1/p_1=j_2/p_2=j_3/p_3=j_4/p_4=j_5/0=ij_{16}/m; \quad (18)$$

and then Eq. (15) becomes equivalent to Dirac's equation *by definition*. But the basis of such definitions, if the quantities thus introduced are to have any connection with the components of momentum, energy and mass, must be either direct experience or Dirac's equations, *from which Eq.* (18) *was originally derived by Eddington.*[8]

To derive Dirac's equation in the form in which p's are replaced by differential operators, Eddington proceeds as follows:[10] Define the operator ∇ as

$$\nabla=\sum_1^{16} E_\mu(\partial/\partial x_\mu). \quad (19)$$

[10] Reference 1, page 118.

Then, Eddington says, "the result of performing the operation ∇ on ψ is another four-valued quantity Ω. We can always find a matrix M such that $\Omega=M\psi$. Generally M will be a function of coordinates." Therefore

$$\nabla\psi=M\psi. \quad (20)$$

This equation is the equation which, according to Eddington, is to be identified with Dirac's equation, when "we limit ourselves to solutions . . . which are functions of four rectangular coordinates (x_1, x_2, x_3, x_4)," so that the summation in Eq. (19) reduces to the first four terms.

The simplicity of this derivation is surprising. But to identify this equation with Dirac's equation implies much more than merely "to ascertain the current nomenclature for . . . M." It is evident from the method of deriving Eq. (20), and from the implication of it being an identity as well, that it must hold for all ψ. On the other hand, Dirac's equation is used *to determine* ψ, as is also done by Eddington in another place. Therefore Dirac's equation cannot be an identity in ψ, and thus cannot be identified with Eq. (20), unless Eq. (20) is interpreted in some way inconsistent with the method of its derivation.

In Eq. (20) M is evidently a function of coordinates which depends upon the choice of ψ; *only in this way can this equation be an identity in* ψ. Dirac's equation makes M a constant independent of ψ. This choice is an induction from physical experience. With this choice Eq. (20) is no longer an identity, but is a restriction of ψ to those functions which have the physical property implied by this choice. To talk of "solutions" of Eq. (20) and to compare it with Dirac's equation implies complete giving up of the assumptions made in its derivation and starting *ab initio* with Dirac's equation, thus accepting all the physical experience and assumptions implied in it.

Nuclear Energy Sources and Stellar Evolution

G. GAMOW
George Washington University, Washington, D.C.
(Received December 16, 1937)

The behavior of a star with a thermonuclear energy source consistent with our present knowledge about nuclear reactions is studied in relation to the problems of stellar evolution and interpretation of the Hertzsprung-Russell diagram and mass-luminosity relation. It is found that in the case of ordinary thermonuclear reactions, with the absence of selective temperature effects (nuclear resonance) the central temperature and luminosity of the star (with constant mass) will rapidly increase in the process of evolution. If, however, such selective effects are present, the energy-production at the center of the star will cease, beginning with the stage when the central temperature reaches the selective value, and energy will be produced only in a spherical shell around the center. This shell will have exactly the selective temperature value corresponding to the thermonuclear reaction in question, and its radius will slowly increase in the process of evolution causing a very slow increase of luminosity. Finally, in the third stage of evolution, when all hydrogen necessary for thermonuclear reactions has been consumed, the star will start a rapid contraction and, passing through the high density stage, will end its life as a cool body. It is also indicated that the star model with a shell source does not possess the property of "super-stability" characteristic for the point-source models.

EQUILIBRIUM CONDITION IN THE INTERIOR OF A STAR[1]

AS was first indicated by Eddington,[2] the distribution of density, pressure, and temperature inside a star can be found by integrating the set of general equations for mechanical and radiative equilibrium in the stellar interior, the equation containing, in addition to the above variables, the average molecular weight, the opacity and the rate of energy production by stellar matter.

Denoting by ρ and p the density and the total pressure at the distance r from the center of the star we can evidently write

$$dp/dr=-GM_r\rho/r^2, \tag{1}$$

$$dM_r/dr=4\pi r^2\rho, \tag{2}$$

where G is the gravitational constant and M_r the total mass inside of the radius r. The total pressure p is composed of the gas pressure p_g of the stellar material and the radiative pressure p_r. It is customary to introduce a new variable β representing the ratio of the gas pressure to the total pressure and write $p_g=\beta p$ and $p_r=(1-\beta)p$. The gas pressure is given by the equation of state of stellar material, so that we have

$$p=f(\rho, T)/\beta \tag{3}$$

or, in the case of an ideal gas

$$p=k\rho T/\beta\mu m_H, \tag{4}$$

where k is Boltzmann's constant, m_H mass of a hydrogen atom and μ the average molecular weight of stellar material. For the radiative pressure we have

$$p_r=p(1-\beta)=\tfrac{1}{3}\sigma T^4, \tag{5}$$

where σ is the Stefan-Boltzmann constant.

To the above set of equations we must add the equation connecting the flow of energy through the stellar material with the gradient of temperature;[2] this equation is

$$\frac{d}{dr}(\tfrac{1}{3}\sigma T^4)=-\frac{1}{c}\kappa\rho\frac{L_r}{4\pi r^2} \tag{6}$$

or

$$\frac{dT}{dr}=-\frac{3}{4}\frac{\kappa}{\sigma c}\rho T^{-3}\frac{L_r}{4\pi r^2}, \tag{7}$$

where κ is the opacity of stellar matter per unit mass and L_r the total flow of radiant energy passing through the surface of the sphere of the radius r. This flow is evidently connected with the rate ϵ of energy-liberation per unit mass by the equation

$$dL_r/dr=4\pi r^2\rho\epsilon. \tag{8}$$

For a star of given chemical constitution the quantities μ, κ, and ϵ can be expressed as functions of density pressure and temperature and,

[1] The discussion of this section closely follows the presentation of the problem by B. Stromgren in Ergebn. Exackt. Naturwiss. **16**, 465 (1937).

[2] A. Eddington, *The Interior Constitution of the Stars* (Cambridge University Press, 1926).

provided the equation of state $p_g=f(\rho, T)$ is also known, the six above equations, along with boundary conditions, completely determine six quantities ρ, p, T, β, M_r, and L_r at any point inside of the star. For given mass we can start with arbitrary values for the radius R and luminosity L and, with the boundary conditions $\rho_R=p_R=T_R=0$; $\beta_R=1$;[3] $M_R=M$ and $L_R=L$, proceed with the integration inwards. In the center of the star we come out with definite values of ρ_0, P_0, T_0, M_0 and L_0 and will have to choose the radius and luminosity R and L with which we started the integration in such a way as to satisfy the conditions $M_0=0$, $L_0=0$. Thus we obtain a definite solution of the problem, the radius of the star, its luminosity and density-temperature-distribution in its interior being completely determined by its mass and chemical constitution. We should notice here that instead of the radius of the star one often uses the so-called effective surface temperature T_{eff}. This temperature is defined as the temperature of the black body which gives the same total radiation per unit surface as the star and, according to definition, is given by $T_{\text{eff}}=(L/4\pi R^2\sigma)^{\frac{1}{4}}$. It can also be determined from the location of the maximum in the continuous spectrum of the star or from relative intensities of absorption lines of the chromosphere.

Some remarks should be made concerning the dependence of μ, κ, and ϵ on the physical state of stellar matter and on its chemical constitution. Because of the very high temperatures in stellar interiors, matter can be considered there as almost completely ionized into nuclei and electrons. Thus the effective molecular weight of an element with atomic number Z and mass number A will evidently be $\mu=A/(Z+1)$. This gives for hydrogen $\mu=\frac{1}{2}$ for helium $\mu=4/3$ and for heavier elements $\mu\leqq 2$. In the calculations of stellar models one often uses the so-called *Russell-mixture* of heavy elements, which represents the simplest approximation to the exact constitutions of stars. This Russell-mixture is given by 50 percent of O; 25 percent of Na and Mg; 6 percent of Si; 6 percent of K and Ca; 13 percent of Fe, and has the average effective molecular weight $\mu=1.85$. In our approximate calculations we can with sufficient accuracy accept the molecular weight of any mixture of heavy elements to be $=2$. If x, y and z represent the fractional amounts of hydrogen, helium and heavy elements in a given star the effective molecular weight will be given by

$$\mu=(2x+\tfrac{3}{4}y+\tfrac{1}{2}z)^{-1}. \tag{9}$$

The opacity of stellar matter, κ, at this high stage of ionization can be calculated on the basis of wave mechanics and its dependence on density and temperature is given by (Kramers' formula)

$$\kappa\sim\kappa_0\rho T^{-3.5}, \tag{10}$$

where κ_0 depends on chemical constitution and for different elements is approximately proportional to Z^2/A. Thus the opacity due to hydrogen and helium can be neglected as compared with the opacity of heavier elements. For the Russell-mixture κ_0 is, for example, calculated to be $3.9\times 10^{+25}$. With the above notations we shall have for our star the effective opacity (per unit mass)

$$\kappa=\kappa_0 z\rho T^{-3.5}, \tag{11}$$

where κ_0 depends only on the relative abundance of different heavy elements and could be accepted to be constant for different stars and for different periods of their life.

According to the present views the energy liberation in stars is due to thermonuclear reactions, i.e., to nuclear transformations caused by violent thermal collisions at the very high temperatures existing inside a star. The more detailed study of such reactions will form the subject of the next section; here we shall notice only that aspect of the problem which relates to the penetration of the barriers surrounding nuclei. The rates of such reactions will increase exponentially with the temperature except for cases of resonance penetration of nuclei where the maximum energy-production will correspond to a resonance temperature T_r.

In case no resonance is present the energy production will be practically concentrated in the center of the star where the temperature is highest. A good approximation in this case will be given by the so-called point-source model; for this model we should write on the right-hand side of (6) L instead of L_r and replace the equa-

[3] We put $\beta_R=1$ on the outer boundary because the radiative pressure decreases with temperature faster than the pressure of gas.

tion (8) by the relation

$$L = F(\rho_0, T_0) \qquad (12)$$

between the total energy production and the density and temperature in the center.

For the point-source model the gradient of temperature will increase towards the center indefinitely (because $dT/dr \sim L/4\pi r^2$) and at a certain distance R^* will become larger than the gradient corresponding to adiabatic temperature change in an element of stellar substance moving along the radius. For $r < R^*$ convection currents will then occur and Eq. (6) will have to be replaced by

$$\frac{1}{T}\frac{dT}{dr} = \frac{2}{3}\frac{d\rho}{\rho}. \qquad (13)$$

It was shown by Cowling[4] that for point-source models the radius of the convection-zone is in constant ratio to the radius of the star $R^* = 0.17R$. The presence of the convection-zone will change somewhat the solution of the star model; in particular it will make the central temperature somewhat lower; however, because of the comparatively small extension of this zone these changes will not be essential. Stromgren has integrated the point-source set of Eqs. ((1), (2), (3), (4), (5), (6)) for our sun and some other stars starting with observed masses, radii and luminosities. In such integrations more detailed dependence of μ and κ_0 on density and temperature was taken into account in the outer regions where the ionization is not complete and the hydrogen content was chosen so as to come out with zero mass remainder when the integration reached the center. For the equation of state the ideal gas expression (4) was taken in the outer region and its validity was checked, step by step, as the integration proceeded inwards. It was found that one should accept the hydrogen content to be about 35 percent and that the ideal gas equation holds for ordinary stars (except white dwarfs) all the way down to the center. The radiative pressure was found to remain (except for very massive stars) very small all the time so that β could be taken with sufficient approximation to be unity for all stars. We should notice here that for ordinary stars such calculations lead to central densities $\rho_0 \leqq 20\bar{\rho}$ and central temperature $T_0 \leqq 4 \cdot 10^7$ °C. As the result of what was said above we can write for a point-source model, not specifying the law of energy production, the set of six equations: Eqs. (1), (2), (4), (12), (13) and

$$\frac{dT}{dr} = -\frac{3}{4}\frac{\kappa_0}{\sigma c}\rho^2 T^{-6.5}\frac{L}{4\pi r^2} \quad (r \geqq R^*). \qquad (14)$$

These equations, together with boundary conditions

$$\rho_R = P_R = T_R = 0, \quad M_R = M, \quad M_0 = 0,$$

define three functions ρ_r, P_r, T_r and two observable characteristics of the star R and L, if the values of the parameters M, μ, κ_0 and the form of the function F are known. Suppose we have a solution for a star of given mass M and given chemical constitution (this defines μ, κ_0 and the coefficients in F) and want to find the change of observable characteristics and internal state of a star if the mass and chemical constitution have been changed. Let us change the mass M by the factor a, the molecular weight μ by the factor b and the opacity-coefficient κ_0 by the factor c. Since we refrain from specifying the law of energy production we shall not use immediately Eq. (12), and denote the change of the total energy-production accompanying the above changes of mass and constitution by the factor d.[5] Substituting $\bar{M} = aM$, $\bar{\mu} = b\mu$; $\bar{\kappa}_0 = c\kappa_0$ and $\bar{L} = dL$ in the five equations (1), (2), (4), (13), (14) we shall have to find such changes of other quantities as will leave these equations invariant. We see at once that Eq. (13) will not change its form for any homogeneous change of variables and that the remaining equations (1), (2), (4), (14) will define the necessary changes of four quantities r, ρ, p and T. Adding the expression for effective temperature $[T_{eff} = (L/4\pi R^2\sigma)^{\frac{1}{4}}]$ we finally obtain the following homologous transformations for the point-source model:

$$\begin{aligned}
&\bar{M} = aM, && \bar{\rho} = a^{-32}b^{-45}c^6d^6\rho,\\
&\bar{\mu} = b\mu, && \bar{p} = a^{-42}b^{-60}c^8d^8p,\\
&\bar{\kappa}_0 = c\kappa_0, && \bar{T} = a^{-10}b^{-14}c^2d^2T,\\
&\bar{L} = d \cdot L, && \bar{T}_{eff} = a^{-5.5}b^{-7.5}c^1d^{5/4}T_{eff},\\
&\bar{r} = a^{11}b^{15}c^{-2}d^{-2}r,
\end{aligned} \qquad (15)$$

[4] T. G. Cowling, Proc. Roy. Astr. Soc. **46**, 42 (1935).

[5] It is clear that for such changes of variable the boundary conditions will always stay invariant.

If we take now a definite dependence of L on ρ_0 and T_0 these equations should give us the change of observable characteristics of the star L and R (or T_{eff}), and its internal density-pressure distribution with the change of mass and chemical constitution.

Analogous homologous transformations could be written for the continuous distribution of energy-sources throughout the star, provided there is a simple law of the form $\epsilon \sim \rho^m T^n$ connecting the energy-production with the density and pressure. Such a transformation, however, will not be of any importance for us in the following discussion.

Thermonuclear Reactions in Star's Interior

It was first indicated by Atkinson and Houtermans[6] on the basis of the wave mechanical theory of nuclear transformations that at the high temperatures ($\geqq 4\times 10^7$ °C) which exist in stellar interiors one should expect considerable probability for the penetration of protons, involved in thermal motion, through the potential barriers of light nuclei. The transparency of the potential barier is given, as is well known,[7] by the expression

$$G \geqq \exp\left[\frac{-2\pi e^2 m^{\frac{1}{2}} Z_1 Z_2}{\hbar (2E)^{\frac{1}{2}}}\right], \tag{16}$$

where m is the reduced mass and Z_1 and Z_2 are the atomic numbers of the colliding nuclei. Integrating over the Maxwell distribution of thermal motion, Atkinson and Houtermans arrived at the expression for the total number of penetrations per unit volume of the given mixture of gases. These calculations have shown that for protons, at stellar temperatures, the appreciable penetration can be expected only in collisions with the first seven or eight elements of the periodic table. As the penetration rapidly decreases with the increasing atomic number of the colliding particles, we may conclude that for α-particles (charge twice and mass four times as large as for protons) there should be expected noticeable penetration only into another α-particle and that the collision between two heavier particles will be always elastic. In order to obtain the formation of heavier elements inside a star it is necessary that some of these thermonuclear reactions between light elements should produce an appreciable number of neutrons, which would then be radiatively captured by heavier nuclei, causing a continuous building up of heavy elements. It seems that the only way in which neutrons can be produced at such comparatively low energies of collision (4×10^7 °C corresponding to an energy of 10 kv) is by the preliminary formation of deuterons, which, as is well known, undergo in mutual collision the following transformations:

$$\begin{aligned} {}_1H^2 + {}_1H^2 &\rightarrow {}_1H^3 + {}_1H^1 \\ &\rightarrow {}_2H^3 + {}_0n^1. \end{aligned} \tag{17}$$

Both possibilities here possess about equal probabilities. One of the simplest thermonuclear reactions which can give rise to deuterons was proposed by Weizsäcker[8] and consists of the following chain:

$$\begin{aligned} {}_2He^4 + {}_1H^1 &\rightarrow {}_3Li^5 + h\nu, \\ {}_3Li^5 &\rightarrow {}_2He^5 + \beta^+, \\ {}_2He^5 + {}_1H^1 &\rightarrow {}_2He^4 + {}_1H^2. \end{aligned} \tag{18}$$

The possibility of this chain rests on the question of the stability of ${}_2He^5$ which is, as yet, undecided. Another possible chain leading to deuterons is

$$\begin{aligned} {}_2He^4 + {}_2He^4 &\rightarrow {}_4Be^8 + h\nu, \\ {}_4Be^8 + {}_1H^1 &\rightarrow {}_5B^9 + h\nu, \\ {}_5B^9 &\rightarrow {}_4Be^9 + \beta^+, \\ {}_4Be^9 + {}_1H^1 &\rightarrow 2\,{}_2He^4 + {}_1H^2. \end{aligned} \tag{19}$$

The possibility of such a chain rests on the stability of ${}_4Be^8$; most recent determinations give, however, for the mass of this nucleus almost exactly twice the mass of an α-particle, the sign of the small difference being uncertain. From inspection of the mass defects of light elements it seems that the above are the only energetically possible reactions which would produce deuterons. We notice that in both chains the original ${}_2He^4$ nuclei which entered the reaction are always set free at the end; the helium acts as a catalyst for the process of transmutation of ordinary hydrogen into heavy hydrogen. However in the reactions (17) the nuclei of mass three (${}_1H^3$ and

[6] R. d'E. Atkinson and F. G. Houtermans, Zeits. f. Physik **54**, 656 (1929).

[7] See, for example, G. Gamow, *Structure of Atomic Nuclei and Nuclear Transformations* (Oxford University Press, 1937).

[8] C. F. Weizsäcker, Physik. Zeits. **38**, 176 (1937).

${}_2He^3$ are formed which, by further capture of a proton may be transformed into ordinary helium.[9] Since heavy nuclei possess much larger cross sections for the capture of neutrons, the neutrons obtained in the above reactions will mainly be used for the increase of the mass of heavy elements. We thus see that the disappearance of 9 units of mass of hydrogen will lead to the formation of 8 units of mass of helium and 1 unit of mass of heavier elements (Russell mixture). If we denote, as above, the hydrogen content by x the content of helium will be $y=8(1-x)/9$ and the content of the Russell mixture $z=(1-x)/9$. For the molecular weight we shall now have

$$\mu \leqq \left[2x+\frac{3}{4}\cdot\frac{8}{9}(1-x)+\frac{1}{2\cdot 9}(1-x)\right]^{-1}=\frac{A}{\alpha+x};$$

$$A=0.78;\quad \alpha=0.56 \qquad (20)$$

and for the coefficient of opacity κ_0:

$$\kappa_0 \leqq 3.9\cdot 10^{25}\cdot(1-x)/9. \qquad (21)$$

We should notice here that in the two limiting cases, where hydrogen is transformed only into helium or only in heavy elements, the coefficient α in (20) will have the values $\alpha_1=0.60$ and $\alpha_2=0.33$.

The rate of energy production per unit mass will be proportional to the number of collisions between the protons and the catalyzing nuclei and can be approximately written in the form:[10]

$$\epsilon \sim xu\rho T^{-\frac{1}{3}}e^{-A/T^{\frac{1}{3}}} \text{ with } A=3\left(\frac{\pi e^2 m^{\frac{1}{2}}Z_1Z_2}{\hbar(2k)^{\frac{1}{2}}}\right)^{\frac{2}{3}}, \qquad (22)$$

where u is the helium content y for the chain (18), ${}_4Be^8$ content for one chain (19) and in general the content of catalizer if some other reaction takes place.

The above formula (22) holds only for the reactions which are due to ordinary penetration through potential barriers. In cases where the nuclei bombarded by protons possess a resonance-maximum in the region of interstellar thermal energies, the penetrations will be mainly due to those protons of the Maxwell energy distribution which possess the resonance energy. If we define the resonance temperature by the relation: $3kT_r/2=E_r$ the rate of reaction will be essentially given by the number of protons of corresponding energy and we shall have

$$\epsilon \sim xu\rho T^{-\frac{1}{3}}e^{-3T_r/2T}. \qquad (23)$$

This expression reaches a maximum for $T \leqq T_r$ and decreases comparatively slowly for lower and higher temperatures.

Another type of selective thermonuclear energy-production (indicated to the author by Dr. E. Teller) can take place if the energy production is mainly due to the reaction-chain (19).

In fact if we assume that the ${}_4Be^8$ nuclei are stable, but possess a very small binding energy Δm, we should expect that the change of temperature will affect the dissociative equilibrium of the reaction

$${}_4Be^8 \rightleftarrows {}_2He^4+{}_2He^4. \qquad (24)$$

For the temperatures below certain $T_s(\leqq \Delta mc^2/k)$ there will be a considerable amount of ${}_4Be^8$, whereas for higher temperatures most of the ${}_4Be^8$ nuclei will dissociate into helium. To obtain an effect for intrastellar temperatures we have to suppose that Δm is about 0.00001 in the hydrogen mass scale, the binding energy being 10–50 kv.

Inasmuch as the reaction chain (19) requires the presence of ${}_4Be^8$ nuclei, the rate of energy-production will be considerably reduced for $T>T_s$. On the other hand the rate of reaction will also decrease for lower temperatures due to the decreasing transparency of the potential barrier surrounding the ${}_4Be^8$ nucleus for small energies. Thus we see that we have here a possible selective temperature effect, the rate of reaction being represented approximately by

$$\epsilon \sim xy^2\rho^2 T^{-\frac{1}{3}}e^{\Delta mc^2/kT}e^{-A/T^{\frac{1}{3}}}/C+e^{\Delta mc^2/kT}, \qquad (25)$$

where C is a constant. Such a reaction also shows a different dependence on the concentration of helium and the density.

[9] We may have

${}_1H^3+{}_1H^1 \rightarrow {}_2He^4+h\nu$ and ${}_2He^3+{}_1H^1 \rightarrow {}_2He^4+\beta^++h\nu$

if one of above nuclei is unstable, the reactions

${}_1H^3 \rightarrow {}_2He^3+\beta^-$ or ${}_2He^3 \rightarrow {}_1H^3+\beta^+$

may take place before the capture of a proton.

[10] The proof and numerical estimate of this formula and also the formulae for the selective temperature effects will be found in the Letter to the Editor by the author and E. Teller in this issue.

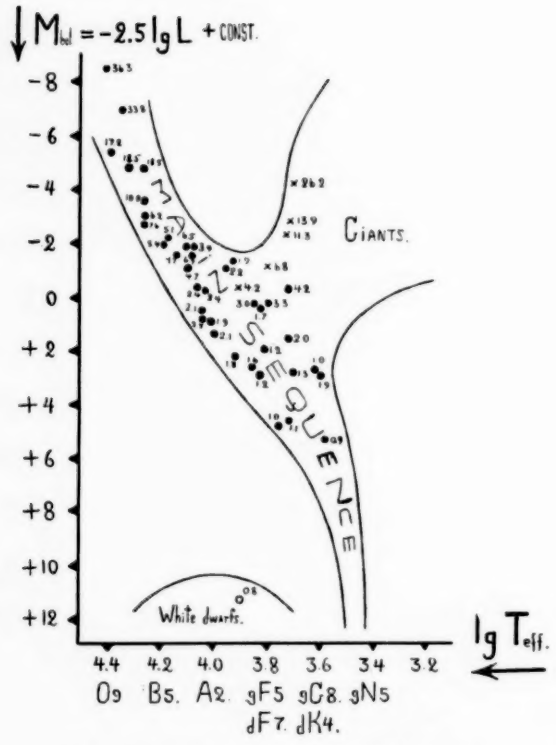

FIG. 1. The Hertzsprung-Russell diagram.

THE EVOLUTION OF A STAR WITH A THERMONUCLEAR SOURCE OF ENERGY

Comparing the behavior of a star model supplied with a thermonuclear source of energy with the observational evidence, we must keep in mind two empirical relations existing between the luminosity, radius (usually expressed through effective temperature) and the mass of the star. The relation between L and T_{eff} (requiring only the knowledge of parallax, stellar magnitude and spectral class of the star) can be studied for a great many stars and is known as the relation of the Hertzsprung-Russell diagram.

It is represented in Fig. 1 where the logarithm of luminosity (absolute magnitude) of different stars is plotted against the logarithm of the effective temperature (expressed through spectral classes). We see that most of the stars are located on a narrow band, the so-called *main sequence*, extending from the cold stars (class N) of small luminosity up to very hot and bright stars (class O). For the stars of the main sequence we have the empirical relation

$$d \lg L / d \lg T_{eff} \leqq 5 \quad (L \sim T_{eff}^{5}). \qquad (26)$$

Apart from the main sequence there is another branch on which the so-called *giants* are located, this region is rather irregular (see Fig. 1) and contains very bright stars of comparatively low effective temperatures. It branches off the main sequence approximately at the class F so that all later classes contain two luminosity groups: giants and the stars of the main sequence which for the purpose of contrast are often called *dwarfs*.

Finally there is a number of very hot stars of small luminosity (evidently due to very small radii) the so-called *white dwarfs*. These stars possess extremely high densities ($\leqq$60,000 relative to water) and, as indicated above, their interiors should be considered in the state of a degenerate Fermi gas of electrons.

Another empirical relation exists between the luminosity and the mass of the star and was first emphasized by Eddington. This *mass luminosity relation* is represented in Fig. 2 where the luminosities are plotted against masses in logarithmic scale for 40 stars (binary variables) for which the most reliable data concerning masses are available.[11] The crosses represent less reliable data for the cepheid variables.[2] We see that the relation can be approximately represented by

$$d \lg L / d \lg M \leqq 3 \quad (L \sim M^{3}). \qquad (27)$$

The scattering of points in Fig. 2 may be partially due to dependence of L (for given mass) on the effective temperature T_{eff} of the star (or on its radius R). In order to check this the stars used in Fig. 2 are also plotted individually in Fig. 1 and

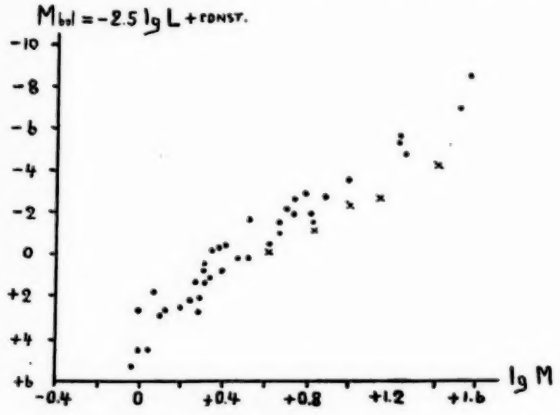

FIG. 2. Mass luminosity relation.

[11] B. Stromgren, Zeits. f. Astrophys. **7**, 222 (1933).

their masses (with respect to that of the sun) are indicated by small figures near each point. Because of large scattering it is difficult to draw lines of equal mass, although it seems that hotter stars have, for the same mass, slightly larger luminosity. It is certain however that whatever the sign of the inclination of constant M, the absolute value of this inclination is much smaller than the inclination of the central line of the main sequence and we may write

$$\left|\frac{d\lg L}{d\lg T_{eff}}\right|_{M=\text{const.}} \ll \left|\frac{d\lg L}{d\lg T_{eff}}\right|_{\text{main sequence}}. \quad (28)$$

In our discussion of the evolution of the stars, due to various thermonuclear reactions in their interior, we shall always suppose that during the total process of evolution the *mass of the star remains constant*. In fact the once favored hypothesis concerning the so-called "annihilation of stellar matter" does not deserve credence in the present development of physics, chiefly because the sources of stellar energy can be sufficiently explained by well-known nuclear transformations. The actual decrease of mass, due to the packing of particles into heavy nuclei, will decrease the mass of the star only in the small percentage of the nuclear mass defects and can be neglected in our present approximate considerations. Finally it is generally accepted that the loss of mass due to emission of material particles from the star's surface (emission necessary for example for explanation of polar lights) is very small and will not lead to any appreciable changes in the total mass during the whole life of the stars.

We have seen above that the only thermonuclear reactions, which can happen at stellar temperatures, are those in which hydrogen is steadily transformed into helium and heavier elements. Such reactions will necessarily lead to an increase of the average molecular weight and the coefficient of opacity of the star according to formulae (20) and (21).

Let us consider the star with no selective temperature effect present, so that the rate of reaction is given by expression (22) where u is the amount of the element primarily responsible for the "burning up" of hydrogen. Not specifying the special type of reaction, we can assume that u increases proportionally to the total number of new nuclei built up by condensation of hydrogen and write $u\sim(1-x)$.

As indicated above, a star with the ordinary thermonuclear source can be described by a point-source model with a convective nucleus and the homologous transformations can be applied. Using the formulae (20) and (21) of the previous section we find that if the hydrogen content changes from x to $\bar{x}=x+dx=x(1+dx/x)$ the molecular weight and coefficient of opacity will change from their original values μ and κ_0 to

$$\bar{\mu}=\mu\left(1-\frac{x}{\alpha+x}\frac{dx}{x}\right)=\mu b, \quad (29)$$

$$\bar{\kappa}_0=\kappa_0\left(1-\frac{x}{1-x}\frac{dx}{x}\right)=\kappa_0 c \quad (30)$$

with $0.33\leqslant\alpha\leqslant 0.60$. Using the homologous transformations with those values of b and c, $a=1$ and arbitrary d we have

$$\bar{\rho}=b^{-45}c^{6}d^{6}\rho, \quad \bar{T}=b^{-14}c^{2}d^{2}T, \quad \bar{L}=d\cdot L. \quad (31)$$

To determine d we have to substitute these values in the formula giving the total liberation of energy. If ω is a small volume around the center in which the energy is mainly produced, the total liberation of energy, i.e., the luminosity of the star, according to (22) and the above remark about u, will be given by

$$L\sim\epsilon\rho_0\omega\sim x(1-x)\rho_0^{2}T_0^{-\frac{1}{3}}e^{-A/T^{\frac{1}{3}}}\omega. \quad (32)$$

For small variations of temperature the exponential dependence in (32) can be represented by a certain power n of temperature. In case of H – He reactions for the intrastellar temperatures around $4\cdot10^{7}$ we have for example: $\epsilon\sim T_0^{7}$; (for heavier elements the exponent will be much larger). With increasing temperature T_0 the volume ω will also increase: this change of ω can be however taken into account by ascribing to the exponent of the temperature a somewhat larger value. The change of the volume ω with the expansion or contraction of the star will also have but small effects on our finite results. We rewrite now the expression (32) in the form:

$$L\sim x(1-x)\rho_0^{2}T_0^{n}. \quad (33)$$

Noticing that

$$\bar{x}(1-\bar{x})=x(1-x)\left(1+\frac{1-2x}{1-x}\frac{dx}{x}\right)$$

and using the expressions (29), (30) and (31) we bring this to the form

$$d=\left(1+\frac{1-2x}{1-x}\frac{dx}{x}\right)\cdot\left(1-\frac{x}{\alpha+x}\frac{dx}{x}\right)^{-(90+14n)}\cdot\left(1-\frac{x}{1-x}\frac{dx}{x}\right)^{12+2n}d^{12+2n}, \quad (34)$$

from which, neglecting higher powers of dx/x, we obtain

$$\bar{L}=d\cdot L=L\left[1-\left(\frac{90+12n}{11+2n}\cdot\frac{x}{\alpha+x}-\frac{12+2n}{11+2n}\cdot\frac{x}{1-x}+\frac{1}{11+2n}\cdot\frac{1-2x}{1-x}\right)\frac{dx}{x}\right], \quad (35)$$

which gives us the change of luminosity accompanying the change of hydrogen content.

Substituting the values of b, c, and d in the transformation for effective temperature we obtain

$$\bar{T}_{eff}=T_{eff}\left\{1-\left[\left(\frac{5}{4}\cdot\frac{90+14n}{11+2n}-\frac{15}{2}\right)\frac{x}{\alpha+x}-\left(\frac{5}{4}\cdot\frac{12+2n}{11+2n}-1\right)\frac{x}{1-x}+\frac{5}{4}\cdot\frac{1}{11+2n}\cdot\frac{1-2x}{1-x}\right]\frac{dx}{x}\right\}. \quad (36)$$

Combining (35) and (36) we obtain finally

$$\frac{d\lg L}{d\lg T_{eff}}=\frac{\frac{\bar{L}}{L}-1}{\frac{\bar{T}_{eff}}{T_{eff}}-1}=\frac{\cdot\ \frac{90+14n}{11+2n}\cdot\frac{x}{\alpha+x}-\frac{12+2n}{11+2n}\cdot\frac{x}{1-x}+\frac{1}{11+2n}\cdot\frac{1-2x}{1-x}}{\left(\frac{5}{4}\cdot\frac{90+14n}{11+2n}-\frac{15}{2}\right)\frac{x}{\alpha+x}-\left(\frac{5}{4}\cdot\frac{12+2n}{11+2n}-1\right)\frac{x}{1-x}+\frac{5}{4}\cdot\frac{1}{11+2n}\cdot\frac{1-2x}{1-x}}. \quad (37)$$

For $n=7$ we have[12]

$$\frac{d\lg L}{d\lg T_{eff}}=4\cdot\frac{0.48+175x-216x^2}{2.4+175x-230x^2}. \quad (37')$$

This expression gives in general very rapid change of luminosity with effective temperature $d\lg L/d\lg T_{eff}\leqq 5$ except near $x=0$ where $d\lg L/d\lg T_{eff}=0.8$. The evolutionary track of a star with such energy-sources, calculated on the basis of Eqs. (35) and (36) is given in Fig. 3 in the frame of Hertzsprung-Russell diagram. We see that such a star would move in the H–R diagram along, or rather parallel to, the main sequence, and only at the end of its evolution the track begins to bend towards the T_{eff} axis (Fig. 3). To follow the time dependence of the evolution, we must write the total energy liberation per unit time as proportional to the decrease of hydrogen content

$$L\sim dx/dt. \quad (38)$$

which shows that the burning up of hydrogen will rapidly increase in the process of evolution and the star will spend only a very small fraction of its life on the slowly ascending part of its evolutionary track in H–R diagram. Let us now keep μ and κ_0 constant and change the mass M of the star. The transformations (15) give us immediately:

$$\bar{M}=aM,\quad \bar{L}=dL,\quad \bar{\rho}=a^{-32}d^6\rho,\quad \bar{T}=a^{-10}d^2T,\quad \bar{T}_{eff}=a^{-5.5}d^{5/4}T_{eff}. \quad (39)$$

Substituting it into (33) with $x=$ const. we get

$$d=a^{-(64+10n)}d^{12+2n} \quad (40)$$

or

$$d=a^{(64+10n)/(11+2n)},$$

$$\left(\frac{d\lg L}{d\lg M}\right)_{x=\text{const.}}=\frac{\lg\alpha}{\lg a}=\frac{64+10n}{11+2n}. \quad (41)$$

For the change in effective temperature we get:

$$\bar{T}_{eff}/T_{eff}=a^{-5.5+(5/4)(64+10n)/(11+2n)} \quad (42)$$

[12] This expression is very insensitive to the exact value of n.

and consequently,

$$\frac{d \lg L}{d \lg T_{eff}} = \frac{\dfrac{64+10n}{11+2n}}{\dfrac{5}{4}\cdot\dfrac{64+10n}{11+2n} - \dfrac{11}{2}}. \qquad (43)$$

Thus the tracks for different masses will be shifted upwards and to the left as indicated in Fig. 3 where the tracks for three different masses (2 : 1 : 1/2) are shown.

Comparing the above results with the real distribution of stars in the H–R diagram we find our results extremely unsatisfactory. In fact the stars of equal masses are located in this diagram on almost horizontal lines, which can be the case for our model only for very small hydrogen content (< 5 percent) where the evolutionary tracks begin to run less steeply. The hypothesis that all known stars correspond to such small hydrogen-content (i.e., are in the last stage of evolution), not only is unsatisfactory in itself, but also contradicts the usual conclusions about high hydrogen content (~35 percent) obtained from the exact calculations of the point-source model. Even if we accept the small hydrogen content in the stars of the main sequence, we will get from the formula (41) much too rapid variation of the luminosity with the mass ($L \sim M^5$) in contradiction to the empirical mass luminosity relation (27).

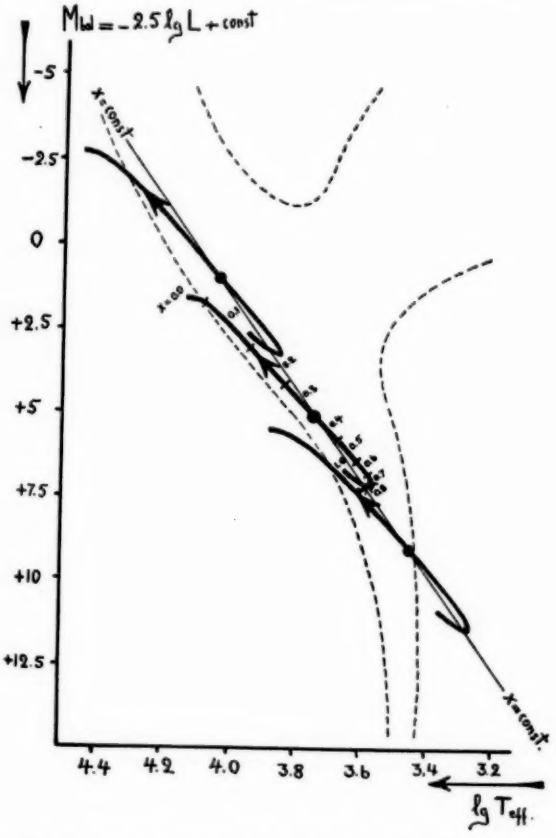

FIG. 3. Evolutionary tracks of three stars (with masses in ratio 2 : 1 : 0.5) in Hertzsprung-Russell diagram. The curves are adjusted in such a way that the point for the star with the mass one and hydrogen-content $x=0.35$ would correspond to the position of the sun in the diagram.

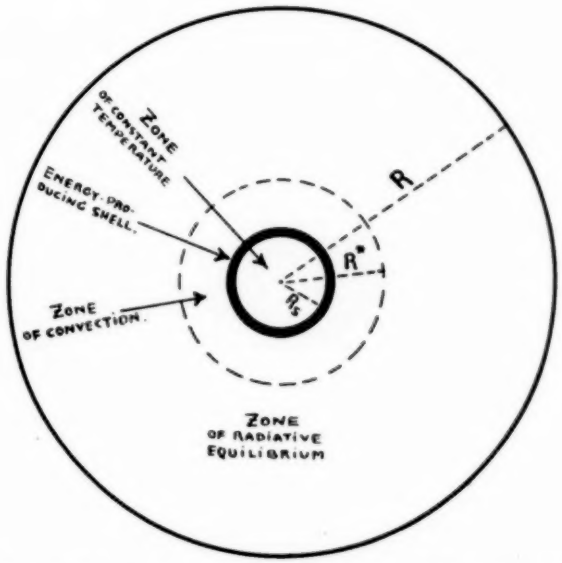

FIG. 4. Schematic representation of the shell source star model. (In reality $R^* = 0.17 \cdot R$.)

It seems that the real behavior of stars cannot be interpreted in terms of ordinary thermonuclear sources of energy, and we now turn our attention to the possibility of selective temperature effects for the nuclear reactions leading to liberation of energy in stellar interiors. Unfortunately a study of the behavior of a star with a selective energy source cannot be pursued by means of simple homologous transformations as used above, because the temperature dependence, possessing a maximum at T_s, in this case, cannot be approximated by definite power of T. This is a necessary condition for the validity of point-source model transformations (15). However, without numerical integration of the fundamental equations (1), (2), (4), (5), (7), (13), which would be necessary for the complete solution of the problem, we can get some idea about the behavior of the star with a selective energy source. Suppose that for steady contraction of the star the temperature in

the center reaches the value corresponding to the resonance energy of the reaction mainly responsible for the energy production. In such a case no further change of the temperature can increase the rate of the energy production and the increase of luminosity which was mainly due to the exponential factor in (32) must become much slower. However, the increasing molecular weight (resulting from burning up of hydrogen) will require the further increase of internal temperature in order to keep the star in mechanical equilibrium. This will result in the shift of the energy production region from the center of the star into a spherical shell as indicated schematically in Fig. 4. The temperature-distribution inside of this *energy producing shell* becomes almost uniform and slightly higher than the selective temperature.[13] No convection-streams will now be expected in the central regions and the convective zone will be located only between the radius of our shell R_s and the outer region of convection R^*.[14]

As the evolution of the star proceeds and its molecular weight and the coefficient of opacity simultaneously increase, we should expect a general rise of temperature inside of the star and, consequently, the slow motion of the energy producing shell towards the outer regions.

Though no direct temperature dependence of the rate of energy-production is present in the case of selective sources, the increase of the volume of the shell, and the decrease of density of stellar matter as the shell moves away from the center, will result in a slow change of the total energy production. Those two effects, acting in opposite directions will give, however, a very slow change, most probably an increase, of the total luminosity of the star.

If we take into account that most probably the star must steadily contract during the above described process (increase of molecular weight and small changes in energy-production) we should expect still slower change of the radius R_s and the general increase of density in homologous points (same r/R); this will not change our conclusions about small changes of luminosity very much. The slow increase of luminosity and steady decrease of the radius of the star will result in the rise of effective temperature $[T_{\text{eff}}=(L/4\pi R^2\sigma)^{\frac{1}{4}}]$ and the star will move towards the hotter part of the H–R diagram, slowly changing its luminosity.

The above considerations justify the hope that the proper treatment of the "shell-source-model" of the star will give us a satisfactory explanation of stellar evolution.[15]

Resuming the above discussion we should imagine the process of stellar evolution as beginning from the state of a comparatively large and cool sphere with a central temperature below the resonance value. This pre-resonance part of the evolution may be described by the point-source model with the rather small total energy liberation due to ordinary penetration. In this stage of evolution the star will rapidly gain in luminosity and effective temperature running along the main sequence from its cool part upwards.

In the succeeding course of evolution, as soon as the central temperature reaches the selective value, the formation of the energy source shell around the center will take place. From this point on, the luminosity and effective temperature of the star will change only very slowly because of the slow increase of the radius of the shell and the star will hold almost constant position in the H–R diagram. After all of the hydrogen in the star is consumed no more nuclear energy will be available and the star will start a rapid contraction, passing through the stage of the *white dwarf* will finally finish its life as a non-luminous body. We should notice here that the shell-model has also a considerable advantage over the point-source model from the point of view of stability. In fact, it was shown by Eddington[2] that the point-source model with strong temperature dependence of energy-source (necessarily existing for ordinary nuclear reactions) will be "superstable:" the amplitude of any small oscillation increasing without limit and leading to the explosion of the star. It is easy to see that the shell model, showing only a very small change of energy-liberation with the change of stellar radius, will be absolutely stable in this respect.

In conclusion I am glad to express my thanks to my friends Dr. E. Teller and Dr. M. Tuve for many helpful discussions of the above problems.

[13] In fact if we suppose that the temperature inside of the shell will be equal to the selective temperature, the energy will be produced in large amounts throughout the sphere and the flow of energy outward from the center will produce a temperature gradient and raise the central temperature above its selective value.

[14] As long as R_s remains smaller than R^*.

[15] Such a treatment is being undertaken at present by the author together with Chas. Critchfield.

LETTERS TO THE EDITOR

Prompt publication of brief reports of important discoveries in physics may be secured by addressing them to this department. Closing dates for this department are, for the first issue of the month, the eighteenth of the preceding month, for the second issue, the third of the month. Because of the late closing dates for the section no proof can be shown to authors. The Board of Editors does not hold itself responsible for the opinions expressed by the correspondents.

Communications should not in general exceed 600 words in length.

An Improvement in Geiger-Müller Tube Design

There have been several methods suggested for the construction of Geiger-Müller tubes.[1] The technique yielding the most satisfactory results in this laboratory has been described by Duffendack, Lifschutz and Slawsky.[2] However, tubes constructed in this manner for use with a magnetic spectrograph were not entirely reliable. Their reliability was further impaired by the presence of nearby charged objects. As a negatively charged rod approached the tube a very high counting rate was observed and as the rod receded the counting rate fell below its original value for a short time. With a positively charged rod the opposite effect was observed.

These effects were found to be prominent only in the presence of light. The counters were known to be slightly sensitive to room light normally. Hence it appeared that the increase in counting rate might be due to an increase in the photoelectric emission of electrons from the metallic film deposited on the glass wall during the sputtering of the elements. An analysis of the effect of the charged bodies shows that during the times of increased counting rate the sputtered film was being charged by induction to a potential more negative than its normal average equilibrium potential. To test this hypothesis we constructed a shield consisting of a layer of copper wire wound around the outside walls of the tube and connected to the anode. It was hoped that this would prevent the photoelectrons ejected from the sputtered film and glass walls from reaching the effective counting volume. The tube was then found to be unaffected by any external bodies. It was no longer appreciably sensitive to room light and its background was considerably reduced.

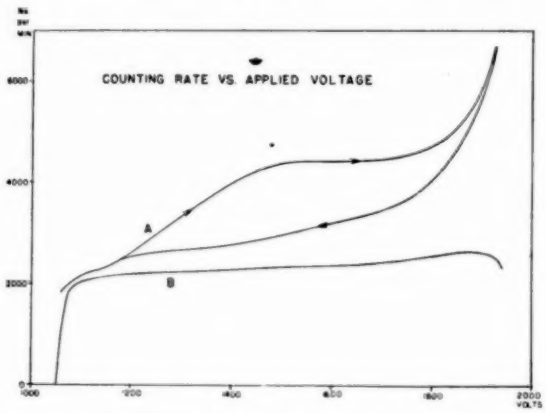

FIG. 1. Counter characteristics with constant source. Curve *A*, unshielded. Curve *B*, shielded.

We had previously noticed that in the determination of the counting rate *vs.* applied voltage the curve obtained in the order of descending voltages invariably was lower than that taken in the reverse order. Measurements were not repeatable because they were dependent upon the voltages that had been previously applied to the counter. Curve *A* of Fig. 1 shows such a behavior. However, with the external copper wire shield at anode potential this same counter showed a long flat plateau, curve *B*, which did not increase rapidly at higher voltages but commenced to decrease at a certain voltage because of an unstable glow discharge within the tube. The plateau was completely stable and repeatable at all times. A similar treatment of five other unsatisfactory counters in every case resulted in a long, flat, stable plateau. This treatment alone does not guarantee good counters for it is still found necessary to clean the tube elements.

A counter having a shield between the cathode and the glass walls was constructed. As the potential on the shield was increased the counting rate with a fixed source decreased asymptotically toward a minimum value until a glow discharge formed around the anode. When the shield was at the potential of the anode, the counting rate had practically reached this minimum value.

In making counters perform in the Neher-Harper circuit it was found satisfactory to connect the external shield directly to the central wire. This, of course, increases the capacity of the tube and hence broadens the pulse. Examination of these pulses, however, shows in most cases a broadening of only fifty percent.

It should be mentioned that in certain circuits the central wire is at ground potential and the cathode at a large negative potential. Counters so arranged in surroundings at ground potential would be shielded in this same manner.

Since this work was carried out it has come to the authors' attention that somewhat similar results have been observed but not reported by G. L. Locher.

This work has been made possible by a grant from the Rackham Trust Fund.

J. L. LAWSON
A. W. TYLER

Department of Physics,
University of Michigan,
Ann Arbor, Michigan,
March 10, 1938.

[1] See for example, L. F. Curtiss, Nat. Bur. Stand. J. Research **4**, 593, 609 (1930), and G. L. Locher, J. Frank. Inst. **216**, 553–558 (1933).
[2] Duffendack, Lifschutz and Slawsky, Phys. Rev. **52**, 1031 (1937).

Electron Capture and Internal Conversion in Gallium 67

In order to establish the fact that nuclei may decay by the capture of orbital electrons, it will be necessary to prove that a nucleus with charge Z transforms into one with charge $Z-1$, and that the characteristic radiation of an atom with charge $Z-1$ is emitted after the process. The K radiation of approximately correct wave-length has been detected in several cases recently[1-3] and has been offered as evidence for the existence of K electron capture. But unless one can show that there are no internally converted gamma-rays from the radioactive body under consideration, the evidence cannot be given too much weight, as it is well known that x-radiation follows internal conversion. Recent experiments have shown that x-rays having the correct absorption coefficients in Al for Fe, Ni, Cu, and Zn $K\alpha$ are emitted by these elements, respectively, after bombardment with high energy deuterons. These x-rays follow both electron and positron periods, which would cast doubt on their interpretation in terms of K electron capture.

An isotope which seems to capture K electrons as well as emit conversion electrons, may be formed by deuteron bombardment of Zn. The activity, of 83 hours half-life, has the chemical properties of Ga, as shown by the solubility of its chloride in ether. It has been assigned to Ga^{67} by Mann,[4] who bombarded Zn with alpha-particles, and separated Ga by chemical means. The radiations emitted are a soft group of electrons, a soft x-ray, and one or two gamma-rays. The electrons have too small an energy for even the first Sargent curve, so their absorption curve was investigated quite carefully. They are absorbed as an 85 kv line spectrum of beta-rays, and this has been confirmed by Mr. E. M. Lyman and Mr. D. C. Kalbfell, who used beta-ray spectrographs with a Geiger counter and a photographic plate, respectively. The spectrum consists of two lines at 90 and 99 kv—corresponding to K and L conversion of a 100 kv line. The 90 kv line is the stronger, as would be expected.

The x-radiation can be shown to be Zn $K\alpha$ and $K\beta$, without question, by absorption measurements in Ni and Cu foils. The wave-lengths of the Zn K lines lie between the critical absorption edges of Ni and Cu, so Ni is several times as effective an absorber. In addition, the absorption edge of Cu splits the K doublet of Zn, so its absorption curve may be resolved into two components giving approximately the correct intensity ratio of $K\alpha$ to $K\beta$.

The gamma-ray absorption curves in Pb and Cu indicate an energy of 0.2–0.3 Mev. Transition curves from Pb to Al show an electron group of this energy and one of lower energy, probably due to the unconverted fraction of the 100 kv line.

It is then evident that a substance which has been shown to be Ga by chemical methods decays into a Zn isotope, as shown by x-ray spectroscopy, and during the process, emits no positrons. (None were observed in a cloud chamber, and no trace of the annihilation radiation could be detected.) In order to show definitely that the transformation is by K electron capture, it is necessary to examine the relative intensities of the various radiations. Perhaps the most direct method would be to show that the x-rays often come off in pairs—one due to an electron captured by the nucleus, and the other due to the converted electron. This will be attempted with the aid of coincidence counters in the near future. From considerations of the geometry of the electroscope and the absorption coefficients, it can be shown that the excitation of the K shell is more frequent than necessary to explain the number of conversion electrons, by about 50 percent. The gamma-ray intensity is more difficult to estimate, but it seems to be roughly equal to that of the electron and x-rays. Professor Oppenheimer and his students have calculated the internal conversion coefficient for a 100 kv γ-ray in zinc, for various orders of multipole, and find that it could easily be 80 percent.

All the data reported above are in agreement with the view that Ga^{67} transforms into Zn^{67} by electron capture, and then emits a K x-ray quantum in half of the cases. (Auger coeff. $=0.5$.) Then the excited state of the Zn^{67} emits either or both a 100 kv and a 0.2–0.3 Mev gamma-ray quantum, the 100 kv line being highly internally converted. Finally another 0.5 quantum of Zn K radiation is emitted.

It is a pleasure to thank Mr. E. M. Lyman and Mr. D. C. Kalbfell for examining the activated zinc in spectrographs of their design, and Professor E. O. Lawrence and Professor J. R. Oppenheimer for continued interest in the problem. The work has been aided by grants from the Research Corporation, the Chemical Foundation, and the Josiah Macy, Jr. Foundation.

LUIS W. ALVAREZ

Radiation Laboratory, Physics Department,
University of California,
Berkeley, California,
March 15, 1938.

[1] L. W. Alvarez, Phys. Rev. **52**, 134 (1937).
[2] O. Oldenberg, Phys. Rev. **53**, 35 (1938).
[3] E. J. Williams and E. Pickup, Nature **141**, 199 (1938).
[4] W. B. Mann, Phys. Rev. **53**, 212 (1938).

Suggestion Regarding the Nature of the Heavy Electron

The existence of heavy particles whose mass appears to be between that of the electron and the proton is indicated by a number of recent experiments on cosmic rays.[1] Jauncey[2] has proposed a theory of the nature of such particles, based on the idea of the addition of photon energy to an electron in the form of increased mass. This theory admits of resultant particles of any mass, depending upon the energy of the captured photon.

An alternative idea is offered in the present note. Relative to an observer at rest, the mass of an electron moving with a speed v is given by

$$m=\frac{m_0}{[1-(v/c)^2]^{\frac{1}{2}}}. \tag{1}$$

The de Broglie wave-length associated with an electron is

$$\lambda=h/mv. \tag{2}$$

Elimination of v between (1) and (2) yields

$$\frac{m}{m_0}=\frac{1}{[1-(h/mc\lambda)^2]^{\frac{1}{2}}}. \tag{3}$$

Suppose that occasionally an electron of suitable speed is able to interact with an atomic nucleus near which it passes in such way that its relativity mass increase is retained in a quasi-stable form provided that the de Broglie wave-length of the electron is equal to $2\pi a$, where $a=e^2/m_0c^2$ is a length representing the range of nuclear forces. This is analogous to the result that the de Broglie wave-length of an electron in the lowest Bohr orbit of an atom is equal to the circumference of the orbit. Substituting $\lambda=2\pi e^2/m_0c^2$ in (3) and calling $m/m_0=R$,

$$R=\frac{1}{[1-(hc/2\pi e^2R)^2]^{\frac{1}{2}}}, \tag{4}$$

or with $hc/2\pi e^2=137$, this becomes

$$R\doteq[1+(137)^2]^{\frac{1}{2}}. \tag{5}$$

Thus the "new" particle should have a mass of about $137m_0$. In view of the fact that $a=e^2/m_0c^2$ is determined only approximately, the result is in accord with experimental values of m so far reported.

The speed of an electron having the apparent mass required by the above relations is given by

$$v/c=137/[1+(137)^2]^{\frac{1}{2}}=0.99997. \tag{6}$$

It is likely that a heavy electron of this kind would ultimately revert to its ordinary state by emission of radiation or by conversion of its excess mass into kinetic energy or both. The behavior of reflected electrons cited by Zwicky[3] may find a ready explanation in terms of such processes.

The total energy given off when a heavy electron of mass $137m_0$ returns to its normal state would be $136m_0c^2$ or about 69 Mev.

IRA M. FREEMAN

Central College,
Chicago, Illinois,
February 28, 1938.

[1] Neddermeyer and Anderson, Phys. Rev. 51, 884 (1937); Street and Stevenson, Phys. Rev. 52, 1003 (1937); Corson and Brode, Bull. Am. Phys. Soc., Dec. 2 (1937).
[2] Jauncey, Phys. Rev. 52, 1256 (1937).
[3] Zwicky, Phys. Rev. 53, 315 (1938).

On the Latitude Effect of the Soft Component of Cosmic Rays

The measurements of Korff, Curtiss, and Astin[1] afford the possibility of evaluating completely the latitude effect of the high altitude part of the absorption curve. The most striking features of this important research are: (a) Almost all ionization measured in the stratosphere is produced by secondary radiation; (b) The shape of the absorption curve does not undergo any considerable change with latitude; (c) The peak of the curve does not shift considerably; (d) The latitude effect, between Washington and Peru, as measured by the heights of the peaks, amounts to 50 percent of the Washington intensity.

We may therefore write for the intensity $I(x)$ measured at a depth X and latitude λ, as a first approximation

$$I(x)=S(x)=S_\lambda\varphi(x) \tag{1}$$

where $S(x)$ is the intensity of the secondary radiation and S_λ a factor only dependent on latitude.

Concerning the energy spectrum of the soft component, different methods of analysis give in the energy range considered here an expression[2]

$$f(\epsilon)d\epsilon=\epsilon^{-n}d\epsilon \tag{2}$$

where n varies between 2.4 and 3 approximately. We may put

$$n=2.5. \tag{3}$$

The number of primaries arriving in a given latitude λ is

$$N_\lambda=c\int_{\epsilon_\lambda}^{\infty}f(\epsilon)d\epsilon=[c/(1-n)]\epsilon_\lambda^{1-n} \tag{4}$$

where ϵ_λ is the threshold energy imposed by the earth's magnetic field. If the intensity of secondaries were directly proportional to the number of primaries, i.e., if $S_\lambda\sim N_\lambda$, an excessively high latitude effect would result. S_λ would be proportional to $\epsilon_\lambda^{-1.5}$. At the latitude of Peru where the threshold energy is as great as three times the corresponding value at Washington (1.2×10^{10} ev against 4×10^9 ev), only 19 percent of the Washington intensity should be observed. In order to obtain a better fit of calculated and observed values a much slower fall of the energy distribution with energy than that given by (2) and (3) would be necessary.

This difficulty may be solved by admitting proportionality between the number of secondaries and the total energy of the incoming rays. This point of view emanates from a general theory based on Swann's formula[3] for the energy loss of corpuscular rays which has already provided an interpretation[4] of a large number of cosmic-ray phenomena. The mathematical deduction will be treated in a subsequent paper. Here let us examine only qualitatively the consequences of this assumption resulting from the behavior of the latitude effect at high altitudes.

With decreasing latitude there is a cut-off of a greater and greater number of soft primaries, but as only small energy is carried by these rays, their efficiency as producers of secondaries is less than that of the remaining rays. Therefore we put

$$S_\lambda\sim E_\lambda=c\int_{\epsilon_\lambda}^{\infty}\epsilon f(\epsilon)d\epsilon=[c/(2-n)]\epsilon_\lambda^{2-n}. \tag{5}$$

The rise of the energy and consequently the rise of the measured intensity, differs from that for the number of primaries by a factor ϵ_λ. There results

$$S_\lambda\sim\lambda^{-0.5}. \tag{6}$$

The intensity at Peru is calculated as 58 percent of that at Washington.

BERNHARD GROSS

Instituto Nacional de Technologia,
do Ministerio do Trabalho,
Rio de Janeiro, Brazil,
February 7, 1938.

[1] S. A. Korff, L. F. Curtiss, A. V. Astin, Phys. Rev. 53, 14 (1938); L. F. Curtiss, A. V. Astin, L. L. Stockmann, B. W. Brown, Phys. Rev. 53, 23 (1938).
[2] G. Pfotzer, Zeits. f. Physik 102, 41 (1936); W. F. G. Swann, Phys. Rev. 50, 1103 (1936); J. F. Carlson, J. R. Oppenheimer, Phys. Rev. 51, 220 (1937); W. Heitler, Proc. Roy. Soc. London A159, 432 (1937).
[3] W. F. G. Swann, Phys. Rev. 46, 432 (1934); 46, 828 (1934); 47, 575 (1935).
[4] B. Gross, Physik. Zeits. 37, 11 (1936); 37, 409 (1936); 38, 201 (1937); G. Pfotzer, reference 2; W. F. G. Swann, Phys. Rev. 48, 641 (1935); 50, 1103 (1936).

The Rate of Selective Thermonuclear Reactions

In the paper of one of us (G.G.)[1] in the present issue, the probable importance of selective temperature effects of thermonuclear reactions for the structure and evolution of stars has been discussed in some detail. It is therefore of interest to obtain quantitative expressions for the rate of energy production in the various reactions involved. The formula for the rate of ordinary thermonuclear penetration followed by radiative capture was first given by Atkinson and Houtermans.[2]

Because of the subsequent development of nuclear physics this formula has to be changed in several respects and we give here the new derivation. Consider a gas consisting of two elements with atomic numbers Z_1 and Z_2 and atomic masses m_1 and m_2. Let x and y be the relative amounts (by weight) of two components, and ρ and T the total density and temperature. The number of collisions between two nuclei of the two different kinds with the collision energy in the interval $[E; E+dE]$ is given by:

$$dN=\frac{4xy\rho\sigma}{(2\pi)^{\frac{1}{2}}m_1m_2m^{\frac{1}{2}}(kT)^{\frac{3}{2}}}e^{-E/kT}EdE, \qquad (1)$$

where $m=m_1m_2/(m_1+m_2)$ is the reduced mass and σ the effective cross section. The effective cross section for radiative capture is given by the cross section for penetration multiplied by the ratio of emission probability of γ-rays $\Gamma_\gamma \gtrsim 10^{+14}$ sec.$^{-1}$ (for the energies involved) and the proper frequency $\hbar/mr_0^2(\gtrsim 10^{22}$ sec.$^{-1})$ of a particle oscillating inside the nucleus. Using the penetration formula we write:

$$\sigma \gtrsim \frac{\Lambda^2}{4\pi}\exp\left[\frac{-2\pi e^2m^{\frac{1}{2}}Z_1Z_2}{\hbar(2E)^{\frac{1}{2}}}+\frac{4e(2mZ_1Z_2r_0)^{\frac{1}{2}}}{\hbar}\right]\cdot\frac{\Gamma_\gamma mr_0^2}{\hbar}, \qquad (2)$$

where $\Lambda=2\pi\hbar/(2mE)^{\frac{1}{2}}$ is the de Broglie wave-length. Substituting (2) into (1) we get an expression possessing a sharp maximum at $E\gtrsim(\pi e^2m^{\frac{1}{2}}Z_1Z_2kT)^{\frac{2}{3}}/(2^{\frac{1}{2}}\hbar)^{\frac{2}{3}}$ the breadth of which is $\Delta E\gtrsim(8/3kT)^{\frac{1}{2}}(2\pi e^2m^{\frac{1}{2}}Z_1Z_2kT^{\frac{1}{2}})/(2^{\frac{1}{2}}\hbar)^{\frac{1}{2}}$. For the total number of captures per unit mass we get:

$$N\gtrsim\frac{\pi^{5/6}}{3^{\frac{1}{2}}}\frac{e^{\frac{1}{3}}\hbar^{\frac{1}{3}}Z_1^{\frac{1}{3}}Z_2^{\frac{1}{3}}r_0^2\Gamma_\gamma}{m_1m_2m^{\frac{1}{3}}} \times\exp\left[\frac{4e(2mZ_1Z_2r_0)^{\frac{1}{2}}}{\hbar}-3\left(\frac{\pi^2e^4mZ_1^2Z_2^2}{2\hbar^2kT}\right)^{\frac{1}{3}}\right]\frac{xy\rho}{(kT)^{\frac{3}{2}}}. \qquad (3)$$

As an example we consider the reaction chain proposed by Weizsäcker (formula (18) in I) though this chain, requiring the stability of $_2He^5$, seems to be in contradiction with the mass defect of this nucleus as determined by Williams, Shepherd and Haxby.[3] Using formula (3) with $Z_1=1$; $Z_2=2$; $m_1=m_H$; $m_2=4m_H$; $x=y=\frac{1}{2}$; $\rho=1$ and $r_0=3\cdot10^{-13}$ cm we obtain the number of chain starting reactions for different temperatures. The total energy libration per gram per second, if we accept the energy balance of each complete chain as 18 Mev, is given by curve A in Fig. 1.

In case there is resonance at a certain energy E_r the dispersion formula has to be used. If Γ_p is the probability of particle re-emission we can write:

$$\dot{\sigma}\gtrsim\frac{\Lambda^2}{4\pi}\frac{\Gamma_p\Gamma_\gamma}{[E-E_r]^2\hbar^{-2}+\frac{1}{4}[\Gamma_p+\Gamma_\gamma]^2}. \qquad (4)$$

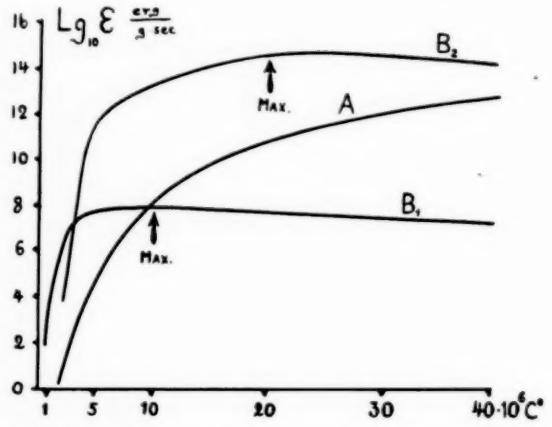

FIG. 1. Energy liberation ϵ in erg per gram per sec. Curve A, energy balance of each complete chain is 18 Mev. Curve B_1 and B_2, energy liberation of Weizsäcker's chain; resonance at 2 Kev and 4 Kev.

If $\Gamma_\gamma\gg\Gamma_p$ we have at the resonance $\sigma\gtrsim\Lambda^2\Gamma_p/\pi\Gamma_\gamma$ and the breadth of the resonance is $\Delta E\gtrsim\hbar\Gamma_\gamma$. Using formula (1) we obtain for the total number of captures per unit mass

$$N\gtrsim 8\left(\frac{\pi}{2}\right)^{\frac{1}{2}}\frac{\hbar^4}{m_1m_2m^{5/2}r_0^2} \times\exp\left[\frac{-2\pi e^2m^{\frac{1}{2}}Z_1Z_2}{\hbar(2E_r)^{\frac{1}{2}}}+\frac{4e(2mZ_1Z_2r_0)^{\frac{1}{2}}}{\hbar}\right]\frac{xy\rho}{(kT)^{\frac{3}{2}}}\cdot e^{-E_r/kT}. \qquad (5)$$

As an example the energy-liberation of Weizsäcker's chain with the resonance lying at 2 Kev and 4 Kev ($T_r=1$ and $2\cdot10^7$ C°) is shown by curves B_1 and B_2 in Fig. 1. We notice that for $E_r=2$ Kev the resonance is comparatively unimportant, whereas for $E_r=4$ Kev and higher the energy liberation at resonance is about 10^4 times larger than in the ordinary case. The energy liberation due to such resonance falls off slowly at high temperatures and therefore the real model of a star with such source will be somewhere between the "shell source model" discussed in I, and the "ball source model" in which the energy production remains constant within a sphere of a certain radius.

Another type of thermonuclear reaction leading to a sharp maximum and therefore to a shell model can be obtained if one assumes the stability of $_4Be^8$ nucleus (formula (19) in I). At low temperatures the rate of energy production will be mainly determined by the reaction $_2He^4+{}_2He^4\rightarrow{}_4Be^8+h\nu$. This rate can be calculated from (3) by putting $Z_1=Z_2=2$ and $m_1=m_2=m=4m_H$. At higher temperatures, however, the chainbreaking reaction $_4Be^8+h\nu\rightarrow{}_2He^4+{}_2He^4$ with the rate N_2 will compete with the next step in the chain $_4Be^8+{}_1H^1\rightarrow{}_5B^9+h\nu$ (rate N_3). The total rate of this complex process will be given by

$$N=\frac{N_1}{1+N_2/N_3} \qquad (6)$$

with

$$\frac{N_2}{N_3}\gtrsim\frac{2^{5/3}\pi^{\frac{1}{2}}}{3^{\frac{1}{2}}}\frac{\hbar^3[\Gamma_\gamma r_0]_3}{m_H^{5/2}[\Gamma_\gamma r_0]_2}\exp\left[\frac{8e}{\hbar}((mr_0)_3^{\frac{1}{3}}-(mr_0)_2^{\frac{1}{2}})\right] \times\frac{x\rho}{(kT)^{\frac{3}{2}}}\exp\left[\frac{E_d}{kT}+1.8\cdot\left(\frac{\pi^2e^4m_H}{\hbar^2kT}\right)^{\frac{1}{3}}\right], \qquad (7)$$

where E_d is the dissociation energy of $_4Be^8$ into two $_2He^4$ nuclei.

The expression (6) shows a sharp maximum for the temperature at which the thermal dissociation of $_4Be^8$ nuclei into two α-particles starts. We should notice here, however, that the possibility of such reaction requires the stability of $_4Be^8$ which at the moment is rather doubtful because of recent experiments of Kirchner, Laaff and Neuert.[4]

It is also questionable, in view of comparatively low probability of α-particle penetration into another α-particle, whether such a chain will give sufficient energy to secure the existence of the star.

George Washington University,
Washington, D. C.
March 4, 1938.

G. GAMOW
E. TELLER

[1] In the following quoted as I.
[2] R. d'E. Atkinson and F. G. Houtermans, Zeits. f. Physik **54**, 656 (1929).
[3] Williams, Shepherd and Haxby, Phys. Rev. **51**, 888 (1937).
[4] F. Kirchner, O. Laaff and H. Neuert. Naturwiss. **39**, 794 (1937).

Multiple States in the High Pressure Discharge

In studying the arc discharge in the one atmosphere range of pressure we have for some time accumulated evidence that there exist, in addition to the "normal arc" and a glow discharge, additional glow states. The possibility that these additional states arise from spurious effects, such as magnetic lengthening of the discharge column, has now been eliminated.

We measure simultaneously the total voltage e, electric gradient E, and the diameter D of the discharge column, all as a function of arc current, i, varying between 10 amperes and zero. In addition to the oscillographically recorded e, E, and D, we have taken motion pictures of the discharge at 1000 frames per second.

The findings are as follows: With hydrogen at one atmosphere pressure and pure carbon electrodes, there exist a normal arc state I, a glow state II, and a glow state III. The normal arc state I has a gradient E that varies (linearly on log-log paper) between 82 v/cm at 10 amperes to 280 v/cm at 2 amperes, and is identical with the hydrogen arc studied by Mackay and Ferguson[1] and Langmuir.[2] In the range 2–0.6 amperes glow II appears, with $530 < E < 900$ v/cm. From 0.6 to 0.1 ampere a glow III is found, with $900 < E < 1300$ v/cm. The transition between I and II is thus accompanied by a change in gradient of 240 (v/cm). The transition between II and III shows no change in gradient, but an abrupt change in total arc voltage.

From measurements of the total voltage e, it is found that the transition between I and II is accompanied by a change in e of 96 volts, the transition between II and III by 130 volts.

The photographs show that I is a highly luminous column, homogeneous along the axis, with a current density of approximately 1000 amp. cm^{-2}. The form II is a less intense striated discharge, with a lower current density, and has a well-developed cathode dark space. The new discharge III has the same column as II, but the cathode dark space is replaced by an intense glow from which streamers emanate. It is evident that the cathode fall of II has increased by 130 volts in going to III.

There is incomplete evidence of an additional fourth state in hydrogen when the electrodes are incandescent tungsten. Further incomplete evidence suggests the presence of a total of four states with copper electrodes in nitrogen.

The results thus point conclusively to the presence of a new discharge type in the high pressure discharge, and suggest the existence of still others. The data are too incomplete at present to allow a conclusion as to the mechanism.

Research Laboratory,
General Electric Company,
Schenectady, N. Y.
March 8, 1938.

C. G. SUITS

[1] Mackay and Ferguson, J. Frank. Inst. **181**, 209 (1916).
[2] Langmuir, Gen. Elec. Rev. **29**, 153 (1926).

Concentration of Radiohalides, and Failure to Observe Gamma-Rays from I^{128}

In connection with experiments in which radioactive iodine, I^{128}, is being used as an indicator in the study of thyroid physiology, it was necessary to determine whether this substance emits gamma-rays. There is disagreement on this point in the literature; Amaldi[1] lists a gamma-ray as present, while Livingston and Bethe[2] do not.

With 150 mC of radon and beryllium, we have prepared sources of I^{128} which emit 10^5 beta-rays per minute, and have been unable to detect with a screen cathode gamma-ray counter any gamma-rays which pass through one-sixteenth of an inch of lead (1.8 g cm^{-2}). This corresponds to less than 0.1 gamma-ray of energy 0.5 Mev, per beta-ray, as determined by comparison with a radium standard.

A modification of the method of concentrating radioactive iodine given by d'Agostino[3] has been used for both iodine and bromine with excellent results. In the case of iodine, a few milligrams of free iodine (e.g., ten) are added to irradiated ethyliodide, and a water solution of the combining weight of sodium bisulphite (e.g., 4.1 mg) is shaken with the ethyliodide until the iodine color disappears. The water layer is separated from the ethyliodide in a separatory funnel, and silver iodide precipitated from it by the addition of an excess of slightly acid silver nitrate solution. Filtration is hastened by heating to boiling before filtering. Almost all the activity can thus be concentrated into a precipitate which may if desired contain as little as one milligram of iodine. The ethyliodide can be used over and over, and the complete separation can be carried out in less than ten minutes.

This work was done at the Massachusetts Institute of Technology under a grant from the Milton Fund of Harvard University.

ARTHUR ROBERTS
JOHN W. IRVINE, JR.

Harvard Medical School and Mass. Inst. of Tech. (A. R.),
Massachusetts Institute of Technology (J. W. I.),
Cambridge, Massachusetts,
March 1, 1938.

[1] Amaldi, Physik. Zeits. **38**, 692 (1937).
[2] Livingston and Bethe, Rev. Mod. Phys. **9**, 246 (1937).
[3] d'Agostino, Gazz. Chem. Ital. **65**, 1071 (1935).

Gamma-Radiation from N^{13}

The momentum distribution of the photoelectrons ejected from lead by the gamma-radiation from N^{13} has been investigated by means of a large cloud chamber recently constructed at this laboratory. A lead radiator of thickness 0.0017 cm was stretched across the center of the cloud chamber, and measurements were made of the radius of curvature of the tracks of the electrons ejected from it. The beam of gamma-rays from the source was collimated with lead so that no recoil electrons could originate in the floor or roof of the chamber. The source of N^{13} was prepared by bombarding a small amount of ash-free charcoal (impurities less than 0.01 percent) with deuterons from the cyclotron.

The source was first surrounded with carbon so that all the positrons were stopped near the source. The distribution obtained in this case is shown in Fig. 1. There are obviously two groups of tracks. The momentum of the most energetic group corresponds closely with that to be expected from the ordinary 510 kv annihilation radiation. This group of tracks is produced by photoelectrons and Compton recoils in about equal numbers, as shown by the smooth curves in the figure. The maximum energy available to the Compton electrons is 340 kv while the energy of the photoelectrons ejected from the K shell of lead should be 420 kv. It is seen that the data obtained are in accord with these predictions. The contribution of the Compton process to the less energetic group of tracks can be neglected, of course. Thus, using the distribution as indicated by the smooth curve, we obtain an energy of 285 ± 30 kv for the gamma-radiation ejecting the photoelectrons. The relative intensity of the two lines can be estimated fairly well from the number of tracks in each. Taking into account the relative cross section for photoelectric absorption at the two energies, one obtains the result that there are 2.5 quanta of 0.5 Mev radiation per quantum of 0.3 Mev radiation. In other words, there are 0.8 quanta of 0.3 Mev radiation for every positron emitted by N^{13}. This intensity estimate is uncertain by a factor 1.5.

It is not difficult to understand why this radiation was not observed in previous experiments, where a radiator of

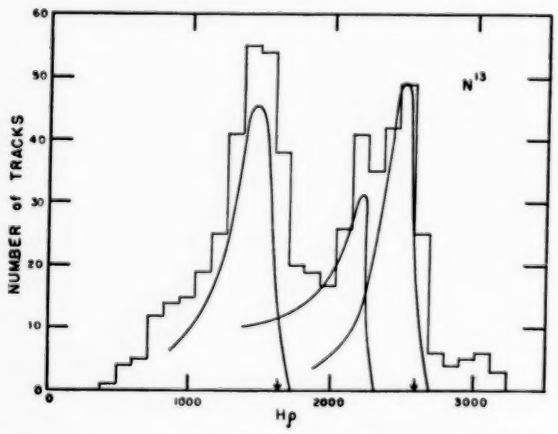

FIG. 1. Distribution of photoelectrons ejected from lead by gamma-radiation from N^{13}.

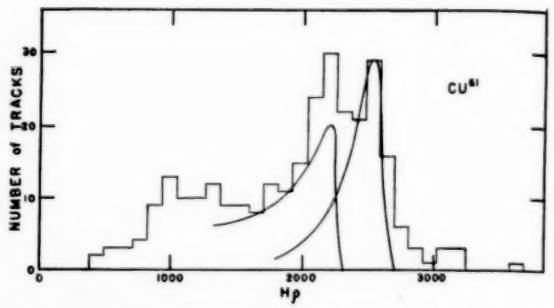

FIG. 2. Distribution of photoelectrons produced by radiation from Cu^{61}.

low atomic number was used, since a radiator of lead is much more sensitive in the low energy region.

Two subsidiary experiments were performed, in order to ascertain if the radiation was connected with the slowing down or annihilation of the positrons from N^{13}. The radiation from a source of Cu^{61}, a positron emitting substance prepared by bombarding nickel with deuterons,[1] was investigated with the same geometrical arrangement and radiator, and the distribution obtained is shown in Fig. 2. It is seen that there are very few tracks which could be ascribed to the low energy group. One would expect a small number of tracks (15) in this region due to the radiation emitted when a positron is annihilated while in motion.[2]

Finally, a thin source of N^{13} was arranged so that most of the positrons were annihilated behind the lead collimating shield. This increased the relative intensity of the low energy line by a factor three, which is all one could hope for, in practice. Thus it is apparent that this radiation is probably nuclear in origin.

The "inspection" upper limit of the positron spectrum of N^{13} is in such apparently good agreement with the difference in the masses of N^{13} and C^{13} (1.25 Mev *vs.* 1.28 Mev) that one hesitates to postulate a gamma-ray of 0.3 Mev following the positron emission. It is possible, of course, that there are two alternative positron transitions, one of 1.3 Mev and one of 1.0 Mev followed by the 0.3 Mev gamma-ray.

Another alternative, which for theoretical reasons would seem much less likely, is that the 0.3 Mev radiation is associated with the process of K electron capture proposed as a possibility by Roberts and Heydenburg[3, 4] to account for the difference in yield of positrons *vs.* neutrons in the formation of N^{13}. It is possible that these questions could be answered by an exact investigation of the positron spectrum of N^{13}.

The writer wishes to thank Professor J. M. Cork and Dr. R. L. Thornton for their interest and cooperation. This research was supported by the Horace H. Rackham Trust Fund.

J. REGINALD RICHARDSON*

University of Michigan,
Ann Arbor, Michigan,
March 12, 1938.

* National Research Fellow.

[1] R. L. Thornton, Phys. Rev. **51**, 893 (1937).
[2] Bethe, Proc. Roy. Soc. **A150**, 129 (1935).
[3] Roberts and Heydenburg, Phys. Rev. **53**, 374 (1938).
[4] Alvarez, Phys. Rev. **53**, 326 (1938).

Change and Exchange of Rest Mass of Elementary Particles During Collisions

In a recent letter I suggested[1] that the possibility of a change of rest mass of elementary particles caused by collisions should be investigated. In general the distribution of energy and of momentum among the various particles which are involved in a collision will be complicated if a change of rest mass is taken into account. In two limiting cases, however, the results may be stated in a simple manner. These two cases are (A) an *exchange* of the rest masses between two elementary particles, and (B) a *change* of the rest mass of one individual particle which passes, for instance, through the field of a nucleus.

We denote with $\mathbf{E}=mc^2/(1-\beta^2)^{\frac{1}{2}}$ the total energy of the particle before the collision. Its kinetic energy is $T=\mathbf{E}-mc^2$. After the collision $\mathbf{E}'=m'c^2/(1-\beta'^2)^{\frac{1}{2}}$ and $T'=\mathbf{E}'-m'c^2$. The limiting case (A) is characterized by $\mathbf{E}'\neq\mathbf{E}$ and $T'=T$, whereas, for the limiting case (B) $\mathbf{E}'=\mathbf{E}$ and $T'\neq T$.

Case (A)

As was suggested in an earlier paper[2] an *exchange of identity* between two elementary particles may take place during a collision, involving for example the exchange of the rest masses m and m' as well as the exchange of the charges e and e'. If the collision takes place next to a heavy third mass whose presence takes care of the change in momentum, the kinetic energy T' of the outgoing particle m' may substantially be equal to the kinetic energy T of the incoming particle m. If the moving particle is analyzed in a uniform magnetic field H the radius ρ of its path will be such that before the collision

$$(H\rho)=(T^2+2mc^2T)^{\frac{1}{2}}/e$$

and after the collision

$$(H\rho)'=(T'^2+2m'c\,T')^{\frac{1}{2}}/e'=(T^2+2m'c^2T)^{\frac{1}{2}}/e'$$

so that $(H\rho)'\gtrless(H\rho)$ for $m'\gtrless m$ if we take $e'=e$.

Case (B)

An elementary particle, such as an electron, may collide with a nucleus and change its rest mass from m to m', so that $\mathbf{E}'=\mathbf{E}=T+mc^2=T'+m'c^2$. In this case

$$(H\rho)=(T^2+2mc^2T)^{\frac{1}{2}}/e$$

and

$$(H\rho)'=[T^2+2mc^2T+(m^2-m'^2)c^4]^{\frac{1}{2}}/e$$

so that $(H\rho)'\gtrless(H\rho)$ for $m'\lesssim m$, respectively.

The change of rest mass therefore produces opposite effects in the cases (A) and (B).

Processes of the type (A) may be expected to take place in nuclear fields where neutrons, protons and possibly electrons of different mass and charge can exchange their identities. The possibility of observing processes of the type (B) however depends on the probability of the transition of an elementary particle from one state of mass and charge into another.

A number of phenomena related to the passage of energetic particles through matter come to mind if the existence of the processes suggested in the preceding is conceded. In particular the apparent changes of energy of fast cosmic-ray particles during their passage through various types of matter may be only partly real and partly caused by a change of the rest mass m or of the charge e. The occurrence of hard and soft showers described by W. Bothe[3] may here find an explanation.

Although the effects on the energy of a change of the charge e in the process (B) cannot be formulated at the present, this possibility also must be carefully examined in view of the fact that the existence of such processes would throw much needed light on the problem of the nature of electric charges and on the problem of the unification of the electromagnetic and the gravitational fields. Some peculiar cloud chamber tracks were pointed out previously which may be due to collisions in which both the rest mass and the charge of elementary particles such as electrons have suffered a change.[1, 2]

F. ZWICKY

California Institute of Technology,
Pasadena, California,
March 13, 1938.

[1] F. Zwicky, Phys. Rev. **53**, 315 (1938).
[2] F. Zwicky, Phys. Rev. **43**, 1031 (1933).
[3] W. Bothe, *Kernphysik*, (Ed. E. Bretscher) (J. Springer, Berlin, 1936), p. 122.

Isomers of Radioindium

In a survey of radioactivity produced by high energy neutron bombardment two long periods, 4 hr. and 2 mo., were found in the indium chemical separation.[1] Lawson and Cork subsequently made a detailed study of the radioactivity induced in indium by various methods of excitation and were able to assign reasonably these two periods, more accurately measured 4.1 hr. and 50 days, as well as the five other periods to definite indium isotopes.[2] They found that the 4.1-hr. period appeared weakly with both deuteron and slow neutron bombardments but strongly with fast neutron bombardment. The 50-day period was obtained only with fast neutrons. Both periods were tentatively assigned to In^{114}.

Recently Mitchell reported that the 50-day period is produced also by slow neutrons but that the 4.1-hr. period is not.[3] The activation of the latter would be expected if the periods were isomeric. He suggested that with slow neutrons the formation of the 4.1-hr. period may be impossible due to energy considerations or forbidden because of some selection rule.

The data obtained during the survey of radioactivity[1] produced by fast neutrons have been used to calculate the branching ratios for the radioactive indium periods here involved. From three specimens bombarded 1, 2 and 4 hours respectively with fast neutrons an average branching ratio for the 50-day to the 4.1-hr. period is about 22. The individual values varied considerably being 25.5, 27.3 and 12.2. The ratio of the abundances of the stable isotopes In^{115} to In^{113} is 21.2. From two observations the ratio for the

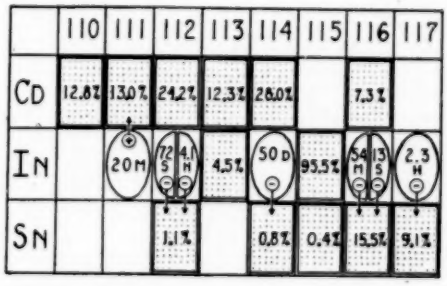

FIG. 1. Stable and radioactive isotopes of indium.

72-sec. period to the 4.1-hr. period is about 2.0. These results therefore indicate that the 4.1-hr. period is best assigned to In^{112}.

If this assignment be made the observations of Lawson and Cork and of Mitchell may be made mutually consistent in view of the following two considerations:

(A) Lawson and Cork accomplished the slow neutron activation by imbedding the specimen in approximately a 4 cm cube of paraffin placed as close as possible to a beryllium target bombarded by 6.3 Mev deuterons. Since the neutrons from this target may have energies up to 10 Mev, 2 cm of paraffin would undoubtedly allow many fast neutrons to impinge upon the indium. These neutrons might then produce the very weak 4.1-hr. period observed.

(B) Many substances when bombarded by high energy deuterons have been shown to emit neutrons which are sufficiently energetic to produce the $n-2n$ reaction.[4] Since the 4.1-hr. period is weaker with direct deuteron bombardment of indium than with the neutrons from the Li – D reaction, it is therefore suggestive that fast secondary neutrons play an important role in the excitation of this period.

Figure 1 shows the stable and radioactive isotopes of indium. In^{112} is shown as an isomeric nucleus having two decay periods, 72 sec. and 4.1 hr.

M. L. Pool

Mendenhall Laboratory of Physics,
Ohio State University,
Columbus, Ohio,
March 15, 1938.

[1] M. L. Pool, J. M. Cork and R. L. Thornton, Phys. Rev. **52**, 239 (1937).
[2] J. L. Lawson and J. M. Cork, Phys. Rev. **52**, 531 (1937).
[3] Allan C. G. Mitchell, Phys. Rev. **53**, 269 (1938).
[4] M. L. Pool, Phys. Rev. **53**, 334 (1938).

Another Circuit for Use with Geiger-Müller Counters

In the most recent circuits for use with the Geiger-Müller counter, a high counting rate has been achieved either by employing the adjustable resistance of a vacuum tube to short-circuit effectively the counter on the initiation of a discharge, (Neher and Harper,[1] Neher and Pickering[2]), or by using two stages of amplification and positive feedback (Getting,[3] and Ruark[4]). In the circuit described below, the automatically adjustable resistance of a vacuum tube is used in series rather than in parallel with the ion counter. The discharge is cut short by increasing the series resistance to a very high value as soon as the counter discharge begins. After deionization has been accomplished the resistance quickly returns to a low value to speed voltage recovery. In counting speed the circuit approaches those of Neher and Harper, Getting, Neher and Pickering, and Ruark, and has some advantages not found in any of these.

As shown in Fig. 1, the high voltage source is connected through a resistance to the center wire of the counter. The cylinder is connected directly to the plate of a pentode, such as the 6C6 or 1B4. Both the cathode of the tube and the negative side of the high voltage source are grounded. The control grid of the tube is capacitance coupled to the counter wire, and is also connected through a grid resistor, (R_g) to a drop wire, by means of which the bias (V_g) may be adjusted. The screen grid is supplied with a positive potential of the order of 1.5 to 3 volts, the value

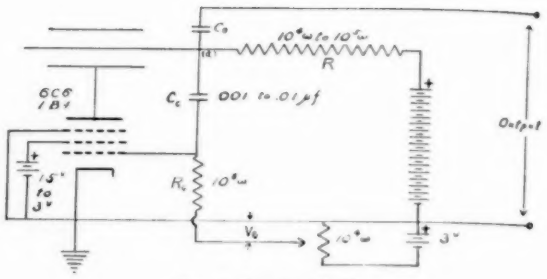

FIG. 1. Counter circuit.

not being critical. The output is most conveniently coupled by capacitance to the counter anode.

When the counter is inactive, no current flows in R, and the full battery voltage reaches the counter. When conduction begins, a current of about 20 microamperes (maximum) flows, causing the potential at point (a) to fall an amount equal to the drop through R. This negative pulse is fed through the coupling condenser (C_c) to the control grid, which swings sufficiently negative to open effectively the circuit and stop the discharge. After the pulse has passed, the grid voltage returns to normal allowing a flow of electrons to the counter cylinder, which quickly brings the counter voltage to normal. In order that the negative pulse received by the grid shall be sufficient to stop conduction in the tube, a certain minimum negative bias (V_g) must be applied. If the bias is less than this critical value, a continuous current results. Increasing the bias serves to reduce the peak current in the circuit during a pulse, thus reducing the magnitude of the output pulse voltage. If the grid is biased too far negative the tube becomes effectively an open circuit and the counter action will be erratic or cease altogether, depending on values of the leakage resistance between various parts of the circuit.

This circuit is similar to those proposed by Neher and Harper, Getting, Ruark, and Neher and Pickering in that low resistances are used, with correspondingly small recovery times, and that a common battery may be used to operate several counters. It differs, however, in the use of the vacuum tube in series with the counter. Since the tube conducts only during a pulse, there is no drain from the high voltage source when the counter is quiescent. Further, by varying the potential applied to the screen grid, the effective resistance in series with the counter may be controlled over a wide range. The cathode of the tube is fixed at ground potential, and all potentials applied to the tube are well below its ratings. The chief disadvantage of this circuit is the varying voltage of the cylinder of the counter tube, making the capacitance to the shield a factor in its operation. In addition, with the output coupled as shown, the output voltage pulses amount to only one or two volts. The output may be coupled to the plate of the tube, but unless the impedance of the coupled circuit is very high the counting rate is affected.

E. W. Yetter

Electrical Engineering Department,
Massachusetts Institute of Technology,
Cambridge, Massachusetts,
March 14, 1938.

[1] H. V. Neher and W. W. Harper, Phys. Rev. **49**, 940–943 (1936).
[2] H. V. Neher and W. H. Pickering, Phys. Rev. **53**, 316 (1938).
[3] I. A. Getting, Phys. Rev. **53**, 103 (1938).
[4] A. Ruark, Phys. Rev. **53**, 316 (1938).

Proceedings of the New England Section of the American Physical Society

MINUTES OF THE NEW HAVEN MEETING, JANUARY 15, 1938

THE twelfth regular meeting of the New England Section was held at Yale University, New Haven, Connecticut, on Saturday, January fifteenth. Five invited papers, listed below, were presented. 100 persons attended the morning session and 125 were present at the afternoon session. A rising vote of thanks was extended to Professor Zeleny and McKeehan and to the other members of the Physics Department of Yale University for their generous hospitality. The next meeting of the Section will be held on Saturday, October 15, at Mt. Holyoke College, South Hadley, Massachusetts.

Morning Session

K. S. VAN DYKE (Wesleyan University): **Viscous Losses in Vibrating Solids**

L. W. MCKEEHAN (Yale University): **Ferromagnetism in Single Crystals**

HARVEY FLETCHER (Bell Telephone Laboratories, Inc.): **Loudness, Masking and Their Relation to the Hearing Process and the Problem of Noise Measurement**

Afternoon Session

E. POLLARD (Yale University): **Transmutations by Alpha-Particles**

R. W. WOOD (The Johns Hopkins University): I. **Demonstration of Forced Vibration and of Resonance by Means of a Conical Pendulum.** II. **Natural Color Motion Pictures of Crystal Growth as seen in Polarized Light**

JOSEPH C. BOYCE,
Secretary-Treasurer,
New England Section